Role of fibrillin-1 in adipose tissue development, homeostasis, and function

By

MUTHU LAKSHMI MUTHU

Department of Anatomy and Cell Biology

Faculty of Medicine and Health Sciences

McGill University

Montreal, Canada

December 2021

A thesis submitted to McGill University in partial fulfillment of the requirements of the degree of

DOCTOR OF PHILOSOPHY

TABLE OF CONTENTS

LIST OF FIGURES AND TABLES ..... **vi**

ACKNOWLEDGEMENTS ..... **ix**

PREFACE ..... **xiii**

CONTRIBUTION OF AUTHORS ..... **xv**

ORIGINAL CONTRIBUTION TO KNOWLEDGE ..... **xvii**

LIST OF ABBREVIATIONS ..... **xviii**

ABSTRACT ..... **xxi**

RÉSUMÉ ..... **xxiii**

CHAPTER 1: REVIEW OF LITERATURE **1**

1.1 Adipose tissue significance **2**

1.2 Adipose tissue biology **2**

1.2.1 White adipose tissue 2

1.2.2 Brown and beige adipose tissue 4

1.2.3 Adipose tissue components 6

1.2.4 Adipose tissue organogenesis 6

1.3 Adipose tissue in disease **9**

1.3.1 Obesity and lipodystrophy 10

1.3.2 Insulin resistance 10

1.3.3 Abnormal adipose tissue expansion 11

1.3.4 Metabolically healthy obesity 16

1.4 Adipogenesis **16**

1.4.1 Transcriptional regulation of adipogenesis 17

1.4.2 Insulin signaling during adipocyte differentiation 18

1.4.3 ECM remodeling during adipogenesis 20

1.5 Fibrillins **22**

1.5.1 Fibrillin structure and isoforms 22

1.5.2 Fibrillin-1 containing microfibrils and growth factor interactions 23

1.5.3 Asprosin, the C-terminal propeptide of fibrillin-1 25

1.6 Marfan syndrome **27**
1.6.1 Cardiovascular abnormalities in MFS 27
1.6.2 Skeletal abnormalities in MFS 28
1.6.3 Adipose tissue abnormalities in MFS 29
1.7 Mouse models of MFS **30**
1.8 Rationale, hypothesis, overall goals, and objectives **32**

CHAPTER 2: FIBRILLIN-1 IS A KEY REGULATOR OF WHITE ADIPOSE TISSUE DEVELOPMENT, HOMEOSTASIS, AND FUNCTION **34**

2.1 Preamble **36**
2.2 Abstract **37**
2.3 Introduction **39**
2.4 Methods **43**
2.4.1 Mice used in this study 43
2.4.2 Systemic metabolism and tissue analysis 44
2.4.3 Histologic analysis and adipocyte size analysis 44
2.4.4 RNA extraction, real-time qPCR, and cDNA sequencing 45
2.4.5 Primary cell isolation and culture 46
2.4.6 Adipogenic differentiation 46
2.4.7 Human tissues 47
2.4.8 Indirect immunofluorescence labeling of tissues and cells 48
2.4.9 Western blotting 49
2.4.10 Cell binding assay 49
2.4.11 Biacore analysis 50
2.4.12 Statistical analysis 51
2.5 Results **51**
2.5.1 Fibrillin-1 in mouse and human white adipose tissue 51
2.5.2 Fibrillin-1 deficiency in mice results in a distinct sexual dimorphism with respect to adipose tissues 53
2.5.3 Reduced fibrillin-1 leads to altered glucose and insulin metabolism in male mice 54
2.5.4 Fibrillin-1 deficient male mice are characterized by adipocyte hypertrophy and increase in adipogenic markers 55
2.5.5 Deficiency of fibrillin-1 enhances adipogenic differentiation 56
2.5.6 Fibrillin-1 restricts adipogenic differentiation in the early commitment phase 58

2.5.7 Fibrillin-1 inhibits adipogenic differentiation via pAKT 60
2.6 Discussion **63**
2.7 Acknowledgements **70**
2.8 Figures and supplemental information **71**
2.9 Bibliography for chapter 2 ..... **91**

CHAPTER 3: MALE MICE WITH FIBRILLIN-1 DEFICIENCY ARE PREDISPOSED TO HIGH FAT DIET INDUCED OBESITY, DIABETES, AND FATTY LIVER **98**

3.1 Preamble **100**
3.2 Abstract **101**
3.3 Introduction **102**
3.4 Material and Methods **104**
3.4.1 Animals and diets 104
3.4.2 Orchiectomy and ovariectomy 104
3.4.3 Measurement of body weight, glucose, insulin and asprosin 105
3.4.4 Biochemical analysis of serum metabolites 105
3.4.5 Body composition using DEXA 105
3.4.6 Tissue collection 106
3.4.7 Histopathological analysis 106
3.4.8 Protein extraction and immunoblotting 106
3.4.9 Statistical analysis 107
3.5 Results **108**
3.5.1 HFD-induced weight gain in MFS mice 108
3.5.2 HFD-induced changes in the adipose tissue mass of MFS mice 108
3.5.3 HFD-induced changes in adipocyte size in MFS mice 109
3.5.4 HFD-induced hyperglycemia and glucose intolerance in MFS mice 110
3.5.5 HFD-induced hyperinsulinemia and insulin intolerance in male MFS mice 110
3.5.6 HFD-induced liver phenotype in male MFS mice is similar to non-alcoholic fatty liver disease (NAFLD) 111
3.6 Discussion **113**
3.7 Acknowledgements **119**
3.8 Figures and supplemental information **120**
3.9 Bibliography for chapter 3 ..... **131**

CHAPTER 4: PRELIMINARY FINDINGS - ADIPOCYTE SPECIFIC DELETION OF FIBRILLIN-1 INHIBITS ADIPOSE TISSUE DEVELOPMENT IN MALE MICE **136**

4.1 Preamble **138**

4.2 Abstract **139**

4.3 Introduction **140**

4.4 Methods **142**

4.4.1 Mice used in this study 142

4.4.2 Analysis of systemic metabolism and tissues 143

4.4.3 Histologic and adipocyte size analysis 143

4.4.4 RNA extraction and real-time qPCR 143

4.4.5 Indirect immunofluorescence 144

4.5 Results **146**

4.5.1 Efficacy of conditional fibrillin-1 deletion in adipocytes 146

4.5.2 Adipocyte specific deletion of fibrillin-1 significantly reduces specific adipose tissue depots 146

4.5.3 Deleted adipocyte specific fibrillin-1 does not alter the overall glucose and insulin metabolism 147

4.5.4 *Fbn1* gene deletion in adipocytes of male mice reduces cell size 147

4.5.5 *Fbn1* deletion in adipocytes slightly reduces adipose tissue inflammation 148

4.6 Discussion **149**

4.7 Ongoing or immediate future experiments **152**

4.8 Acknowledgements **153**

4.9 Figures and supplemental information **154**

4.10 Bibliography for chapter 4 ..... **159**

CHAPTER 5: OVERALL DISCUSSION AND CONCLUSIONS **163**

5.1 Significance of the study **164**

5.2 Key findings **164**

5.3 Overall discussion and future directions **166**

5.3.1 Regulation of TGF-β signaling by fibrillin-1 in adipose tissue 166

5.3.2 Potential reasons for sex differences observed in MFS mice 167

5.3.3 Therapeutic potential of fibrillin-1 fragments to target adipogenesis 169

5.3.4 Fibrillin-1 and asprosin turnover 170

5.4 Limitations of the study **172**
5.5 Concluding remarks and broader implications **173**
5.6 Bibliography for chapter 1 and 5 ..... **174**
APPENDIX **195**

LIST OF FIGURES AND TABLES

Chapter 1

Figure 1.1: Schematic diagram of subcutaneous and visceral adipose tissue depots in mice

Figure 1.2: Light microscopic images of white adipose tissue and brown adipose tissue

Figure 1.3: Schematic stages of adipogenesis in relation to ECM protein expression

Figure 1.4: Isoforms and domain organisation of fibrillins

Figure 1.5: Furin processing of profibrillin-1 leads to microfibril assembly and asprosin release

Figure 1.6: The role of asprosin in metabolic organs

Chapter 2

Figure 2.1: Fibrillin-1 in mouse and human white adipose tissues

Figure 2.2: Analysis of metabolic indices of fibrillin-1 deficient mice

Figure 2.3: Analysis of glucose and insulin metabolism of fibrillin-1 deficient mice

Figure 2.4: Quantification of adipocyte size in iWAT of fibrillin-1 deficient mice

Figure 2.5: Analysis of adipogenic and inflammatory gene expression markers in iWAT of mgR/mgR mice

Figure 2.6: Lack of fibrillin-1 enhances adipogenic differentiation in cell culture

Figure 2.7: Fibrillin-1 inhibits adipogenesis in cell culture

Figure 2.8: Fibrillin-1 sequesters insulin and attenuates the insulin signaling pathway

Figure S2.1: *Magp1* mRNA expression analysis in subcutaneous white adipose tissue

Figure S2.2: Weight analysis of liver and spleen in mgR/mgR and C1041G/+ mice

Figure S2.3: Adipogenic and inflammatory gene expression analysis of iWAT from C1041G/+ mice

Figure S2.4: Fibrillin-1 deposition of non-differentiated and adipocyte differentiated MSCs

Figure S2.5: Analysis of adipogenesis and adipogenic markers after 10 days of adipocyte differentiation

Figure S2.6: Surface plasmon resonance spectroscopy of the components in the adipogenic cocktail with immobilized rFBN1-N and rFBN1-C

Table 2.1: Sequence of primers used in this study

Chapter 3

Figure 3.1: Diet-induced weight gain in MFS mice and their wild type littermates

Figure 3.2: Diet-induced changes in adiposity in MFS mice and their wild type littermates

Figure 3.3: Diet-induced changes in adipocyte size of MFS mice and their wild type littermates

Figure 3.4: Diet-induced changes in glucose homeostasis in MFS mice and their wild type littermates

Figure 3.5: Diet-induced changes in insulin homeostasis in MFS mice and their wild type littermates

Figure 3.6: Diet-induced changes in liver adiposity in $Fbn1^{C1041G/+}$ mice and their wild type littermates

Figure 3.7: ER-stress in the liver of $Fbn1^{C1041G/+}$ mice and their wild type littermates

Figure S3.1: Female *Fbn1*$^{mgR/mgR}$ mice increase lean mass when fed with HFD

Figure S3.2: Male or female *Fbn1*$^{mgR/mgR}$ mice do not demonstrate liver adiposity when fed HFD

Figure S3.3: Female *Fbn1*$^{C1041G/+}$ demonstrate only a mild lipid accumulation in the liver when fed with HFD

Figure S3.4: The spleen weight is not changed in MFS mutant mice when fed with HFD

Chapter 4

Figure 4.1: Generation of adipocyte specific fibrillin-1 knockout (Fbn1-AKO) mice

Figure 4.2: Analysis of whole body and tissue weights of adipocyte specific fibrillin-1 knockout mice

Figure 4.3: Analysis of glucose and insulin metabolism of adipocyte specific fibrillin-1 knockout mice

Figure 4.4: Quantification of adipocyte size in eWAT of adipocyte specific Fbn1-AKO mice

Figure 4.5: Analysis of inflammatory markers in eWAT of adipocyte specific Fbn1-AKO knockout mice

Chapter 5

Figure 5.1: Hypothesized working model of the role of fibrillin-1 in adipogenesis and adipose tissue homeostasis

ACKNOWLEDGEMENTS

My graduate school experience has been a truly unforgettable experience in my life. This journey was only possible and successful because of all the wonderful people around me. I would like to take this opportunity and space to sincerely thank each one of them for their support and motivation.

First and foremost, my heartfelt gratitude goes to my PhD mentor, Dr. Dieter Reinhardt for believing in me and giving me the opportunity to work in his lab. His expert guidance and support have been instrumental in helping me achieve so much during my PhD program. I am very grateful for his open-door policy, constant motivation, and detailed teaching. His sincerity and unwavering enthusiasm in science and research have inspired and empowered me to always do my best and to go the extra mile. His lab infrastructure and organization has facilitated a smooth PhD experience. I also want to thank him for the numerous opportunities he provided me during my tenure in his lab, including the involvement in grant applications and the training of undergraduate and graduate students which honed my scientific writing and teaching skills. His constant encouragement to present my projects in various conferences has given me the exposure and confidence to communicate my research data effectively, which led to several presentation and travel awards over the years. I will proudly carry forward what I have learned from him, and I am sincerely thankful for his impact on my professional growth.

I am very thankful to my co-supervisor, Dr. Svetlana Komarova for always pushing me to the right direction. Her positivity and unparalleled enthusiasm in research and mentoring students are contagious and has been truly inspirational. I thank her for being a great role model of a successful

female scientist. Dr. Kerstin Tiedemann deserves my deepest appreciation and thanks for her unwavering support and guidance. I truly believe her patience, work ethic and the vast knowledge in science and research methods have greatly helped me throughout my PhD journey. I am grateful for her kindness, support, motivation, and willingness to help me at all times.

I also would like to express my special thanks to my previous supervisors, Dr. Andreas Herrlich and Dr. Eirini Kefalogianni for initially sparking my interest in a PhD project. It has been an honor to have started my scientific career under their guidance. I thank them for their constant support, advice, and positive words, that significantly helped to propel me to where I am now. I am always indebted for their mentorship both professionally and personally.

I feel fortunate to have joined the Reinhardt lab where I met amazing colleagues and friends along the way. My sincere appreciation and thanks go to all past and present Reinhardt lab members I have interacted with, for their professional help and moral support throughout my PhD program. First of all, I would like to thank my previous lab members, Dr. Heena Kumra, Dr. Rongmo Zhang and Dr. Hana Hakami for being my best friends and colleagues in the lab. I would like to thank them for all the scientific discussions, suggestions and criticisms which contributed to the development of my research abilities. I thank all the undergraduate students I have supervised, Domenico Lopez, Rajpreet Kaler, Merve Younussi, and Kelly Jung for helping me in my projects. It has been my privilege and a truly rewarding experience to have guided them. I am grateful for the work of the awesome lab managers, previously Jason Lee and currently Dr. Ling Li for the smooth organization of all aspects in the lab. I also would like to appreciate and thank my current lab members Neha Dinesh, Cori Lau, Iram Siddiqui and Elahe Mirzarazi for their kindness and

moral support in the final phases of my PhD project. I extend my appreciation to Dr. Valentin Nelea for being a great colleague and for reviewing the French translation of the thesis abstract. Also, I would like to thank the Komarova lab members Dr. Iris Borasachi, Turney McKee, and Dr. Gulzhakhan Sadvakassova for being supportive every time I was working at the Shriners Hospital. I am incredibly grateful to each one of all these individuals for making my life at McGill very pleasant.

I would like to sincerely thank my committee members Dr. Monzur Murshed, Dr. Lisbet Haglund and Dr. Chantal Autexier for their timely advice and support. I would also like to thank Dr. Autexier for being the best Graduate Program Director I could ever ask for. I thank her for swiftly responding to all my emails and for being a great mentor always with a smile and diligence. I express my sincere appreciation to Dr. Craig Mandato, Joelle Denomy, Joseph Dube, Anne Marie Contofalsky, and other administrative coordinators for being supportive throughout my graduate studies in the Department of Anatomy and Cell Biology at McGill University. I am very fortunate and thankful to have received scholarships, tuition assistance fellowships and differential fee waivers during my tenure as a PhD student from various funding agencies, including the Fonds de recherche de Quebec (FRQS), the Réseau de recherche en santé buccodentaire et osseuse (RSBO), and the Department of Anatomy and Cell Biology, McGill University.

All my friends from India and in Montreal deserve a huge thank you for being my go-to buddies. Many thanks to Dr. Ramya Kalyana Kumar and Bhaavana Krishnan, I don’t have enough words to appreciate both of you for just being there for me, for listening and for showing me a way out of every stumbling block. Also, I appreciate Siva Kumar Natarajan, Sharmila Srinivasan, Dr.

Vaishali Krishnadoss and Kiruthiga Thangavel for tolerating me over the last 10 years and for constantly being available every time I needed help. I would also like to thank all my Montreal friends, particularly Felix Raja Rodriguez and Swathi Adinarayanan for their continued kindness and support. I am also indebted to Manjusha Karanam, Sharadha Swaminathan and Sushmetha Mohan for helping me very much when I broke my leg during the third year of my PhD project. Thank you for all the food, for accompanying me to every hospital trip and most importantly for the moral support you provided to surpass the toughest phase of my PhD, far away from home. I extend my heartfelt appreciation and respect to Arobindh Balaji Viswanathan for being my pillar of strength during the last 4 years. I want to thank him for always being there for me, in good and bad times. I am sincerely grateful for all the efforts he took to make and keep me happy every single day. I would have never been able to get where I am today, without his unconditional love, encouragement and most importantly the trust he has in me.

Last but not least, I express my heartfelt thanks and gratitude to mom and dad (Muthu and Janaki) for their endless love, unconditional support, patience and understanding through all these years. They always encouraged me to pursue opportunities they never had. I am very fortunate to have them as my parents and I truly hope that I am making them proud. I am grateful for all the sacrifices they made to let me achieve my scientific goals. I am also very obliged to my brother and sister-in-law (Alagappan and Annapoorani) for being my support system and for standing by me at all times. Finally, I would like to thank my little niece Meenakshi for bringing enormous amount of joy and happiness in my life. I am very blessed to have the support of my family and I dedicate my PhD to them.

PREFACE

The work described in this thesis is published, submitted or to be submitted as follows:

1. **Chapter 1**

   Fibrillin-1 and fibrillin-1-derived asprosin in adipose tissue function and metabolic disorders.

   Muthu L. Muthu, Dieter P. Reinhardt

   J. Cell Commun. Signal. 14, 159–173 (2020)

2. **Chapter 2**

   Fibrillin-1 is a key regulator of white adipose tissue development, homeostasis, and function

   Muthu L. Muthu*, Kerstin Tiedemann*, Julie Fradette, Svetlana Komarova[#], Dieter P. Reinhardt[#], *Co-first authors, [#]Co-last authors

   The journal requested a second revision which was submitted on April 12th, 2022.

3. **Chapter 3**

   Male mice with fibrillin-1 deficiency are predisposed to high fat diet induced obesity, diabetes, and fatty liver

   Kerstin Tiedemann*, Muthu L. Muthu*, Dieter P. Reinhardt[#], Svetlana V. Komarova[#], *Co-first authors, [#]Co-last authors

   The journal requested a revision which will be submitted in April 2022.

4. **Chapter 4**

   Adipocyte specific deletion of fibrillin-1 inhibits adipose tissue development in male mice

   Muthu L. Muthu, Dieter P. Reinhardt

   Preliminary findings – Work in progress

According to the guidelines of McGill University, Chapter 1 and 5 have a common bibliography on pages 174-194, and Chapter 2, 3 and 4 have individual bibliographies at the end of each chapter.

CONTRIBUTION OF AUTHORS

Chapter 1 and 5:

Some selected parts of these chapters were directly taken from the published review article written by me and extensively reviewed and edited by Dr. Dieter Reinhardt (Muthu ML, Reinhardt DP, *J. Cell Commun. Signal.* 14, 159–173 (2020)). The remainder of these chapters were generated by me and reviewed and edited by Dr. Reinhardt.

Chapter 2:

The study presented in chapter 2 were conceptualised and planned by me, Dr. Tiedemann, Dr. Komarova and Dr. Reinhardt. All mouse breeding, and experiments using *Fbn1*$^{mgR/mgR}$ mice shown in Fig. 2.1-2.5, the cell culture experiments in Fig. 2.6-2.8 and the experiments for supplemental Figs. S2.1-2.5 were conducted by me. *Fbn1*$^{C1041G/+}$ mice colony were maintained and dissected by Dr. Tiedemann and the data in Figs. 2.2-2.4 were generated by Dr. Tiedemann. Tissues from C1041G/+ mice were provided to me, and I performed all immunofluorescence and sequencing experiments for Fig. 2.1. Dr. Nelea performed the Biacore experiments in Fig. 2.8 and Fig. S2.6. Dr. Fradette provided the human white adipose tissue samples for analysis. The data analysis and interpretation were performed by me, Dr. Tiedemann, Dr. Komarova and Dr. Reinhardt. All figures were designed and generated by me. The first draft of the manuscript was written by me, followed by extensive reviewing, and editing by Dr. Reinhardt with inputs from other authors.

Chapter 3:

The study presented in chapter 3 were conceptualised and planned by me, Dr. Tiedemann, Dr. Komarova and Dr. Reinhardt. All experiments using mgR/mgR mice presented in Figs. 3.1-3.5 and Figs. S3.1-3.2 were conducted by me. The experiments using C1041G/+ mice in Figs. 3.1-3.7

and Figs. S3.1, 3.3 and 3.4 were conducted by Dr. Tiedemann. The data analysis and interpretation were performed by me, Dr. Tiedemann, Dr. Komarova and Dr. Reinhardt. All figures were compiled by Dr. Tiedemann with my participation for the data obtained from mgR/mgR mice. The first draft of the manuscript was written by Dr. Tiedemann followed by careful reviewing and editing by Dr. Komarova, Dr. Reinhardt and me.

Chapter 4:

The study presented in chapter 4 was conceptualised by me and Dr. Reinhardt. Generation of the mouse model and all the *in vivo* experiments in this chapter were conducted by me and the data were analysed by me. All figures and the manuscript were compiled and generated by me, followed by thorough reviewing and editing by Dr. Reinhardt.

ORIGINAL CONTRIBUTION TO KNOWLEDGE

The work presented in this thesis contributes the following novel findings about essential roles of fibrillin-1 in adipose tissue development, function, and homeostasis.

1. Fibrillin-1 is present around mature adipocytes in mouse and human white adipose tissue.
2. Reduced fibrillin-1, but not a missense mutation leading to Marfan syndrome (MFS), promotes excess fat deposition, adipocyte hypertrophy and insulin resistant phenotypes in male mice.
3. At the mesenchymal cell stage, fibrillin-1 acts as a negative regulator of adipogenic differentiation to maintain tissue homeostasis.
4. The C-terminal half of fibrillin-1 mediates this negative regulation through a dual mechanism, by direct cell binding and by insulin sequestration, merging at the level of AKT signaling.
5. High fat diet fed to male MFS mice further exacerbates the obesity and insulin resistance phenotypes, whereas female MFS mice remain protected from weight gain and metabolic alterations.
6. High fat diet fed male MFS mice were susceptible to an endoplasmic stress induced fatty liver phenotype, which was reduced after orchiectomy.
7. Deletion of fibrillin-1 in mature adipocytes leads to reduced adipose tissue deposition in male mice, recapitulating the adipose tissue phenotype frequently observed in MFS patients. This highlights the positive role of fibrillin-1 in the maintenance of mature adipocytes.

LIST OF ABBREVIATIONS

Adipoq.....Mouse adiponectin gene/mRNA

AgRP.....Agouti-related protein

AKT .....Protein kinase B

ATP.....Adenosine triphosphate

aP2.....Adipocyte protein 2

BAT.....Brown adipose tissue

BMI.....Body mass index

BMP .....Bone morphogenetic protein

cAMP .....Cyclic adenosine monophosphate

cbEGF .....Calcium-binding Epidermal Growth Factor

CD.....Control diet

CD31 .....Cluster of differentiation 31

C/EBP .....CCAAT enhancer binding protein

Cebpa .....Mouse ccaat/enhancer-binding protein α gene/mRNA

C1041G/+.....$Fbn1^{C1041G/+}$ mice

CLS .....Crown like structures

DAPI .....4′, 6-diamidino-2-phenylindole

ECM.....Extracellular matrix

Erk.....Extracellular signal-regulated kinases

eWAT.....Epididymal white adipose tissue

Fabp4.....Fatty Acid-Binding Protein 4

FBN1.....Fibrillin-1 protein

Fbn1 .....Mouse fibrillin-1 gene/mRNA

Fbn2 .....Mouse fibrillin-2 gene/mRNA

Fbn3 .....Mouse fibrillin-3 gene/mRNA

Fbn1-FL .....Mice flanked by 2 loxP sites for fibrillin-1

Fbn1-AKO.....Adipocyte specific fibrillin-1 knockout mice

gWAT .....Gonadal or visceral white adipose tissue

GLUT4.....Glucose transporter 4

Glut4 .....mouse Glucose transporter 4 gene/mRNA

GTT.....Glucose tolerance test

HFD.....High fat diet

HIF-1α.....Hypoxia inducible factor-1α

IL-1β Interleukin-1β

IL-6 ..... Interleukin 6

IL-10 .....Interleukin 10

IR.....Insulin receptor

IRS .....Insulin receptor substrate

ITT .....Insulin tolerance test

iWAT .....Inguinal or subcutaneous white adipose tissue

KD.....Equilibrium dissociation constant

LC .....Littermate controls

Lep .....Mouse leptin gene/ mRNA

LTBP.....Latent TGF-β binding protein

MAGPs .....Microfibril-associated glycoproteins

Magp1 .....Mouse microfibril-associated glycoprotein 1 gene/ mRNA

MCP1 .....Monocyte chemoattractant protein 1

MEF .....Mouse embryonic fibroblasts

MFS.....Marfan syndrome

MPLS .....Marfanoid progeroid lipodystrophy syndrome

MSCs.....Mesenchymal stem cells

mgR/mgR..... $Fbn1^{mgR/mgR}$ mice

mTOR ..... Mechanistic target of rapamycin

NAFLD ..... Non-alcoholic fatty liver disease

NASH..... Non-alcoholic steatohepatitis

NPS ..... Neonatal progeroid syndrome

ob/ob ..... $Leptin^{ob/ob}$ mice

PDGFR..... Platelet-derived growth factor receptor

PERK ..... Protein kinase-like endoplasmic reticulum kinase

PI3K ..... Phosphoinositide 3-kinase

Plin ..... Mouse perilipin gene/mRNA

PPARγ ..... Peroxisome proliferator-activated receptor gamma

Pparg ..... Mouse peroxisome proliferator-activated receptor gamma gene/mRNA

rFBN1-N/C ..... Recombinant fibrillin-1 N terminal half/ C terminal half

RANKL..... Receptor activator of nuclear factor κβ ligand

RGD ..... Arginine- Glycine- Aspartate

RT ..... Room temperature

sWAT..... Subcutaneous white adipose tissue

TAA ..... Thoracic aortic aneurysm

TGF-β..... Transforming growth factor beta

TBS/TBST ..... Tris buffered saline / Tris buffered saline containing Tween 20

TNFα ..... Tumour necrosis factor alpha

UCP1..... Uncoupling protein 1

vWAT ..... Visceral white adipose tissue

Wt..... Wild-type littermates

WAT ..... White adipose tissue

Zfp423..……. Mouse zinc finger protein 423 gene/ mRNA

ABSTRACT

Introduction

Adipose tissue is a dynamic metabolic organ, that undergoes significant remodeling during development. The extracellular microenvironment of adipose tissue orchestrates differentiation, remodeling, and function of adipocytes and modulates systemic metabolism. Fibrillin-1 is a large glycoprotein that forms the backbone of microfibrils in the extracellular matrix, present in almost all tissues. Mutations in fibrillin-1 lead to Marfan syndrome (MFS), characterized by severe lipodystrophy and aortic aneurysms, among other complications. However, subgroups of MFS patients were identified by a high body mass index, especially aging individuals due to altered adipose tissue metabolism. Therefore, this study addresses the hypothesis that fibrillin-1 regulates the development of adipocytes and plays a vital role in adipose tissue function and homeostasis.

Results

Using two different MFS mouse models (*Fbn1*$^{mgR/mgR}$ and *Fbn1*$^{C1041G/+}$), we determined that reduction of, but not a missense mutation in fibrillin-1 leads to altered adipose tissue metabolism. This was strongly dependent on the biological sex, because only male *Fbn1*$^{mgR/mgR}$ mice with reduced fibrillin-1 levels were prone to excess fat deposition associated with adipocyte hypertrophy and an insulin resistance phenotype. The study shows that expression of fibrillin-1 by mesenchymal stem cells maintains adipogenic homeostasis, whereas fibrillin-1 deficiency at this stage enhances adipogenic differentiation. Mechanistically, we demonstrate that fibrillin-1 negatively regulates adipogenic differentiation via the insulin signaling pathway. Fibrillin-1 acts via a dual mechanism that merges at the level of AKT signaling, through direct interaction with mesenchymal stem cells and through insulin sequestration.

The diet composition can alter adipose tissue homeostasis and may in turn contribute to increased cardiovascular complications in MFS. To understand the role of fibrillin-1 in diet-induced obesity, we investigated the consequence of high fat diet on the metabolic functions of *Fbn1*$^{mgR/mgR}$ and *Fbn1*$^{C1041G/+}$ mice. Overall, the data show that dietary fat leads to significantly altered metabolism in MFS mice which strongly depends on the biological sex. Specifically, male mice with MFS developed obesity, more pronounced insulin resistance phenotype, as well as a non-alcoholic fatty liver phenotype, which was reduced in orchiectomized mice. On the other hand, female MFS mice, were protected from these metabolic and liver phenotypes. We expect that the results from this study may in the longer-term help define personalized dietary guidelines for individuals affected with MFS.

Finally, to decipher the role of fibrillin-1 in mature adipocytes, we developed a conditional Cre-LoxP knockout mouse model using the Adipoq-Cre transgene to delete the *Fbn1* gene in mature adipocytes. Surprisingly, the weight of epididymal white adipose tissue in male mice was significantly reduced at 16 and 30 weeks of age with considerable reduction in adipocyte size. This resembles the lipodystrophic phenotype in MFS patients and points to a promoting role of fibrillin-1 in the maintenance of mature adipocytes.

Conclusions

Overall, this study established a novel role of fibrillin-1 in normal and abnormal adipose tissue development and homeostasis. Altered adipose tissue metabolism observed in fibrillin-1 deficient mice depends on the type of fibrillin-1 deficiency, dietary intervention, and biological sex. More specifically, fibrillin-1 has a dual role in adipocyte differentiation, **i)** inhibiting commitment in the early phase and **ii)** supporting maintenance and function in mature adipocytes.

RÉSUMÉ

Introduction

Le tissu adipeux est un organe métabolique dynamique qui subit un remodelage important au cours du développement. Son microenvironnement extracellulaire orchestre la différenciation, le remodelage et la fonction des adipocytes, La fibrilline-1 est une glycoprotéine à large masse moléculaire des microfibrilles de la matrice extracellulaire. Des mutations de la fibrilline-1 conduisent au syndrome de Marfan (MFS), caractérisé par une lipodystrophie sévère et des anévrismes aortiques. Des sous-groupes de patients MFS étaient caractérisés par un indice de masse corporelle élevé, en particulier chez les personnes âgées. Cette étude investigue l'hypothèse selon laquelle la fibrilline-1 régule le développement des adipocytes et joue un rôle vital dans l'homéostasie du tissu adipeux.

Résultats

À l'aide de deux modèles de souris MFS différents (*Fbn1*$^{mgR/mgR}$ and *Fbn1*$^{C1041G/+}$), nous avons établi qu'une réduction, mais pas une mutation faux-sens de la fibrilline-1, entraîne une altération du métabolisme du tissu adipeux. Seules les *souris* mâles *Fbn1*$^{mgR/mgR}$ avec des niveaux d'expression de fibrilline-1 réduits étaient sujettes à un excès de dépôt de graisse associé à une hypertrophie des adipocytes et à un phénotype de résistance à l'insuline. L'expression de la fibrilline-1 par les cellules souches mésenchymateuses maintient l'homéostasie adipocytaire, tandis que la carence en fibrilline-1 à ce stade améliore la différenciation adipocytaire. La fibrilline-1 régule négativement la différenciation adipeuse via la voie de signalisation de l'insuline. La fibrilline-1 agit via un double mécanisme qui fusionne au niveau de la signalisation AKT, via une interaction directe avec les cellules souches mésenchymateuses et via la séquestration de l'insuline.

La composition du régime alimentaire peut altérer l'homéostasie du tissu adipeux et peut contribuer à l'augmentation des complications cardiovasculaires dans la MFS. Pour comprendre le rôle de la

fibrilline-1 dans l'obésité induite par l'alimentation, nous avons étudié les conséquences d'un régime riche en graisses sur les fonctions métaboliques des souris *Fbn1*$^{mgR/mgR}$ et *Fbn1*$^{C1041G/+}$. Nos données montrent que les graisses alimentaires entraînent une modification significative du métabolisme chez les souris MFS, qui dépend fortement du sexe biologique. Les souris mâles MFS ont développé une obésité, un phénotype de résistance à l'insuline plus prononcé, ainsi qu'un phénotype de stéatose hépatique non alcoolique, qui a été réduit chez les souris orchiectomisées. Les souris femelle MFS ont été protégés contre ces phénotypes métaboliques et du foie. Nous nous attendons à ce que nos résultats puissent aider à long terme à définir des directives alimentaires personnalisées pour les personnes atteintes de MFS.

Pour décrypter le rôle de la fibrilline-1 dans les adipocytes matures, nous avons développé un modèle de souris knock-out Cre-LoxP conditionnel en utilisant le transgène Adipoq-Cre qui supprime le gène *Fbn1* dans les adipocytes matures. Le poids du tissu adipeux blanc de l'épididyme chez les souris mâles était significativement réduit à l'âge de 16 et 30 semaines avec une réduction considérable de la taille des adipocytes. Cela ressemble au phénotype lipodystrophique chez les patients MFS et indique un rôle promoteur de la fibrilline-1 dans le maintien des adipocytes matures.

Conclusion

Cette étude a identifié un nouveau rôle de la fibrilline-1 dans le développement et l'homéostasie normaux et anormaux du tissu adipeux. L'altération du métabolisme du tissu adipeux observé chez les souris déficientes en fibrilline-1 dépend du type de carence en fibrilline-1, de l'intervention alimentaire et du sexe biologique. La fibrilline-1 a un double rôle dans la différenciation adipocytaire, **i)** en inhibant l'engagement dans la phase précoce et **ii)** en soutenant le maintien et la fonction des adipocytes matures.

CHAPTER 1: REVIEW OF LITERATURE

1.1 Adipose tissue significance

Energy homeostasis involves a balanced action of energy intake, storage and expenditure maintained by inter-organ crosstalk in the body [*Hill et al., 2012*]. The central organ is the brain, that cross talks with the peripheral organs including stomach, intestine, liver, adipose tissue, pancreas, and skeletal muscles. Body weight changes when energy intake is not equal to the energy expenditure, in a given time [*Galgani & Ravussin, 2008; Hill et al., 2012*]. Due to body's limitation to store carbohydrates and protein as energy for long-term use, 90% of excess energy is stored as fat in adipose tissue. Thus, fat is the main nutrient that can cause energy imbalance, and adipose (fat) tissue plays a major role in maintaining energy homeostasis [*Hill et al., 2000; Hill et al., 2012*]. Although adipose tissue is recognised as a metabolically dynamic organ, its importance was heightened with the increasing prevalence of obesity worldwide in the past several decades, which alarmingly increases metabolic conditions such as insulin resistance, type 2 diabetes mellitus and cardiovascular disease.

1.2 Adipose tissue biology

Adipose tissue is a unique form of loose connective tissue critically important to regulate energy storage and expenditure [*Fruhbeck, 2008*]. Besides that, adipose tissue has various other functions such as insulation, control of thermogenesis, regulation of insulin sensitivity, and also as an endocrine organ [*Choe et al., 2016*]. Adipose tissue is classified based on morphology, location, and function into white, brown, and beige adipose tissues [*Choe et al., 2016*] (Fig. 1.1).

1.2.1 White adipose tissue

White adipose tissue (WAT) is present throughout the body and functions primarily as storage of energy-rich lipids [*Gesta et al., 2007*]. It was initially considered as a caloric reservoir of triglycerides until the discovery of the hormone leptin [*Zhang et al., 1994b*]. Now it is well known

that white adipose tissue secretes a wide variety of "adipokines" and represents as a major endocrine organ. Important adipokines include leptin, adiponectin, resistin, and asprosin [*Zhang et al., 1994b; Minokoshi et al., 1999; Gesta et al., 2007; Denroche et al., 2012; Choe et al., 2016; Romere et al., 2016; D'Souza A et al., 2017*]. White adipocytes are larger in size (20-300 μm) compared to brown adipocytes (see section 1.2.2) and have a unilocular appearance with single lipid droplet, occupying 85% area of the total cell (Fig. 1.2). In both humans and mice, based on the differences in location and function, white adipose tissue is majorly classified into two types, the subcutaneous (sWAT) and the visceral (vWAT) white adipose tissue. In humans, sWAT is found in thighs, hips, and abdomen, whereas vWAT or the abdominal fat surrounds the internal organs in the peritoneal cavity [*Bjorndal et al., 2011*]. In mice, sWAT is present below the skin and is further subdivided into interscapular and inguinal WAT (iWAT), present in the upper and the lower body regions, respectively (Fig. 1.1a). vWAT is located deep in the abdomen surrounding the peritoneal cavity and some internal organs. vWAT is further categorised into 3 major depots: gonadal WAT (gWAT) located around the reproductive organs in both male (epididymal) and female (periovarian), mesenteric WAT lining the intestines in the mesentery and retroperitoneal WAT located around the kidneys on both sides (Fig. 1.1b) [*Wronska & Kmiec, 2012; Berry et al., 2013*]. Further, higher amounts of vWAT are known to cause greater metabolic complications than increased sWAT. Possible explanations include that there are differential adipokines secreted from vWAT versus sWAT that are pro-inflammatory which quickly enters the major metabolic organs such as liver due to its close vicinity and thereby causes metabolic complications [*Kissebah & Krakower, 1994; Fried et al., 1998; Cancello et al., 2006*]. Females are more protected from obesity due to the higher accumulation of sWAT than vWAT. Increased vWAT is more commonly observed in males leading to central obesity and metabolic syndrome

[*Krotkiewski et al., 1983*]. Perivascular WAT surrounds the blood vessels in the thoracic and abdominal aortic regions (Fig. 1.1 b) contributing to the health and functioning of aorta in physiological and pathological conditions [*Hildebrand et al., 2018; Chang et al., 2020*].

1.2.2 Brown and beige adipose tissue

Brown adipose tissue (BAT) is mainly involved in thermogenesis [*Smith & Horwitz, 1969; Saely et al., 2012*]. Both in humans and mouse, the major BAT depot is located in the neck region (Fig 1.1a) just under the interscapular WAT. The unique brownness of this fat tissue originates from high mitochondrial density expressing UCP1 (uncoupling protein-1), a marker of brown adipose tissue [*Smith & Horwitz, 1969; Saely et al., 2012*]. Brown adipocytes are relatively small (10-25 μm) compared to white adipocytes and have a multilocular appearance with several small lipid droplets, occupying only 50% of the total cell area (Fig. 1.2). In humans, BAT is highly abundant in newborns, and it significantly reduces in size with increasing age. There is a third form of adipose tissue called the beige adipose tissue which also plays a role in thermogenesis, but it requires induction [*Wu et al., 2012*]. This is brown-like white fat tissue that expresses, like BAT, high amounts of uncoupling protein-1 on prolonged stimulation to cold temperatures or conditions that induce cyclic AMP. BAT and beige adipose tissue can be difficult to distinguish due to the similarity in morphology. Both are also found in other regions of the neck, in the mediastinum surrounding the aorta, and sometimes within the sWAT and skeletal muscles [*Saely et al., 2012; Choe et al., 2016*]. It has also been shown that white adipocytes in sWAT are prone to transdifferentiate into beige adipocytes compared to white adipocytes from vWAT and this is also explained as one of the reasons why sWAT is healthier than vWAT. Like white adipocytes, brown

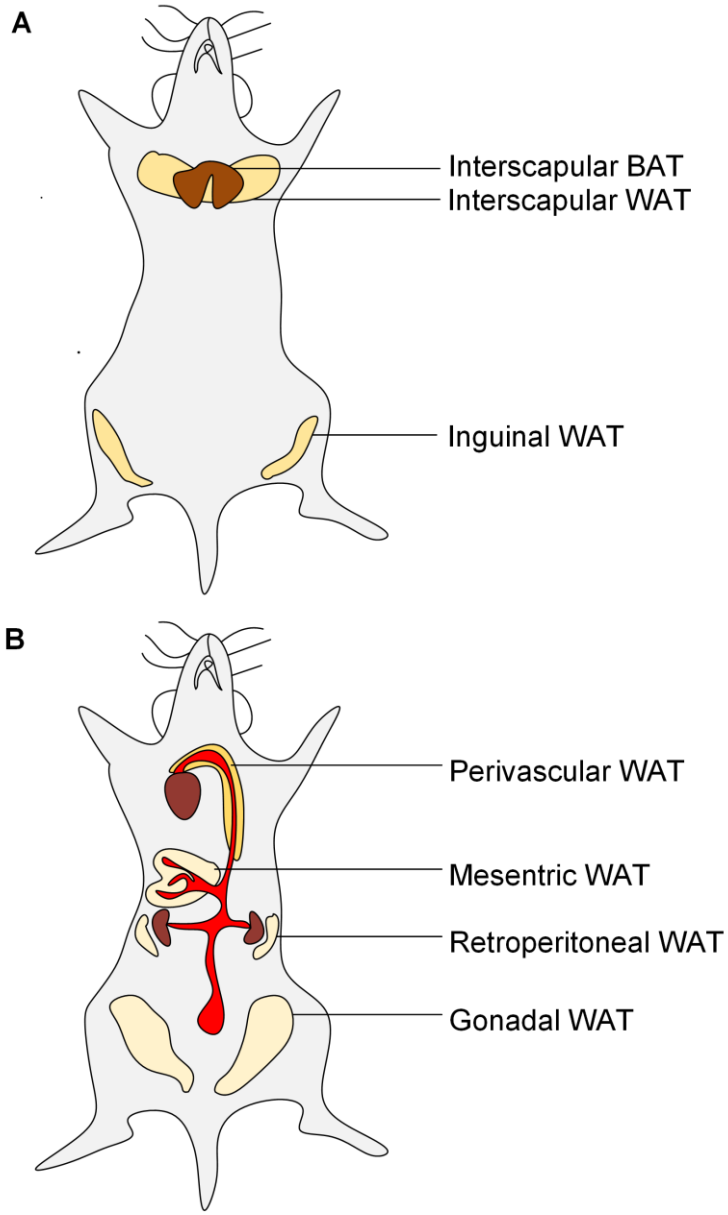

Figure 1.1. Simplified schematic diagram of subcutaneous (A) and visceral (B) adipose tissue depots in mice. (A) Shown are interscapular BAT and WAT located in the neck region, and inguinal WAT present beneath the skin in the lower body. **(B)** Highlighted are perivascular WAT surrounding the thoracic and abdominal aortas, mesenteric WAT lining the mesentery in the abdominal area, retroperitoneal WAT around the kidneys, and gonadal WAT in the abdominal cavity. BAT-Brown adipose tissue, WAT-White adipose tissue. Adapted with modifications based on [*Hildebrand et al., 2018*] with permission from Frontiers.

and beige adipocytes also secrete hormones and growth factors termed “batokines” that regulate glucose homeostasis [*Kajimura et al., 2015*].

1.2.3 Adipose tissue components

Adipose tissue is a dynamic connective tissue that consists of both cellular components and non-cellular extracellular matrix (ECM) components. The cellular components include adipocytes, pre-adipocytes, mesenchymal stem cells, fibroblasts, pericytes, endothelial cells, macrophages, and T cells [*Eto et al., 2009; Garcia-Rubio et al., 2018*]. The main ECM components in adipose tissues include fibronectin, fibrillin-1, elastin, collagen I, III, IV, V and VI, as well as laminin α2 and α4 [*Junghyo et al., 2009; Mariman & Wang, 2010; Martinez-Santibanez et al., 2015; Davis et al., 2016*]. Adipocytes primarily originate from mesenchymal stem cells (MSCs), which can also transform into osteoblasts, myocytes, and chondrocytes.

1.2.4 Adipose tissue organogenesis

Adipose tissue organogenesis involves two key events. 1) Adipose tissue development 2) Adipose tissue maintenance [*Berry et al., 2016*]. Both in case of humans and mice, the principals of adipose tissue organogenesis remain the same. However, relevant to the scope of this thesis, only the details of murine adipose tissue organogenesis will be introduced in detail. Development of both WAT and BAT starts at the embryonic stage and continues during the postnatal period [*Berry et al., 2016*]. Lineage tracing studies demonstrated that sWAT and BAT starts developing during embryogenesis between E13.5 and E18.5 [*Wang et al., 2013; Jiang et al., 2014*] and between E9.5 and E11.5 [*Lepper & Fan, 2010*] respectively (E-embryonic day). vWAT starts developing postnatally between P3 and P21 [*Berry et al., 2013; Wang et al., 2013*] (P-postnatal day). The

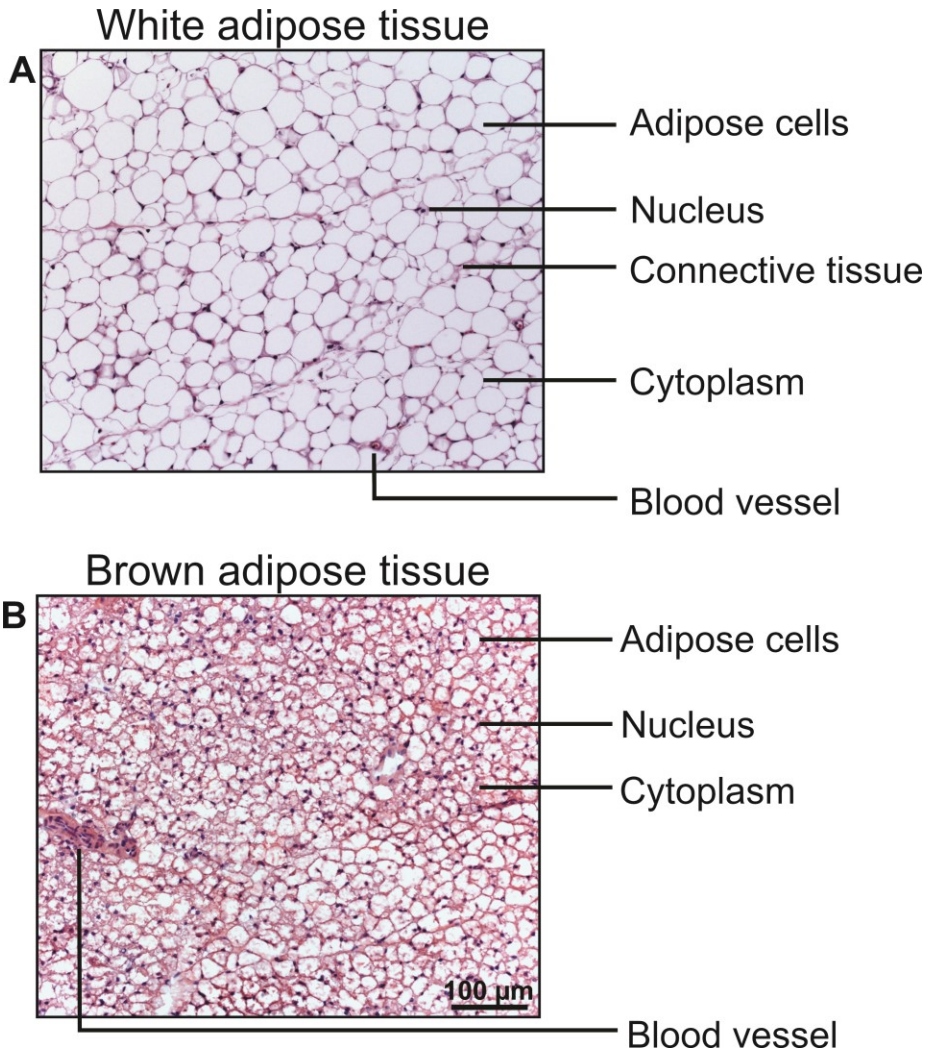

Figure 1.2. Light microscopic images of white adipose tissue (A) and brown adipose tissue **(B).** Hematoxylin and eosin staining of mouse white adipose tissue (top) and brown adipose tissue (bottom) analyzed at 16 weeks of age. White adipose tissue has unilocular big adipocytes filled with lipid droplets compared to brown adipose tissue which has multilocular smaller adipocytes. Nuclei are displaced peripherally to the plasma membrane by a lipid vacuole. Blood vessels and connective tissues are present in the stromal layer which also contains endothelial cells, macrophages, smooth muscle cells, mesenchymal stem cell, and preadipocytes. The scale bar represents 100 mm for both images.

development of sWAT or BAT in the embryonic period may denote its function and requirement at that stage [*Berry et al., 2016*]. Collectively, adipose tissue organogenesis is site specific and develops in a systematic and timed manner.

Adipocytes in different adipose tissue originates from distinct cellular progenitors. Some of the critical studies identifying the key precursors are highlighted here. Various cell lineage tracing studies performed in mice show that both sWAT and vWAT originate from adipogenic progenitor cells expressing platelet-derived growth factor receptor alpha and beta (PDGFRα and β), zinc finger protein 423 (ZFP423), and peroxisome proliferator-activated receptor gamma (PPARγ) [*Chawla & Lazar, 1994; Lee et al., 2012; Berry & Rodeheffer, 2013; Jiang et al., 2014*]. PRX1 (Paired related homeobox-1) positive cells only give rise to sWAT progenitors [*Sanchez-Gurmaches et al., 2015*], whereas WT1 (Wilms' tumour 1) expressing cells gives rise to vWAT progenitors [*Chau et al., 2014*]. Similarly, MYF5 (myogenic factor 5) and aP2 (adipocyte protein 2) expressing progenitors in the stromal vascular fraction were shown to be precursors of both WAT and BAT [*Seale et al., 2008; Seale et al., 2009; Shan et al., 2013; Sanchez-Gurmaches & Guertin, 2014*]. Although there is some evidence that distinct precursors are involved in the development of sWAT and vWAT, there are also obvious overlaps, however, the full spectrum is not completely understood yet [*Chau et al., 2014*].

Postnatal development of WAT involves two mechanisms, adipocyte hyperplasia marked by an increase in the number of adipocytes and hypertrophy characterized by an increase in adipocyte size [*Wang et al., 2013*]. Depending on the adipose tissue depot, 10–20% of new adipocytes are formed per month in mice fed with normal chow diet [*Jiang et al., 2014*]. Human studies showed that 10% of adipocytes are replenished each year with new adipocytes, and the average adipocyte age is about 10 years in lean individuals [*Spalding et al., 2008*]. Additionally, PPARγ deletion in

mice demonstrated the inability to form new adipocytes under homeostatic conditions [*Chawla & Lazar, 1994; Jiang et al., 2014*]. This resulted in reduced adipose tissue development and abnormal glucose homeostasis [*Chawla & Lazar, 1994; Jiang et al., 2014*]. Together, the data clearly define that adipocyte precursor cells are necessary for adipose tissue maintenance and overall body metabolism.

1.3 Adipose tissue in disease

Obesity and lipodystrophy, when associated with insulin resistance, hyperglycemia, hyperinsulinemia, dyslipidemia, high blood pressure and liver hepatic steatosis can lead to increased risk of developing diabetes mellitus and cardiovascular diseases, collectively termed metabolic syndrome [*Herranz et al., 2008; Unger & Scherer, 2010; Virtue & Vidal-Puig, 2010; Kassi et al., 2011; Bindlish et al., 2015; Czech, 2017*]. Diabetes mellitus is a chronic health condition caused due to changes in lifestyle, genetic or environmental factors leading to either reduced secretion or function of insulin resulting in sustained increase in blood glucose levels (hyperglycemia) [*Yaribeygi et al., 2019*]. Diabetes mellitus is categorized into type 1 and type 2 diabetes mellitus. Type 1 diabetes mellitus is an autoimmune disorder, which typically occurs in individuals <35 years of age, whereas type 2 occurs at an older age and is mostly caused by environment or lifestyle factors. Many obese people with type 2 diabetes mellitus develop insulin resistance due to the defects in insulin sensitive cells, such as muscles and adipocytes, disabling their ability to utilize glucose [*Yaribeygi et al., 2019*]. This leads to chronic elevation of blood glucose levels damaging certain tissues, such as nerves and blood vessels. This in turn elevates the complications of cardiovascular disease [*Wilcox, 2005*]. Around 2.3 million people in Canada have been diagnosed with type 2 diabetes mellitus. The prevalence of diabetes among was 13.7% among

obese Canadians, 6.8% among overweight and 3.6% among normal weight category (www150.statcan.gc.ca).

1.3.1 Obesity and lipodystrophy

Dysfunctional adipose tissue can lead to conditions such as obesity and lipodystrophy [*Garg, 2006*]. Obesity is characterized by excessive or abnormal accumulation of overall body fat. World Health Organization proposes the body mass index (BMI) as a determinant of obesity, which is calculated by dividing body weight in kilograms by the height in meters squared (kg/m^2). Unhealthy individuals with BMI greater than 30 are considered obese. On the other hand, individuals with reduced or abnormal distribution of body fat are diagnosed with lipodystrophy. Like obesity, lipodystrophy also results in abnormal energy storage and metabolism due to the presence of dysfunctional adipose tissue. In both situations, obesity and lipodystrophy, due to limitations of the adipocyte storage capacity, excess dietary triglycerides are accumulated in other metabolic organs such as the liver or skeletal muscles causing lipid toxicity [*Garg, 2006; Samuel et al., 2010*].

1.3.2 Insulin resistance

According to World Health Organization, insulin resistance was identified as a major underlying risk factor and evidence for the diagnosis of metabolic syndrome [*Takamiya et al., 2004*]. Insulin is a small peptide hormone (~6 kDa) produced by β cells of the pancreatic islets. Insulin physiologically functions in maintaining the blood glucose levels by stimulating cellular uptake of glucose by target tissues like skeletal muscles and WAT [*Wilcox, 2005*]. In humans, skeletal muscle accounts for up to 60%, liver 30%, and adipose tissue 10% of whole-body insulin stimulated glucose uptake and clearance. Skeletal muscle cells and liver acts as a storage repository for glucose in the form of glycogen [*Wang et al., 1999; Smith, 2002*]. Glucose transporter proteins

(GLUT) upon stimulation translocate from the intracellular vesicular compartment to the plasma membrane and facilitates glucose entry [*Wang et al., 1999; Smith, 2002*]. From the family of glucose transporters, GLUT-4 is entirely dependent upon insulin and represents the primary glucose transporter for adipose tissue and skeletal muscle cells [*Olefsky, 1999; Wilcox, 2005*]. Additionally, insulin suppresses hepatic gluconeogenesis and maintains glucose concentrations during fasting [*Wilcox, 2005*]. Overall, the core physiological function of insulin is to keep blood glucose concentrations under control [*Wilcox, 2005*]. However, the importance of insulin is highlighted more due to its critical role in risk factors such as insulin resistance, hyperglycemia, hyperinsulinemia, and obesity together contributing to metabolic syndrome [*Yaribeygi et al., 2019*]. Various factors including obesity, excess food consumption and lack of exercise can promote hyperinsulinemia and insulin resistance through stimulation of insulin secretion, triglyceride synthesis, and adipose tissue accumulation together with down-regulation of insulin receptors signalling [*Wilcox, 2005; Yaribeygi et al., 2019*]. Insulin resistance during obesity or lipodystrophy can cause dyslipidemia [*Krauss & Siri, 2004; Wilcox, 2005*]. Importantly, dyslipidemia contributes to accumulation of fat (ectopic fat deposits) in the liver leading to the development of non-alcoholic fatty liver disease or hepatic steatosis [*Geisler & Renquist, 2017*]. Dyslipidemia leads to higher blood triglyceride levels, increased low density lipoproteins and reduced high-density lipoprotein [*Krauss & Siri, 2004*]. Increased lipid content in the liver not only causes non-alcoholic fatty liver disease but also contributes to liver specific insulin resistance and inflammation eventually leading to liver cirrhosis [*Dam-Larsen et al., 2004*].

1.3.3 Abnormal adipose tissue expansion

During obesity or lipodystrophy, adipose tissue has the capacity to expand or reduce in size from the original volume. Intrinsic modifications associated with the changes in adipose tissue size

includes adipocyte hypertrophy (increase in cell size) and adipocyte hyperplasia (increase in cell number), inflammation, fibrosis, hypoxia, reduced angiogenesis and altered secretion of adipokines. WAT expansion and dysfunction in obesity is typically associated with insulin resistance, glucose intolerance and hyperinsulinemia leading to increased risk of developing type 2 diabetes mellitus and cardiovascular disease [*Weyer et al., 2000; Connell et al., 2010; Betteridge, 2011*].

1.3.3.1 Hypertrophy/ Hyperplasia

Until the last decade, it was assumed that adipocyte number was pre-set at a very early age and only adipocyte size changes with the nutritional state, environmental, or genetic factors. However, recent studies showed that around 10% of adipocytes renew annually in humans. This introduced a new concept in the field that, at early stages or in childhood obesity, adipose tissue increases in size due to a combination of both adipocyte hyperplasia and hypertrophy [*Salans et al., 1973; Wajchenberg, 2000*]. However, in later stages or in adulthood obesity, adipocytes mostly undergo hypertrophy [*Hirsch & Han, 1969; Hirsch & Knittle, 1970*]. It has also been shown that during obesity both the mass of sWAT and vWAT increases in humans. However, in rodents, the generation of new adipocytes in response to high fat diet (HFD) are age and depot specific. In young or adolescent mice, new adipocytes form primarily in vWAT followed by sWAT, whereas adult mice showed lower adipogenic potential [*Wang et al., 2013; Kim et al., 2014*]. Additionally, when mice fed with HFD reached a body weight of around 40 g, vWAT stopped expanding, while sWAT continued to grow [*Kloting et al., 2010*]. During obesity, increases in sWAT mass are directly linked to adipocyte hyperplasia rather than adipocyte hypertrophy due to the presence of increased adipocyte precursor cells [*Hirsch & Han, 1969; Hirsch & Knittle, 1970; Giordano et al., 2013; Kim et al., 2015*]. Hypertrophic adipocytes are characteristic of metabolic disorder and

are also linked with insulin resistance and inflammation in healthy adults who are genetically predisposed to type 2 diabetes mellitus [*Okuno et al., 1998; Rong et al., 2007; Henninger et al., 2014*]. On the other hand, mice lacking collagen VI have enlarged adipocytes due to uninhibited expansion of adipocytes, but these mice have improved metabolic health [*Khan et al., 2009*]. Thus, these murine and human studies show that adipocyte size is not an absolute indicator of metabolic homeostasis, and changes in metabolic factors can occur in the presence or absence of altered adipocyte size. Concludingly, a balanced combination of adipocyte hypertrophy and adipocyte hyperplasia is important for adipose tissue and metabolic homeostasis.

1.3.3.2 Inflammation

Chronic low-grade inflammation is a typical characteristic of obese and lipodystrophic adipose tissues [*Xu et al., 2003; Hanna-Mitchell et al., 2014; Saltiel & Olefsky, 2017; Zatterale et al., 2019*]. Typically, resident macrophages are localised in the stromal vascular fraction of the adipose tissue but when adipocytes undergo apoptosis, additional macrophages infiltrate into the adipose tissue and arrange into "crown like structures" (CLS) around the dead adipocyte to irradicate them [*Weisberg et al., 2003; Cinti et al., 2005; Pajvani et al., 2005*]. It has been shown that macrophage infiltration was twice as high in vWAT compared to sWAT [*Kralova Lesna et al., 2016*]. Macrophages have been broadly classified as M1 or M2 macrophages [*Castoldi et al., 2015*]. M1 (proinflammatory) macrophages are highly present in obese adipose tissue where they produce pro-inflammatory cytokines such as tumour necrosis factor alpha (TNFα), interleukin 6 (IL6), monocyte chemoattractant protein 1 (MCP1), and interleukin 1β. Lean adipose tissue has typically a higher number of M2 (anti-inflammatory) macrophages that produce anti-inflammatory cytokines such as interleukin 10, and interleukin 1 receptor antagonist [*Hotamisligil et al., 1995; Castoldi et al., 2015*]. Chronic adipose tissue inflammation also leads to impaired insulin

signalling and continued deterioration of adipose tissue function [*Cinti et al., 2005; Lumeng et al., 2007; Crewe et al., 2017*]. On the other hand, hyperinsulinemia and excess circulating lipids promote pro-inflammatory cytokines, leading to decline in metabolic health [*Weisberg et al., 2003; Cinti et al., 2005; Crewe et al., 2017*]. However, it is important to note that the field of adipose tissue inflammation is rapidly evolving and some pro-inflammatory cytokines, including TNFα and oncostatin M, are required for maintaining adipose tissue homeostasis and insulin sensitivity in mice [*Wernstedt Asterholm et al., 2014; Schultze, 2015; Stephens et al., 2018*].

1.3.3.3 Fibrosis, hypoxia, and reduced angiogenesis

Generally, in obesity or lipodystrophy, the alterations in the adipose tissue initiate fibrosis which is further enhanced by inflammatory mechanisms [*Buechler et al., 2015*]. In fibrotic human and murine fat tissues, several collagens are deposited in large quantities [*Huber et al., 2007; Khan et al., 2009; Pasarica et al., 2009*]. In particular, collagen VI is upregulated in adipose tissue of obese individuals as well as in leptin receptor-deficient obese mice [*Khan et al., 2009; Pasarica et al., 2009*]. Genetic ablation of collagen VI in WAT leads to adipocyte hypertrophy and obesity but protects mice from metabolic complications [*Halberg et al., 2009; Khan et al., 2009*]. This suggests that fibrosis limits adipocyte hypertrophy and impairs adipocyte functionality [*Abdennour et al., 2014; Pellegrinelli et al., 2014*]. Additionally, fibrosis in vWAT of obese mice also limits adipose tissue expansion and metabolic complications [*Dalmas et al., 2015*]. Hypoxic conditions that occur during the adipose tissue expansion in obese mice induce hypoxia inducible factor-1α (HIF-1α), a critical molecule regulated by oxygen levels in the cellular microenvironment which initiates adipose tissue fibrosis [*Halberg et al., 2009; Trayhurn, 2013*]. Hypoxia and HIF-1α are implicated in adipose tissue dysfunction via several proposed mechanisms such as reducing adiponectin levels as well as stimulating inflammation and fibrosis

[*Halberg et al., 2009*]. Among the underlying processes, adipose tissue hypoxia is well-recognized to induce ECM accumulation leading to fibrosis [*Halberg et al., 2009*]. Elastin is present in the ECM of WAT where it provides structural elasticity and interacts with collagens [*Khan et al., 2009; Alkhouli et al., 2013*]. During the development of adipose tissue fibrosis in obese mice and humans, the level of elastin is downregulated in fibrotic areas compared to lean white adipose control tissue [*Khan et al., 2009; Spencer et al., 2011; Martinez-Santibanez et al., 2015*]. This results in structural rigidity of the white adipose tissue [*Halberg et al., 2009*]. Therefore, it is possible that the fibrotic ECM in fat tissue establishes a mechanical barrier for the transport of metabolic hormones, including glucose and insulin, which may lead to defective insulin signaling and insulin resistance [*Williams et al., 2015*]. In addition, altered mechanical properties and hypoxia of the adipose tissue modifies angiogenesis that leads to adipose tissue dysfunction [*Corvera & Gealekman, 2014*].

1.3.3.4 TGF-β signaling

There is also evidence that TGF-β is upregulated in obesity. 184 non-diabetic obese human subjects from a diverse background showed increased circulating TGF-β levels [*Yadav et al., 2011*]. In addition, the levels of TGF-β positively correlated with the levels of adipose tissue mass and negatively correlated with the energy expenditure in overweight subjects [*Yadav et al., 2011*]. Another study identified that the levels of TGF-β from WAT positively correlated with the body mass index from 13 female individuals after a bariatric surgery [*Fain et al., 2005*]. Two mouse models of obesity, Leptin$^{ob/ob}$ and HFD-induced obesity, showed increased TGF-β in circulating plasma and in WAT, as well as increased TGF-β signaling in WAT [*Samad et al., 1997; Yadav et al., 2011*]. In addition, intraperitoneal injection of TGF-β increased the gene expression levels of

adipogenic markers in WAT [*Yadav et al., 2011*]. Therefore, abnormal adipose tissue metabolism strongly correlates with elevated TGF-β levels in both humans and mice.

1.3.4 Metabolically healthy obesity

Insulin resistance and obesity are typically associated with reduced plasma adiponectin levels. However, a subgroup of obese individuals presented with higher plasma adiponectin levels and normal insulin sensitivity, and thus they are considered metabolically healthy obese individuals [*Aguilar-Salinas et al., 2008*]. Metabolically healthy individuals are characterized by higher accumulation of sWAT as compared to vWAT, which is associated with an improved metabolic profile in both obese and non-obese individuals [*Ahl et al., 2015*]. Also, adiponectin over-expressing transgenic Leptin$^{ob/ob}$ mice are obese, but they show improvements in insulin sensitivity, which prevents ectopic accumulation of fat in peripheral tissues leading to improved metabolism [*Kim et al., 2007*]. Metabolically healthy but obese individuals also present with an improved inflammatory profile [*Bluher, 2020*].

1.4 Adipogenesis

Adipogenesis is a multistep differentiation process by which mature adipocytes develop and accumulate in the adipose tissue (Fig. 1.3). Adipogenesis involves two critical events, an early commitment, and a subsequent differentiation phase. Pluripotent or multipotent mesenchymal stem cells are committed to become pre-adipocytes and are then terminally differentiated into mature adipocytes characterized by round shapes and the accumulation of lipids (Fig. 1.3) [*Gregoire et al., 1998; Rosen & MacDougald, 2006*].

1.4.1 Transcriptional regulation of adipogenesis

Adipogenic differentiation is characterized by sequential changes in two key transcription factors, CCAAT enhancer binding protein (C/EBPs) and PPARγ [*Rosen et al., 2000*]**.** As adipogenic differentiation occurs, C/EBPβ and δ directly induces the expression of PPARγ, the master regulator of adipogenesis [*Wu et al., 1996*]. C/EBPβ or C/EBPδ knockout mouse embryonic fibroblast (MEF) displayed decreased adipogenesis and double knockout MEFs of C/EBPβ and C/EBPδ did not differentiate into adipocytes, showing the importance of these two transcription factors in adipogenesis [*Wu et al., 1996*]. Further, the induced PPARγ facilitates adipogenesis with the help of CEBPα [*Tontonoz et al., 1994; Kubota et al., 1999; Rosen et al., 1999; Rosen et al., 2000*]. Also, PPARγ knockout MEFs which express very little C/EBPα despite normal levels of C/EBPβ and δ did not differentiate into adipocytes [*Kubota et al., 1999; Rosen et al., 1999*]. Interestingly, C/EBPα−/− MEFs express reduced levels of PPARγ and do not form adipocytes [*Wu et al., 1999*]. However, when C/EBPα was added back to these cells, PPARγ expression and the ability to differentiate into adipocytes were restored [*Wu et al., 1999*]. This shows a positive feedback loop where PPARγ and C/EBPα mutually induce each other, and once initiated the adipogenesis is maintained [*Rosen et al., 2000*]. Alternative splicing of PPARγ generates two isoforms: PPARγ1 and PPARγ2 [*Tontonoz et al., 1994; Fajas et al., 1997*]. PPARγ1 is expressed in several tissues, whereas PPARγ2 is primarily present in adipocytes [*Mueller et al., 2002*]. However, knockout of either of the isoforms does not affect adipogenesis due to the compensatory action by the other isoform [*Mueller et al., 2002*]. Finally, PPARγ and CEBPα induces transcription of mature adipogenic genes, including adiponectin and perilipin, as well as the formation of lipid droplets [*Rosen et al., 2000*].

1.4.2 Insulin signaling during adipocyte differentiation

Insulin binds to the insulin receptor (IR) on the cell surface to regulate downstream signaling events important for glucose uptake by adipocytes and for adipogenesis. IR is present on the surface of all cells, importantly on mesenchymal stem cells and adipocytes. The IR consist of a heterotetramer containing two α- and two β-subunits linked by disulphide bonds [*Kido et al., 2001*]. Insulin binds to the α-subunit of the IR exposed to the extracellular space, which induces a conformational change enabling ATP to bind to the membrane spanning β-subunits, which triggers autophosphorylation [*Wolever, 1990; Wilcox, 2005*]. This enables activation of insulin receptor substrate proteins (IRS-1 and IRS-2) and src homology and collagen protein (Shc). IRS-1/2 further regulate the metabolic signalling of insulin, whereas Shc regulates mitogenic signalling of insulin which in turn activates cell proliferation [*Wilcox, 2005*]. Metabolic signaling is highly predominant in the adipocytes since it regulates adipogenesis and GLUT4 translocation required for glucose uptake [*Bryant et al., 2002; Wilcox, 2005*]. IRS-1/2 further activates phosphatidylinositol-3 kinase (PI3K) and stimulates the protein kinase B (PKB/AKT) signaling pathway. Inhibition of PI3K/AKT has been shown to inhibit adipogenesis and AKT deficient mice demonstrated a lipoatropic phenotype [*Garofalo et al., 2003*]. Further, AKT controls the translocation of GLUT4 to the plasma membrane in adipose tissue [*Wang et al., 1999*]. In another independent pathway, insulin regulates adipogenesis by phosphorylating the cAMP response element binding protein (CREB) [*Klemm et al., 2001*].

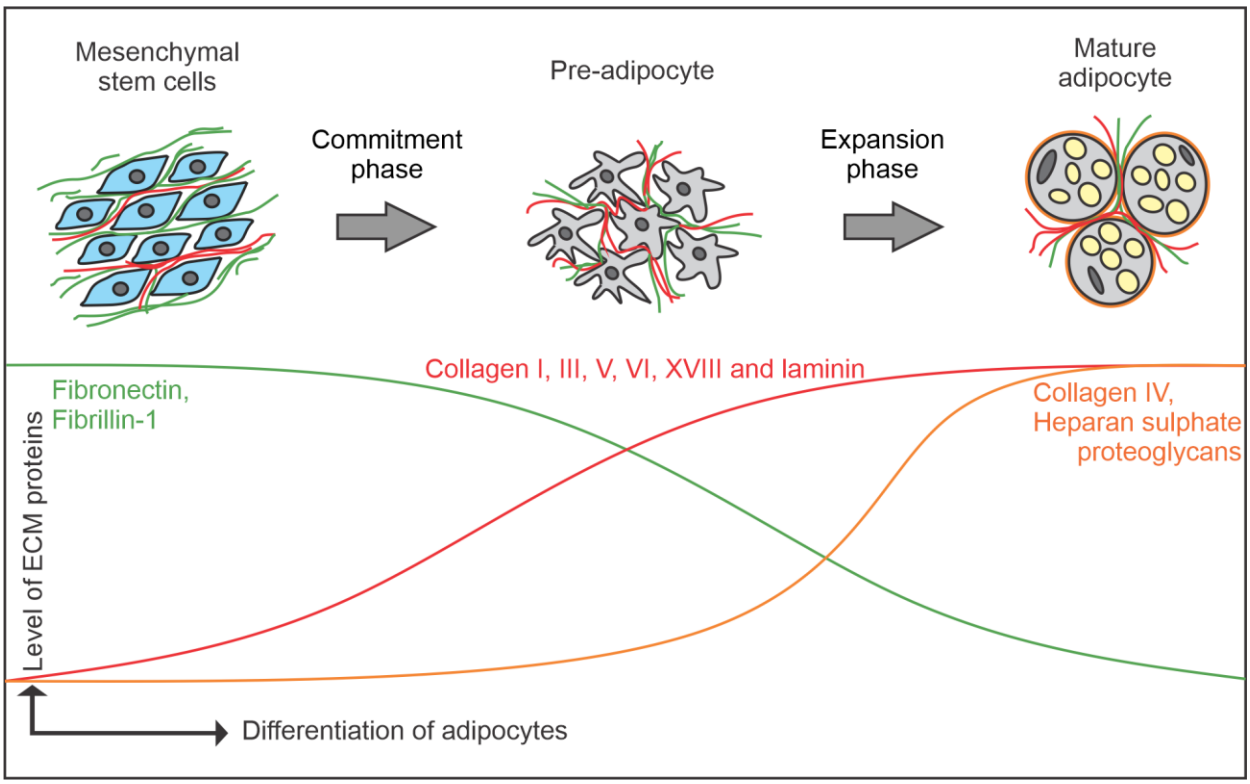

Figure 1.3. Schematics of adipogenesis in relation to ECM protein expression. Key steps of adipogenesis are indicated. Relative ECM protein expression is shown as curves. Fibronectin and fibrillin-1 (green curve) are present in the early commitment phase and decreases during adipocyte differentiation, whereas collagen I, III, V, VI, XVIII and laminin (red curve) appear during mid-differentiation and increase further until maturation. Basement membrane components, including collagen IV and heparan sulfate proteoglycans (orange curve) are mainly present when adipocytes are differentiated. Adapted from [*Muthu & Reinhardt, 2020*] with permission from Elsevier.

1.4.3 ECM remodeling during adipogenesis

The ECM microenvironment of adipose tissue orchestrates differentiation, remodeling, and function of adipocytes and maintains systemic energy metabolism (Fig. 1.3). Although not well studied, some evidence shows the importance of ECM-adipocyte interactions in adipogenesis. Several ECM proteins in the adipose tissue including fibronectin, fibrillin-1, elastin, collagens, laminins, and proteoglycans are synthesized and degraded at various stages of differentiation (Fig. 1.3). ECM remodeling is typically characterized by the conversion of fibrillar networks present at the pre-adipocyte stage to a basement membrane sheet-like network at the mature adipocyte stage. Fibronectin appears early at the pre-adipocyte stage of adipogenesis, but is degraded during the differentiation process [*Kubo et al., 2000*]. Preadipocyte factor 1, an inhibitor of adipocyte differentiation directly interacts with fibronectin and downregulates the integrin signaling cascade to inhibit adipocyte differentiation [*Wang et al., 2010*]. Several interstitial ECM collagens (collagen I, III, V, VI, XVIII), as well as the basement membrane protein laminin appear during mid differentiation and are present until later stages [*Kubo et al., 2000*]. Collagen VI which is enriched in the ECM of mature adipocytes, negatively regulates adipocyte cell size [*Khan et al., 2009*], whereas collagen XVIII promotes adipose tissue accumulation by adipocyte hyperplasia [*Aikio et al., 2014*]. Other basement membrane components (collagen IV and heparan sulfate proteoglycan) are detectable around mature adipocytes [*Pierleoni et al., 1998; Kubo et al., 2000; Mariman & Wang, 2010; Vaicik et al., 2014*]. Thus, the composition and regulation of the pericellular ECM is pivotal for the differentiation and function of adipocytes [*Divoux & Clement, 2011*]. However, the role of fibrillin-1 in this context has not been well studied.

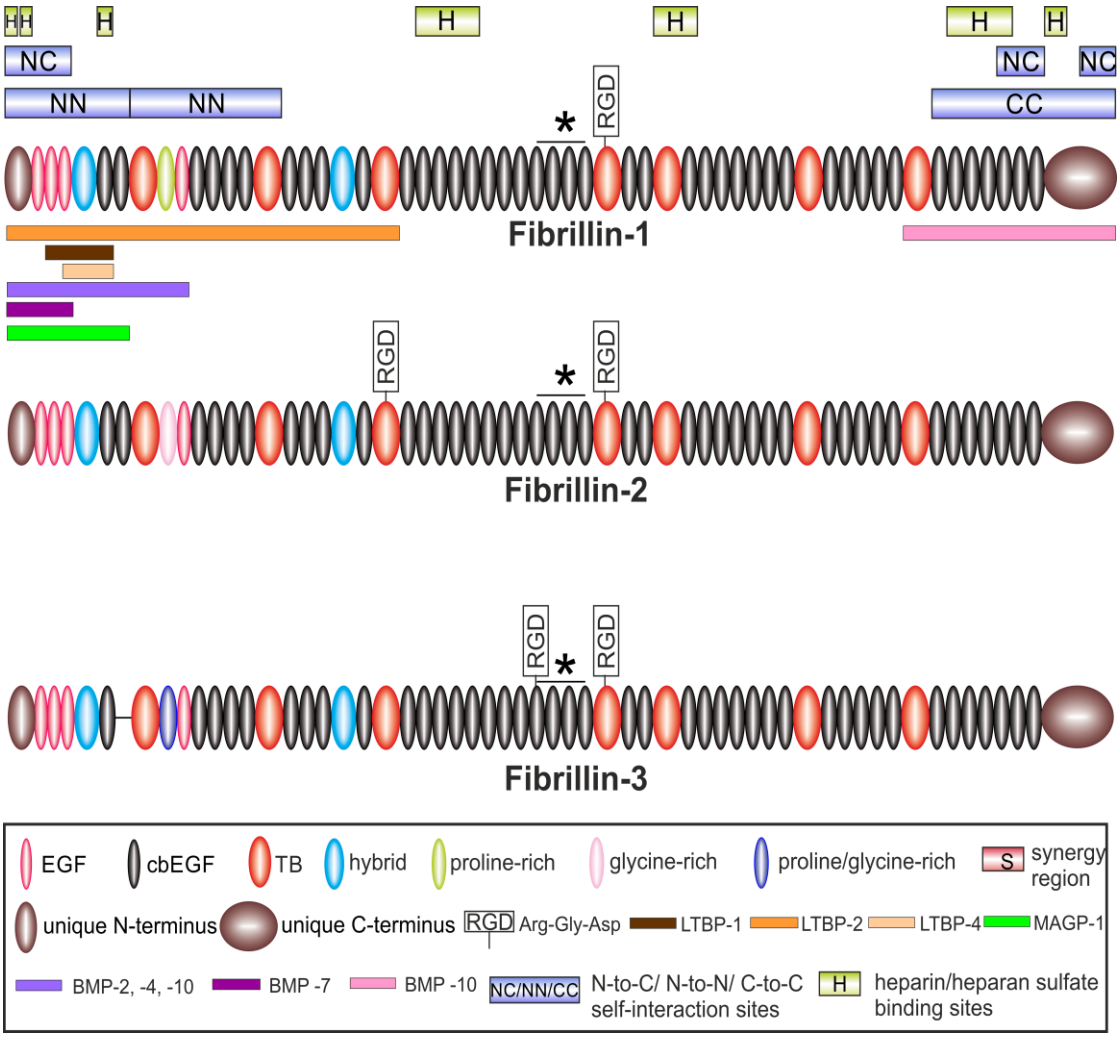

Figure 1.4. Isoforms and domain organization of fibrillins. All three fibrillin isoforms consist of epidermal growth factor (EGF) and calcium-binding EGF domains, separated by TB and hybrid domains. Indicated are the RGD cell binding sites (RGD), heparin/heparan sulphate binding sites (H), synergy sites in cbEGF 19-21 (S), non-homologous proline/glycine rich domains located near the N-terminus, unique N- and C-terminal domains, and N-to-N (NN), N-to-C (NC), C-to-C (CC) self-interaction sites, BMP interaction sites and LTBP binding sites are indicated.

1.5 Fibrillins

1.5.1 Fibrillin structure and isoforms

In humans and most other mammals, fibrillins are encoded by three active genes *FBN1*, *FBN2* and *FBN3*, whereas in rodents the *FBN3* gene is inactivated [*Zhang et al., 1995; Corson et al., 2004; Piha-Gossack et al., 2012*]. Fibrillin-1 is expressed throughout life, whereas fibrillin-2 and -3 is mainly present during the fetal and embryonic development [*Zhang et al., 1995; Corson et al., 2004; Sabatier et al., 2011*] (Fig. 1.4). Fibrillins are ~350 kDa glycoproteins with high cysteine content (12-13%) and are typically synthesized by cells of mesenchymal origin [*Summers et al., 2010; Hubmacher & Reinhardt, 2011; Hubmacher et al., 2011; Davis et al., 2014*]. Fibrillins are multi-domain proteins containing 47 epidermal growth factor-like EGF domains [*Pereira et al., 1993*], the majority of them (42-43) bind calcium [*Handford et al., 1991; Corson et al., 1993; Downing et al., 1996*] (Fig. 1.4). Both, EGFs and cbEGF domains are stabilized by intradomain disulfide bonds between six conserved cysteine residues in a C1–C3, C2–C4 and C5–C6 fashion [*Downing et al., 1996; Hubmacher & Reinhardt, 2011*]. Other prominent domains in fibrillins include seven transforming growth factor beta (TGF-β) binding protein domains (TB domain) stabilized by intradomain disulfide bonds between 8 cysteine residues in a C1–C3, C2–C6, C4–C7, and C5–C8 pattern, and two hybrid domains containing 4 intradomain disulfide bond formation in a C1–C3, C2–C5, C4–C6, and C7–C8 manner [*Yuan et al., 1997; Jensen et al., 2009*]. Fibrillin-1 further contains one unique N- and C-terminal domain. The domain organization share 100% homology between the 3 isoforms and ~95-97% between species, whereas 60-70% homology is found between the 3 fibrillin isoforms at the amino acid level [*Piha-Gossack et al., 2012*]. However, there are also some key differences between the three isoforms. There is one unique domain near the N-terminus which is rich in proline residues in fibrillin-1, rich in glycine

residues in fibrillin-2 and a mixture of glycine and proline residues in fibrillin-3 [*Corson et al., 1993; Zhang et al., 1994a; Corson et al., 2004*]. Few other differences include the number and position of the conserved RGD cell binding site(s) and the predicted N-glycosylation sites. All three isoforms contain a synergy site, located in between cbEGF 19-21, which enhances the RGD binding to integrins [*Bax et al., 2007*]. The focus of the following text and throughout the thesis is on fibrillin-1.

1.5.2 Fibrillin-1 containing microfibrils and growth factor interactions

Fibrillin-1 is synthesized as a precursor profibrillin which is processed by furin-type endoproteases in the N- and C-terminal prodomains giving rise to the mature ~320 kDa fibrillin-1 [*Milewicz et al., 1995; Reinhardt et al., 1996b; Lönnqvist et al., 1998*] (Fig. 1.5). Processed fibrillin-1 assembles with other proteins, including microfibril-associated glycoproteins (MAGPs) into bead-on-a-string microfibrils with a diameter of 10-12 nm and with periodicities of 50-60 nm via N-to-C-terminal interactions [*Low, 1962; Wright & Mayne, 1988; Keene et al., 1991; Wallace et al., 1991; Reinhardt et al., 1996a; Hubmacher et al., 2008*]. One of the main functions of fibrillin-containing microfibrils is their essential contribution in providing a scaffold for elastic fiber formation in elastic tissues. In non-elastic tissues fibrillin-containing microfibrils can serve structural roles by intersecting firmly with basement membranes, such as in the eye or kidney [*Kriz et al., 1990; Tiedemann et al., 2005*].

Another crucial function of fibrillin-1 containing microfibrils is to regulate TGF-β bioavailability in the ECM through direct interaction with latent TGF-β binding proteins (LTBPs) [*Isogai et al., 2003; Neptune et al., 2003; Chaudhry et al., 2007; French et al., 2012*]. TGF-β is secreted from the cells as a part of the large latent TGF-β complex (LLC) [*Hyytiäinen et al., 2004; Rifkin, 2005*]. This LLC is comprised of the small latent complex (SLC) including TGF-β and the latency

associated protein (LAP) which is covalently bound to the members of LTBPs [*Saharinen et al., 1996; Hyytiäinen et al., 2004; Rifkin, 2005*]. LTBP-1 and -3 bind to all three TGF-β isoforms, LTBP-4 only binds to TGF-β1 and LTBP-2 does not interact with any of the TGF-β isoforms [*Saharinen & Keski-Oja, 2000*]. It has also been revealed that LTBP -1, -3 and -4 interacts with the SLC by direct disulfide bond formation between Cys33 of the LAP monomer and a cysteine residue in the TB3 domain of LTBPs [*Saharinen et al., 1996; Lack et al., 2003*]. On the other hand, TGF-β and LAP in the SLC each homodimerize through disulfide bond formation and they form non-covalent interactions with each other after proteolytic cleavage [*Shi et al., 2011*]. In this complex, LAP controls the latency of TGF-β [*Saharinen et al., 1996; Saharinen & Keski-Oja, 2000; Koli et al., 2001*]. TGF-β in its latent form does not bind to its receptor, it needs to be released from the ECM either through conformational changes in the SLC or proteolytic degradation. Among others, integrins play a significant role in the conformational change of SLC by exerting forces on LAP which in turn activates TGF-β [*Wipff et al., 2007*]. The N-terminus of fibrillin-1 has been shown to interact with the C-terminus of LTBP-1, -2 and -4 in the LLC (Fig. 1.4) [*Isogai et al., 2003; Hirani et al., 2007; Ono et al., 2009*], and the N terminus of LTBP-1 and 4 is known to interact with fibronectin in the ECM [*Fontana et al., 2005; Kantola et al., 2008*]. Loss of interaction between fibrillins and LTBPs leads to increased free active TGF-β which further causes aberrant downstream TGF-β signaling [*Ramirez et al., 2008*].

In addition to controlling the bioavailability of TGF-β isoforms, fibrillin-1 also sequesters other bioactive molecules in the TGF-β superfamily, for example the bone morphogenetic protein (BMP)-2, -4, -5, -7 and -10 and renders them latent [*Sengle et al., 2011; Wohl et al., 2016*]. Similar to TGF-β, BMP-7 is also secreted as a stable complex in which the pro-domain is non-covalently bound to the growth factor dimer. It has been shown that the N-terminal region of fibrillin-1

contains binding sites for the BMP-7 prodomain or the BMP-7 complex as a whole but not the growth factor dimer alone [*Gregory et al., 2005*]. Binding of the BMP-7 complex renders the growth factor latent through a conformational change [*Wohl et al., 2016*]. Activation of this complex occurs via matrix metalloproteinase 13 cleavage in the prodomain [*Furlan et al., 2021*]. The prodomains of BMP-2, -4, -5, -10 were also shown to interact with high affinity with the N-terminal region of fibrillin-1 [*Sengle et al., 2008; Sengle et al., 2011*]. Contrary to fibrillin-dependent mechanisms, the microfibril-associated MAGP-1 binds the active forms of TGF-β and BMP-7, also suggesting a critical role in microfibril-mediated growth factor signaling [*Weinbaum et al., 2008; Broekelmann et al., 2020*].

1.5.3 Asprosin, the C-terminal propeptide of fibrillin-1

Asprosin is the C-terminal prodomain of fibrillin-1 cleaved during or directly after secretion by the furin-type proprotein convertases, giving rise to a bioactive 140 amino acid cleavage product [*Lönnqvist et al., 1998; Wallis et al., 2003; Romere et al., 2016*] (Fig. 1.5). This propeptide migrates much higher than expected in SDS gels (~30-32 kDa), likely due to the presence of three N-linked glycans [*Lönnqvist et al., 1998*]. Processing of the C-terminal propeptide is a prerequisite for the ~320 kDa mature fibrillin-1 to assemble into the typical bead-on-the-string microfibrils [*Raghunath et al., 1999; Jensen et al., 2014*] (Fig. 1.5). The propeptide blocks a critical N- to C-terminal self-interaction site in fibrillin-1 to prevent premature microfibril assembly during secretion [*Hubmacher et al., 2008; Jensen et al., 2014*]. Circulating asprosin was reported to be primarily secreted from WAT during fasting conditions or in obesity [*Romere et al., 2016*] (Fig. 1.6). It promotes hepatic glucose production through the OLFR734 receptor and increases insulin

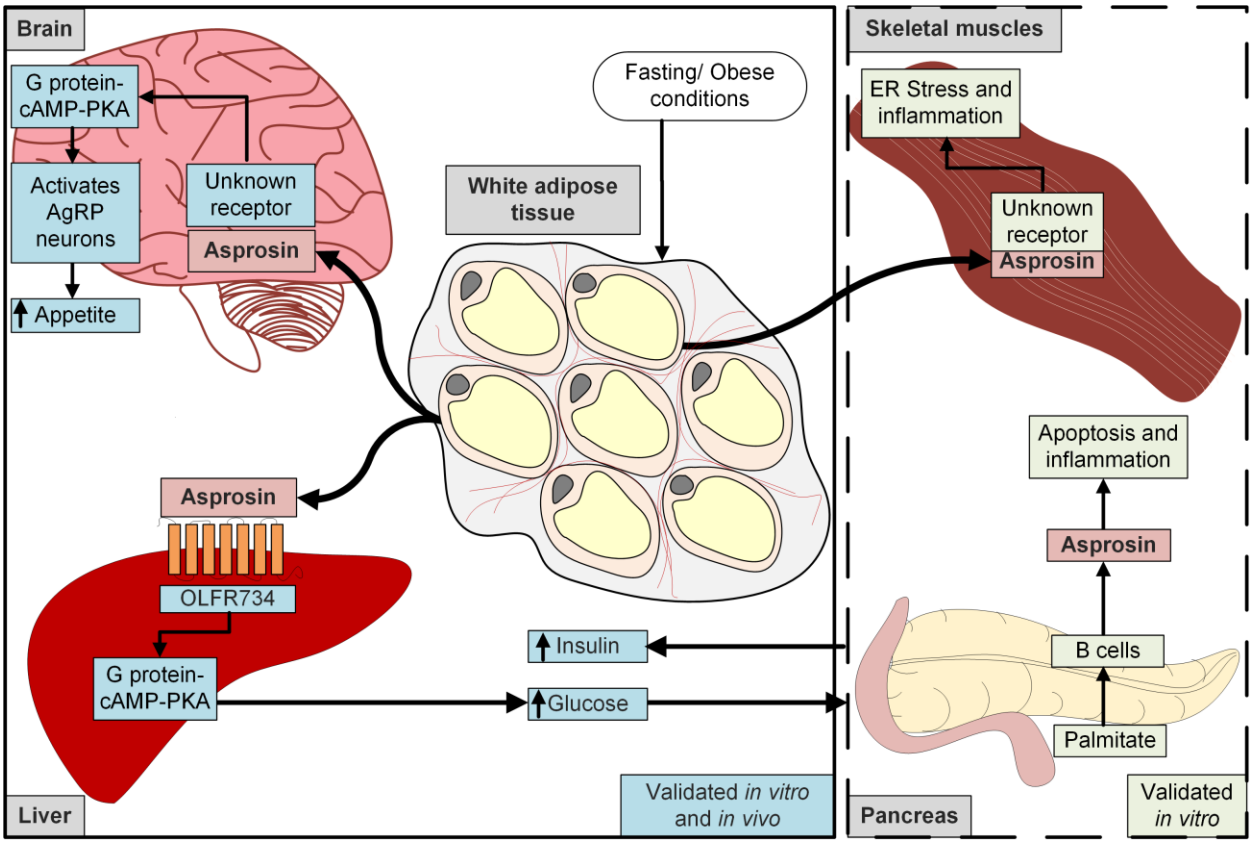

Figure 1.6. The role of asprosin in metabolic organs. Left solid box: During fasting or in obesity, increased circulating asprosin promotes hepatic glucose production and increases insulin secretion from the pancreas. Asprosin activates the AgRP neurons in the brain and increases appetite. Both asprosin functions have been tested and validated *in vivo* and *in vitro* experiments. **Right dashed box**: Other *in vitro* studies have shown that increased asprosin levels lead to apoptosis and inflammation in pancreatic B cells, and to inflammation and endoplasmic reticulum stress in skeletal muscle cells. However, further *in vivo* validation is required for these functional aspects. Reproduced from [*Muthu & Reinhardt, 2020*] with permission from Elsevier.

secretion from the pancreas [*Romere et al., 2016; Li et al., 2019*]. It also stimulates the appetite by activating the AgRP neurons in the brain [*Duerrschmid et al., 2017*] (Fig.1.6). *In vitro* studies have shown that increased asprosin levels lead to pancreatic B cell malfunction [*Lee et al., 2019*], and to inflammation and endoplasmic reticulum (ER) stress in skeletal muscle cells leading to abnormal glucose homeostasis [*Jung et al., 2019*] (Fig.1.6).

1.6 Marfan syndrome

Mutations in the fibrillin-1 gene cause a wide spectrum of type I fibrillinopathies [*Dietz et al., 1991; Collod-Beroud et al., 2003*]. While most of them are relatively rare disorders, Marfan syndrome (MFS) is more common with a prevalence of about 2-3 in 10,000 [*Judge & Dietz, 2005; Groth et al., 2015*]. Type I fibrillinopathies are characterized by clinical symptoms in the aorta, skeletal system, adipose tissue, and eye [*Pyeritz, 2000; Summers et al., 2005; Robinson et al., 2006; Yetman & McCrindle, 2010*]. More than 1,800 different mutations in *FBN1* leading to MFS have been reported [*Collod-Beroud et al., 2003*]. The underpinning pathogenetic mechanism leading to MFS can include a dominant negative mechanism, where mutated fibrillin-1 becomes incorporated into microfibrils and compromises their function, or by haploinsufficiency with reduced fibrillin-1 protein present in the ECM due to a variety of mechanisms, including nonsense mediated mRNA decay or secretion deficiency [*Hubmacher & Reinhardt, 2011*]. The effective physiological outcome in both cases is a reduced level of fully functional microfibrils in tissues and elevated levels of active TGF-β [*Hubmacher & Reinhardt, 2011*].

1.6.1 Cardiovascular abnormalities in MFS

Aortic rupture resulting from progressive thoracic aortic aneurysms (TAA) is the main cause of premature death in MFS patients [*Gray & Davies, 1996b; Gray & Davies, 1996a*]. Aortic dilation is present in around ~60% of both children and adults suffering from MFS [*van Karnebeek et al.,*

2001]. Average life expectancy of patients with MFS is around 45 years without surgical intervention [*Murdoch et al., 1972*]. However, surgical treatments have drastically improved the life expectancy of MFS patients to 70 years [*Finkbohner et al., 1995; Silverman et al., 1995*]. Non-canonical TGF-β signaling through the extracellular signal-regulated kinase (Erk) 1 and 2 is critical in aneurysm formation [*Holm et al., 2011*]. Losartan, an angiotensin II type 1 receptor blocker, reduces excessive TGF-β-mediated Erk activation and thereby prevents aortic aneurysm formation in MFS mouse models [*Habashi et al., 2006; Habashi et al., 2011*]. These findings sparked considerable interest among researchers and clinicians to use losartan for the treatment of human patients. However, several randomized clinical trials reported controversial results [*Singh & Lacro, 2016; Rurali et al., 2018*]. Overall, the trials did not fully support the use of angiotensin II type 1 receptor blocker over β-adrenergic receptor antagonists for the treatment of MFS. Later, it was identified that increased activity of TGF-β in MFS is not the primary cause of the disease but rather a consequence of defective mechanosensing, and that TGF-β might be a non-productive activity of smooth muscle cells to rescue this phenotype [*Franken et al., 2015*].

1.6.2 Skeletal abnormalities in MFS

Major skeletal defects associated with MFS include long bone overgrowth, arachnodactyly, dolichostenomelia, pectus deformity (pectus excavatum and pectus carinatum), kyphosis, scoliosis and osteopenia [*Pyeritz, 2000*]. Pectus excavatum occurs and it is visible in 60-70% of the MFS patients [*Scherer et al., 1988*]. Abnormal curvature of the bone leading to kyphosis and scoliosis are also a common feature of MFS patients [*Sponseller et al., 1995; Sponseller et al., 1997*]. Osteopenia (low bone mineral density) is present in both women [*Kohlmeier et al., 1993; Kohlmeier et al., 1995*] and men [*Carter et al., 2000*] with MFS. Although the osteoporosis diagnosis is complicated in children because they are taller than average [*Rauch et al., 2008*], it

was shown that children with MFS have significantly lower bone mineral density compared to healthy height-matched controls [*Kohlmeier et al., 1995; Moura et al., 2006*]. Low bone mass has also been reported in a mouse model of MFS [*Nistala et al., 2010*].

1.6.3 Adipose tissue abnormalities in MFS

Many individuals affected with MFS have an asthenic (thin) body habitus. A subgroup of MFS patients classified as marfanoid progeroid lipodystrophy syndrome (MPLS) caused by mutations in the C-terminal domain of fibrillin-1 [*Passarge et al., 2016*], exhibit a progeroid (premature aging) appearance together with a lipodystrophic phenotype [*Goldblatt et al., 2011; Horn & Robinson, 2011; Takenouchi et al., 2013; Garg & Xing, 2014; Jacquinet et al., 2014; Lin et al., 2019*]. Similarly, neonatal progeroid syndrome (NPS) can also be caused by C-terminal fibrillin-1 mutations and is characterized by lipodystrophy from birth and signs of premature aging [*O'Neill et al., 2007; Romere et al., 2016*]. However, a study reported that there is a subgroup of MFS patients with a median age of 21 who fall under the overweight category with a body mass index of 25-30 kg/m^2 (14%) or even under obese category with a body mass index of >30 kg/m^2 (22%) [*Yetman & McCrindle, 2010*]. Since the percentage of obese population (22%) in MFS is similar to the common population, these patients are not protected from obesity. In addition, most people diagnosed with MFS accrue adiposity as they age, which predisposes them to insulin resistance and type 2 diabetes mellitus [*Erkula et al., 2002; Yetman & McCrindle, 2010; von Kodolitsch et al., 2019; Hansen et al., 2020*]. Together these metabolic complications increase the risk of pre-existing cardiovascular complications, such as aneurysm formation and aortic dissection [*Orio et al., 2007; Bastien et al., 2012*]. None of the studies reported of any gender-based differences in the adipose tissue abnormalities seen in MFS patients. Several mutations in the C-terminal fibrillin-1 propeptide giving rise to MFS inhibit processing of the propeptide [*Milewicz et al.,*

1995; Lönnqvist et al., 1998]. Other mutations in this region lead to NPS and MPLS [*Graul-Neumann et al., 2010; Goldblatt et al., 2011; Horn & Robinson, 2011; Takenouchi et al., 2013; Garg & Xing, 2014; Jacquinet et al., 2014; Romere et al., 2016; Lin et al., 2019*], indicating a role of the fibrillin-1 C-terminal prodomain (asprosin) in the regulation of adipose tissue (Fig. 1.6). Asprosin is elevated in humans and mice affected with insulin resistance, obesity and type 2 diabetes mellitus [*Romere et al., 2016; Alan et al., 2019; Wang et al., 2019; Zhang et al., 2019*], but it is decreased in NPS patients [*Romere et al., 2016*]. It is also important to note that obese women were identified with increased *FBN1* gene expression levels in WAT [*Davis et al., 2016*]. Together, the clinical data clearly suggests that fibrillin-1 plays an important and dynamic role in adipose tissue homeostasis.

1.7 Mouse models of MFS

Various mouse models were developed over the last two decades to study MFS. The first reported mouse model was the *Fbn1*$^{mg\Delta/mg\Delta}$ model, in which exons 19 to 24 of *Fbn1* were deleted. These mice express only 10% fibrillin-1 protein compared to normal wild type levels and die of a severe cardiovascular phenotype around 3 weeks after birth. Homozygous *Fbn1*$^{mgR/mgR}$ mice contain a neomycin cassette inserted in the intron between exon 18 and 19 leading to transcriptional interference with the *Fbn1* gene. *Fbn1*$^{mgR/mgR}$ mice express normal fibrillin-1 at about 20-25% of the level in wild-type mice [*Pereira et al., 1999*]. These mice represent one of the generally accepted mouse models for severe MFS with typical disease features in the cardiovascular, skeletal, and pulmonary systems and an average lifespan of ~4 months [*Nistala et al., 2010*]. Fibrillin-1 null mice (*Fbn1*$^{mgN/mgN}$) die within the first two weeks after birth due to aortic rupture and pulmonary manifestations [*Carta et al., 2006*].

Another mouse model of MFS carries a heterozygous and dominant negative C1041G mutation in the cbEGF11 domain of fibrillin-1 (*Fbn1*$^{C1041G/+}$) [*Judge et al., 2004*]. The C1041G mutation alters a cysteine residue in mouse fibrillin-1, which is homologous to a C1039Y mutation leading to MFS in humans. This unique mouse model represents the only currently available MFS model with a causative heterozygous missense mutation. These mice gradually develop aortic aneurysms and skeletal phenotypes later in life (6 months) which represents a milder MFS phenotype [*Judge et al., 2004*]. Another line of fibrillin-1 mutant mice (*Fbn1*$^{H1\Delta/H1\Delta}$) where exon 7 was deleted, resulting in deletion of the first hybrid domain of fibrillin-1. But these mice survived normally and manifested neither defects in microfibril structure nor MFS phenotypes [*Charbonneau et al., 2010*]. Recently, two additional animal models were developed harboring a C-terminal deletion of fibrillin-1 (asprosin), *Fbn1*$^{NPS/+}$ (mice) [*Duerrschmid et al., 2017*] and *Fbn1* Het (rabbit) [*Kim & Kim, 2012*].

From the above described fibrillin-1 relevant mice models, three models with a relatively mild MFS (*Fbn1*$^{C1041G/+}$), or no MFS at all (*Fbn1*$^{H1\Delta/H1\Delta}$; *Fbn1*$^{mg+/-}$) were previously analyzed for a metabolic phenotype [*Walji et al., 2016*]. All three mouse models did not display a lipodystrophic phenotype, but rather had slightly increased body and adipose tissue mass with an insulin resistant phenotype. Additionally, both *Fbn1*$^{NPS/+}$ (mice) [*Duerrschmid et al., 2017*] and *Fbn1* Het (rabbit) [*Kim & Kim, 2012*] harboring C-terminal deletion show a severe lipodystrophic phenotype.

1.8 Rationale, hypothesis, overall goals, and objectives

Rationale

Individuals with MFS caused by mutations in fibrillin-1 are characterized by adipose tissue dysfunction (obesity and lipodystrophy). This predisposes the patients to metabolic complications and serves as a causative factor for the progression of aortic aneurysm and rupture. *FBN1* gene expression was shown to be highly expressed in adipose tissue of obese women compared to non-obese women, correlating with an increase in adipocyte size. While these clinical and scientific data clearly show that fibrillin-1 is indispensable in fat tissue homeostasis, virtually nothing is known about the mechanisms by which fibrillin-1 determines the level of adipose tissue.

Hypothesis

We hypothesize that fibrillin-1 regulates adipocyte development and plays a vital role in adipose tissue homeostasis. We further postulate that fibrillin-1 has distinct but critical roles in both early and late phases of adipogenesis.

Overall goals and objectives

The overarching goal of this study is to define the contribution of fibrillin-1 in adipose tissue metabolism. To fulfill this goal, we took a stepwise approach with four specific objectives.

1. To determine the physiological and pathological roles of fibrillin-1 in adipose tissue homeostasis using two MFS mouse models (Chapter 2).
2. To study the molecular signaling mechanisms of fibrillin-1 regulated adipogenesis (Chapter 2).

3. To examine the role of fibrillin-1 in diet-induced obesity using two MFS mouse models (Chapter 3).

4. To generate a mouse model that will allow us to delineate the adipocyte specific role of fibrillin-1 in adipose tissue and systemic metabolism (Chapter 4).

CHAPTER 2: FIBRILLIN-1 IS A KEY REGULATOR OF WHITE ADIPOSE TISSUE DEVELOPMENT, HOMEOSTASIS, AND FUNCTION

Fibrillin-1 is a key regulator of white adipose tissue development, homeostasis, and function

Muthu L. Muthu[1*], Kerstin Tiedemann[2,3*], Julie Fradette[4,5], Svetlana Komarova[2,3#], Dieter P. Reinhardt[1,2#]

[1]Faculty of Medicine and Health Sciences, Department of Anatomy and Cell Biology, McGill University, Montreal, Canada

[2]Faculty of Dental Medicine and Oral Health Sciences, McGill University, Montreal, Canada

[3]Shriners Hospital for Children – Canada, Montreal, Canada

[4]Centre de recherche en organogénèse expérimentale de l'Université Laval / LOEX, Division of Regenerative Medicine, CHU de Québec Research Center - Université Laval, QC, Canada.

[5]Department of Surgery, Faculty of Medicine, Université Laval, Québec, QC, Canada.

[*] Co-first authors, [#]Co-corresponding authors

Keywords: Fibrillin-1, Extracellular matrix, Microfibrils, Marfan syndrome, Adipose tissue, Adipocyte differentiation

2.1 Preamble

Adipose tissue is a dynamic metabolic organ that undergoes significant remodeling during weight gain or loss. The extracellular matrix microenvironment of adipose tissue is of critical importance for the differentiation, remodeling, and function of adipocytes. Fibrillin-1 is a key component of microfibrils and an important player in this process. Mutations in fibrillin-1 lead to MFS and other heritable disorders, often characterized by adipose tissue and cardiovascular dysfunction among others. Therefore, the work described in this chapter identifies the impact of global fibrillin-1 deficiency and a fibrillin-1 missense mutation in the development of adipocytes and adipose tissue as a whole, using the haplo-insufficient $Fbn1^{mgR/mgR}$ and the dominant negative $Fbn1^{C1041G/+}$ MFS mouse models. Further, we also delineate the signaling mechanisms by which fibrillin-1 controls adipogenic commitment and differentiation.

2.2 Abstract

Fibrillin-1 is an extracellular glycoprotein present throughout the body. Mutations in fibrillin-1 cause a wide spectrum of type I fibrillinopathies, including Marfan syndrome characterized by clinical manifestations in adipose tissues, among others. This study addresses the hypothesis that fibrillin-1 regulates adipocyte development and plays a vital role in adipose tissue homeostasis. We employed two mouse models - *Fbn1*$^{mgR/mgR}$ (20-25% of normal fibrillin-1) and *Fbn1*$^{C1041G/+}$ (missense mutation in fibrillin-1) to examine the role of fibrillin-1 in adipose tissue development and homeostasis. Fibrillin-1 was detected around mature adipocytes in both mouse and human white adipose tissues. As expected, *Fbn1*$^{mgR/mgR}$ mice displayed a significant reduction of fibrillin-1 in white adipose tissue, whereas no change was observed for *Fbn1*$^{C1041G/+}$ mice. Male *Fbn1*$^{mgR/mgR}$ mice had more white and brown adipose tissues, whereas female *Fbn1*$^{mgR/mgR}$ and both male and female *Fbn1*$^{C1041G/+}$ showed no difference compared to wild-type littermates. Consistent with this data, male *Fbn1*$^{mgR/mgR}$ mice displayed hyperinsulinemia and an insulin resistance phenotype with higher levels of cholesterol and high-density lipoproteins in the serum. Fibrillin-1 deficiency in male *Fbn1*$^{mgR/mgR}$ mice also promoted adipogenic gene expression and led to hypertrophic expansion of mature adipocytes. To further elucidate the fibrillin-1-dependent adipogenic mechanisms in cell culture, we used primary bone marrow derived mesenchymal stem/stromal cells (MSCs) from *Fbn1*$^{mgR/mgR}$, *Fbn1*$^{C1041G/+}$ and wild-type mice. Increased lipid content, adipogenic differentiation and pAKT levels were observed when MSCs from both male and female *Fbn1*$^{mgR/mgR}$ mice were in vitro differentiated. Furthermore, a recombinant fragment spanning the C-terminal half of fibrillin-1 significantly reduced adipocyte differentiation i) by binding to MSCs and inhibiting adipogenic commitment, and ii) by sequestering insulin, together suppressing the AKT signaling pathway. This fibrillin-1 fragment also rescued enhanced adipogenic differentiation of MSCs derived from *Fbn1*$^{mgR/mgR}$ mice. Overall, this study shows that

altered adipose tissue homeostasis observed in fibrillin-1 deficient mice depends on the type of fibrillin-1 deficiency and the biological sex, and it shows that fibrillin-1 is a negative regulator of adipogenesis.

2.3 Introduction

White adipose tissue (WAT) is a dynamic endocrine organ that regulates energy balance and releases a wide variety of adipokines. Physiological development of WAT involves a multi-step orchestrated sequence of events where mesenchymal precursor cells differentiate into mature lipid-filled adipocytes during the early commitment and late expansion phase [*Ghaben & Scherer, 2019*]. Growth and expansion of WAT in the postnatal phase involves two central mechanisms, adipocyte hyperplasia marked by an increase in the number of adipocytes and hypertrophy characterized by an increase in adipocyte size [*Wang et al., 2013*]. Imbalance in either one of these mechanisms could lead to excessive adipose tissue deposition resulting in obesity, or dysregulated adipose tissue deposition (lipodystrophy), and both can be a causative risk factor for metabolic disease [*Herranz et al., 2008; Kassi et al., 2011; Bindlish et al., 2015; Czech, 2017*]. The extracellular matrix (ECM) microenvironment positioned around adipocytes is constantly remodeled during the development and expansion of WAT. Key ECM proteins in WAT include fibronectin, fibrillin-1, elastin, collagens, laminins, and proteoglycans. Fibronectin emerges early in the undifferentiated mesenchymal stem cell stage and degrades as mature adipocytes develop [*Kubo et al., 2000*]. Preadipocyte factor 1 interacts with fibronectin and inhibits adipocyte differentiation [*Wang et al., 2010*]. Collagen VI is enriched in the ECM of mature adipocytes and negatively regulates cell size [*Khan et al., 2009*], whereas collagen XVIII promotes adipose tissue accumulation by adipocyte hyperplasia [*Aikio et al., 2014*]. Other basement membrane proteins typically appear later in the differentiation process [*Kubo et al., 2000; Mariman & Wang, 2010; Vaicik et al., 2014*]. Thus, the composition and regulation of the pericellular ECM is pivotal for the differentiation and function of adipocytes [*Divoux & Clement, 2011*]. However, the role of fibrillin-1 in this microenvironment is not explored.

Fibrillin-1 constitutes the major backbone protein of extracellular microfibrils and is encoded by the *FBN1* gene in humans and rodents [*Sakai et al., 1986*]. Fibrillin-containing microfibrils assemble as highly ordered bead-on-the-string macromolecular structures [*Keene et al., 1991; Reinhardt et al., 1996; Lönnqvist et al., 1998*]. Fibrillin-1 is primarily produced by cells of mesenchymal origin, and it is expressed throughout life [*Zhang et al., 1995; Summers et al., 2010; Davis et al., 2016*]. Processing of profibrillin-1 into the mature ~320kDa protein is mediated through cleavage of the N- and C-terminal prodomains by furin-type proteases [*Milewicz et al., 1995; Ritty et al., 1999; Muthu & Reinhardt, 2020*]. The C-terminal pro-peptide is released primarily from the WAT into the blood stream as a hunger hormone termed asprosin, known to promote hepatic gluconeogenesis and insulin secretion [*Romere et al., 2016; Duerrschmid et al., 2017*]. Consistent with these aspects, mouse (*Fbn1*$^{NPS/+}$) and rabbit (*Fbn1* het) models harboring deletions in the C-terminal fibrillin-1 pro-peptide show severe lipodystrophic phenotypes [*Romere et al., 2016; Chen et al., 2018*]. Fibrillin-1 in microfibrils not only provides structural support for elastic fiber formation and for stability of basement membranes, but also regulates the bioavailability of important growth factors and cytokines. For example, it interacts with LTBP-1 and -4 to position the latent form of transforming growth factor beta (TGF-b) to microfibrils [*Isogai et al., 2003; Neptune et al., 2003; Chaudhry et al., 2007*]. Fibrillin-1 also directly interacts with several bone morphogenetic proteins (BMP) including BMP-2, -4, -7 and -10 [*Sengle et al., 2008; Wohl et al., 2016*], and osteoclastogenic cytokine receptor activator of nuclear factor κβ ligand (RANKL) in various cellular microenvironments [*Tiedemann et al., 2013*].

Marfan syndrome (MFS) and Marfanoid progeroid lipodystrophy syndrome are caused by mutations in fibrillin-1 and are often characterized by lipodystrophic phenotypes of various

severities [*Herranz et al., 2008; Graul-Neumann et al., 2010; Goldblatt et al., 2011; Takenouchi et al., 2013; Jacquinet et al., 2014; Passarge et al., 2016; Romere et al., 2016*]. A significant subset of MFS patients (36%), however, is typified as overweight or even obese with elevated body mass indices of >30 kg/m^2 [*Yetman & McCrindle, 2010*]. MFS patients also frequently accrue adiposity as they age [*Erkula et al., 2002; von Kodolitsch et al., 2019; Hansen et al., 2020*]. Abnormal adipose tissue deposition in MFS patients not only predisposes to metabolic abnormalities such as insulin resistance and type 2 diabetes mellitus but also increases the risk of pre-existing cardiovascular conditions [*Erkula et al., 2002; Orio et al., 2007; Graul-Neumann et al., 2010; Yetman & McCrindle, 2010; Goldblatt et al., 2011; Bastien et al., 2012; Jacquinet et al., 2014; Passarge et al., 2016; von Kodolitsch et al., 2019; Hansen et al., 2020*]. Fibrillin-1 is upregulated in adipose tissue of obese women correlating to the size of adipocytes [*Davis et al., 2016*]. Together, the data show that fibrillin-1 holds a central role in the development and homeostasis of WAT. It was previously shown that fibrillin-1 is secreted by primary rat adipocytes [*Mariman & Wang, 2010*]. Also, the fibrillin-1 deficient mouse models *Fbn1*$^{+/-}$ and *Fbn1*$^{C1041G/+}$ were characterized previously showing slightly excess WAT deposition and reduced insulin sensitivity compared to wild-type mice [*Walji et al., 2016*]. However, the specific role of fibrillin-1 in adipocyte differentiation and the underpinning molecular mechanisms that lead to either reduced or increased fat deposition is virtually unknown.

The overarching aim of this study was to determine the physiological and pathological roles of fibrillin-1 in adipose tissue development and metabolism. We used two MFS mouse models, *Fbn1*$^{mgR/mgR}$ (mgR/mgR) and *Fbn1*$^{C1041G/+}$ (C1041G/+) mice, as well as primary bone marrow derived mesenchymal stem/stromal cells (MSCs) isolated from both mouse models to delineate

the role of fibrillin-1 haploinsufficiency versus a fibrillin-1 mutation in adipose differentiation. Mechanistically, we define the stage-specific role of fibrillin-1 in adipogenic differentiation and in modulating the AKT signaling pathway. The study establishes fibrillin-1 as a dynamic ECM protein in adipose tissue physiology and systemic metabolism.

2.4 Methods

2.4.1 Mice used in this study

All experimental procedures were approved by the McGill University Animal Care Committee in accordance with the guidelines of the Canadian Council on Animal Care (Protocol#2014-7561). *Fbn1*$^{mgR/mgR}$ mice, kindly provided by Dr. Francesco Ramirez, have a neomycin cassette inserted in the *Fbn1* gene between exons 18 and 19 leading to a reduced level (20-25%) of normal fibrillin-1 [*Pereira et al., 1999*]. *Fbn1*$^{C1041G/+}$ mice harboring a missense mutation at p.Cys1041Gly were purchased from the Jackson Laboratories (B6.129-Fbn1tm1Hcd/J). This mouse model was designed based on a human MFS mutation and is identical with the originally described *Fbn1*$^{C1039G/+}$ mice [*Judge et al., 2004*]. mgR/mgR mice are phenotypically characterized by severe aortic aneurysms leading to death around 16 weeks of age [*Pereira et al., 1999*], whereas the C1041G/+ mice represent a milder MFS mouse model that develop aneurysms much later in life [*Judge et al., 2004*]. The mgR/mgR and the C1041G/+ mouse colonies were kept in two different animal facilities using slightly different regular facility grain-based diet. mgR/mgR mice received for 16 weeks grain-based diet purchased from Envigo, USA (Cat#2920X), and C1041G/+ mice received for 35 weeks grain-based diet purchased from Charles River, Canada (Cat#5075). For that reason, only Wt littermates from each colony were used to compare with the respective mutant mice. All mice were housed under standard conditions (12 hours of light-dark cycles) and were fed with conventional grain-based diet. Wild-type (Wt) mice (C57BL/6J strain) from the same breeding were used as littermate controls for the study. To determine the food intake, each mouse was individually housed for 10 days and provided on day 0 with known food quantities. The beddings in the mouse cage were not changed and the mice were left undisturbed for 10 days. The remaining food after 10 days was weighed and the food consumption per day was calculated. For

other experiments, 2-5 littermates were kept in one cage. For genotyping, genomic DNA was isolated from tail snips and amplified by polymerase chain reaction (PCR) using the protocol and the components of the Mouse Direct PCR Kit (Bimake, Cat#B40015). The sequences of primers used for genotyping mice are detailed in Supplemental Table 1, as published in the original studies [*Pereira et al., 1999; Kubo et al., 2000; Judge et al., 2004*].

2.4.2 Systemic metabolism and tissue analysis

Mice were fasted for 6 h and 16 h before performing Insulin tolerance test (ITT) and Glucose tolerance test (GTT), respectively, 1 week prior to the experimental end points (16 weeks for mgR/mgR mice and 35 weeks for C1041G/+ mice). For both ITT and GTT, blood glucose was measured using a blood glucometer (Verio Flex, OneTouch) with a drop of blood from the tail tip immediately before (time 0) and 15, 30, 60, 90, and 120 min after intraperitoneal injection of 0.75 U/kg insulin or 2 g/kg glucose, respectively. During terminal analysis, blood was collected through cardiac puncture and centrifuged at 6,000×g for 8 min to separate serum from blood cells. Samples were analyzed for cholesterol, triglycerides, and high-density lipoproteins by the diagnostic and research support services of the McGill Animal Resource Center. Insulin levels were measured in serum using an ELISA kit following the manufacturer's instructions (Cristal Chem, Cat#90080). Mice were euthanized at the experimental endpoint and iWAT, BAT, gWAT, liver, and spleen were dissected and weighed before further analysis.

2.4.3 Histologic analysis and adipocyte size analysis

Formalin fixed iWAT was paraffin embedded and cut in 5 μm sections, and deparaffinized by incubating slides at 65°C for 30 min followed by 2 changes of CitriSolv (Decon Labs) for 5 min

each. The sections were rehydrated with a decreasing ethanol gradient and distilled water (100% ethanol – 0% ethanol), followed by hematoxylin and eosin staining. Images were captured at 200× magnification using an AxioImager M2 bright field microscope (Zeiss) equipped with a AxioCam ICc5 color camera at 3 different areas per sample in the center of the WAT. Adipose tissue histomorphometry was performed to quantify the number and size of adipocytes using the ImageJ software (Version 1.53n) following established procedures [*Schneider et al., 2012; Parlee et al., 2014*].

2.4.4 RNA extraction, real-time qPCR, and cDNA sequencing

iWAT was harvested from mice, immediately snap frozen, and pulverized using a BioPulverizer (BioSpec, Cat#59012MS), followed by total RNA extraction using the RNeasy kit (Qiagen, Cat#74104). To obtain total RNA from cells in culture, cells were lysed at the experimental endpoint and RNA was extracted using the RNeasy kit following the manufacturer's instructions. cDNA generation was performed with 0.5-1 μg of RNA using the Protoscript First Strand cDNA Synthesis kit (New England Biolabs, Cat#E6560L). For quantification of the respective genes, real-time qPCR was performed using a SYBR Select Master Mix (Applied Biosystems, Cat# LS4472908). The primers for each gene were purchased from Alpha DNA, Montreal, Canada or Integrated DNA Technologies, Coralville, USA and are included in Supplemental Table 1. Relative gene expression levels were determined using the comparative delta-delta Ct method. Sanger sequencing was performed by the McGill Genome Centre (Montreal, Canada) using the cDNA of iWAT with the primers listed in Supplemental Table 1.

2.4.5 Primary cell isolation and culture

To isolate MSCs, tibiae and femurs were dissected from both male and female Wt, mgR/mgR, and C1041G/+ mice after euthanasia at 4-6 weeks of age. Bone marrow was aspirated, washed, and plated in αMEM culture medium (Gibco, Cat#12571063) containing 10% heat-inactivated fetal bovine serum and penicillin-streptomycin-glutamine (basal media) for 6-7 days under a 5% CO_2 atmosphere at 37°C. Cells from each mouse were cultured separately. Floating cells were aspirated, and adherent cells (MSCs) were trypsinized after 7 days and seeded at a density of 50,000 cells/cm^2 in standard expansion αMEM media for 24 h followed by induction of differentiation with or without the addition of recombinant fibrillin-1 fragments.

2.4.6 Adipogenic differentiation

MSCs were induced to differentiate into adipocytes by adding an adipogenic differentiation culture medium from day 1-4, containing a cocktail of 7.5 nM insulin (Sigma-Aldrich, Cat#I2643), 1 µM dexamethasone (Sigma-Aldrich, Cat#D4902), 500 µM 1-methyl-3-isobutyl-xanthin (IBMX) (Sigma-Aldrich, Cat#I5879), and 50 µM indomethacin (Sigma-Aldrich, Cat#I7378) added to the basal media as mentioned above [*Watchareewan & Thanaphum, 2021*]. The concentration of insulin in the adipogenic cocktail was standardized for this study. The cells were then maintained from day 4-10 in an adipogenic maintenance medium containing only insulin (50 ng/ml) and dexamethasone (1 µM) added to the basal media. To investigate the consequences of fibrillin-1 fragments on adipogenesis, recombinant N- (rFBN1-N) and C-terminal (rFBN1-C) halves were produced as described previously [*Jensen et al., 2001*]. The recombinant fragments in 50 mM Tris-HCl, pH 7.4, 150 mM NaCl, 2 mM $CaCl_2$ (TBS) were added to the culture medium at 50 µg/mL final concentration, for either d 1-4 or d 1-10, depending on the experimental set up.

For the buffer control, the same volumes of TBS were added to the cells. The positive control contained only adipogenic differentiation media, whereas the negative control contained basal media. The medium with either fragments or buffer control was replenished every 3 days. To address insulin sequestration of fibrillin-1, increasing concentrations of insulin (0.75 nM, 0.75 µM, 7.5 µM) were added to the culture medium without altering the other components of the adipogenic cocktail. Adipocyte differentiation at day 10 was assessed morphologically using the Oil Red-O staining method [*Sikkeland et al., 2014*]. Briefly, cells were fixed with 10% formalin for 1 h at RT, rinsed with 60% isopropanol for 5 min, air dried for 20 min, stained with Oil Red O solution (Sigma-Aldrich, Cat#O0625) for 15 min and finally washed with distilled water before quantification. Red lipid droplets within adipocytes were imaged at 100× magnification using a Zeiss Axiovert 40 CFL inverted microscope, and the area of the adipocytes were outlined and quantified using ImageJ [*Schneider et al., 2012*]. The cell viability was assessed on live cells parallelly using Live and Dead Cell Assay kit on day 10 (Abcam, Cat#ab115347).

2.4.7 Human tissues

Subcutaneous white adipose tissues were obtained from 6 female donors undergoing cosmetic surgery procedures (lipectomy), following informed consent and according to protocols approved by the Institutional review board of the CRCHU de Québec-Université Laval (DR-002--1117). Mean age of the donors was 39.5 years (range 31 to 42 years) and mean body mass index was 24.85 kg/m^2 (range 20.4 to 28.8). Tissue samples were fixed with 10% buffered formalin, paraffin embedded and cut in 5 µm sections.

2.4.8 Indirect immunofluorescence labeling of tissues and cells

Tissue sections were deparaffinized and rehydrated as described above under *Histological analysis and adipocyte size estimation.* Antigen retrieval was performed using citric acid buffer (10 mM citric acid, pH 6.0, 0.05% Tween 20) at 95°C, followed by treatment with 10 µM Protease XXIV (Sigma-Aldrich, Cat#P8038) dissolved in 50 mM Tris-HCl, pH 7.6 for 5 min. The sections were washed with TBS and blocked with 2% bovine serum albumin for 1 h at room temperature (RT). Immunofluorescence staining of cells was performed by plating the cells on plastic 8-well chamber slides (Thermo Fisher Scientific, Cat# CA62407-335A) at a density of 50,000 cells/cm^2. At the experimental endpoint, cells were fixed with 70% methanol/30% acetone and blocked with 10% v/v normal goat serum. Tissues or cells were then incubated with primary antibodies using the α-rF6H polyclonal anti-fibrillin-1 antiserum [*Tiedemann et al., 2001*], or anti-perilipin (Cell Signaling Technologies, Cat#3470S) at a 1:1,000 dilution, overnight at 4°C or 2 h at RT, respectively. Goat anti-rabbit Cyanine5 or Cyanine3 (Jackson ImmunoResearch Laboratories, Cat#111-165-003) was used as secondary antibodies for 1 h at RT at a 1:200 dilution. Vectashield with 4′, 6-diamidino-2-phenylindole (DAPI) (Vector labs, Cat#VECTH1200) was used for nuclear counter staining and mounting. To control for non-specific binding, no primary antibody control was additionally performed in each experiment. Immunofluorescence images were taken with an Axio Imager M2 microscope fitted with an ORCA-flash4.0 camera. Mean intensity of fibrillin-1 and perilipin staining in each image were quantified using ImageJ as mentioned previously [*Zhang et al., 2019*].

2.4.9 Western blotting

Cells were lysed using RIPA buffer (50 mM Tris, pH 8.0, 150 mM NaCl, 0.5% sodium deoxycholate, 1% Triton X-100, and 0.1% sodium dodecyl sulfate) supplemented with 2% v/v protease inhibitor cocktail (Roche, Basel, Switzerland, Cat#11697498001) and 1% v/v phosphatase inhibitor cocktail (Sigma-Aldrich, St. Louis, MO, USA, Cat#P5726). To remove cell debris, lysates were centrifuged, and supernatants were transferred to a new tube. The concentration was measured using the BCA protein assay kit (Thermo Fisher Scientific, Cat#23225). 15 μg protein was loaded and resolved on a 10% SDS-PAGE gel, and then wet-transferred to a 0.45 μm pore size nitrocellulose membrane (Bio-Rad, Berkeley, CA, Cat#1620115). The membranes were blocked with 5% non-fat dry milk for 1 h at RT and incubated overnight at 4°C with primary antibody diluted 1:1,000 in 2% non-fat dry milk or 5% bovine serum albumin. All antibodies were purchased from Cell Signaling Technologies: anti-pAKT (Ser473, Cat#4508), anti-AKT (Cat#9272), and anti-GAPDH (Cat#2118). Horse radish peroxidase-conjugated goat anti-rabbit secondary antibody (Jackson ImmunoResearch Laboratories, Cat#111-035-003) was diluted 1: 800 and incubated for 2 h at RT. Super signal chemiluminescent western blotting substrate (Thermo Fisher Scientific, Cat#34580) was used to develop and image the Western blots with a Chemi Doc MP imaging system (Bio-Rad). The intensity of the bands was quantified using ImageJ and normalized to the band intensity of the GAPDH loading control.

2.4.10 Cell binding assay

MSCs interaction with the recombinant halves of fibrillin-1 were tested with an end-point cell binding assay using crystal violet staining. 96-well Nunc plates (Thermo Fisher Scientific, Cat#439454) were coated with 25 μg/mL rFBN1-N or rFBN1-C recombinant proteins in triplicates

at 4ºC overnight. Plasma fibronectin and bovine serum albumin were used as a positive and a negative cell binding control, respectively. The coated wells were blocked for 45 min with 100 µL of 10 µg/mL bovine serum albumin. Cells were removed from the parent flask using 0.05% trypsin solution, containing 0.53 mM EDTA for 3 min to minimize the cleavage of cell surface receptors, plated at a density of 25,000 cells/well on the 96-well plates in basal media, and incubated for 2 h to allow cell adhesion at 37ºC. Adherent cells were fixed with freshly prepared 5% glutaraldehyde solution diluted in phosphate buffered saline for 10 min and stained with 0.1% crystal violet in 200 mM 2-(4-morpholino)-ethane sulfonic acid, pH 6 for 45 min. The cells were visualized and imaged using a Zeiss Axiovert 40 CFL inverted microscope. For quantification, the dye was solubilized from the attached cells with 10% glacial acetic acid for 10 min. The absorbance was measured at 570 nm using a spectrophotometer microplate reader (Beckman Coulter, Model# DTX 880).

2.4.11 Biacore analysis

Surface plasmon resonance spectroscopy was used to perform binding analysis of recombinant fibrillin-1 fragments to insulin (Biacore X; Cytiva). rFBN1-N and rFBN1-C was covalently coupled to a CM5 chip using the standard chemistry, resulting in immobilization of 200-1,000 resonance units. Kinetic analyses were performed at 0-15 µg/mL insulin at a 10 µL/min flow rate for 180 s (association), and dissociation was monitored for 1,000 s. The affinity constants were calculated from the kinetics data (fitted rate constants) (BIAevaluation software 4.1; Cytiva), using the module "Fit Kinetics Separate k_a/k_d" with the 1:1 Langmuir binding model. The equilibrium dissociation constant (K_D) was calculated as the ratio of k_d/k_a.

2.4.12 Statistical analysis

Data are represented as means ± Standard Error of the Mean (SEM) or ± Standard Deviation (SD), depending on the experimental requirement. $p<0.05$ was considered statistically significant. Experiments were performed as duplicates or triplicates depending on the experimental setup. For experiments with two conditions, significance was evaluated using Student t-test, otherwise one or two-way ANOVA post Bonferroni test was used as specified in each figure legend. Statistical analyses for ITT and GTT were performed using two-way ANOVA with repeated measures post-Bonferroni test. All statistical analyses were performed using the OriginPro version 2021 software (OriginLab). Outlier analysis was performed using the Grubb's test with confidence levels of 95%. For representation of the data obtained from real-time qPCR, immunofluorescence imaging, and Western blots, the value of control or Wt littermate was set to either 1 or 100%.

2.5 Results

2.5.1 Fibrillin-1 in mouse and human white adipose tissue

To investigate the role of fibrillin-1 in white adipose tissue development, we first analyzed its presence and localization in wild-type (Wt; C57BL/6J strain) mouse in subcutaneous inguinal white adipose tissue (iWAT) by indirect immunofluorescence with specific fibrillin-1 antibodies. Strong fibrillin-1 staining was observed around each mature adipocyte in the stromal vascular compartment (Fig. 2.1A-D). The staining was not different in male and female mice. The fibrillin-1 staining colocalized with a strong autofluorescence in the 450-550 nm range, typical for higher order macro-assemblies of elastin and collagens in the extracellular matrix. We then determined adipose tissue specific levels of fibrillin-1 in two mouse models with altered fibrillin-1, the

mgR/mgR and the C1041G/+ mice. The mgR/mgR mice develop a phenotypic spectrum in several tissues within 3-4 months of age caused by low levels (20-25%) of normal fibrillin-1 [*Pereira et al., 1999; Nistala et al., 2010*]. The C1041G/+ mice generally develop a milder phenotypic spectrum later in life (6-12 months) due to a single heterozygous amino acid substitution (p.C1041G) in fibrillin-1 [*Judge et al., 2004*]. Therefore, iWAT was harvested from mgR/mgR mice at 16 weeks and from C1041G/+ mice at 35 weeks. As expected, the *Fbn1* mRNA levels were lower in male (42%) and female (32%) mgR/mgR mice compared to Wt littermates (Fig. 2.1E). The deposited fibrillin-1 in iWAT, determined by quantification of the IF signals, was significantly reduced by 90% for male mgR/mgR mice relative to Wt littermates (Fig. 2.1A,F). This was different for female mgR/mgR mice, where reduced fibrillin-1 deposition did not reach statistical significance in comparison with Wt mice (Fig. 2.1B,F). Heterozygous male and female C1041G/+ mice did not show any difference in either the *Fbn1* mRNA or the deposited fibrillin-1 levels (Fig. 2.1C,D,G,H). Interestingly, both female mgR/mgR and C1041G/+ mice showed a significant increase in deposited fibrillin-1 compared to the male mgR/mgR and C1041G/+ mice (Fig. 2.1F,H). To test whether the allele harboring the missense mutation (c.3121T>G) in the C1041G/+ mice was indeed transcribed into mRNA, we sequenced amplified DNA after reverse transcription of mRNA isolated from iWAT of male and female mice (Fig. 2.1I). The allele with the missense mutation (c.3121G) was present at 43% in male mice and 33% in female mice relative to the Wt allele (c.3121T), based on peak area quantification. This result validates that the c.3121T>G mutation did not cause haploinsufficiency on the mRNA level. Together these data demonstrate that reduced levels of fibrillin-1 (mgR/mgR mice) in iWAT lead to lower fibrillin-1 deposition primarily in male mice, whereas the p.C1041G missense mutation in fibrillin-1 did not show a deposition phenotype. To analyze the presence of fibrillin-1 in human adipose tissue, we

performed immunofluorescence analysis of female WAT harvested after lipectomy procedures. Similar to mouse tissues, fibrillin-1 was strongly present in the ECM around each adipocyte (Fig. 2.1J).

2.5.2 Fibrillin-1 deficiency in mice results in a distinct sexual dimorphism with respect to adipose tissues

Individuals with MFS are characterized by abnormal adipose tissue, which led us to the hypothesis that fibrillin-1 haploinsufficiency and/or alteration leads to an abnormal adipose metabolism. To test this hypothesis, we continued to use the haploinsufficient mgR/mgR and the dominant negative C1041G/+ mouse models at 16 weeks and 35 weeks of age, respectively (we refer to both defects as "deficiency"). Fibrillin-1 deficiency did not alter the overall body weight of male or female mgR/mgR or C1041G/+ mice, compared to Wt littermates (Fig. 2.2A). However, excess adiposity (1.5 to 1.8-fold higher) was observed in male mgR/mgR mice in various fat depots including brown adipose tissue (BAT) (Fig. 2.2B), iWAT (Fig. 2.2C), and gonadal visceral white adipose tissue (gWAT) (Fig. 2.2D). To control for potential effects from altered eating habits, we monitored the food intake, which did not differ between male Wt and mgR/mgR mice (Fig. 2.2E). Representative images of iWAT and gWAT in Fig. 2.2F exemplify the size differences of the adipose tissues between male Wt and mgR/mgR mice. No differences in adipose tissue weights relative to Wt littermates were observed for female mgR/mgR (Fig. 2.2B-D), as well as male and female C1041G/+ (Fig. 2.2B,C). As expected, female mgR/mgR and C1041G/+ mice displayed significantly lower body weights and metabolic adipose tissue indices compared to their male counterparts (Fig. 2.2A-C).

Processed fibrillin-1 assembles into bead-on-a-string microfibrils together with other proteins, such as Microfibril-associated glycoprotein-1 (MAGP-1) which has been previously shown to promote obesity in mice [*Craft et al., 2014*]. However, we confirmed by real-time qPCR analysis that the mRNA expression levels of *Magp1* was not altered in mgR/mgR and C1041G/+ mice (Fig. S2.1). Therefore, excess adiposity observed in male mgR/mgR mice is likely a direct consequence of fibrillin-1 haploinsufficiency. The weight of other metabolic organs such as liver and spleen did not differ in mgR/mgR and C1041G/+ relative to Wt mice (Fig. S2.2). Total cholesterol (Fig. 2.2G) and high-density lipoproteins (Fig. 2.2H) were significantly elevated in male but not in female mgR/mgR mice. Serum triglyceride levels (Fig. 2.2I) did not differ in male and female mgR/mgR mice compared to Wt. Cholesterol, high-density lipoproteins and triglycerides levels were similar in male and female C1041G/+ mice and Wt littermates (Fig. 2.2G-I). Overall, reduced fibrillin-1, but not the heterozygous p.C1041G mutation, resulted in increased deposition of various fat depots as well as elevated markers of lipid metabolism in male mice. However, female mice were protected from these consequences.

2.5.3 Reduced fibrillin-1 leads to altered glucose and insulin metabolism in male mice

The glucose and insulin metabolism of the fibrillin-1 deficient mice was assessed by tolerance tests through bolus injections of 2 g/kg glucose or 0.75 U insulin, respectively. At baseline, male but not female mgR/mgR mice displayed reduced blood glucose levels compared to Wt mice after 16 h fasting (Fig. 2.3A). However, glucose tolerance tests revealed normal glucose clearance similar to Wt in both male and female mgR/mgR mice (Fig. 2.3B). Neither male nor female C1041G/+ mice showed different glucose levels at baseline (Fig. 2.3C) compared to Wt mice, and males displayed relatively lower glucose clearance, while females were more sensitive after

glucose injection (Fig. 2.3D). Male, but not female mgR/mgR mice demonstrated a significant hyperinsulinemia at baseline (Fig. 2.3E), as well as an insulin resistance phenotype compared to Wt littermates (Fig. 2.3F), correlating with the excess fat accumulation in male mgR/mgR mice. Baseline serum insulin levels and insulin sensitivity of male and female C1041G/+ mice were comparable to Wt mice (Fig. 2.3G,H). Altogether, male mgR/mgR mice had reduced blood glucose levels, but they were hyper-insulinemic and insulin resistant, possibly due to a compensatory mechanism to maintain the insulin-glucose homeostasis. C1041G/+ mice on the other hand demonstrated a much milder phenotype.

2.5.4 Fibrillin-1 deficient male mice are characterized by adipocyte hypertrophy and increase in adipogenic markers

Metabolic disturbance is usually associated with adipocyte hypertrophy, hyperplasia or a combination of both. Therefore, we assessed the adipocyte size in the adipose tissue of fibrillin-1 deficient mice (Fig. 2.4). At 16 weeks of age iWAT adipocytes were clearly larger in male mgR/mgR mice compared to Wt mice, but not in male C1041G/+ mice (Fig. 2.4A-D). On average, adipocytes in mgR/mgR male mice were ~2 fold larger compared to Wt mice (Fig. 2.4A). Consequently, the frequency of small adipocytes (0-4,000 μm^2) was lower, and the frequency of larger adipocytes (4,001-6,000 μm^2) was higher in male mgR/mgR compared to Wt mice (Fig. 2.4B). Adipocyte size was similar in male C1041G/+ and Wt mice (Fig. 2.4C,D). On the other hand, the mean size of adipocytes in female mgR/mgR and C1041G/+ mice was about 0.8-fold lower compared to Wt mice (Fig. 2.4E-H), consistent with a higher frequency of smaller adipocytes (0-2,500 μm^2 and 1,000-2,500 μm^2, respectively) compared to Wt littermates (Fig. 2.4F,H).

To further understand and address the underlying mechanisms for adipocyte hypertrophy in male mgR/mgR mice, real-time qPCR analysis of iWAT was performed for several relevant adipogenic, metabolic and inflammatory markers. Consistent with adipocyte hypertrophy, an increased adipogenic and metabolic gene expression profile was detected in the iWAT of male mgR/mgR mice compared to Wt controls. Particularly, markers of adipocyte differentiation (peroxisome proliferator activated receptor gamma (*Pparg*), CCAAT enhancer binding protein alpha (*Cebpa*), typical white adipose tissue markers (*Adipoq*, *Lep*), glucose uptake transporter (*Glut4*) and fatty acid binding protein 4 (*Fabp4*) were all upregulated in iWAT of male mgR/mgR mice compared to Wt (Fig. 2.5A,B). Chronic inflammation in adipose tissue is a hallmark often associated with hypertrophic adipocytes [*Cancello et al., 2006*]. However, none of several key inflammatory marker mRNAs, including monocyte chemoattractant protein-1 (*Mcp1*), interleukin 1 beta (*Il1b*), and tumor necrosis factor alpha (*Tnfa*) were different between male mgR/mgR and Wt mice (Fig. 2.5C). All analyzed mRNA levels did not differ from Wt controls in female mgR/mgR mice as well as in male and female C1041G/+ mice (Fig. 2.5A-C; Fig. S3). These results further support the data that the observed adipose tissue phenotype is strongly dependent on the biological sex and the type of fibrillin-1 deficiency (reduced normal fibrillin-1 versus missense mutation).

2.5.5 Deficiency of fibrillin-1 enhances adipogenic differentiation

Based on the *in vivo* data, we hypothesized that fibrillin-1 might play a role in the adipogenic differentiation of mesenchymal precursor cells. To test this hypothesis, we used bone marrow derived mesenchymal stem/stromal cells (MSCs), commonly used in adipogenic differentiation experiments. During the multi-step adipogenic process, where adipocyte precursors develop into mature adipocytes, the ECM around adipocytes is extensively remodeled and strongly influences

the formation of adipocytes [*Mariman & Wang, 2010*]. The isolated MSCs were differentiated into adipocytes with an adipogenic cocktail including insulin, dexamethasone, 3-Isobutyl-1-methylxanthine (IBMX), and indomethacin. A schematic overview of the experimental procedure is shown in Fig. 2.6A. To determine *Fbn1* mRNA expression levels during adipocyte differentiation, we performed a time dependent real-time qPCR analysis from 1-10 d of differentiation in cells harvested from Wt mice (Fig. 2.6B). The *Fbn1* mRNA was significantly and progressively downregulated during the expansion phase at d6 to 35% and at d10 to 15%, as the mature adipocytes develop, and the surrounding ECM is remodeled. This was consistent with altered fibrillin-1 deposition in adipocyte-differentiated MSCs *vs.* non-differentiated MSCs (Fig. S2.4A). Similar qualitative changes of the fibrillin-1 network were observed for MSCs from mgR/mgR and C1041G/+ mice (Fig. S2.4B,C). *Zfp423* is a critical positive regulator of committing progenitors to the adipogenic lineage. To control for differences of *Zfp423* possibly affecting early adipogenic commitment of un-differentiated MSCs obtained from Wt, mgR/mgR or C1041G/+ mice, we analyzed Zfp423 mRNA expression levels, which did not reveal any differences (Fig. 2.6C).

We then analyzed the level of mature adipogenesis on day 10 based on perilipin and Oil red O staining. Compared to Wt, MSCs from male and female mgR/mgR mice showed a 2-3.8-fold increase in overall adipogenesis (Fig. 2.6D). Real-time qPCR analysis of total RNA extracted from mature adipocytes on day 10 showed that the *Fbn1* mRNA was significantly reduced to 15% in the adipocyte differentiated MSCs of mgR/mgR mice compared to Wt mice (Fig. 2.6E). Both male and female mgR/mgR mice showed a significant increase in early (*Pparg, Cebpa)*, and late (*Adipoq*) adipogenic markers as well as the glucose transporter *Glut4* (Fig. 2.6E). Adipocyte-

differentiated MSCs from C1041G/+ mice did not differ in the *Fbn1* mRNA levels (Fig. 2.6G). Consistent with this data, no differences were observed in adipocyte numbers or adipogenic marker gene expression in the adipocytes differentiated from C1041G/+ MSCs compared to MSCs isolated from Wt mice (Fig. 2.6F, G). All the above-described experiments with primary MSCs (Fig. 2.6B-G) were performed with cells extracted from both male and female mice. Results of both sexes were also analyzed separately (Fig. S2.5). The enhanced adipogenic differentiation observed in the mgR/mgR mice was independent of the biological sex (Fig. 2.6D,E; cells obtained from male (green diamonds) and female (orange diamonds) mice are denoted separately).

To further validate whether lack of fibrillin-1 promotes adipogenesis, we used mouse embryonic fibroblasts (MEFs) isolated from the global fibrillin-1 knockout and Wt littermates and differentiated them into adipocytes using the adipogenic cocktail. The lipid droplets were visualized by perilipin staining on day 10 (Fig. 2.6H). The fibrillin-1 knockout cells demonstrated ~1.5-fold higher perilipin staining intensity compared to Wt cells. This data was also supported by mRNA expression analysis from mature day 10 adipocytes. As expected, *Fbn1* mRNA was detectable only in the Wt but not the KO cells (Fig. 2.6I). In the absence of fibrillin-1, the adipogenic markers *Pparg*, *Adipoq*, and *Cebpa* were significantly upregulated (Fig. 2.6I).
Overall, these results confirmed our hypothesis that lack of fibrillin-1 during adipogenesis enhances differentiation. Therefore, fibrillin-1 should have an inhibitory role in this process.

2.5.6 Fibrillin-1 restricts adipogenic differentiation in the early commitment phase

To directly test whether fibrillin-1 protein inhibits adipogenic differentiation, we employed recombinant proteins produced by HEK293 cells. Since full length fibrillin-1 cannot be generated

recombinantly due to its propensity to aggregate [*Lin et al., 2002*], we used two established recombinant halves of human fibrillin-1 (rFBN1-N, rFBN1-C) that span the entire protein, except the N- and C-terminal pro-peptides (Fig. 2.7A) [*Jensen et al., 2001*]. We first tested whether MSCs adhere and interact with immobilized rFBN1-N or rFBN1-C over a period of 2 h using a standard cell attachment assay. MSCs strongly adhered to the C-terminal rFBN1-C similar to the positive control (PC) plasma fibronectin [*Veevers-Lowe et al., 2011*], whereas only background binding was observed for the N-terminal rFBN1-N fragment (Fig. 2.7B). Since adipogenic differentiation experiments require MSCs to adhere to the culture flasks, and since we observed differences for rFBN1-N and rFBN1-C in cell adherence, we used soluble recombinant proteins in the following experiments to study the consequence of fibrillin-1 in adipogenic differentiation. MSCs extracted from the bone marrow of Wt mice were differentiated for 10 d with adipogenic cocktail in the presence or absence of 50 µg/mL rFBN1-N or rFBN1-C and subjected to Oil red O staining, followed by quantification of the number and size of adipocytes (Fig. 2.7C-E). Treatment with rFBN1-C significantly disrupted the formation of adipocytes when added either during the commitment phase from days 1-4 (70%) or during the entire time course (90%) of the adipogenic differentiation compared to the buffer control (Fig. 2.7C,D). For both treatment regimens, we also observed significantly reduced adipocyte sizes (~40-50%) (Fig. 2.7C,E). In contrast, the size and number of adipocytes were not altered when rFBN1-N was present in both experimental setups (Fig. 2.7C-E). Cell viability was not affected at d10 by the addition of either buffer alone (TBS/2 mM Ca^{2+}, BC), or 50 µg/mL rFBN1-N or rFBN1C in this buffer compared to the positive control which contained only the adipogenic cocktail (Fig. 2.7F). To determine whether inhibition in the lipid accumulation was accompanied by changes in adipogenic gene expression markers, total RNA was extracted from the cells at the experimental endpoint (10 d) and real-time qPCR analysis

was performed. The adipogenic markers *Pparg*, *Cebpa, Adipoq*, and *Glut4* were upregulated after differentiation, as expected. Addition of rFBN1-C reduced the mRNA levels significantly for all adipogenic markers (Fig. 2.7G). However, the presence of rFBN1-N did not significantly affect any of these adipogenic mRNA levels (Fig. 2.7G). The endogenous fibrillin-1 mRNA levels and the extracellular fibrillin-1 deposition was significantly downregulated after adipocyte differentiation, and addition of the soluble recombinant fragments did not alter those parameters (Fig. 2.7H,I). Since fibrillin-1 deficiency enhanced adipogenic differentiation of MSCs and addition of rFBN1-C inhibited adipogenesis *in vitro* under Wt conditions, we attempted to rescue fibrillin-1 deficiency of mgR/mgR MSCs with rFBN1-C. Addition of rFBN1-C indeed normalized the enhanced adipogenic differentiation properties of mgR/mgR MSCs to Wt levels (Fig. 2.7J). Altogether, these data established i) that fibrillin-1 protein inhibits adipogenic differentiation, ii) the presence of fibrillin-1 during the commitment phase is sufficient for this inhibition, and iii) this activity is conferred through the C-terminal half of fibrillin-1.

2.5.7 Fibrillin-1 inhibits adipogenic differentiation via pAKT

It is well known that fibrillin-1 sequesters directly or indirectly several bioactive factors such as TGF-β, BMPs and the osteoclastogenic cytokine RANKL [*Tiedemann et al., 2013*]. Therefore, we hypothesized that fibrillin-1 may regulate adipocyte differentiation through sequestration of insulin in the adipogenic cocktail. Surface plasmon resonance spectroscopy with immobilized fibrillin-1 fragments showed for rFBN1-C a strong binding interaction with soluble insulin with a K_D of 184 ± 28.8 nM. rFBN1-N also interacted with insulin, but with a considerably lower K_D of 404 ± 90 nM (Fig. 2.8A). We also verified that none of the other components in the adipogenic cocktail (dexamethasone, indomethacin, IBMX) interacted with the fibrillin-1 fragments (Fig.

S2.6). Moreover, the rFBN1-C-mediated inhibition of adipogenesis was partially rescued when increasing concentrations of insulin (0.75 nM - 7.5 μM) were added to the adipogenic cocktail together with rFBN1-C (Fig. 2.8B, left panel). Although high insulin concentrations (7.5 μM) increased adipogenesis ~2-3-fold under buffer control and rFBN1-N conditions, it did elevate adipogenesis by ~20-fold when rFBN1-C was present, compared to the lowest insulin concentration used (Fig. 2.8B, right panel). Thus, the inhibition of adipogenesis mediated by rFBN1-C was partially rescued by increasing concentrations of insulin.

Since insulin is an essential regulator of adipogenic differentiation of MSCs, we hypothesized that the mechanism by which fibrillin-1 regulates adipogenesis acted (at least partially) through the insulin signaling pathway (PI3K/AKT/mTOR). Therefore, we incubated Wt MSCs with rFBN1-N or rFBN1-C for 24h or 72h together with the adipogenic cocktail during the early commitment phase. The presence of rFBN1-C for 72h significantly inhibited phosphorylation of AKT (Ser473), whereas the presence of rFBN1-N did not (Fig. 8C). We further tested if MSCs isolated from both male and female mgR/mgR mice (reduced fibrillin-1) differentiated for 10 d into mature adipocytes also exhibited an altered insulin signaling pathway. Consistent with the cell culture data, in the presence of basal insulin levels in the adipogenic cocktail, MSCs from mgR/mgR mice showed a significant increase (~2.4-fold) in AKT phosphorylation (Ser473), compared to the Wt mice, irrespective of the biological sex (Fig. 2.8D). We then expanded this experimental setup to include selective inhibitors of PI3K (LY294002) and mTOR (rapamycin) signaling (Fig. 2.8E). Inhibition of PI3K signaling caused a substantial reduction of adipogenic differentiation of MSCs from mgR/mgR mice, however not to the level observed with Wt MSCs. Inhibition of mTOR signaling completely abrogated adipogenesis of MSCs from both Wt and mgR/mgR mice. This

data suggested i) a partial contribution of PI3K as well as an PI3K-independent contribution upstream of AKT and ii) an essential role of mTOR signaling downstream of AKT for the fibrillin-1 regulated adipogenic differentiation of MSCs.

2.6 Discussion

Individuals with MFS commonly exhibit abnormal metabolism and are frequently characterized by a lipodystrophic phenotype. A subgroup of MFS patients as well as aging patients, however, show excess adiposity and even obesity [*Erkula et al., 2002; Graul-Neumann et al., 2010; Yetman & McCrindle, 2010; Goldblatt et al., 2011; Jacquinet et al., 2014; Passarge et al., 2016; von Kodolitsch et al., 2019; Hansen et al., 2020*]. These adipose tissue abnormalities represent two extremes of the adiposity spectrum and excess adiposity often worsens the progression of aortic aneurysm formation [*Yetman & McCrindle, 2010*]. The present study shows that male mgR/mgR mice that have a reduced level of normal fibrillin-1 mimic the excess adiposity phenotype subgroup and aging individuals with MFS. Consistently, fibrillin-1 reduction also led to hypertrophic expansion of white adipocytes and a pre-diabetic phenotype. Fibrillin-1 deficient male mice showed an increased adipogenic differentiation via elevated pAKT signaling, whereas female mgR/mgR mice and male and female C1041G/+ mice were protected from excess adiposity and enhanced adipogenic differentiation. A soluble fragment spanning the C-terminal half of fibrillin-1 restrained adipogenesis i) by binding to MSCs regulating the early commitment into the adipogenic lineage, and ii) through partial insulin sequestration from the adipogenic cocktail. Both mechanisms merged in reduced pAKT signaling. Altogether, the data obtained from these *in vivo* and cell culture studies show that fibrillin-1 has an inhibitory function in the early mesenchymal commitment phase of adipogenesis and global deficiency of fibrillin-1 acts as a negative regulator of adipogenesis and tissue adiposity.

Fibrillin-1 localized in WAT to the pericellular ECM around adipocytes, overlapping with the autofluorescence emitted by elastic fibers and collagen fibrils. The general existing paradigm for

mgR/mgR mice states a reduction of fibrillin-1 to 20-25% of the wild-type level. This was determined on the mRNA levels in skin and protein levels assembled by skin fibroblast [*Pereira et al., 1999*]. However, in WAT we determined fibrillin-1 mRNA levels of ~42% in male and ~32% in female mgR/mgR mice compared to Wt littermates. Due to the fact that fibrillin-1 is crosslinked in microfibrils, extraction of fibrillin-1 for quantification by Western blotting is not reliable. Instead, we quantified deposited fibrillin-1 by IF, which showed a differential reduction on the assembled microfibril level of 90% for male mice and no significant difference for female mice. These data exemplify that the fibrillin-1 mRNA levels in the mgR/mgR mice strongly depend on the type of cells and tissues as well as on the biological sex. It also shows that the assembled microfibrils in the pericellular space not necessarily correlate with the fibrillin-1 mRNA levels. The latter aspect likely reflects differences in the degradation and turnover of microfibrils between male and female mice. We also tested the levels of fibrillin-2 in WAT to exclude possible compensatory mechanisms caused by fibrillin-1 deficiency. However, we did not find evidence for an upregulation of fibrillin-2. For the C1041G/+ mice, the normal and the mutated mRNA allele were present at approximately similar levels in male and female mice, correlating well with similar fibrillin-1 protein levels between C1041G/+ and wild-type mice. This suggests that the originally reported haploinsufficiency caused by the C1041G missense mutation was only present on the level of assembled fibrillin-1 containing microfibrils, but not on the mRNA level [*Judge et al., 2004*]. MAGP-1 is an important structural component of fibrillin-1 containing microfibrils, and ablation of MAGP1 in mice results in an obese phenotype via increased TGF-β signaling [*Craft et al., 2014; Craft, 2015; Walji et al., 2016*]. Therefore, we tested MAGP1 mRNA levels in both mgR/mgR and C1041G/+ mice but observed no significant differences compared to the Wt littermates, excluding the possibility that MAGP1 has a role in the observed adipose phenotypes.

Overall, our data show that reduction of fibrillin-1 protein in microfibrils is sufficient to lead to increased adiposity. A missense mutation in fibrillin-1, however, has much milder phenotypic consequences with respect to adipose tissue. Therefore, the level of fibrillin-1 protein in WAT determines adiposity and can explain the phenotypic differences between the two mouse models.

A distinct sexual dimorphism was observed at various levels in mgR/mgR mice. Male mutant mice developed insulin resistance with excess fat deposition and a higher proportion of hypertrophic adipocytes, whereas female littermates were protected from these phenotypic changes. This is consistent with a report showing that estrogen protected Wt female mice on a high-fat diet from adipocyte hypertrophy and insulin resistance [*Stubbins et al., 2012*]. Also consistent with these findings is that postmenopausal women undergoing hormone replacement therapy by exogeneous treatment of estrogen displayed improved insulin sensitivity [*Salpeter et al., 2006*]. It also has been shown that 17-β estradiol protects against the progression of thoracic aortic aneurysm (TAA) by increasing fibrillin-1 secretion from smooth muscle cells, whereas androgens accentuated the severity of TAA [*Son et al., 2005; Zhao et al., 2007; Renard et al., 2017; Tashima et al., 2020*]. Therefore, it is likely that female sex hormones play a major role in the protective metabolic and adipose tissue phenotype of female mice by increasing fibrillin-1 protein synthesis in adipocytes. This view correlated well with our results demonstrating that female mgR/mgR and C1041G/+ mice had increased fibrillin-1 protein levels in deposited microfibrils in WAT and showed a protective metabolic phenotype, compared to male mgR/mgR and C1041G/+ mice. We predict that increased deposition of fibrillin-1 translates into improved organization of the adipocyte pericellular ECM that in turn exerts a stabilizing role in terms of adipose tissue expansion and metabolism. The data also correlate with the fact that MSCs harvested from male and female MFS

mice and cultured in the absence of sex hormones displayed similar fibillin-1 levels and behaved similarly in terms of adipogenesis. Although, sexual dimorphism has been widely reported with respect to adipose tissue deposition and obesity in humans, until now no study has addressed potential sexual dimorphisms of adipose tissues in human MFS patients. Future studies will have to investigate the role of sex hormones in fibrillin-1 regulated adipogenesis in mouse models and cell culture and assess correlations with MFS patients who are either lipodystrophic or overweight.

In line with a previous study [*Davis et al., 2016*], we demonstrate with cell culture differentiation experiments that fibrillin-1 is synthesized, secreted, and assembled at the MSC stage with qualitatively long fibers, and in lower amounts at the mature adipocyte stage with shorter fibers. This correlates with the fibrillin-1 mRNA expression levels at the early and late stages of adipocyte differentiation, and it shows that microfibrils are turned over and remodeled during in vitro adipogenesis. Global reduction of fibrillin-1 in the mgR/mgR mice or a complete knockout of fibrillin-1 in MEFs clearly shows that fibrillin-1 is required in the early phase to inhibit excess adipogenic differentiation. Further, our results demonstrate that addition of soluble C-terminal rFBN1-C, but not the N-terminal rFBN1-N fragment, during the commitment phase (d 1-4) or during the entire adipogenic differentiation (d 1-10) similarly inhibited adipogenic differentiation of MSCs (number and size of mature adipocytes) by decreasing the expression of early and late adipogenic markers. This solidifies that fibrillin-1 acts in the early commitment phase as a negative regulator of adipogenesis, and that the C-terminal half is sufficient for this activity. Additionally, our cell binding data demonstrate that MSCs bind to rFBN1-C but not the rFBN1-N fragment, suggesting the fibrillin-1 binding site for MSCs is localized within the C-terminal half of fibrillin-1 which contains an integrin and several heparan sulfate binding sites [*Pfaff et al., 1996; Sakamoto*

et al., 1996; Tiedemann et al., 2001; Bax et al., 2003; Sabatier et al., 2014]. Indeed, the major fibrillin-1 integrin receptors (α5β1 and αvβ3), and several syndecans and glypicans are present on MSCs [*Valdivia et al., 2020; Yu et al., 2020*]. Integrins (α5 and αv) and syndecan-1 are also known to negatively control MSC proliferation and adipogenic lineage differentiation [*Zaragosi et al., 2015; Morandi et al., 2016; Yu et al., 2020; Ruiz-Ojeda et al., 2021*]. Thus, it is possible that fibrillin-1 regulates adipogenesis either via integrins through the RGD binding site located in the TB4 domain of fibrillin-1, or through the three heparan sulfate binding sites localized in the C terminal half [*Tiedemann et al., 2001; Ritty et al., 2003*], or a combination of both. It is known that the RGD motif in fibrillin-1 initiates the integrin downstream targets FAK and Src [*Zeyer et al., 2019; Zhang et al., 2021*], and FAK activation negatively regulates adipogenesis via the insulin signaling PI3K/AKT/mTOR cascade [*Lee et al., 2017; Hyvari et al., 2018; Kim et al., 2020*]. This is consistent with our results showing that deficiency of fibrillin-1 enhanced adipogenesis by increased pAKT signaling, and rFBN1-C containing the integrin binding site inhibited pAKT signaling. This was further confirmed by using a specific PI3K inhibitor which rescued enhanced adipogenesis observed under fibrillin-1 deficient conditions. We also identified that fibrillin-1 directly interacts with insulin, a key adipogenic hormone that induces adipogenic differentiation [*Klemm et al., 2001*]. Insulin interacted with both the N- and the C-terminal halves of fibrillin-1, albeit with a higher affinity with the C-terminal rFBN1-C. These data show that there are more than one binding sites for insulin present on fibrillin-1. Importantly, the inhibition of adipogenesis by rFBN1-C was rescued by increasing concentrations of insulin in the cell culture adipogenesis assay. This shows the ability of fibrillin-1 to sequester insulin, which is an additional mechanism contributing to the inhibition of adipogenic differentiation. Taken together, these data show that

fibrillin-1 negatively regulates adipogenic differentiation via PI3K/AKT/mTOR cascade, by cell binding and insulin sequestration mechanisms.

Some MFS mutations render fibrillin-1 more susceptible to proteolysis in vicinity of the mutated site, whereas other MFS mutations do not increase protease susceptibility, depending on the location and the mutated amino acid residues [*McGettrick et al., 2000; Reinhardt et al., 2000; Kirschner et al., 2011*]. Individuals with TAA/MFS indeed show increased levels of circulating fibrillin-1 fragments [*Marshall et al., 2013*]. That study used sandwich ELISAs containing capture and detector antibody pairs that were able to detect circulating proteolytic fragments from the N-terminal half of fibrillin-1 in plasma. The study result predicts that there are also circulating fragments derived from the C-terminal half of fibrillin-1, possibly similar to the rFBN1-C fragment used in the present study. Such circulating fibrillin-1 fragments may inhibit adipogenesis in a negative feedback mechanism which would lead to the frequently observed lipodystrophic phenotypes. In MFS patients with an overweight phenotype, dependent on the location and identity of the mutations in fibrillin-1, there might be less circulating fibrillin-1 fragments, or the fragments adopt a different conformation, which may repress the adipose-inhibiting properties. For mgR/mgR mice, such a scenario is likely, because it is a hypomorph model with reduced levels of normal fibrillin-1 that should not be susceptible to proteolytic fragmentation. In this context it will be important to define better the identity of circulating fibrillin-1 fragments in MFS patients with a lipodystrophic versus overweight phenotypes.

Taken together our findings demonstrate that reduction of fibrillin-1 in the adipocyte pericellular ECM enhances adipocyte hypertrophy, thereby leading to excess adipose tissue expansion and

deposition. Further, adipose tissue homeostasis is maintained by fibrillin-1 through inhibition of the insulin signaling pathway in the early adipogenic commitment phase by cell binding and insulin sequestration. This study thus identifies the extracellular matrix protein fibrillin-1 as an important regulator of adipose tissue development, homeostasis, and function.

2.7 Acknowledgements

We express our gratitude to Dr. Francesco Ramirez for providing *Fbn1*$^{mgR/mgR}$ mice. We thank Dr. Dirk Hubmacher for kindly providing mouse embryonic fibroblasts from *Fbn1*$^{-/-}$ mice. We would also like to thank Rajpreet Kaler for quantifying adipocytes, Turney McKee for performing some preliminary experiments, and Valentin Nelea for executing the SPR analyses.

Declarations of Interest: None

Author contributions

MLM, KT, SV, and DPR conceptualized the study, contributed to the design of the experiments, and wrote or edited the manuscript. MLM and KT performed all experiments and analyzed the data. JF provided resources for the project and contributed to the writing. DPR and SV supervised, acquired the funding, and provided the resources for the project.

Funding

This work was supported by the Canadian Institutes of Health Research (MOP-137091 to SK and DPR; PJT-162099 to DPR), the Marfan Foundation (USA), and the Fonds de recherche de Quebec (fellowship to MLM).

2.8 Figures and supplemental information

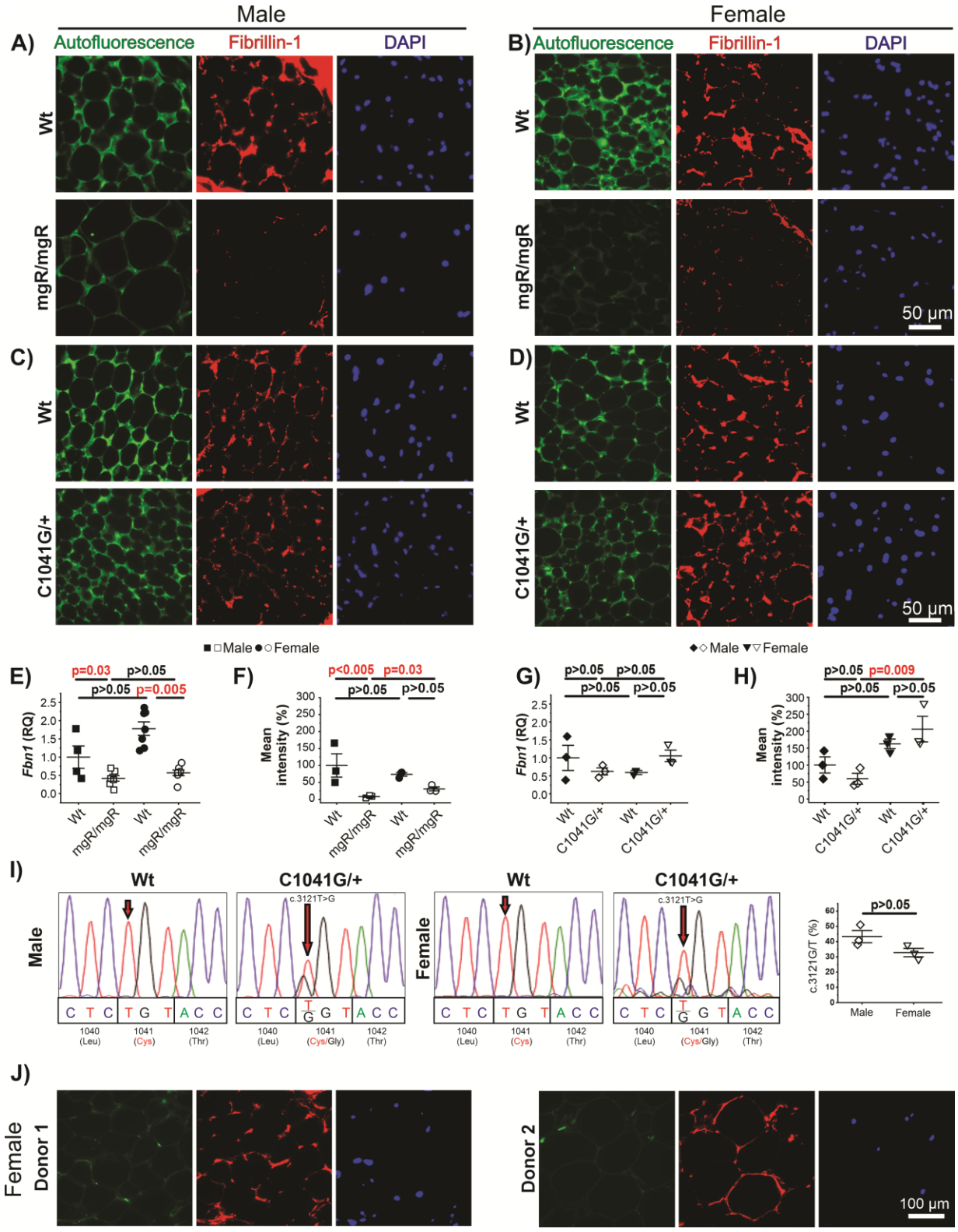

Figure 2.1. Fibrillin-1 in mouse and human white adipose tissues. (Figure legend next page)

Figure 2.1. Fibrillin-1 in mouse and human white adipose tissues. (Figure legend continued)

Subcutaneous inguinal white adipose tissue (iWAT) was isolated and analyzed from Wt and mgR/mgR mice at 16 weeks or Wt and C1041G/+ mice at 35 weeks. **(A-D)** Immunofluorescence analysis of fibrillin-1 in male **(A)** and female **(B)** mgR/mgR mice, and male **(C)** and female **(D)** C1041G/+ mice, compared to their respective Wt littermates. Immunofluorescence images: green channel (Autofluorescence), red channel (Fibrillin-1), Blue channel (DAPI, nuclei stain). (**E, G)** Real-time qPCR analyses of *Fbn1* mRNA levels normalized to *Gapdh,* isolated from iWAT of mgR/mgR or C1041G/+ mice, compared to Wt littermates. (**F, H)** Quantification of the deposited fibrillin-1 intensity from immunofluorescence images such as shown in **(A-D)** using ImageJ. The mean intensity of Wt mice was set to 100% and all other mice were normalized to that data point. **(E-H)** Each data point denotes an individual mouse, error bars represent ± SEM, n=3-7 mice per group (Wt and mgR/mgR mice) and n=2-3 mice per group (Wt and C1041G/+ mice). Significance was evaluated by two-way ANOVA with Bonferroni post-test. Symbol legend: Wt and mgR/mgR male (squares) and female (circles) mice; Wt and C1041G/+ male (diamonds) and female (triangles) mice. **(I)** Sequence analysis of *Fbn1* mRNA isolated from white adipose tissue of heterozygous C1041G/+ mice and Wt littermates. Total RNA was extracted from subcutaneous white adipose tissue (iWAT) of both male and female mice, reverse transcribed to cDNA, PCR-amplified and Sanger-sequenced. Left panels show the sequencing chromatograms for Wt mice and C1041G/+ heterozygous male and female mice with the c.3121T>G peak indicated by red arrows. Right panel shows the quantification of the c.3121G missense allele (coding for G1041) relative to the c.3121T Wt allele (coding for C1041) by peak area quantification normalized to the average of 3 other peak areas of the respective nucleotides at different positions of the same mouse using ImageJ. Experiments were performed on 3 mice for each genotype. **(J)** Immunofluorescence analysis of fibrillin-1 performed on human female WAT samples (6 donors analyzed, representative images of 2 donors are shown).

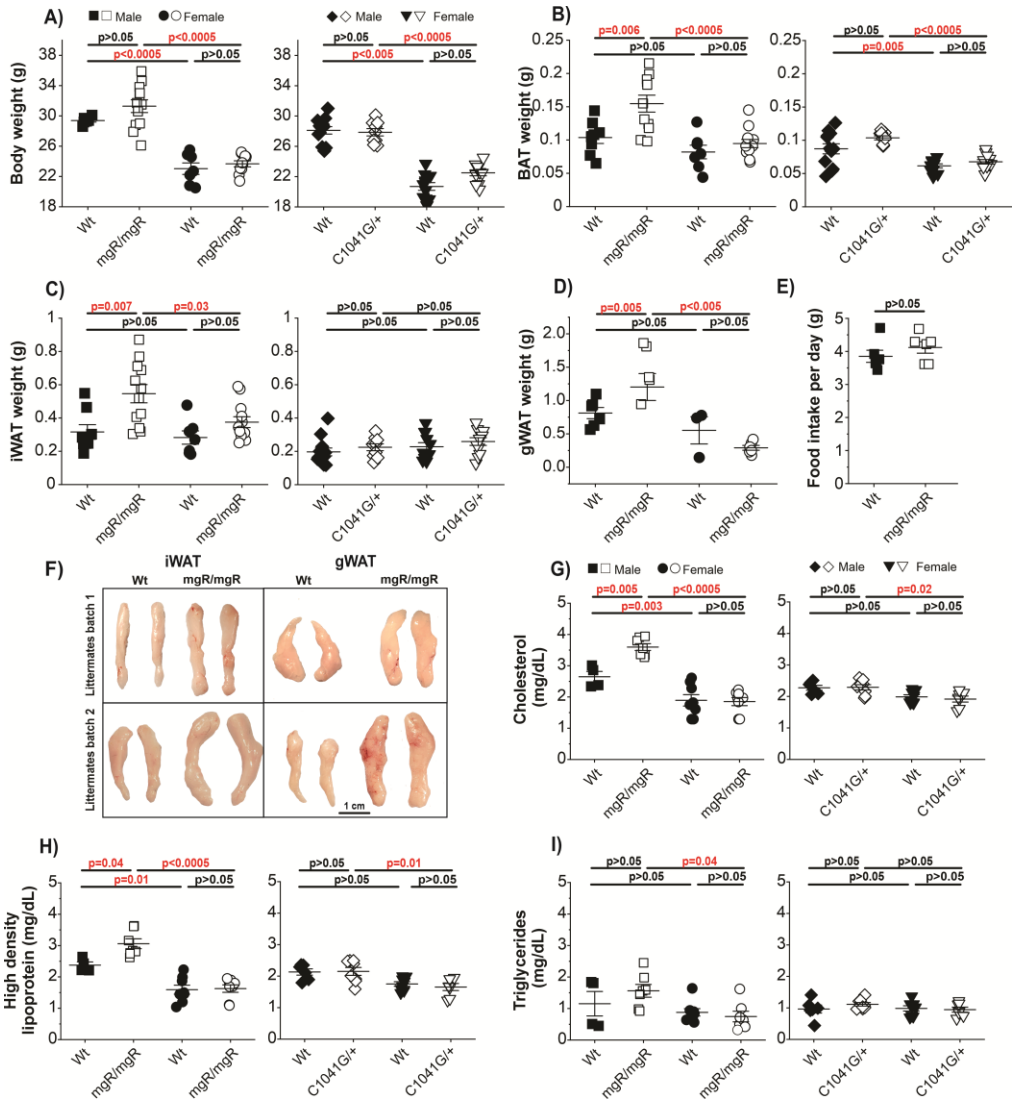

Figure 2.2. Analysis of metabolic indices of fibrillin-1 deficient mice. The parameters indicated below were analyzed in male and female Wt and mgR/mgR mice at 16 weeks or Wt and C1041G/+ mice at 35 weeks. **(A)** Whole body mass, **(B)** brown adipose tissue (BAT) weight, **(C)** inguinal or subcutaneous white adipose tissue (iWAT) weight, **(D)** gonadal or visceral white adipose tissue (gWAT) weight of mgR/mgR and C1041G/+ mice compared to their respective Wt littermates. **(E)** Food intake of mgR/mgR mice at 16 weeks of age. **(F)** Representative images of freshly isolated iWAT and gWAT of male Wt and mgR/mgR littermates. **(G)** serum cholesterol levels (mg/dL), **(H)** serum high-density lipoprotein levels (mg/dL), and **(I)** serum triglyceride levels (mg/dL) of mgR/mgR and C1041G/+ mice compared to their respective Wt littermates. Each data point represents an individual mouse and error bars represent ± SEM, n= 3-12 mice per group. Significance was assessed by two-way ANOVA with Bonferroni post-test. Symbol legend: Wt and mgR/mgR male (squares) and female (circles) mice, Wt and C1041G/+ male (diamonds) and female (triangles) mice.

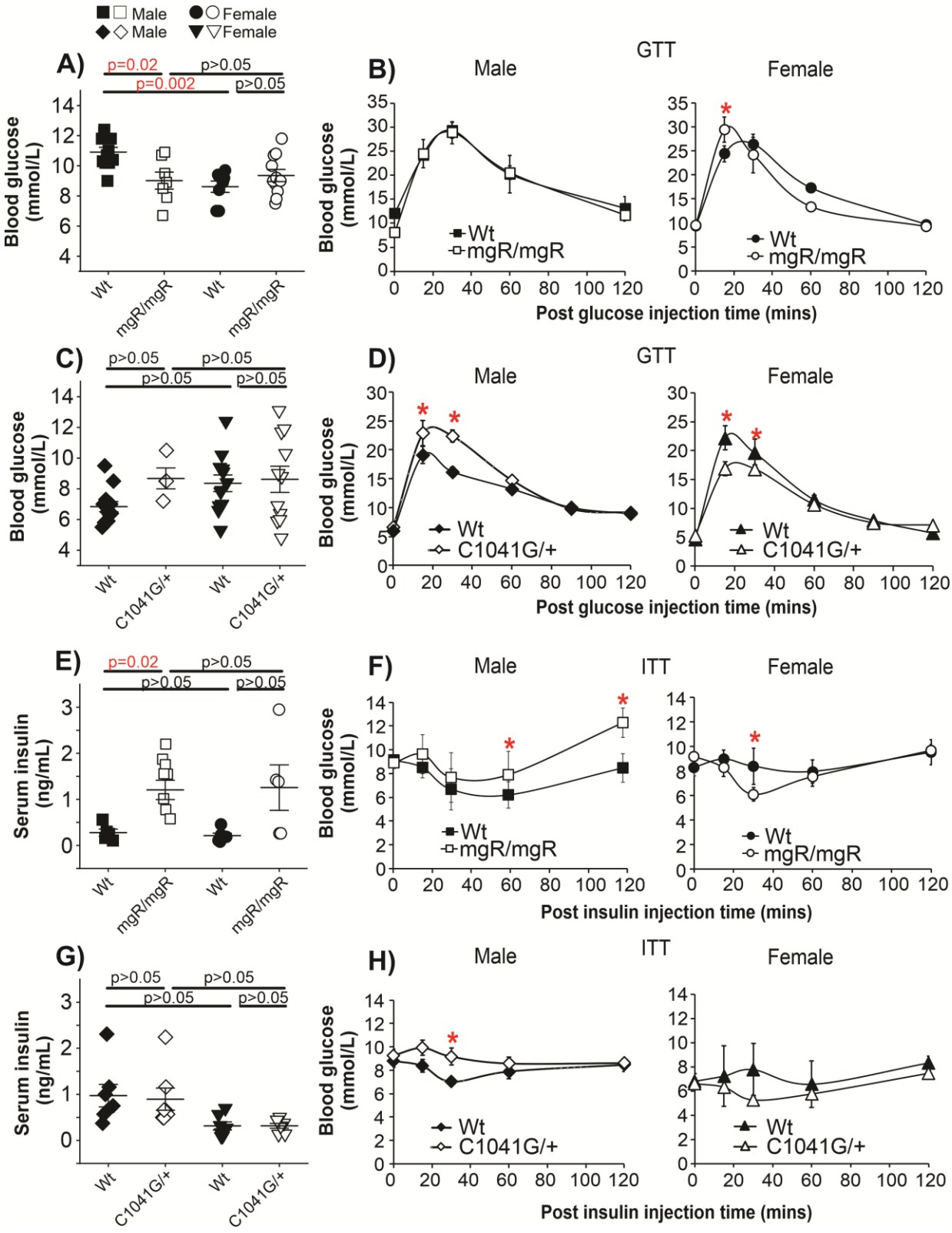

Figure 2.3. Analysis of glucose and insulin metabolism of fibrillin-1 deficient mice.
(Figure legend next page)

Figure 2.3. Analysis of glucose and insulin metabolism of fibrillin-1 deficient mice.
(Figure legend continued)

(A,C) Fasting blood glucose levels (mmol/L) determined from 16-week-old Wt and mgR/mgR mice **(A),** or 35-week-old Wt and C1041G/+ mice **(C)**. **(B,D)** Glucose tolerance test (GTT) was performed in male and female wild-type (Wt) and mgR/mgR mice after overnight fasting, by injecting 2mg/kg of glucose at 14 weeks of age **(B)**. GTT in Wt and C1041G/+ mice were performed at 20 weeks **(D)**. **(E,G)** Insulin levels (ng/mL) were determined by ELISA from the serum collected at 16 weeks from Wt and mgR/mgR mice **(E),** or at 35 weeks from Wt and C1041G/+ mice **(G)**. **(F,H)** Insulin tolerance test (ITT) was performed in male and female wild-type (Wt) and mgR/mgR mice after 6 hours of fasting, by injecting 0.75U of insulin at 15 weeks of age **(F)**. ITT in Wt and C1041G/+ mice were performed at 24 weeks **(H)**. **(A,C,E,G)** Each data point denotes an individual mouse and error bars represent ± SEM, n= 3-12 mice per group (Wt and mgR/mgR) and n=6-7 mice per group (Wt and C1041G/+). Significance was assessed by two-way ANOVA with Bonferroni post-test. **(B,D,F,H)** Data represent means ± SEM, n=3-8 mice per group. Statistics was performed using two-way ANOVA repeated measures with Bonferroni post-test and *$p<0.05$. Symbol legend: Wt and mgR/mgR male (squares) and female (circles) mice, Wt and C1041G/+ male (diamonds) and female (triangles) mice.

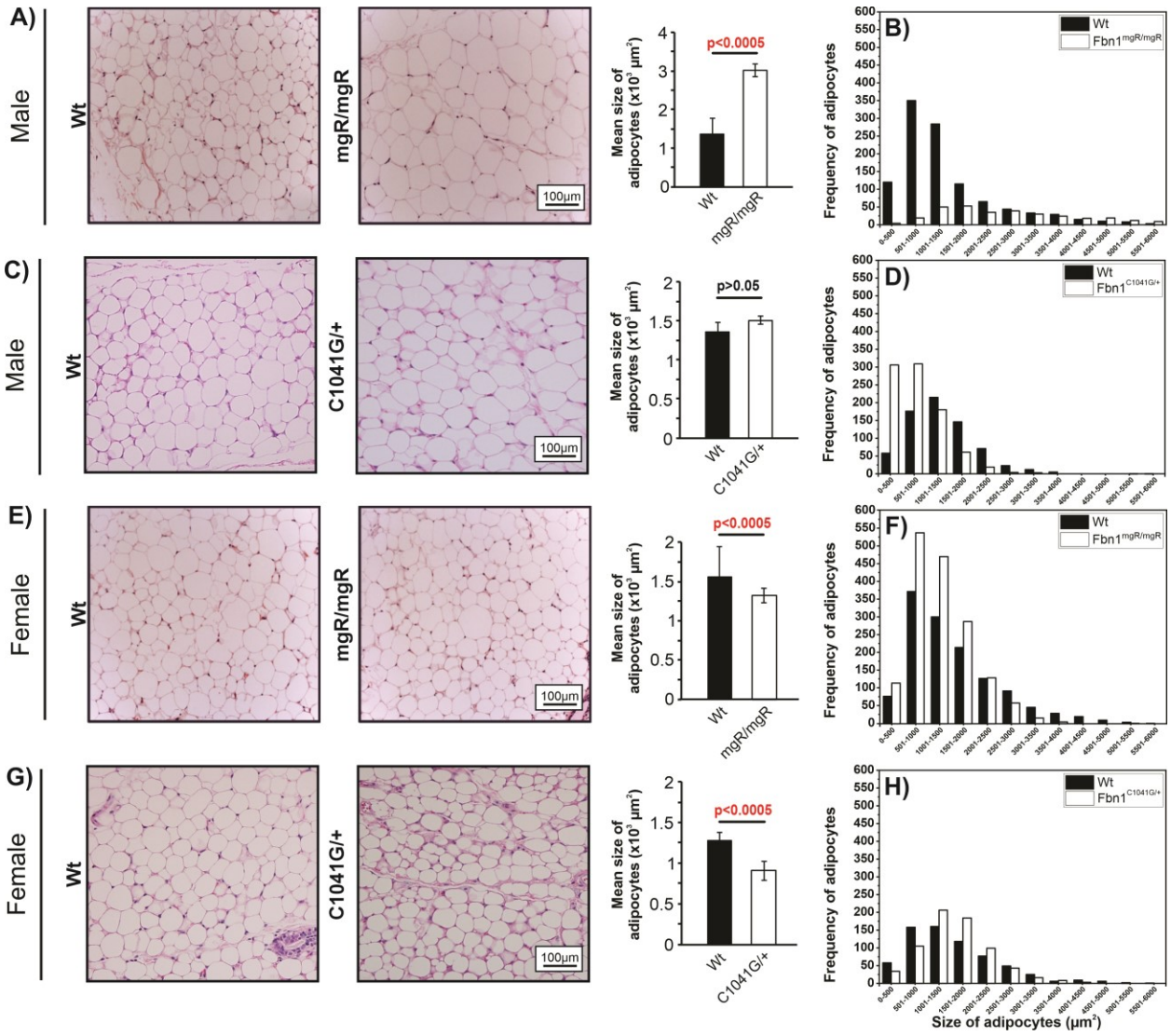

Figure 2.4. Quantification of adipocyte size in iWAT of fibrillin-1 deficient mice. The adipocyte size (area in μm^2) was quantified in the iWAT of male and female Wt and mgR/mgR mice at 16 weeks of age or C1041G/+ mice at 35 weeks of age, using ImageJ (see methods section). **(A,C,E,G)** Shown are representative images of hematoxylin/eosin-stained tissue sections of iWAT from male and female Wt and mgR/mgR mice or Wt and C1041G/+ mice as indicated. Quantification of mean areas of adipocytes are shown on the right. Data are shown as means ± SEM; Statistical analysis was performed with the unpaired student two tailed t-test**. (B,D,F,H)** Frequency histograms of iWAT adipocyte areas binned in 500 μm^2 steps of mgR/mgR **(B, F)** and C1041G/+ **(D, H)** mice. n=3 mice for each condition. The number of analyzed adipocytes for each mouse was >300.

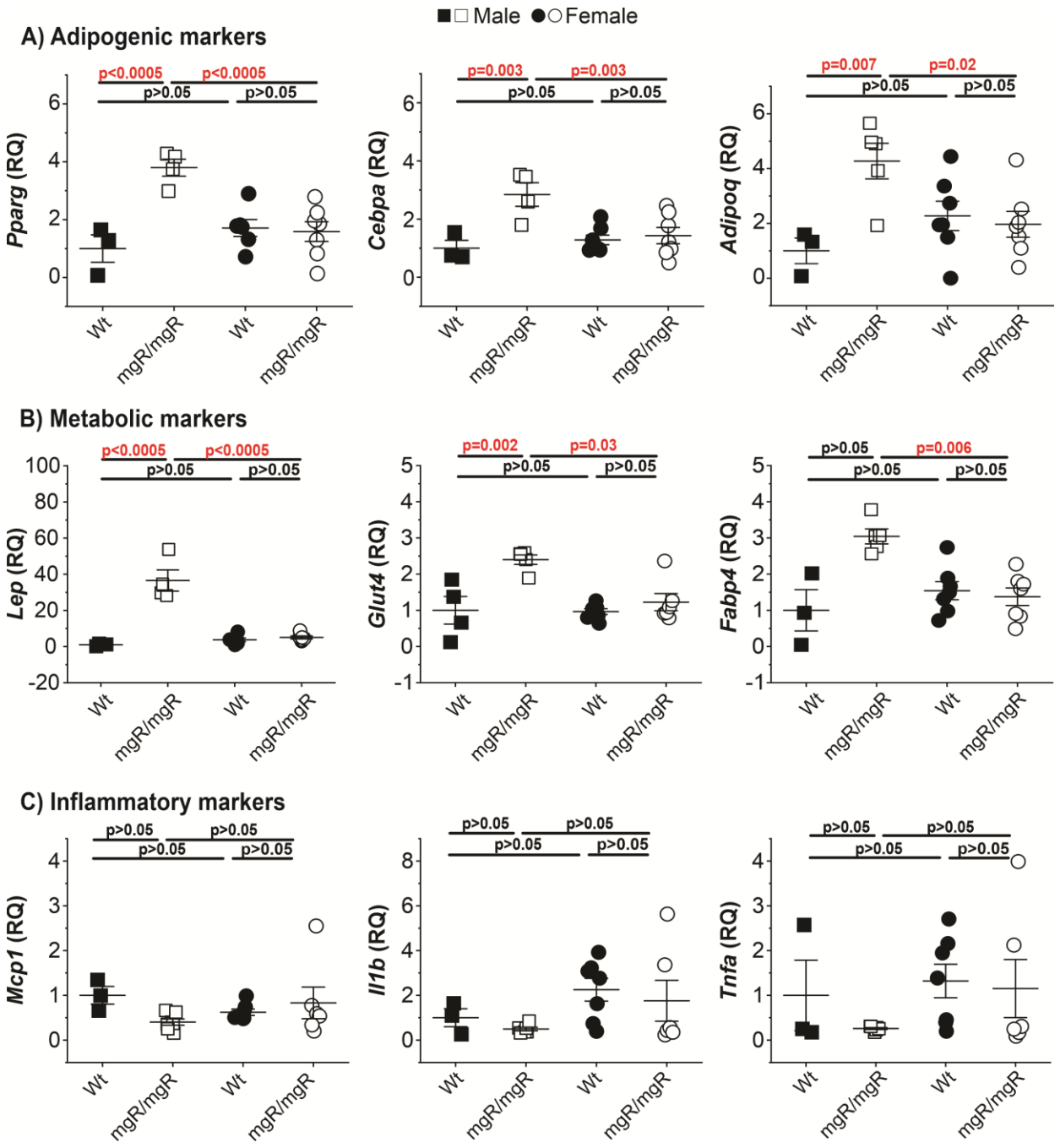

Figure 2.5. Analysis of adipogenic and inflammatory gene expression markers in iWAT of mgR/mgR mice. Real-time qPCR analyses were performed with total RNA extracted from iWAT of male and female Wt and mgR/mgR mice at 16 weeks. mRNA expression levels relative to *Gapdh* are shown in each graph. **(A)** Adipogenic markers *(Pparg, Cebpa, Adipoq),* **(B)** metabolic markers (*Lep, Glut4, Fabp4),* **(C)** inflammatory markers (*Mcp1, Il1b, Tnfa)*. Each data point represents an individual mouse and error bars are denoted as ± SEM; n= 3-7 mice per group. Significance was assessed by two-way ANOVA with Bonferroni post-test. Symbol legend: Wt and mgR/mgR male (squares) and female (circles) mice.

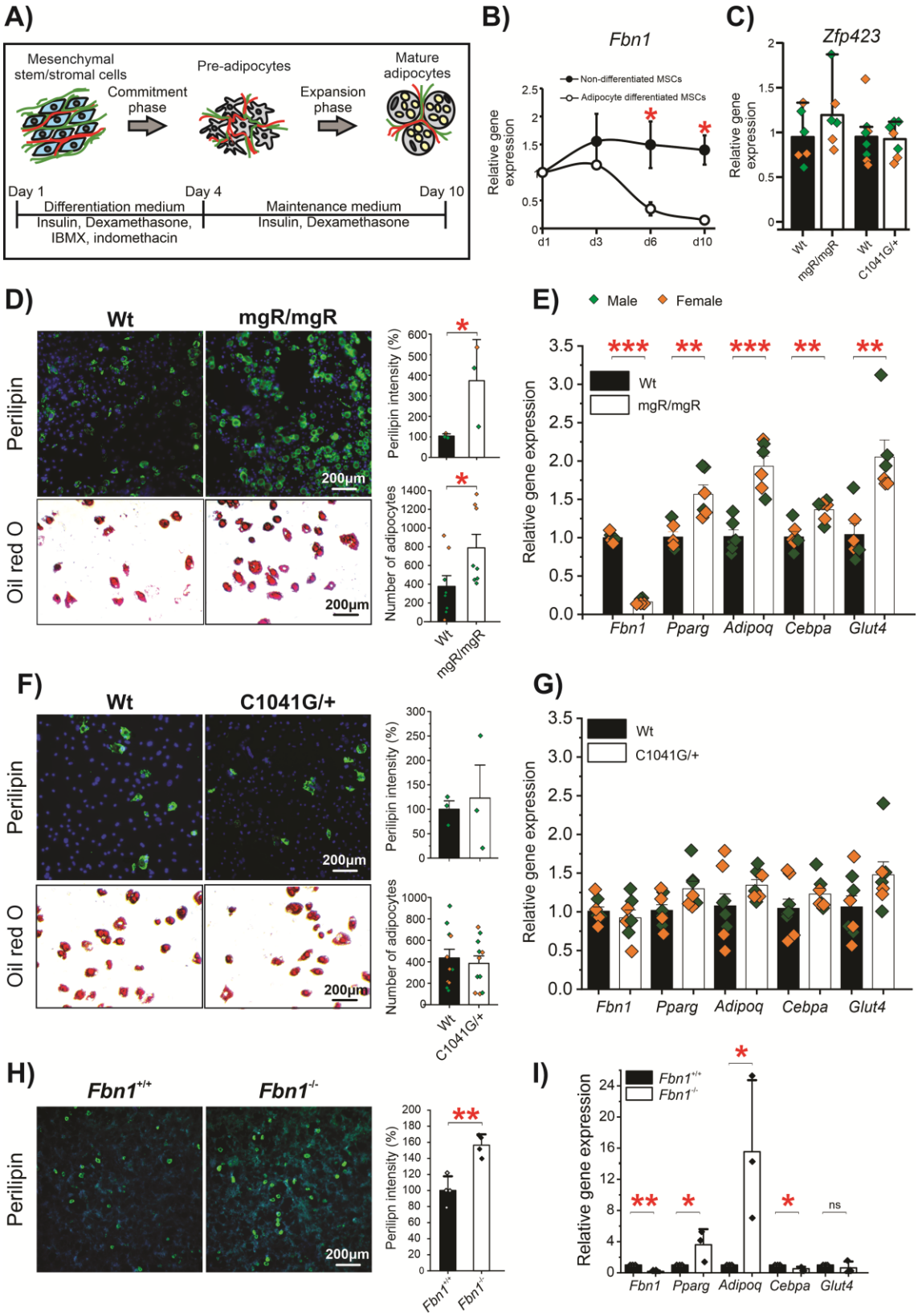

Figure 2.6. Lack of fibrillin-1 enhances adipogenic differentiation in cell culture.
(Figure legend next page)

Figure 2.6. Lack of fibrillin-1 enhances adipogenic differentiation in cell culture.
(Figure legend continued)

Primary bone marrow derived mesenchymal stem cells (MSCs) were isolated from 6–8-week-old Wt and mgR/mgR or Wt and C1041G/+ mice and differentiated into adipocytes with the adipogenic cocktail consisting of 7.5 nM of insulin, 50 µM Indomethacin, 1 µM dexamethasone, 500 mM IBMX for 4 d followed by only 7.5 nM of insulin and 1 µM dexamethasone for 10 days. **(A)** Schematic of the experimental cell culture procedure. **(B)** Real-time qPCR analysis of *Fbn1* relative to *Gapdh* at d1-10 in non-differentiated and adipocyte differentiated MSCs harvested from Wt mice. Data are means ± SD; n=2 mice. **(C)** Real-time qPCR analysis of *Zfp423*, an early pre-adipocyte marker expressed in non-differentiated MSCs isolated from mgR/mgR and C1041G/+ mice and their respective Wt littermates. **(D, F)** Representative images of adipocyte differentiated MSCs isolated from male and female mgR/mgR and C1041G/+ and their respective Wt littermates stained with perilipin and Oil red O on day 10. Quantification of the perilipin intensity (Wt was set to 100%) and Oil red O staining (counting of Oil red O-stained adipocytes) indicative for lipid accumulation is shown to the right of the images. **(E, G)** Real-time qPCR analyses of *Fbn1* and adipogenic markers *Pparg*, *Adipoq*, *Cebpa*, and *Glut4* relative to *Gapdh* after 10 days of adipogenic differentiation. Relative gene expression of Wt was set to 1. Each data point in figures C-G represents an individual mouse. Data are means ± SEM. Symbol color representation: Cells from male (green diamonds) and from female (orange diamonds) mice. **(H)** Representative images of Mouse Embryonic Fibroblast (MEF) cells isolated from Wt ($Fbn1^{+/+}$) and fibrillin-1 knockout ($Fbn1^{-/-}$) pups, differentiated into adipocytes for 10 days and stained for perilipin. Quantification of the perilipin staining intensity is shown to the right of the images. The intensity of the $Fbn1^{+/+}$ MEFs was set to 100%. **(I)** Real-time qPCR analyses of *Fbn1* and the adipogenic markers *Pparg, Adipoq, Cebpa,* and *Glut4* relative to *Gapdh* after 10 days of adipogenic differentiation. The relative quantification of the $Fbn1^{+/+}$ MEFs for all genes was set to 1. Each data point in figure **H, I** represent experimental replicates using different passages of MEF cells. Data are means ± SD. **(B-I)** Statistics for all figures was performed using unpaired student two tailed t-test, comparing two conditions. *p<0.05, **p<0.005, ***p<0.0005.

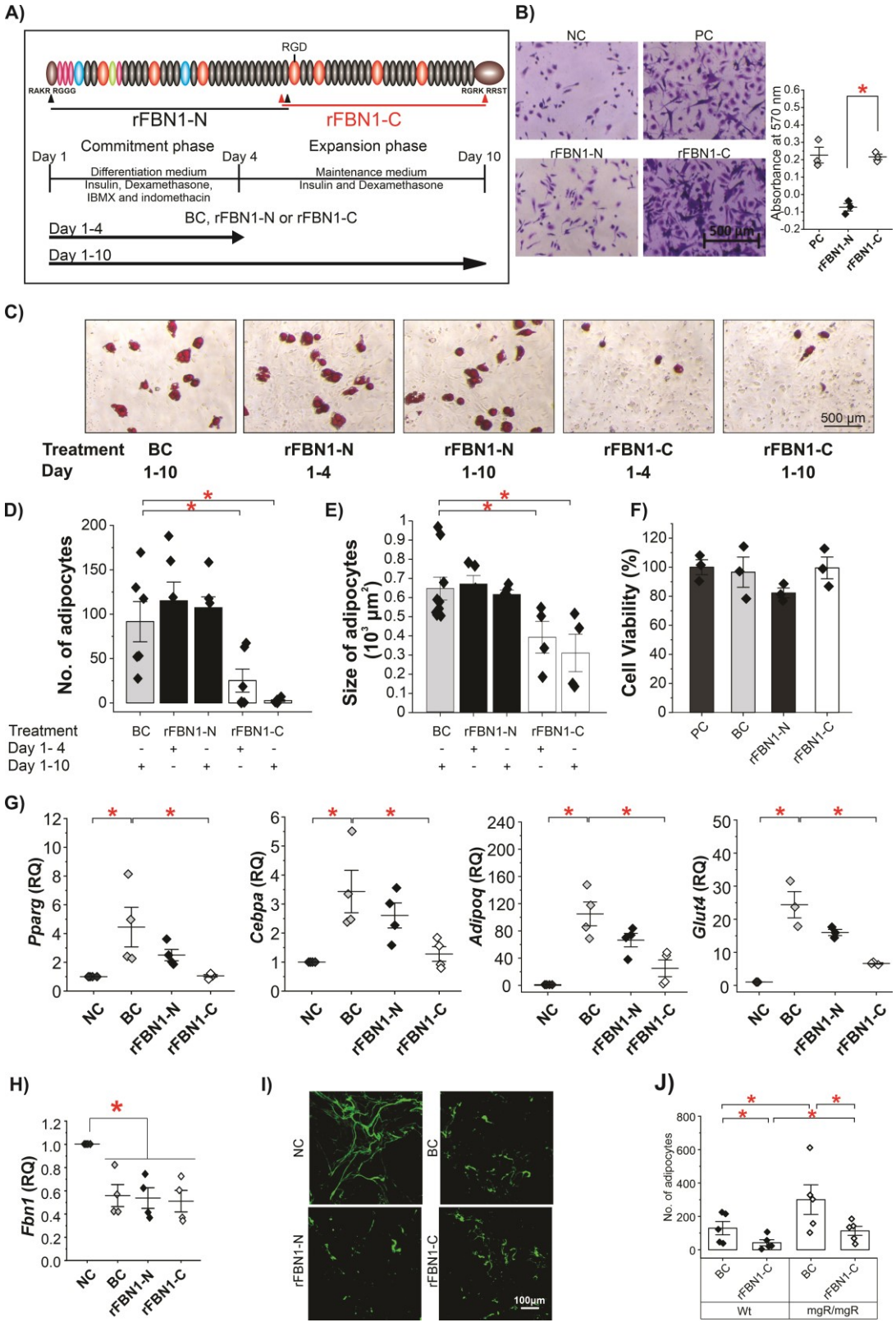

Figure 2.7. Fibrillin-1 inhibits adipogenesis in cell culture. (Figure legend next page)

Figure 2.7. Fibrillin-1 inhibits adipogenesis in cell culture. (Figure legend continued)

MSCs isolated from Wt mice were differentiated into adipocytes with the adipogenic cocktail detailed in figure legend 6 with or without the addition of TBS/2 mM Ca^{2+} (BC), or 50 µg/mL N-terminal (rFBN1-N) or C-terminal (rFBN1-C) halves of fibrillin-1. **(A)** Domain structure of fibrillin-1 and the location of the rFBN1-N (black bar) and rFBN1-C (red bar) halves of human fibrillin-1 without the propeptides (cleavage site indicated by arrowheads). Experimental timelines for the addition of BC, rFBN1-N or rFBN1-C. **(B)** Representative images of MSC adhesion on wells coated with 25 µg/mL of the negative control (NC) bovine serum albumin, the positive control (PC) plasma fibronectin, rFBN1-N, and rFBN1-C visualized by crystal violet staining. Quantification of MSC adhesion by absorbance measurements at 570 nm of the solubilized crystal violet is shown on the right. The experiment was performed in triplicate wells and each data point denotes MSCs from an individual mouse. The data is normalized to the NC. **(C)** Representative images of Oil red O staining after the addition of BC, rFBN1-N or rFBN1-C either only during the adipogenic commitment phase during day 1-4 or during the entire adipogenic differentiation procedure during day 1-10, as indicated below each figure**. (D,E)** Quantitative assessment of the number **(D)** and size **(E)** of Oil red O positive adipocytes using ImageJ. **(F)** Cell viability was determined by LIVE/DEAD cytotoxicity assay at day 10 and quantified by ImageJ. PC was set to 100%. **(G)** Real-time qPCR analyses of adipogenic markers *Pparg*, *Adipoq*, *Cebpa*, and *Glut4* were performed with total RNA extracted from non-differentiated (NC) and adipocyte-differentiated MSCs after addition of BC, rFBN1-N or rFBN1-C for 10 d during the entire course of the experiment. Relative quantification of NC was set to 1. **(H)** Real-time qPCR quantification of *Fbn1* mRNA levels on day 10 in non-differentiated and adipocyte-differentiated MSCs after the addition of BC, rFBN1-N or rFBN1-C. Relative *Fbn1* gene expression of NC was set to 1. Statistical analysis between experimental conditions compared to BC was performed using the unpaired student two tailed t-test. *$p<0.05$, **$p<0.005$, ***$p<0.0005$. **(I)** Immunofluorescence analysis of extracellular fibrillin-1 fibers on day 10 after the addition of BC, rFBN1-N or rFBN1-C. **(J)** MSCs were isolated from Wt and mgR/mgR mice of both sexes and were treated either with BC, or 50 µg/mL of rFBN1-C together with the adipogenic cocktail; Shown is the quantification of the adipocytes after Oil red O staining at day 10 of adipogenic differentiation. For the entire figure, each data point represents the analysis of MSCs isolated from an individual mouse. Data are means ± SEM; n=3 experiments with each experiment containing 1-3 biological samples and two technical replicates. Statistics was assessed by unpaired student two tailed t test with *$p<0.05$.

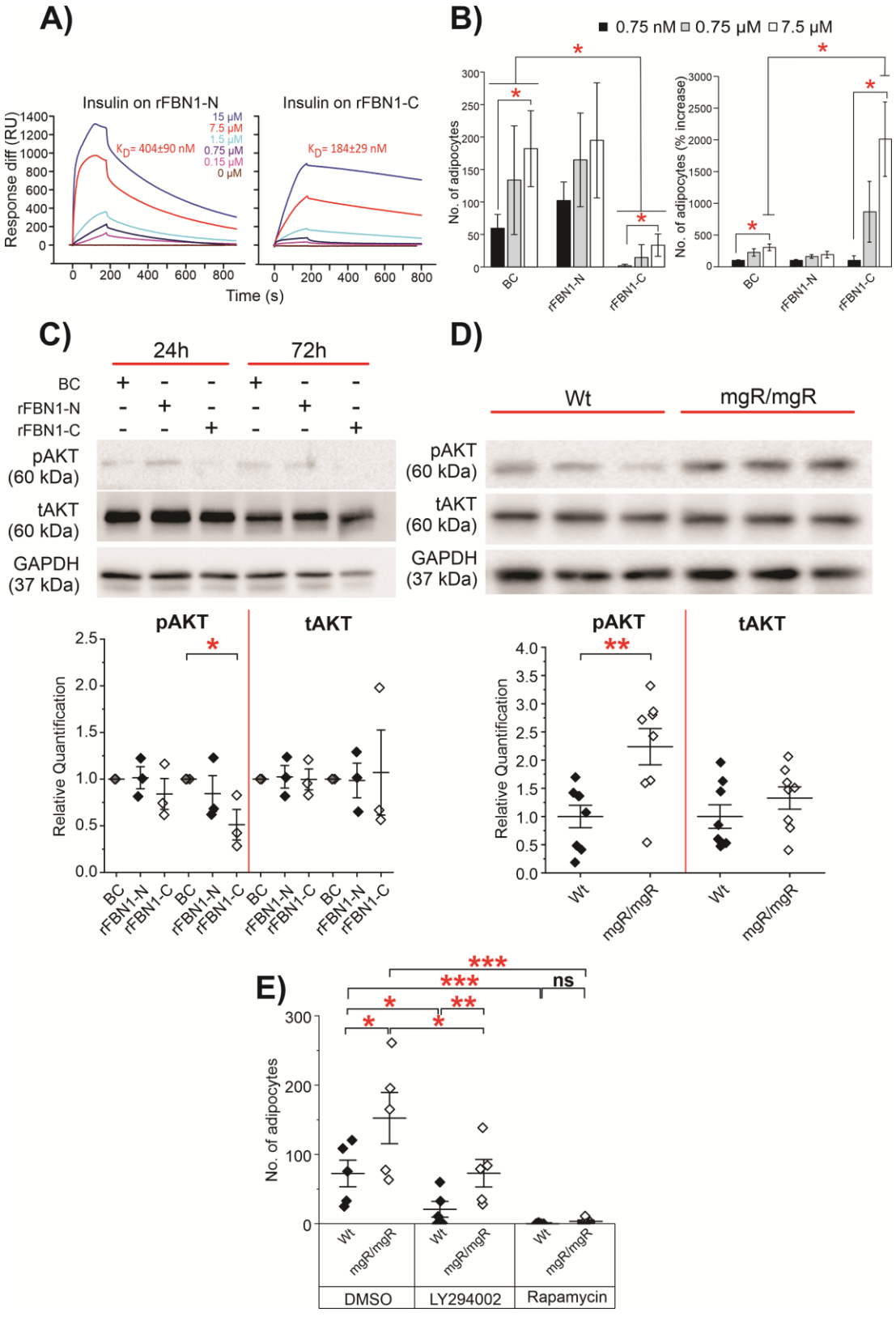

Figure 2.8. Fibrillin-1 sequesters insulin and attenuates the insulin signaling pathway. (Figure legend next page)

Figure 2.8. Fibrillin-1 sequesters insulin and attenuates the insulin signaling pathway. (Figure legend continued)

(A) Surface plasmon resonance spectroscopy of the interaction of soluble insulin with immobilized rFBN1-N or rFBN1- C. Five insulin concentrations were used in each experiment ranging from 0-15 μM. A representative experiment is shown for each condition. The experiments were repeated with similar results. Response difference (Response units, RU) on the Y axis is the difference between experimental and blank sensor chips. **(B)** Insulin sequestration experiments performed in an adipogenic differentiation experiment of MSCs isolated from Wt mice under standard conditions as detailed in Fig. 6, but with increasing concentrations of insulin (0.75 nM, 0.75 μM, 7.5 μM) present during the entire time course of adipogenesis for 10d. Shown is the quantification of the adipocytes after Oil red O staining at day 10 of adipogenic differentiation (left graph). The same data are plotted on a relative scale with the number of adipocytes at the lowest insulin concentration set to 100% (right graph); n=3-6 mice per group. The experiment was performed in duplicates with error bars denoted as ± SEM. Statistics was evaluated by unpaired student two tailed t test with *$p<0.05$. **(C)** MSCs were incubated with BC, or 50 μg/mL of rFBN1-N or rFBN1-C for 24 h and 72 h together with the adipogenic differentiation medium. Protein lysates were immunoblotted for phospho-AKT (pAKT, 60 kDa), total AKT (tAKT, 60 kDa) and GAPDH (37 kDa). A representative immunoblot of the protein lysate from one mouse is shown; n=3 mice per group. Densitometric analysis of pAKT and tAKT normalized to GAPDH is shown in the bottom panel. The average relative quantification of BC was set to 1. Each data point represents an individual mouse; error bars are denoted as ± SEM. Statistics was assessed by unpaired student two tailed t test with *$p<0.05$. **(D)** MSCs isolated from Wt and mgR/mgR male and female mice at 6 weeks of age were differentiated into adipocytes with adipogenic differentiation medium. Protein lysates were immunoblotted for pAKT, tAKT and GAPDH. Densitometric analysis of pAKT and tAKT normalized to GAPDH is shown in the bottom panel. The average relative intensity of Wt mice was set to 1; n=8 mice per condition. **(E)** MSCs were isolated from Wt and mgR/mgR mice of both sexes and treated either with a solvent control (0.01% DMSO), or with 2 μM LY294002 or 10 nM rapamycin for 10 d in addition to the adipogenic cocktail; n=5 and the experiment was performed in duplicates. Each data point represents an individual mouse. Statistics was assessed by unpaired student two tailed t test with *$p<0.05$; **$p<0.005$; ***$p<0.0005$.

Supplemental Figures

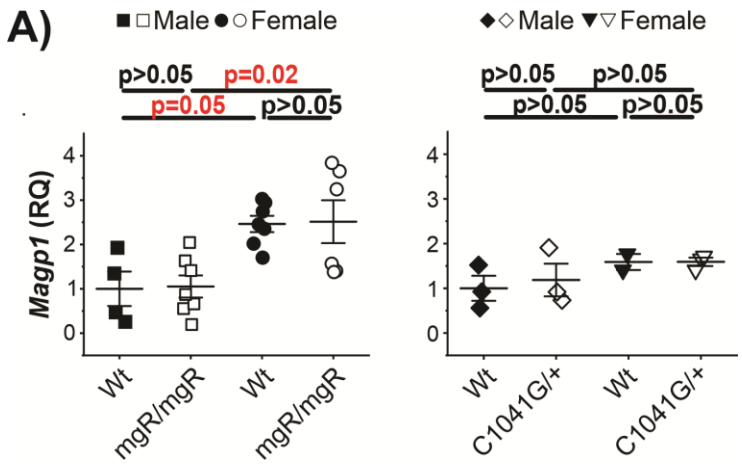

Figure S2.1. *Magp1* mRNA expression analysis in subcutaneous white adipose tissue. Real-time qPCR analysis for *Magp1* was performed with total RNA isolated from iWAT of Wt and mgR/mgR littermates, or from Wt and C1041G/+ mice. Each data point denotes an individual mouse and error bars represent ± SEM; n= 3-7 mice per group (Wt and mgR/mgR) and n=2-3 mice per group (Wt and C1041G/+). Significance was assessed by two-way ANOVA with Bonferroni post-test. Symbol legend: Wt and mgR/mgR male (squares) and female (circles) mice; Wt and C1041G/+ male (diamonds) and female (triangles) mice.

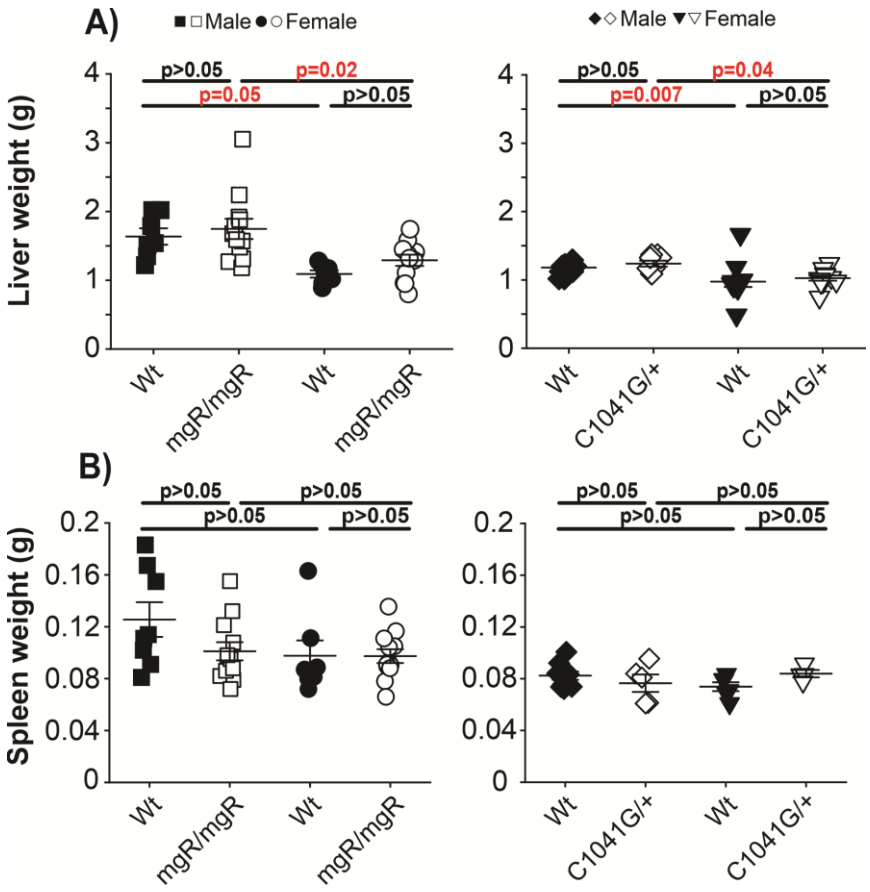

Figure S2.2. Weight analysis of liver and spleen in mgR/mgR and C1041G/+ mice. (A) Weight of livers and **(B)** weight of spleens at 16 weeks for mgR/mgR and at 35 weeks for C1041G/+ mice, compared to Wt littermates. Each data point represents an individual mouse and error bars are denoted as ± SEM; n= 6-12 mice per group (Wt and mgR/mgR), and n=6-7 mice per group (Wt and C1041G/+). Significance was assessed by two-way ANOVA with Bonferroni post-test. Symbol legend: Wt and mgR/mgR male (squares) and female (circles) mice, or Wt and C1041G/+ male (diamonds) and female (triangles) mice.

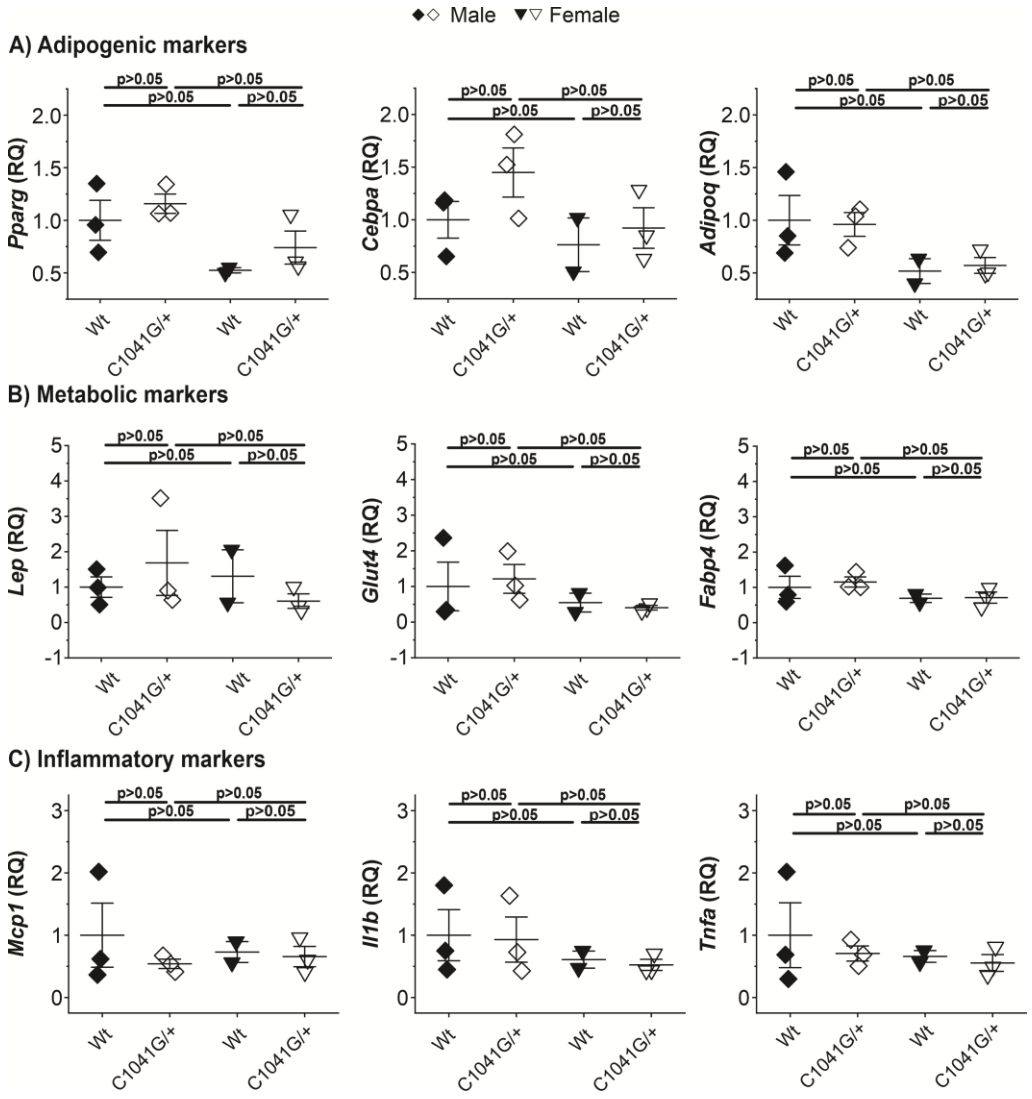

Figure S2.3. Adipogenic and inflammatory gene expression analysis of iWAT from C1041G/+ mice. Real-time qPCR analysis was performed with total RNA extracted from iWAT of male and female Wt and C1041G/+ mice at 35 weeks of age. mRNA expression levels relative to *Gapdh* are shown in each graph. **(A)** Adipogenic markers *(Pparg, Cebpa, Adipoq),* **(B)** metabolic markers (*Lep, Glut4, Fabp4),* **(C)** inflammatory markers (*Mcp1, Il1b, Tnfa)*. Each data point denotes an individual mouse and error bars represent ± SEM; n=2-3 mice per group (Wt and C1041G/+). Significance was assessed by two-way ANOVA with Bonferroni post-test. Symbol legend: Wt and C1041G/+ male (diamonds) and female (triangles) mice.

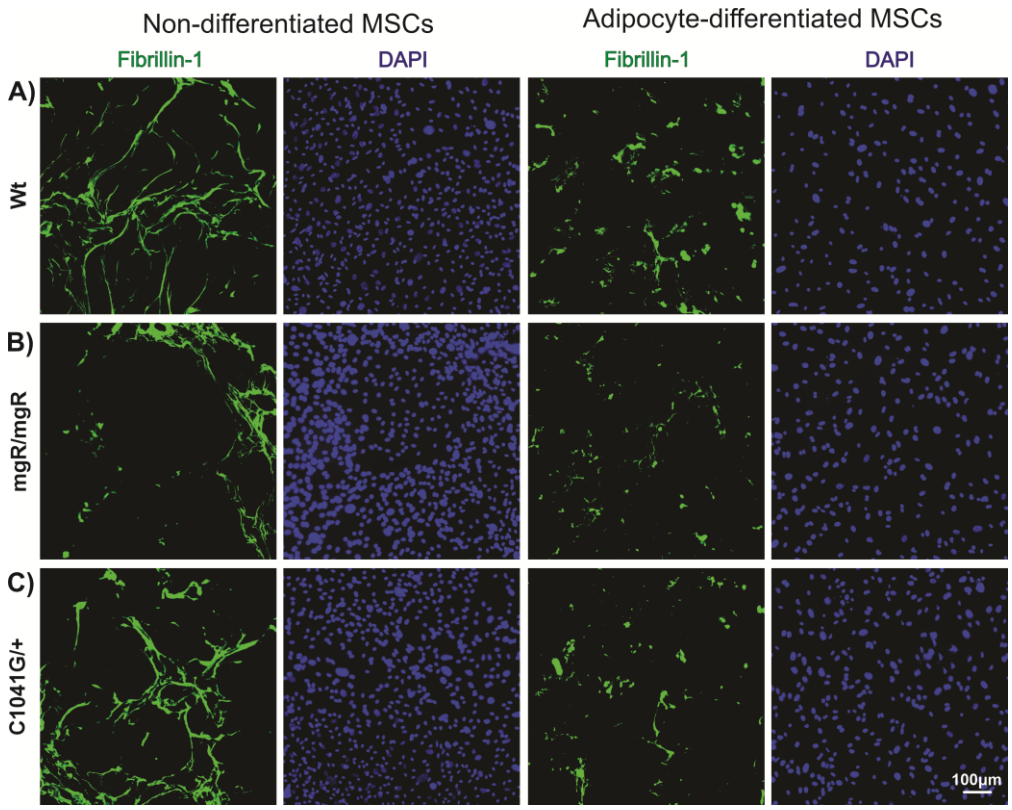

Figure S2.4. Fibrillin-1 deposition of non-differentiated and adipocyte differentiated MSCs. MSCs were isolated from Wt **(A)**, mgR/mgR **(B)** and C1041G/+ **(C)** mice and cultivated either with basal medium (non-differentiated) or with adipogenic differentiation medium (adipocyte-differentiated). At day 10 of culture, immunofluorescence analysis was performed with a specific anti-fibrillin-1 antiserum in both the conditions. Green channel (Fibrillin-1), blue channel (DAPI).

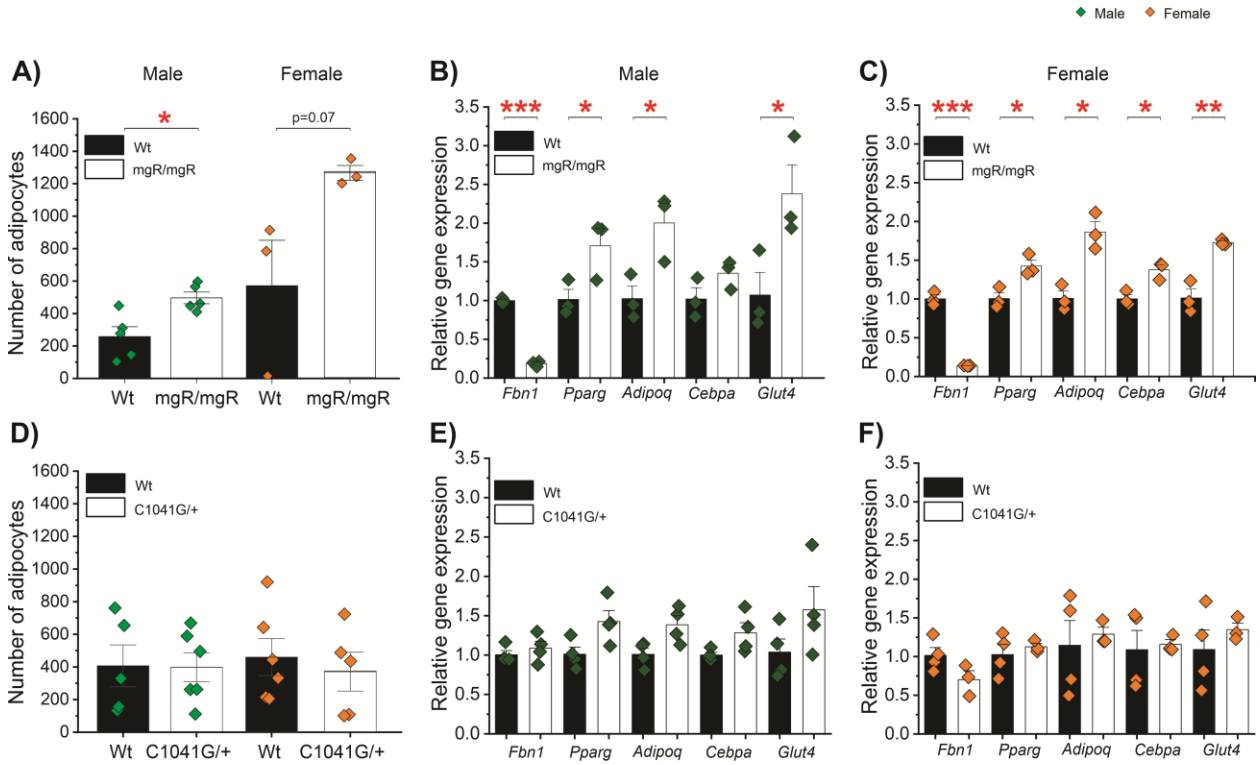

Figure S2.5. Analysis of adipogenesis and adipogenic markers after 10 days of adipocyte differentiation. The same data from figure **Fig. 6 D-G** was replotted, but male and female mice are analyzed separately and displayed in different graphs. **(A, D)** Quantification of Oil red O-stained adipocytes from male and female mgR/mgR, C1041G/+, and respective Wt mice on day 10 **(B-F)** Real-time qPCR analyses of *Fbn1* and adipogenic markers *Pparg*, *Adipoq*, *Cebpa*, and *Glut4* relative to *Gapdh* after 10 days of adipogenic differentiation from male **(B, E)** and female **(C, F)** mgR/mgR, C1041G/+, and respective Wt mice. Relative gene expression of Wt was set to 1. **(A-F)** Data are means ± SEM. Each data point represents an individual mouse. Symbol color representation: Cells from male (green diamonds) and from female (orange diamonds) mice. Statistics for all figures was performed using unpaired student two tailed t-test, comparing two conditions. *p<0.05, **p<0.005, ***p<0.0005.

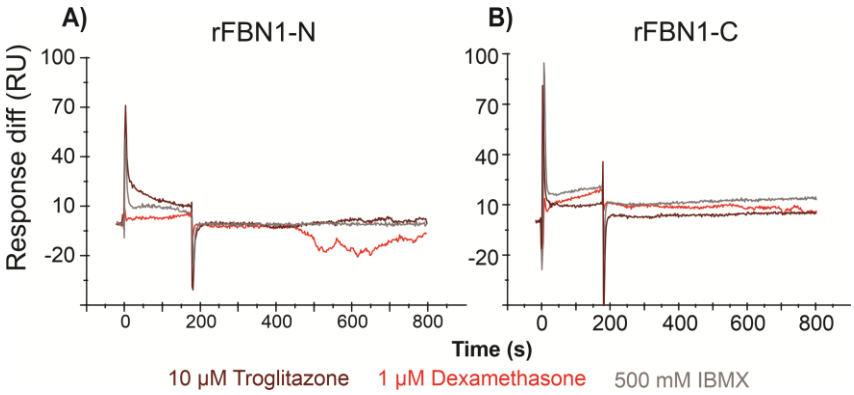

Figure S2.6. Surface plasmon resonance spectroscopy of the components in the adipogenic cocktail with immobilized rFBN1-N and rFBN1-C. Interaction studies of 10 µM troglitazone (brown profile), 1 µM dexamethasone (red profile), and 500 mM IBMX (gray profile) on chips coated with rFBN1-N **(A)** or rFBN1-C **(B)**.

Supplemental Table 1: Sequence of primers used in this study.

Gene	Primer	Sequence 5'-3'	Purpose
Fbn1	Sense	GGGTAAAGGATGCACATATGTAAAGTGGTGC	mgR/mgR genotyping
	Antisense	AATCCAGTACTAGGAGGAGAAGGCCATG	mgR/mgR genotyping
Neo	Antisense	GCCAAGTTCTAATTCCATCAGAAGCTGGTC	mgR/mgR genotyping
Fbn1	Sense	CTCATCATTTTTGGCCAGTTG	C1041G/+ genotyping
	Antisense	GCACTTGATGCACATTCACA	C1041G/+ genotyping
Fbn1	Sense	ATGCTACAGGAAGAATCTGTCTTGAC	cDNA sequencing
	Antisense	CTGACATTCATCAATATCCATGCAGT	cDNA sequencing
Adipoq	Sense	TGTTCCTCTTAATCCTGCCCA	Real-time qPCR
	Antisense	CCAACCTGCACAAGTTCCCTT	Real-time qPCR
Cebpa	Sense	GCAAAGCCAAGAAGTCGGTG	Real-time qPCR
	Antisense	TCTCCACGTTGCGTTGTTTG	Real-time qPCR
Fabp4	Sense	AGCTGGTGGTGGAATGTGTTA	Real-time qPCR
	Antisense	ATTTCCATCCAGGCCTCTTCC	Real-time qPCR
Fbn1	Sense	GGTAGTGGATTCTCTGAGAC	Real-time qPCR
	Antisense	GGCGTATTGCACATGCTGTG	Real-time qPCR
Gapdh	Sense	CACTCTTCCACCTTCGATGC	Real-time qPCR
	Antisense	CACCACCCTGTTGCTGTAGC	Real-time qPCR
Glut4	Sense	GAGCAGGAGGTGAAACCCAG	Real-time qPCR
	Antisense	GAGGGAGTCTGGGTGGAGAG	Real-time qPCR
Il1b	Sense	TCTCGCAGCAGCACATCAACA	Real-time qPCR
	Antisense	CCTGGAAGGTCCACGGGAAA	Real-time qPCR
Lep	Sense	TCACACACGCAGTCGGTATC	Real-time qPCR
	Antisense	ACTCAGAATGGGGTGAAGCC	Real-time qPCR
Magp1	Sense	GGTCTGCTTCTACAGCCTCC	Real-time qPCR
	Antisense	TGGAGAACTTGTCTCGGCAC	Real-time qPCR
Mcp1	Sense	CAGCCAGATGCAGTTAACGC	Real-time qPCR
	Antisense	GCCTACTCATTGGGATCATCTTG	Real-time qPCR
Pparg	Sense	ATTCTCAGTGGAGACCGCCC	Real-time qPCR
	Antisense	CAGCTGAGAGGACTCTGGGT	Real-time qPCR
Tnfa	Sense	AGCCCCCAGTCTGTATCCTT	Real-time qPCR
	Antisense	GGTCACTGTCCCAGCATCTT	Real-time qPCR
Zfp423	Sense	GCTGCCCTGAATGTAACGTG	Real-time qPCR
	Antisense	TGACGTCTGGGCACCTTTCC	Real-time qPCR

2.9 Bibliography for chapter 2

Aikio M, Elamaa H, Vicente D, Izzi V, Kaur I, Seppinen L, Speedy HE, Kaminska D, Kuusisto S, Sormunen R, Heljasvaara R, Jones EL, Muilu M, Jauhiainen M, Pihlajamaki J, Savolainen MJ, Shoulders CC, Pihlajaniemi T. (2014). Specific collagen XVIII isoforms promote adipose tissue accrual via mechanisms determining adipocyte number and affect fat deposition. *Proc Natl Acad Sci USA* **111**, E3043-E3052

Bastien M, Dagenais F, Dumont E, Vadeboncoeur N, Dion B, Royer M, Gaudet-Savard T, Poirier P. (2012). Assessment of management of cardiovascular risk factors in patients with thoracic aortic disease. *Blood Press Monit* **17**, 235-242

Bax DV, Bernard SE, Lomas A, Morgan A, Humphries J, Shuttleworth A, Humphries MJ, Kielty CM. (2003). Cell adhesion to fibrillin-1 molecules and microfibrils is mediated by alpha5 beta1 and alphav beta3 integrins. *J Biol Chem* **278**, 34605-34616

Bindlish S, Presswala LS, Schwartz F. (2015). Lipodystrophy: Syndrome of severe insulin resistance. *Postgrad Med* **127**, 511-516

Cancello R, Tordjman J, Poitou C, Guilhem G, Bouillot JL, Hugol D, Coussieu C, Basdevant A, Bar Hen A, Bedossa P, Guerre-Millo M, Clement K. (2006). Increased infiltration of macrophages in omental adipose tissue is associated with marked hepatic lesions in morbid human obesity. *Diabetes* **55**, 1554-1561

Chaudhry SS, Cain SA, Morgan A, Dallas SL, Shuttleworth CA, Kielty CM. (2007). Fibrillin-1 regulates the bioavailability of TGF-beta1. *J Cell Biol* **176**, 355-367

Chen M, Yao B, Yang Q, Deng J, Song Y, Sui T, Zhou L, Yao H, Xu Y, Ouyang H, Pang D, Li Z, Lai L. (2018). Truncated C-terminus of fibrillin-1 induces Marfanoid-progeroid-lipodystrophy (MPL) syndrome in rabbit. *Dis Model Mech* **11**, dmm031542

Craft CS, Pietka TA, Schappe T, Coleman T, Combs MD, Klein S, Abumrad NA, Mecham RP. (2014). The extracellular matrix protein MAGP1 supports thermogenesis and protects against obesity and diabetes through regulation of TGF-beta. *Diabetes* **63**, 1920-1932

Craft CS. (2015). MAGP1, the extracellular matrix, and metabolism. *Adipocyte* **4**, 60-64

Czech MP. (2017). Insulin action and resistance in obesity and type 2 diabetes. *Nat Med* **23**, 804-814

Davis MR, Arner E, Duffy CR, De Sousa PA, Dahlman I, Arner P, Summers KM. (2016). Expression of FBN1 during adipogenesis: Relevance to the lipodystrophy phenotype in Marfan syndrome and related conditions. *Mol Genet Metab* **119**, 174-185

Divoux A, Clement K. (2011). Architecture and the extracellular matrix: the still unappreciated components of the adipose tissue. *Obes Rev* **12**, e494-503

Duerrschmid C, He Y, Wang C, Li C, Bournat JC, Romere C, Saha PK, Lee ME, Phillips KJ, Jain M, Jia P, Zhao Z, Farias M, Wu Q, Milewicz DM, Sutton VR, Moore DD, Butte NF, Krashes MJ, Xu Y, Chopra AR. (2017). Asprosin is a centrally acting orexigenic hormone. *Nat Med* **23**, 1444-1453

Erkula G, Jones KB, Sponseller PD, Dietz HC, Pyeritz RE. (2002). Growth and maturation in Marfan syndrome. *Am J Med Genet* **109**, 100-115

Ghaben AL, Scherer PE. (2019). Adipogenesis and metabolic health. *Nat Rev Mol Cell Biol* **20**, 242-258

Goldblatt J, Hyatt J, Edwards C, Walpole I. (2011). Further evidence for a marfanoid syndrome with neonatal progeroid features and severe generalized lipodystrophy due to frameshift mutations near the 3' end of the FBN1 gene. *Am J Med Genet A* **155A**, 717-720

Graul-Neumann LM, Kienitz T, Robinson PN, Baasanjav S, Karow B, Gillessen-Kaesbach G, Fahsold R, Schmidt H, Hoffmann K, Passarge E. (2010). Marfan syndrome with neonatal progeroid syndrome-like lipodystrophy associated with a novel frameshift mutation at the 3' terminus of the FBN1-gene. *Am J Med Genet A* **152A**, 2749-2755

Hansen LB, von Kodolitsch Y, Schroeder F, Benninghoven D. (2020). Body image in patients with Marfan syndrome. *J Clin Med* **9**

Herranz P, de Lucas R, Perez-Espana L, Mayor M. (2008). Lipodystrophy syndromes. *Dermatol Clin* **26**, 569-578, ix

Hyvari L, Ojansivu M, Juntunen M, Kartasalo K, Miettinen S, Vanhatupa S. (2018). Focal adhesion kinase and ROCK signaling are switch-like regulators of human adipose stem cell differentiation towards osteogenic and adipogenic lineages. *Stem Cells Int* **2018**, 2190657

Isogai Z, Ono RN, Ushiro S, Keene DR, Chen Y, Mazzieri R, Charbonneau NL, Reinhardt DP, Rifkin DB, Sakai LY. (2003). Latent transforming growth factor beta-binding protein 1 interacts with fibrillin and is a microfibril-associated protein. *J Biol Chem* **278**, 2750-2757

Jacquinet A, Verloes A, Callewaert B, Coremans C, Coucke P, de Paepe A, Kornak U, Lebrun F, Lombet J, Pierard GE, Robinson PN, Symoens S, Van Maldergem L, Debray FG. (2014). Neonatal progeroid variant of Marfan syndrome with congenital lipodystrophy results from mutations at the 3' end of FBN1 gene. *Eur J Med Genet* **57**, 230-234

Jensen SA, Reinhardt DP, Gibson MA, Weiss AS. (2001). Protein interaction studies of MAGP-1 with tropoelastin and fibrillin-1. *J Biol Chem* **276**, 39661-39666

Judge DP, Biery NJ, Keene DR, Geubtner J, Myers L, Huso DL, Sakai LY, Dietz HC. (2004). Evidence for a critical contribution of haploinsufficiency in the complex pathogenesis of Marfan syndrome. *J Clin Invest* **114**, 172-181

Kassi E, Pervanidou P, Kaltsas G, Chrousos G. (2011). Metabolic syndrome: definitions and controversies. *BMC Med* **9**, 48

Keene DR, Maddox BK, Kuo HJ, Sakai LY, Glanville RW. (1991). Extraction of extendable beaded structures and their identification as fibrillin-containing extracellular matrix microfibrils. *J Histochem Cytochem* **39**, 441-449

Khan T, Muise ES, Iyengar P, Wang ZV, Chandalia M, Abate N, Zhang BB, Bonaldo P, Chua S, Scherer PE. (2009). Metabolic dysregulation and adipose tissue fibrosis: role of collagen VI. *Mol Cell Biol* **29**, 1575-1591

Kim JY, Park S, Lee HJ, Lew H, Kim GJ. (2020). Functionally enhanced placenta-derived mesenchymal stem cells inhibit adipogenesis in orbital fibroblasts with Graves' ophthalmopathy. *Stem Cell Res Ther* **11**, 469

Kirschner R, Hubmacher D, Iyengar G, Kaur J, Fagotto-Kaufmann C, Brömme D, Bartels R, Reinhardt DP. (2011). Classical and neonatal Marfan syndrome mutations in fibrillin-1 cause differential protease susceptibilities and protein function. *J Biol Chem* **286**, 32810-32823

Klemm DJ, Leitner JW, Watson P, Nesterova A, Reusch JE, Goalstone ML, Draznin B. (2001). Insulin-induced adipocyte differentiation. Activation of CREB rescues adipogenesis from the arrest caused by inhibition of prenylation. *J Biol Chem* **276**, 28430-28435

Kubo Y, Kaidzu S, Nakajima I, Takenouchi K, Nakamura F. (2000). Organization of extracellular matrix components during differentiation of adipocytes in long-term culture. *In Vitro Cellular & Developmental Biology - Animal* **36**, 38-44

Lee H, Lee YJ, Choi H, Seok JW, Yoon BK, Kim D, Han JY, Lee Y, Kim HJ, Kim JW. (2017). SCARA5 plays a critical role in the commitment of mesenchymal stem cells to adipogenesis. *Sci Rep* **7**, 14833

Lin G, Tiedemann K, Vollbrandt T, Peters H, Bätge B, Brinckmann J, Reinhardt DP. (2002). Homo- and heterotypic fibrillin-1 and -2 interactions constitute the basis for the assembly of microfibrils. *J Biol Chem* **277**, 50795-50804

Lönnqvist L, Reinhardt DP, Sakai LY, Peltonen L. (1998). Evidence for furin-type activity-mediated C-terminal processing of profibrillin-1 and interference in the processing by certain mutations. *Hum Mol Genet* **7**, 2039-2044

Mariman EC, Wang P. (2010). Adipocyte extracellular matrix composition, dynamics and role in obesity. *Cell Mol Life Sci* **67**, 1277-1292

Marshall LM, Carlson E, O'Malley JP, Snyder CK, Charbonneau N, Hayflick S, Coselli JS, Lemaire SA, Sakai LY. (2013). Thoracic aortic aneurysm frequency and dissection are associated with fibrillin-1 fragment concentrations in circulation. *Circ Res* **113**, 1159-1168

McGettrick AJ, Knott V, Willis A, Handford PA. (2000). Molecular effects of calcium binding mutations in Marfan syndrome depend on domain context. *Hum Mol Genet* **9**, 1987-1994

Milewicz DM, Grossfield J, Cao SN, Kielty C, Covitz W, Jewett T. (1995). A mutation in FBN1 disrupts profibrillin processing and results in isolated skeletal features of the Marfan syndrome. *J Clin Invest* **95**, 2373-2378

Morandi EM, Verstappen R, Zwierzina ME, Geley S, Pierer G, Ploner C. (2016). ITGAV and ITGA5 diversely regulate proliferation and adipogenic differentiation of human adipose derived stem cells. *Sci Rep* **6**, 28889

Muthu ML, Reinhardt DP. (2020). Fibrillin-1 and fibrillin-1-derived asprosin in adipose tissue function and metabolic disorders. *J Cell Commun Signal* **14**, 159-173

Neptune ER, Frischmeyer PA, Arking DE, Myers L, Bunton TE, Gayraud B, Ramirez F, Sakai LY, Dietz HC. (2003). Dysregulation of TGF-beta activation contributes to pathogenesis in Marfan syndrome. *Nat Genet* **33**, 407-411

Nistala H, Lee-Arteaga S, Carta L, Cook JR, Smaldone S, Siciliano G, Rifkin AN, Dietz HC, Rifkin DB, Ramirez F. (2010). Differential effects of alendronate and losartan therapy on osteopenia and aortic aneurysm in mice with severe Marfan syndrome. *Hum Mol Genet* **19**, 4790-4798

Orio F, Jr., Palomba S, Cascella T, Savastano S, Lombardi G, Colao A. (2007). Cardiovascular complications of obesity in adolescents. *J Endocrinol Invest* **30**, 70-80

Parlee SD, Lentz SI, Mori H, MacDougald OA. (2014). Quantifying size and number of adipocytes in adipose tissue. *Methods Enzymol* **537**, 93-122

Passarge E, Robinson PN, Graul-Neumann LM. (2016). Marfanoid-progeroid-lipodystrophy syndrome: a newly recognized fibrillinopathy. *Eur J Hum Genet* **24**, 1244-1247

Pereira L, Lee SY, Gayraud B, Andrikopoulos K, Shapiro SD, Bunton T, Biery NJ, Dietz HC, Sakai LY, Ramirez F. (1999). Pathogenetic sequence for aneurysm revealed in mice underexpressing fibrillin-1. *Proc Natl Acad Sci USA* **96**, 3819-3823

Pfaff M, Reinhardt DP, Sakai LY, Timpl R. (1996). Cell adhesion and integrin binding to recombinant human fibrillin-1. *FEBS Lett* **384**, 247-250

Reinhardt DP, Keene DR, Corson GM, Pöschl E, Bächinger HP, Gambee JE, Sakai LY. (1996). Fibrillin 1: Organization in microfibrils and structural properties. *J Mol Biol* **258**, 104-116

Reinhardt DP, Ono RN, Notbohm H, Müller PK, Bächinger HP, Sakai LY. (2000). Mutations in calcium-binding epidermal growth factor modules render fibrillin-1 susceptible to proteolysis: A potential disease-causing mechanism in Marfan syndrome. *J Biol Chem* **275**, 12339-12345

Renard M, Muino-Mosquera L, Manalo EC, Tufa S, Carlson EJ, Keene DR, De Backer J, Sakai LY. (2017). Sex, pregnancy and aortic disease in Marfan syndrome. *PLoS One* **12**, e0181166

Ritty TM, Broekelmann T, Tisdale C, Milewicz DM, Mecham RP. (1999). Processing of the fibrillin-1 carboxyl-terminal domain. *J Biol Chem* **274**, 8933-8940

Ritty TM, Broekelmann TJ, Werneck CC, Mecham RP. (2003). Fibrillin-1 and -2 contain heparin-binding sites important for matrix deposition and that support cell attachment. *Biochem J* **375**, 425-432

Romere C, Duerrschmid C, Bournat J, Constable P, Jain M, Xia F, Saha PK, Del Solar M, Zhu B, York B, Sarkar P, Rendon DA, Gaber MW, LeMaire SA, Coselli JS, Milewicz DM, Sutton VR, Butte NF, Moore DD, Chopra AR. (2016). Asprosin, a fasting-induced glucogenic protein hormone. *Cell* **165**, 566-579

Ruiz-Ojeda FJ, Wang J, Backer T, Krueger M, Zamani S, Rosowski S, Gruber T, Onogi Y, Feuchtinger A, Schulz TJ, Fassler R, Muller TD, Garcia-Caceres C, Meier M, Bluher M, Ussar S. (2021). Active integrins regulate white adipose tissue insulin sensitivity and brown fat thermogenesis. *Mol Metab* **45**, 101147

Sabatier L, Djokic J, Hubmacher D, Dzafik D, Nelea V, Reinhardt DP. (2014). Heparin/heparan sulfate controls fibrillin-1, -2 and -3 self-interactions in microfibril assembly. *FEBS Lett* **588**, 2890-2897

Sakai LY, Keene DR, Engvall E. (1986). Fibrillin, a new 350-kD glycoprotein, is a component of extracellular microfibrils. *J Cell Biol* **103**, 2499-2509

Sakamoto H, Broekelmann T, Cheresh DA, Ramirez F, Rosenbloom J, Mecham RP. (1996). Cell-type specific recognition of RGD- and non-RGD-containing cell binding domains in fibrillin-1. *J Biol Chem* **271**, 4916-4922

Salpeter SR, Walsh JM, Ormiston TM, Greyber E, Buckley NS, Salpeter EE. (2006). Meta-analysis: effect of hormone-replacement therapy on components of the metabolic syndrome in postmenopausal women. *Diabetes Obes Metab* **8**, 538-554

Schneider CA, Rasband WS, Eliceiri KW. (2012). NIH Image to ImageJ: 25 years of image analysis. *Nat Methods* **9**, 671-675

Sengle G, Charbonneau NL, Ono RN, Sasaki T, Alvarez J, Keene DR, Bachinger HP, Sakai LY. (2008). Targeting of bone morphogenetic protein growth factor complexes to fibrillin. *J Biol Chem* **283**, 13874-13888

Sikkeland J, Jin Y, Saatcioglu F. (2014). Methods to assess lipid accumulation in cancer cells. *Methods Enzymol* **542**, 407-423

Son ED, Lee JY, Lee S, Kim MS, Lee BG, Chang IS, Chung JH. (2005). Topical application of 17beta-estradiol increases extracellular matrix protein synthesis by stimulating TGF-beta signaling in aged human skin in vivo. *J Invest Dermatol* **124**, 1149-1161

Stubbins RE, Najjar K, Holcomb VB, Hong J, Nunez NP. (2012). Oestrogen alters adipocyte biology and protects female mice from adipocyte inflammation and insulin resistance. *Diabetes Obes Metab* **14**, 58-66

Summers KM, Raza S, van Nimwegen E, Freeman TC, Hume DA. (2010). Co-expression of FBN1 with mesenchyme-specific genes in mouse cell lines: implications for phenotypic variability in Marfan syndrome. *Eur J Hum Genet* **18**, 1209-1215

Takenouchi T, Hida M, Sakamoto Y, Torii C, Kosaki R, Takahashi T, Kosaki K. (2013). Severe congenital lipodystrophy and a progeroid appearance: Mutation in the penultimate exon of FBN1 causing a recognizable phenotype. *Am J Med Genet* **161A**, 3057-3062

Tashima Y, He H, Cui JZ, Pedroza AJ, Nakamura K, Yokoyama N, Iosef C, Burdon G, Koyano T, Yamaguchi A, Fischbein MP. (2020). Androgens accentuate TGF-beta dependent Erk/Smad activation during thoracic aortic aneurysm formation in Marfan syndrome male mice. *J Am Heart Assoc* **9**, e015773

Tiedemann K, Bätge B, Müller PK, Reinhardt DP. (2001). Interactions of fibrillin-1 with heparin/heparan sulfate: Implications for microfibrillar assembly. *J Biol Chem* **276**, 36035-36042

Tiedemann K, Boraschi-Diaz I, Rajakumar I, Kaur J, Roughley P, Reinhardt DP, Komarova SV. (2013). Fibrillin-1 directly regulates osteoclast formation and function by a dual mechanism. *J Cell Sci* **126**, 4187-4194

Vaicik MK, Thyboll Kortesmaa J, Moverare-Skrtic S, Kortesmaa J, Soininen R, Bergstrom G, Ohlsson C, Chong LY, Rozell B, Emont M, Cohen RN, Brey EM, Tryggvason K. (2014). Laminin alpha4 deficient mice exhibit decreased capacity for adipose tissue expansion and weight gain. *PLoS One* **9**, e109854

Valdivia A, Cardenas A, Brenet M, Maldonado H, Kong M, Diaz J, Burridge K, Schneider P, San Martin A, Garcia-Mata R, Quest AFG, Leyton L. (2020). Syndecan-4/PAR-3 signaling regulates focal adhesion dynamics in mesenchymal cells. *Cell Commun Signal* **18**, 129

Veevers-Lowe J, Ball SG, Shuttleworth A, Kielty CM. (2011). Mesenchymal stem cell migration is regulated by fibronectin through alpha5beta1-integrin-mediated activation of PDGFR-beta and potentiation of growth factor signals. *J Cell Sci* **124**, 1288-1300

von Kodolitsch Y, Demolder A, Girdauskas E, Kaemmerer H, Kornhuber K, Muino Mosquera L, Morris S, Neptune E, Pyeritz R, Rand-Hendriksen S, Rahman A, Riise N, Robert L, Staufenbiel I, Szocs K, Vanem TT, Linke SJ, Vogler M, Yetman A, De Backer J. (2019). Features of Marfan syndrome not listed in the Ghent nosology - the dark side of the disease. *Expert Rev Cardiovasc Ther* **17**, 883-915

Walji TA, Turecamo SE, DeMarsilis AJ, Sakai LY, Mecham RP, Craft CS. (2016). Characterization of metabolic health in mouse models of fibrillin-1 perturbation. *Matrix Biol* **55**, 63-76

Wang QA, Tao C, Gupta RK, Scherer PE. (2013). Tracking adipogenesis during white adipose tissue development, expansion and regeneration. *Nat Med* **19**, 1338-1344

Wang Y, Zhao L, Smas C, Sul HS. (2010). Pref-1 interacts with fibronectin to inhibit adipocyte differentiation. *Mol Cell Biol* **30**, 3480-3492

Watchareewan RS, Koranis, P. Prasit, P., Thanaphum OC, S. (2021). Tailored generation of insulin producing cells from canine mesenchymal stem cells derived from bone marrow and adipose tissue. *Sci Rep* **11**

Wohl AP, Troilo H, Collins RF, Baldock C, Sengle G. (2016). Extracellular regulation of bone morphogenetic protein activity by the microfibril component fibrillin-1. *J Biol Chem* **291**, 12732-112746

Yetman AT, McCrindle BW. (2010). The prevalence and clinical impact of obesity in adults with Marfan syndrome. *Can J Cardiol* **26**, 137-139

Yu C, Peall IW, Pham SH, Okolicsanyi RK, Griffiths LR, Haupt LM. (2020). Syndecan-1 facilitates the human mesenchymal stem cell osteo-adipogenic balance. *Int J Mol Sci* **21**

Zaragosi LE, Dadone B, Michiels JF, Marty M, Pedeutour F, Dani C, Bianchini L. (2015). Syndecan-1 regulates adipogenesis: new insights in dedifferentiated liposarcoma tumorigenesis. *Carcinogenesis* **36**, 32-40

Zeyer KA, Zhang RM, Kumra H, Hassan A, Reinhardt DP. (2019). The fibrillin-1 RGD integrin binding site regulates gene expression and cell function through microRNAs. *J Mol Biol* **431**, 401-421

Zhang H, Hu W, Ramirez F. (1995). Developmental expression of fibrillin genes suggests heterogeneity of extracellular microfibrils. *J Cell Biol* **129**, 1165-1176

Zhang RM, Kumra H, Reinhardt DP. (2019). Quantification of extracellular matrix fiber systems related to ADAMTS proteins. *Methods Mol Biol* **2043**, 237-250

Zhang RM, Zeyer KA, Odenthal N, Zhang Y, Reinhardt DP. (2021). The fibrillin-1 RGD motif posttranscriptionally regulates ERK1/2 signaling and fibroblast proliferation via miR-1208. *FASEB J* **35**, e21598

Zhao Y, Wen Y, Polan ML, Qiao J, Chen BH. (2007). Increased expression of latent TGF-beta binding protein-1 and fibrillin-1 in human uterine leiomyomata. *Mol Hum Reprod* **13**, 343-349

CHAPTER 3: MALE MICE WITH FIBRILLIN-1 DEFICIENCY ARE PREDISPOSED TO HIGH FAT DIET INDUCED OBESITY, DIABETES, AND FATTY LIVER

Male mice with fibrillin-1 deficiency are predisposed to high fat diet induced obesity, diabetes, and fatty liver

Kerstin Tiedemann[1,2,§], Muthu L. Muthu[3,§], Dieter P. Reinhardt[1,3,#], Svetlana V. Komarova[1,2,#]

[1]Faculty of Dental Medicine and Oral Health Sciences, McGill University, Montréal, Canada

[2]Shriners Hospital for Children – Canada, Montréal, Canada

[3]Faculty of Medicine and Health Sciences, Department of Anatomy and Cell Biology, McGill University, Montréal, Canada

[§] Co-first authors; [#] Co-corresponding authors

Keywords: Fibrillin-1, high fat diet, metabolism, liver, ER-stress

3.1 Preamble

Chapter 2 of this thesis discovered novel sex specific differences in adipose tissue development and metabolism using two MFS mouse models fed with a normal chow diet. We also found that only male mice haplo-insufficient for fibrillin-1 are prediabetic with increased adipose tissue deposition and adipocyte hypertrophy. However, the role of fibrillin-1 in the development of diet induced obesity and metabolic complications have not been studied. Therefore, the overarching goal of this chapter is to study the adipose tissue and metabolic phenotypes of the two MFS models fed with a HFD and a matched control diet.

3.2 Abstract

Gene mutations in the extracellular matrix protein fibrillin-1 cause connective tissue disorders including Marfan syndrome (MFS) with clinical symptoms in the cardiovascular, skeletal, and ocular systems. In addition, MFS patients exhibit alterations in adipose tissues, which in some individuals leads to a lipodystrophy, while in others to obesity. We have recently demonstrated that fibrillin-1 regulates adipose tissue homeostasis. In this study we examined how fibrillin-1 abnormality affects metabolic adaptation to different diets. We used two MFS mouse models: *Fbn1*$^{mgR/mgR}$ mice with fibrillin-1 haploinsufficiency resulting in severe MFS, and *Fbn1*$^{C1041G/+}$ mice with a dominant negative missense mutation leading to relatively mild MFS. When *Fbn1*$^{mgR/mgR}$ mice were fed with high fat diet (HFD) for 12 weeks (limited due to the phenotype severity), male mice were heavier than littermate controls (LC), while female mice gained less weight compared to LC. Female *Fbn1*$^{C1041G/+}$ mice fed HFD for 24 weeks were similarly protected from weight gain. Even though male *Fbn1*$^{C1041G/+}$ mice were similar to their LC in HFD-induced weight gain, they demonstrated higher insulin level, insulin resistance, circulating levels of cholesterol and high-density lipoproteins. Moreover, male HFD-fed *Fbn1*$^{C1041G/+}$ mice showed a higher liver weight with a fatty liver disease phenotype, which was reduced to LC levels after orchiectomy. Phosphorylation of protein kinase-like endoplasmic reticulum kinase (PERK) in livers of HFD-fed male *Fbn1*$^{C1041G/+}$ mice was elevated compared to LC, and reduced after orchiectomy, suggesting the contribution of endoplasmic reticulum stress. These data demonstrate that male MFS mice are susceptible to HFD-induced obesity, diabetes, and fatty liver phenotype, correlated by increased endoplasmic reticulum stress due to the processing of abnormal fibrillin-1. In contrast, female MFS mice appeared to be protected from the negative consequence of HFD.

3.3 Introduction

Fibrillins are large cysteine-rich glycoproteins found ubiquitously in elastic and non-elastic tissues throughout the body. The fibrillin super-family is comprised of fibrillin-1, -2, and -3 and the related latent transforming growth factor (TGF)-β-binding proteins (LTBPs). Fibrillins constitute the backbone components of extracellular microfibrils, which are important for structural and functional integrity of all connective tissues, and the regulation of growth factor signaling [*Hubmacher et al., 2006; Ramirez & Dietz, 2007*]. There are presently over 1800 mutations known in the fibrillin-1 gene [*Collod-Beroud et al., 2003*], which cause connective tissue disorders including Marfan syndrome (MFS) with wide clinical symptoms in the cardiovascular, skeletal and ocular systems [*Pyeritz, 2000; Summers et al., 2005; Robinson et al., 2006*]. In addition, individuals with MFS are frequently lipodystrophic with very little overall body fat [*Takenouchi et al., 2013*]. However, the adipose tissue phenotype is complex and variable, with documented obesity in a subgroup of MFS patients [*Yetman & McCrindle, 2010*], and high visceral fat deposits in older individuals [*von Kodolitsch et al., 2019*]. The pathophysiology of the MFS-associated adipose tissue phenotype is not well understood.

There are multiple mouse models that recapitulate different aspects of MFS pathology. *Fbn1*$^{mgR/mgR}$ mice [*Pereira et al., 1999; Nistala et al., 2010*] have low levels (20-25%) of normal fibrillin-1, which is commonly observed in patients [*Mátyás et al., 2007; Hilhorst-Hofstee et al., 2011; Aubart et al., 2015; Franken et al., 2015; Franken et al., 2016; Franken et al., 2017*]. *Fbn1*$^{C1041G/+}$ mice [*Judge et al., 2004*] harbor a single amino acid substitution in fibrillin-1 which mimics a mutation observed in MFS patients [*Robinson & Godfrey, 2000; Boileau et al., 2005*]. Previously, reduced insulin sensitivity was demonstrated in several MFS mouse models, including *Fbn1*$^{C1041G/+}$ [*Walji*

et al., 2016]. Importantly, Romere *et al*, discovered that the C-terminal propeptide of fibrillin-1, named asprosin, functions as a circulating hormone that affects glucose homeostasis [*Romere et al., 2016*]. Asprosin levels were elevated in humans and mice during starvation, insulin resistance, obesity, and diabetes [*Romere et al., 2016; Alan et al., 2019; Wang et al., 2019; Muthu & Reinhardt, 2020; Zhang et al., 2020*]. We have recently found that fibrillin-1 negatively regulates the development and homeostasis of adipose tissue, due to its interaction with adipocyte progenitor cells and the ability to sequester insulin (chapter 2). These data clearly show a central role of fibrillin-1 in adipose tissue development and homeostasis. However, the consequences of a high-fat diet (HFD) in MFS mouse models have not yet been analyzed.

The goal of this study was to examine the metabolic adaptation to HFD in $Fbn1^{mgR/mgR}$ and $Fbn1^{C1041G/+}$ MFS mouse models. The $Fbn1^{mgR/mgR}$ mice represent a severe MFS model, in which the mice die at 3-4 months of age due to aortic rupture [*Pereira et al., 1999; Nistala et al., 2010*]. In contrast, the $Fbn1^{C1041G/+}$ mice have relatively mild MFS, which develop vascular and skeletal phenotypes later in life (6-12 months) [*Judge et al., 2004*]. We compared the weight gain, insulin and glucose homeostasis, serum lipids, adipose tissues, and liver health in male and female $Fbn1^{mgR/mgR}$ and $Fbn1^{C1041G/+}$ mice and corresponding littermate control (LC) mice fed with HFD (60% fat) or a matched control diet (CD, 10% fat). Because of the differences in longevity between the two MFS models, the duration of the diet study in $Fbn1^{mgR/mgR}$ mice was for 12 weeks, and in $Fbn1^{C1041G/+}$ for 24 weeks. The role of androgens on liver disease was also investigated by performing orchiectomy on male $Fbn1^{C1041G/+}$ mice fed with HFD.

3.4 Material and Methods

3.4.1 Animals and diets

All experimental procedures were approved by the McGill University Animal Care Committee in accordance with the guidelines of the Canadian Council on Animal Care (Protocol#2014-7561). *Fbn1*$^{C1041G/+}$ mice used in this study were purchased from Jackson Laboratories (B6.129-Fbn1tm1Hcd/J, stock number 012885), and *Fbn1*$^{mgR/mgR}$ mice were a gift from Dr. Francesco Ramirez (Icahn School of Medicine, Mount Sinai) [*Carta et al., 2006*]. Female and male wild type and MFS (*Fbn1*$^{mgR/mgR}$; *Fbn1*$^{C1041G/+}$) mice were on the C57BL/6J background. The mice were housed in a pathogen-free animal facility and fed with a Teklad special HFD (60% fat, TD.06414) and a matched control diet (10% fat, TD.06416), both purchased from Envigo, Madison Wisconsin USA. The diets were provided during the age of 4-16 weeks for the *Fbn1*$^{mgR/mgR}$ mice or 4-28 weeks for the *Fbn1*$^{C1041G/+}$ mice and the experimental endpoints were 16 and 28 weeks, respectively.

3.4.2 Orchiectomy and ovariectomy

After 8-10 weeks on HFD, male *Fbn1*$^{C1041G/+}$ mice were orchiectomized and female *Fbn1*$^{C1041G/+}$ mice were ovariectomized. For orchiectomy, the male mice were under isoflurane induced anesthesia, the testes were descended into the scrotal sac, a small midline incision was made in the scrotum, the tunica was pierced, and the testes were pushed out. Before cauterization of the vas deferens and the spermatic blood vessels, surrounding fat was gently dissected. This was repeated for the second testis. For ovariectomy, female mice were under isoflurane induced anesthesia, a

small incision (0.5 cm) on the mid-dorsal aspect of the mouse was created, the skin was removed, and the peritoneal layer was cut through to retrieve and excise the ovary on each flank.

3.4.3 Measurement of body weight, glucose, insulin and asprosin

The body weight was measured weekly. For glucose tolerance tests (GTTs), mice were fasted 16 h, and a fasting blood glucose value was recorded before intraperitoneal injection of glucose (2 g/kg). The circulating blood glucose levels were measured using a glucometer (Onetouch, Verio) at 0, 15, 30, 60, 90 and 120 min after injection. Four days after GTT, an insulin tolerance test (ITT) was performed. The mice were fasted 5 h, a fasting blood glucose value was recorded before intraperitoneal injection (200 µl) of insulin (0.60 U/kg body weight) was performed. The glucose values were measured at 0, 15, 30, 60, 90 and 120 min after injection. Insulin (Cristal Chem, Cat#90080) and asprosin (MyBiosources, Cat#MBS3807092) levels were measured in serum using an ELISA kit following the manufacturer's instructions.

3.4.4 Biochemical analysis of serum metabolites

Lipid profiling of cholesterol, high-density lipoproteins (HDL) and triglycerides were measured in serum of fasted mice at the respective experimental endpoints at the Comparative Medicine and Resources Center at McGill University, Montreal, Canada.

3.4.5 Body composition using DEXA

Live whole-mouse radiographs were captured with the digital specimen radiology instrument (GE Lunar PIXImus II) at an energy rate of 80 kV and 400 µA at the Center for Bone and Periodontal Research at McGill University, Montreal, Canada. Three parameters were assessed: (a) the total

tissue mass (b) the total lean mass and (c) the total fat percentage of the mouse. From these parameters, the total fat mass was calculated.

3.4.6 Tissue collection

Tissues were collected at the experimental endpoints of 16 (*Fbn1*$^{mgR/mgR}$) and 28 (*Fbn1*$^{C1041G/+}$) weeks of age. The mouse fur was sprayed with 70% ethanol, and then the interscapular brown adipose tissue (BAT), subcutaneous inguinal white adipose tissues (iWAT), liver lobes, and spleen were dissected. Tissues were either snap frozen in liquid nitrogen or fixed in 10% formalin.

3.4.7 Histopathological analysis

Liver and iWAT were fixed in 10% buffered formalin, dehydrated by an ethanol gradient, and stored in 70% ethanol at 4°C before paraffin embedding. Four-micron tissue sections were stained with hematoxylin and eosin. Images were taken using a Leica DMRB light microscope equipped with the Olympus Nano Zoomer 2.0-HT System with NDP scan 2.5 image software [*Schneider et al., 2012*]. For quantification of adipocyte size, we used ImageJ software following a published protocol [*Parlee et al., 2014*].

3.4.8 Protein extraction and immunoblotting

Between 25-50 mg (ratio 0.1 g tissue/0.4 ml RIPA buffer) of frozen mouse liver was homogenized using an ice-cold bio-pulverizer and total protein was extracted in RIPA buffer (50 mM Tris-HCl pH 7.4; 150 mM NaCl, 1 % NP-40, 1 mM EDTA) containing 1 mM phenylmethylsulfonyl fluoride

and broad-spectrum proteinase inhibitors retrieved from protease inhibitor cocktail mini tablets (Roche, Cat#11836153001). After homogenization, the samples were centrifuged at 12,000×g for 10 min at 4°C, the supernatant was collected, and protein was measured using a Quant-iT protein assay kit (Invitrogen, Q33211). 50-75 μg protein was separated by 7.5% SDS-PAGE and transferred onto a nitrocellulose membrane (0.45 μm, 162-0115, Bio-Rad) using non-buffered 10 mM sodium borate buffer. The membranes were blocked in either 5% milk or 5% bovine serum albumin for 1 h at room temperature followed by overnight incubation at 4°C with primary antibodies: anti–pPERK (1:100, bs-3330-TR, BIOSS), anti–PERK (1:100, bs-2469R-TR, BIOSS), and anti–HRP-GAPDH (1:1000, Cell Signaling Technology). The blots were washed, incubated with horseradish peroxidase–conjugated secondary antibodies (1:1000, anti-rabbit, 170-5046; Bio-Rad), and visualized with a chemiluminescence system (SuperSignal West Pico; 34,080, Pierce). Immunoblots were quantified using densitometry with ImageJ.

3.4.9 Statistical analysis

Data are means ± Standard Error of the Mean (SEM) or ± Standard Deviation (SD), depending on the experimental design. Significance was assessed using Student t-test, one-way, two-way, or two-way repeated measures ANOVA followed by Tukey post-test, with $p<0.05$ considered as statistically significant. Statistical analysis for each figure is detailed in the respective figure legend. Statistical analysis was performed using the OriginPro version 2021 (OriginLab).

3.5 Results

3.5.1 HFD-induced weight gain in MFS mice

MFS mice (*Fbn1*$^{mgR/mgR}$ and *Fbn1*$^{C1041G/+}$) and wild type LCs were fed with a HFD or a matched CD starting after weaning (4 weeks of age) up to 16 weeks for *Fbn1*$^{mgR/mgR}$ or 28 weeks for *Fbn1*$^{C1041G/+}$ mice. LC mice responded to the HFD with an expected change in weight (Fig. 3.1A-D). Male *Fbn1*$^{mgR/mgR}$ mice increased their body weight significantly more than LC after 12 weeks of HFD (Fig. 3.1E), whereas male *Fbn1*$^{C1041G/+}$ mice did not differ from LC after 24 weeks of HFD (Fig. 3.1F). In contrast, female *Fbn1*$^{mgR/mgR}$ (Fig. 3.1C and E) and *Fbn1*$^{C1041G/+}$ (Fig. 3.1D and F) mice fed with HFD gained less weight compared to their LC. Thus, male mice of the more severely affected hypomorphic *Fbn1*$^{mgR/mgR}$ genotype were more susceptible to HFD-induced obesity compared to their LC, whereas female mice from both MFS mouse models were protected from the HFD-induced weight gain.

3.5.2 HFD-induced changes in the adipose tissue mass of MFS mice

We assessed tissue composition of MFS mice and their LC by DEXA at the experimental end points (16 weeks of age for *Fbn1*$^{mgR/mgR}$ and 28 weeks of age for *Fbn1*$^{C1041G/+}$). MFS mice and their LC fed with HFD significantly increased the total mass (Fig. 3.2A-B) and the fat mass (Fig. 3.2C-D), compared to the corresponding mice fed with CD. However, for female *Fbn1*$^{mgR/mgR}$ mice fed with HFD the fat mass was significantly lower (Fig. 3.2C) and the lean mass was significantly higher (Fig. S3.1) compared to their LC on HFD. We next examined the mass of isolated iWAT and BAT. HFD resulted in a significant increase in iWAT mass compared to CD in LC mice, as well as male *Fbn1*$^{mgR/mgR}$ and *Fbn1*$^{C1041G/+}$ mice, however not in female *Fbn1*$^{mgR/mgR}$ and

Fbn1$^{C1041G/+}$ mice (Fig. 3.2E-F). Moreover, compared to their LC, female *Fbn1*$^{mgR/mgR}$ and *Fbn1*$^{C1041G/+}$ mice displayed a significantly lower iWAT mass when fed with a HFD (Fig. 3.2E-F). BAT weight did not differ in *Fbn1*$^{mgR/mgR}$ and their LC (Fig. 3.2G), or in female *Fbn1*$^{C1041G/+}$ mice and their LC (Fig. 3.2H) on either HFD or CD. Interestingly, male *Fbn1*$^{C1041G/+}$ mice on HFD presented with a significant increase in the BAT mass compared to the LC (Fig. 3.2H), suggesting that the lack of difference in weight gain in male *Fbn1*$^{C1041G/+}$ compared to LC required adaptative changes in potentially energy-dissipating BAT in these MFS mice.

3.5.3 HFD-induced changes in adipocyte size in MFS mice

To evaluate the specific consequence of diet on individual adipocytes, we examined adipocyte size in histological samples of iWAT at the experimental end points. HFD induced a significant increase in average adipocyte size compared to CD in all mice, however the degree of change was genotype- and sex-dependent (Fig. 3.3). On HFD, only female *Fbn1*$^{mgR/mgR}$ mice had significantly smaller adipocytes compared to their LC mice (Fig. 3.3A-B). This was reflected in the differences in the adipocyte size distributions between MFS mice and their LC on HFD but not on CD (Fig. 3.3C-F). In this regard, even the female *Fbn1*$^{C1041G/+}$ mice on HFD, which did not show a significant difference in average adipocyte size (Fig. 3.3H), demonstrated higher prevalence of small sized cells on HFD compared to their LC (Fig. 3.3L). These data suggest that global fibrillin-1 abnormality interferes with lipid accumulation within individual adipocytes, which in female MFS mice results in low weight gain on HFD. The fact that male mice are able to gain weight in excess of their LC even though the individual adipocytes are similar strongly suggest that the proliferation of adipocytes is induced by HFD in male MFS mice.

3.5.4 HFD-induced hyperglycemia and glucose intolerance in MFS mice

We evaluated glucose metabolism in male and female *Fbn1*$^{mgR/mgR}$ and *Fbn1*$^{C1041G/+}$ mice and their LC on HFD or CD. Fasting glucose levels assessed at the experimental endpoints were normal for both male and female *Fbn1*$^{mgR/mgR}$ mice (Fig. 3.4A) and female *Fbn1*$^{C1041G/+}$ mice (Fig. 3.4B), compared to their respective LCs. Only the male *Fbn1*$^{C1041G/+}$ and their LC demonstrated a higher fasting blood glucose value when fed a HFD compared to CD (Fig. 3.4B). GTT performed at the age of 15 weeks for *Fbn1*$^{mgR/mgR}$ and at 20 weeks for *Fbn1*$^{C1041G/+}$ demonstrated that male MFS and LC mice became glucose intolerant on HFD (Fig. 3.4C-D). Female *Fbn1*$^{mgR/mgR}$ and LC mice on HFD remained similar to those on CD (Fig. 3.4E), whereas female *Fbn1*$^{C1041G/+}$ and LC started to demonstrate signs of glucose intolerance (Fig. 3.4F). The area under the curve (AUC) was significantly higher in male *Fbn1*$^{C1041G/+}$ or LC mice on HFD compared to CD (Fig. 3.4G-H). Thus, the MFS genotype did not lead to significant differences in glucose levels or tolerance on HFD.

3.5.5 HFD-induced hyperinsulinemia and insulin intolerance in male MFS mice

Insulin levels at the experimental endpoints were similar in HFD versus CD fed male and female *Fbn1*$^{mgR/mgR}$ mice (Fig. 3.5A), female *Fbn1*$^{C1041G/+}$ mice (Fig. 3.5B), and male LC from the *Fbn1*$^{C1041G/+}$ colony (Fig. 3.5B). Only the male *Fbn1*$^{C1041G/+}$ demonstrated higher insulin levels when fed with HFD compared to CD (Fig. 3.5B). No change in asprosin levels, in either of the MFS mice on CD or HFD, was observed (Fig. 3.5C-D). We further evaluated insulin sensitivity in male *Fbn1*$^{C1041G/+}$ mice and their LC after 16 weeks of HFD, 4 days after performing the GTT. The ITT demonstrated an initial delay in clearing glucose in both *Fbn1*$^{C1041G/+}$ and their LC (Fig. 3.5E), however the AUC for the ITT was similar in *Fbn1*$^{C1041G/+}$ and their LC (Fig. 3.5F). Thus,

postprandial insulin level was affected in male *Fbn1*$^{C1041G/+}$ mice further suggesting that even though HFD-induced weight gain in male *Fbn1*$^{C1041G/+}$ is comparable to LC, there are specific HFD-induced metabolic changes in these MFS mice.

3.5.6 HFD-induced liver phenotype in male MFS mice is similar to non-alcoholic fatty liver disease (NAFLD)

We evaluated liver histology and weight in male and female *Fbn1*$^{mgR/mgR}$ and *Fbn1*$^{C1041G/+}$ and the LC mice after they were fed a HFD or CD. In male *Fbn1*$^{C1041G/+}$ mice on HFD liver demonstrated severely pathological appearance, with an increase in lipid droplets and ballooning of the hepatocytes compared to CD or HFD-fed LC (Fig. 3.6A). The average liver weight of male *Fbn1*$^{C1041G/+}$ mice on HFD was significantly higher compared to CD (Fig. 3.6B). In male *Fbn1*$^{mgR/mgR}$ mice, which spent much less time on HFD than the *Fbn1*$^{C1041G/+}$ mice, liver weights were similar to the diet-matched LC (Fig. S3.2). No significant difference was observed in liver weight of female MFS mice compared to their LC, even though female *Fbn1*$^{C1041G/+}$ livers demonstrated a mild lipid accumulation (Fig. S3.3). The spleen weight was similar in MFS mice compared to their sex- and diet-matched LC (Fig. S3.4). We examined serum lipids and have found that in HFD-fed *Fbn1*$^{C1041G/+}$ circulating levels of cholesterol (Fig. 3.6C) and HDL (Fig. 3.6D), but not triglycerides (Fig. 3.6E) were significantly increased. Since testosterone was previously shown to be associated with NAFLD [*Jia et al., 2018; Okamura et al., 2020*], we examined if reducing testosterone levels with orchiectomy interferes with HFD-induced NAFLD in *Fbn1*$^{C1041G/+}$ mice. After 7-8 weeks on HFD, a subgroup of male *Fbn1*$^{C1041G/+}$ were orchiectomized and then continued on HFD (HFD/X) until the experimental endpoint. Orchiectomy interfered with the development of NAFLD, decreasing the liver adiposity and weight (Fig. 3.6A-B) and

improving lipid profile (Fig. 3.6C, D). Since testosterone-induced endoplasmic reticulum (ER) stress was suggested to play a critical role in NAFLD [*Jia et al., 2018*], we evaluated an essential ER-stress marker in the liver of male *Fbn1*$^{C1041G/+}$ and LC mice after they were fed a HFD for 24 weeks. We found a relative ~7-fold increase in the level of phosphorylated protein kinase-like endoplasmic reticulum kinase (PERK) in male *Fbn1*$^{C1041G/+}$ compared to LC (Fig. 3.7A-B). We also assessed the expression of sterol regulatory element-binding transcription factor 1 (*Srebp1*). *Srebp1* plays a key role in liver lipogenesis, and it was significantly increased in the liver of HFD-induced male *Fbn1*$^{C1041G/+}$ (Fig. 3.7C). Thus, long term exposure of male *Fbn1*$^{C1041G/+}$ mice to HFD leads to the development of NAFLD, associated with an increased ER stress.

3.6 Discussion

In this study, we show that male and female MFS mice respond differently to a HFD challenge. We compared the response to HFD in fibrillin-1 hypomorphic *Fbn1*$^{mgR/mgR}$ mice that develop severe MFS, and in mice with a missense mutation in fibrillin-1, *Fbn1*$^{C1041G/+}$, that exhibit moderate MFS. We demonstrate that male MFS mice were more susceptible to HFD-induced obesity compared to their wild type littermates whereas female mice with reduced or mutated fibrillin-1 were protected against HFD-induced weight gain. On HFD, white fat adipocyte size was similar in male MFS mice compared to their respective Wt littermates, while it was lower in female MFS mice with reduced or mutated fibrillin-1 compared to their littermates, suggesting that adipocyte numbers are increased in male mice. We observed a earlier weight gain in hypomorphic *Fbn1*$^{mgR/mgR}$ mice compared to *Fbn1*$^{C1041G/+}$. Because of dissecting aortic aneurysms and the associated reduced life span, the duration of HFD was limited to 12 weeks for the *Fbn1*$^{mgR/mgR}$ mice, while moderately affected *Fbn1*$^{C1041G/+}$ were followed for 24 weeks. Such long-term exposure to HFD led to the development of hyperinsulinemia and non-alcoholic fatty liver phenotype in male MFS mice. We demonstrate that non-alcoholic fatty liver phenotype was correlated with ER stress, which was likely elevated due to processing of mutated fibrillin-1 and reduced after orchiectomy. Taken together, we demonstrate that deficiencies in fibrillin-1 lead to susceptibility to HFD-induced metabolic disease in male mice, while protecting the female mice.

An asthenic body habitus was described in many individuals with MFS [*Muthu & Reinhardt, 2020*]. However, in keeping with a large variability in fibrillin-1 mutations leading to MFS [*Collod-Beroud et al., 2003*], differences in adipose tissue presentation have been reported. On one hand, there are patients with marfanoid progeroid lipodystrophy syndrome due to mutations

in the C-terminal domain of fibrillin-1 [*Passarge et al., 2016*]. On the other hand, the proportion of obese individuals (body mass index of > 30 kg/m^2) among MFS patients was reported to be similar to the general population [*Yetman & McCrindle, 2010*], suggesting that not all patients are protected from diet-induced obesity. This becomes especially important since the longevity of individuals with MFS approaches that of the general population [*von Kodolitsch et al., 2019*]. In older patients, deposition of visceral fat has been noted [*von Kodolitsch et al., 2019*], which is known to increase the risk of type 2 diabetes and cardiovascular disease [*Despres & Lemieux, 2006*]. Fibrillin-1 levels were also reported to increase in the adipose tissue of obese women in correlation with adipocyte size, but not the number [*Davis et al., 2016*]. Thus, there is strong evidence for the association of fibrillin-1 expression and adipocyte homeostasis in individuals with or without MFS.

Adipose tissue homeostasis was previously investigated in multiple fibrillin-1 deficient mouse models spanning the wide spectrum of MFS pathology, from very mildly to severely affected. The mouse models included *Fbn1*$^{mgR/mgR}$ **(chapter 2)**, *Fbn1*$^{C1041G/+}$ [*Walji et al., 2016*] and **(chapter 2)**, haploinsufficient *Fbn1*$^{+/-}$ mice, and *Fbn1*$^{H1\Delta/H1\Delta}$ mice with a homozygous deletion in exon 7 [*Walji et al., 2016*]. The expression pattern of normal fibrillin-1 in adipose differentiation has also been examined **(chapter 2)**. We have shown that when *Fbn1*$^{mgR/mgR}$ and *Fbn1*$^{C1041G/+}$ mice were fed the conventional grain-based diet, male, but not female MFS mice, had higher white and brown adipose tissue mass **(chapter 2)**. These data are consistent with the findings in male *Fbn1*$^{C1041G/+}$, *Fbn1*$^{+/-}$ and *Fbn1*$^{H1\Delta/H1\Delta}$ mice that displayed an increase in overall adiposity and a reduced insulin sensitivity when fed a grain-based diet [*Walji et al., 2016*]. Furthermore, male *Fbn1*$^{mgR/mgR}$ mice, not *Fbn1*$^{C1041G/+}$, fed with a grain-based diet, demonstrated an increase in the adipocyte size in

iWAT compared to their LC, whereas females from both mouse models demonstrated a significant decrease in iWAT adipocyte size compared to their LC **(chapter 2)**. In contrast to previous papers, this study used a commercially available control diet (CD, 10% kcal from fat), which is a purified diet containing high quality ingredients in controlled amounts (Envigo). The CD is thus different from the grain-based diets, which often contain trace amounts of "non-nutrients" and impurities and high concentrations of both soluble and in-soluble fibers [*Pellizzon & Ricci, 2020*]. Comparing the findings for the adipose tissue on different diets, we have realized that on grain-based diet male *Fbn1*$^{mgR/mgR}$ mice exhibit higher adiposity compared to their LC **(chapter 2)**, while on CD there was no difference between *Fbn1*$^{mgR/mgR}$ and LC (this study). Further comparing the adipose tissues from mice fed with grain-based and CD, we observed that male (but not female) *Fbn1*$^{mgR/mgR}$ and *Fbn1*$^{C1041G/+}$ mice have a significantly higher mean adipocyte size on grain-based, by two-fold for *Fbn1*$^{mgR/mgR}$ and by 1.2-fold for *Fbn1*$^{C1041G/+}$. Male LC mice fed with the grain-based diet did not demonstrate increased adiposity compared to the CD. These data importantly demonstrate that the type of diet that is fed to laboratory mice can have important implication beyond the value of caloric intake.

To our knowledge, this study is the first to report the outcome of an exposure to HFD in MFS mice. The mice were fed a commercial HFD (60% kcal from fat) and in parallel the matched CD (10% kcal from fat). We identified a strong sexual dimorphism in the response in mice with MFS phenotype to the HFD challenge. On HFD, male mice with severe MFS gained weight faster, and the mildly affected MFS mice became hyperinsulinemic faster than their corresponding LC. Adipocyte size in iWAT was smaller in all male mice with reduced or mutated fibrillin-1 compared to their LCs, suggesting that adipocyte proliferation is induced in male mice. Interestingly,

metabolic conditions, such as type 2 diabetes and insulin resistance, have been associated with a wider distribution of smaller adipocytes [*McLaughlin et al., 2007; Pasarica et al., 2009; McLaughlin et al., 2014; Fang et al., 2015*]. In contrast, in female MFS mice, HFD-induced accumulation of white fat was attenuated, resulting in their protection from severe weight gain on HFD. Although we could not study *Fbn1*$^{mgR/mgR}$ mice beyond 16 weeks of age because of their shorter life span due to cardiovascular mortality [*Pereira et al., 1999*], we extended the diet intervention of moderately affected *Fbn1*$^{C1041G/+}$ mice to 24 weeks. This allowed us to detect the long-term changes in the metabolic phenotype of MFS mice, which included hyperinsulinemia and fatty liver disease. The liver phenotype in HFD fed male *Fbn1*$^{C1041G/+}$ mice was associated with fat accumulation in hepatocytes, increase in fatty acid synthesis, cholesterol and triglycerides as well as an insulin intolerance, all closely resembling NAFLD that commonly results in non-alcoholic steatohepatitis (NASH) [*Dorn et al., 2010; Knebel et al., 2012; Nakamura & Terauchi, 2013*]. We did not observe the signs of NAFLD or NASH in wild type C57Bl/6J littermates after 24 weeks of diet, consistent with previous studies demonstrating that only very long, 30–60-week exposure to HFD is required for these mice to develop NASH [*Nakamura & Terauchi, 2013*]. Thus, having MFS exacerbated the negative outcomes of HFD for male mice, while attenuated the harmful effects of HFD for female mice.

We have considered several potential reasons for the differences in the responses of MFS mice to HFD. One recently identified link between fibrillin-1 and whole-body bioenergetics is asprosin, the C-terminal prodomain of fibrillin-1 that is cleaved during or directly after secretion into the extracellular environment [*Lönnqvist et al., 1998; Wallis et al., 2003*]. Asprosin acts as a circulating glucogenic hormone, that responds very fast by releasing glucose from the liver to the

circulation during fasting conditions [*Romere et al., 2016*]. Previous studies have shown that asprosin is elevated in humans and mice affected with insulin resistance, obesity, and diabetes mellitus [*Romere et al., 2016; Alan et al., 2019; Wang et al., 2019; Zhang et al., 2020*]. In contrast, a decreased level of plasma asprosin was found in 87 obese children, with even lower levels of asprosin in boys than in girls, demonstrating a clear sexual dimorphism [*Long et al., 2019*]. Although our study found a similar sexual dimorphism in MFS mice responding to HFD, no difference in circulating levels of asprosin in either male MFS or LC mice was observed. The discrepancy between the Romere study, that found that male $Fbn1^{mgR/mgR}$ mice displayed a 70% decrease in circulating asprosin, and our study, might be explained by the difference using the defined HFD and CD in our study versus the "normal chow" likely representing a grain-based diet commonly used in animal facilities in the study by Romere et al. [*Romere et al., 2016*].

As an alternative mechanism, we explored the potential contribution of ER stress, specifically to the development of NAFLD-like liver phenotype, which was previously shown to be associated with testosterone-induced ER stress after the long term HFD of WT mice [*Jia et al., 2018*]. Knowing that the missense mutation in $Fbn1^{C1041G/+}$ mice leads to a disorganized ECM which is associated with ER stress [*Siegert et al., 2019*], we hypothesized that the liver in $Fbn1^{C1041G/+}$ mice is under chronic ER-stress. Indeed, we have found that orchiectomy reduced the NAFLD-like liver phenotype in MFS mice and demonstrated upregulated phosphorylation of PERK, a known downstream effector of ER-stress and the unfolded protein response [*Ozcan et al., 2004; Boot-Handford & Briggs, 2010*]. We also found an increased level of Srebp1, the activation of which is induced during ER-stress, and which also increases PERK phosphorylation [*Hu et al., 2020*]. A similar increase in the ER-stress followed by an increasing PERK-phosphorylation were identified in WT mice that were fed a long-term HFD [*Ozcan et al., 2004*] Furthermore, it was also reported

that the liver in MFS patients is commonly enlarged and can contain an increased number of cysts [*von Kodolitsch et al., 2019*]. Thus, our data suggest that fibrillin-1 deficiency in MFS results in increased ER stress, which is exacerbated by HFD, and ultimately can lead to a liver condition that resembles the phenotype of NAFLD.

HFD is characterized by a high content fat, and its negative effect on general health is of utmost concern [*Johnson et al., 2021*]. Here we demonstrate that HFD leads to weight gain and susceptibility to poor metabolic outcomes in male mice affected with MFS. The association of male sex with worse metabolic outcomes due to HFD was previously reported in both mice and humans [*Hwang et al., 2010; Long et al., 2019; Hasegawa et al., 2020*]. Our study provides a rationale to examine metabolic manifestations in older MFS patients, which is consistent with a recent study that presented numerous clinical manifestations in MFS patients, beyond those listed in the Ghent nosology [*von Kodolitsch et al., 2019*]. Understanding the pathophysiology, the life course, and the environmental contributors to the progression of MFS paves the way for personalized dietary recommendations for these patients, which will eventually improve their quality of life.

3.7 Acknowledgements

We express our gratitude to Dr. Francesco Ramirez for the provision of *Fbn1*$^{mgR/mgR}$ mice. We would also like to thank Nour Pop and Merve Younussi for quantifying the adipocytes. We are also grateful to the animal facility staff at the Shriners Hospital for Children for technical assistance with the *in vivo* study.

Declarations of Interest: None

Author's contribution

The conception and design of the study: KT, MLM, DPR, SVK

The acquisition of data: KT, MLM

Analysis and interpretation of data: KT, MLM, DPR, SVK

Drafting the article: KT, MLM, DPR, SVK

Critical revision: KT, MLM, DPR, SVK

Approval of the final version: All co-authors

Funding

This work was supported by a research grant of the Canadian Institute of Health Research MOP-137091 and PJT-152926, the Marfan Foundation (USA), and a fellowship to MLM from the Fonds de recherche de Quebec.

3.8 Figures and supplemental information

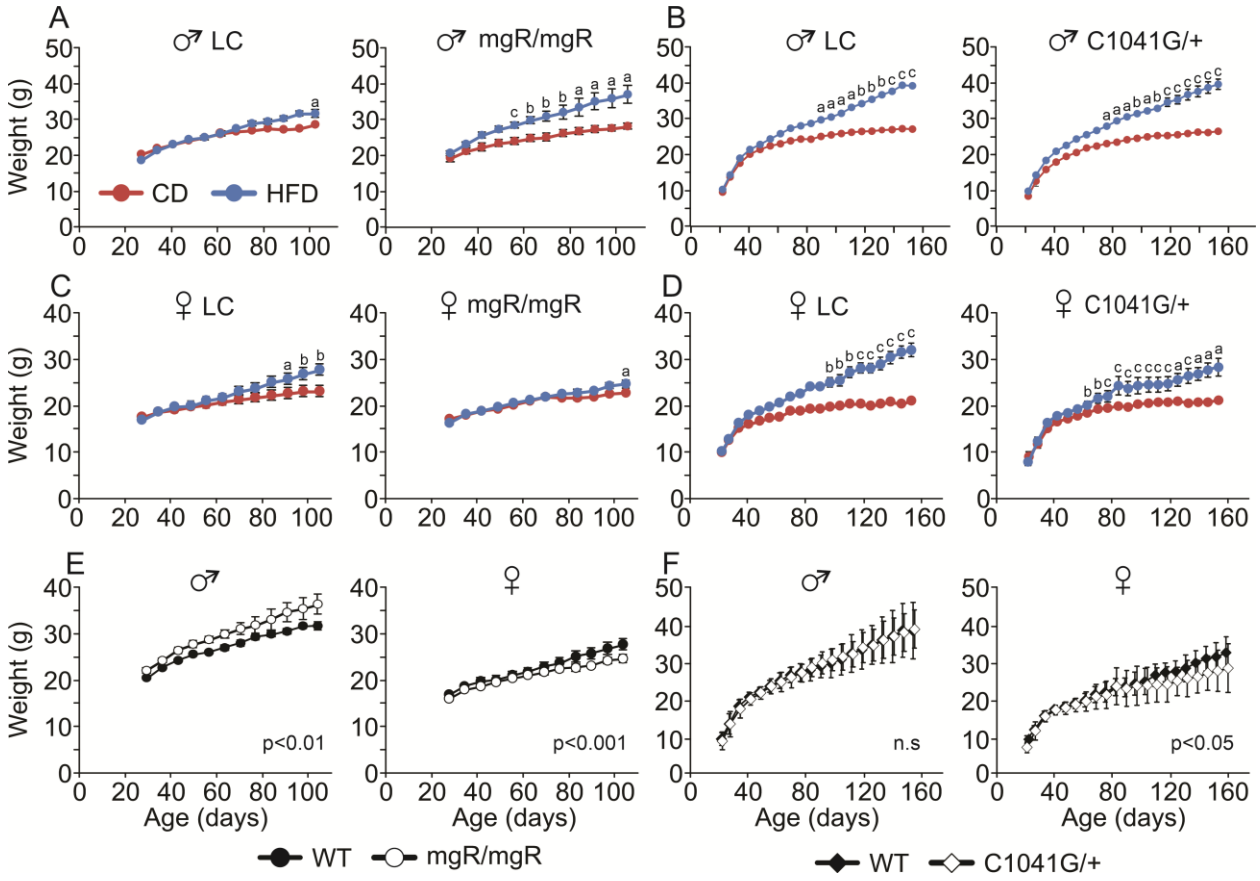

Figure 3.1. Diet-induced weight gain in MFS mice and their wild type littermates. Male and female mgR/mgR, C1041G/+ and littermate control (LC) mice were fed with a control diet (CD), or a high fat diet (HFD) starting from 4 weeks of age. **(A-D)** Average weight of male **(A, B)** and female **(C, D)** mgR/mgR and LC during 12 weeks on CD and HFD **(A, C)** or C1041G/+ and LC during 24 weeks on CD and HFD **(B, D)**. **(E, F)** Average weight gain of male and female mgR/mgR **(E)** and C1041G/+ **(F)** with corresponding LC. Data are means ± SEM, n= 5-12 mice per group (mgR/mgR cohort) and n=7-9 mice per group (C1041G/+), for A-F the letters indicate significance as *a* $p<0.05$; *b* $p<0.01$; *c* $p<0.001$ assessed by two-way repeated measures ANOVA with Tukey post-test.

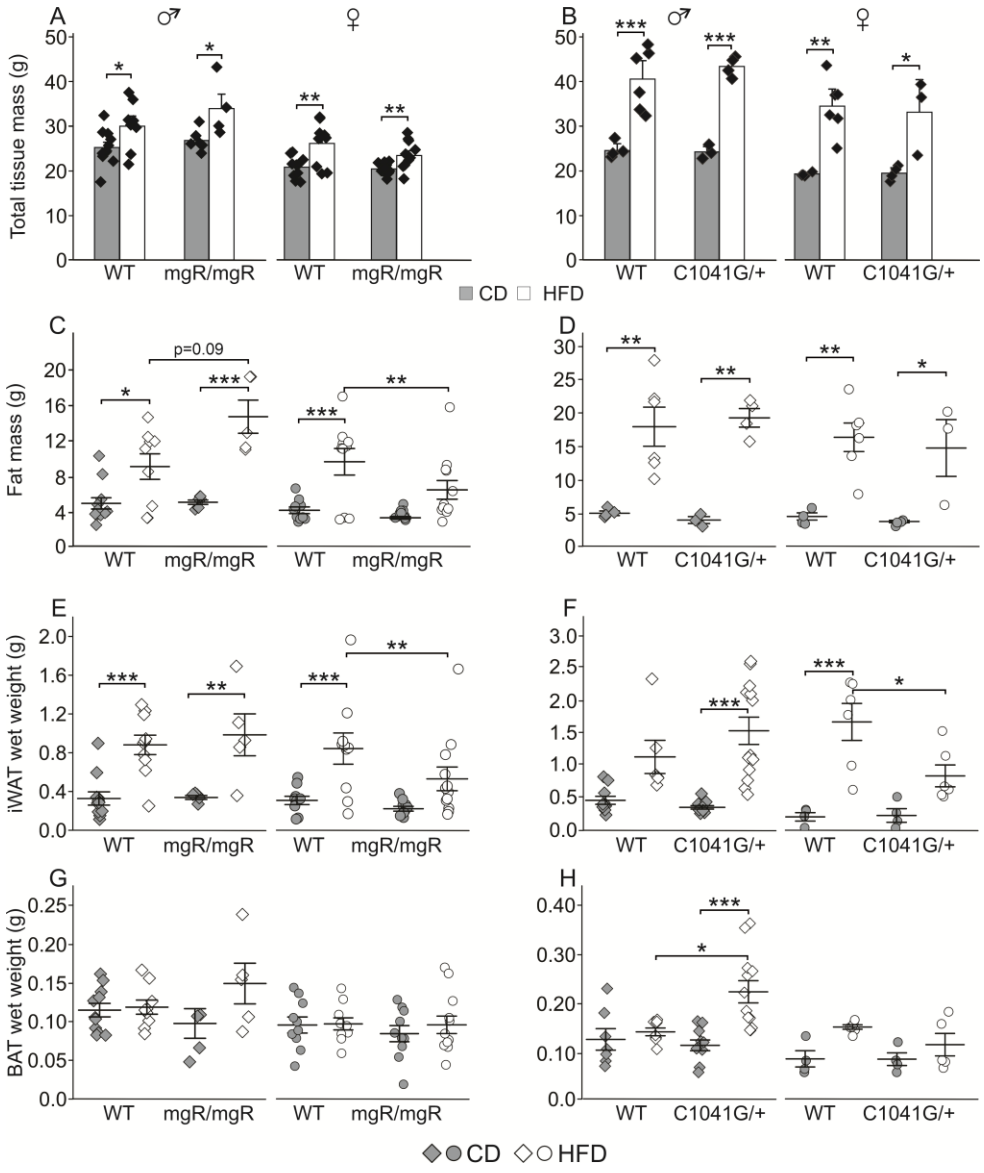

Figure 3.2. Diet-induced changes in adiposity in MFS mice and their wild type littermates. The tissue composition in male (d*iamonds*) and female (*circles*) mgR/mgR and C1041G/+ and littermate control (LC) mice, fed with a control diet (CD, *grey symbols*), or a high fat diet (HFD, *white symbols*) starting from 4 weeks of age for 12 weeks for mgR/mgR, or 24 weeks for C1041G/+ mice. The mice were first analyzed using DEXA, then inguinal white adipose tissue (iWAT) and interscapular brown adipose tissue (BAT) was dissected and weighed. **(A-D)** DEXA analysis of total tissue mass **(A-B)**, and fat mass **(C-D)** of mgR/mgR and LC **(A, C)** and of C1041G/+ and LC **(B, D)**. **(E-H)** The average weight of iWAT **(E, F)** and BAT **(G, H)** in mgR/mgR and LC **(E, G)** and C1041G/+ and LC **(F, H)** on CD or HFD. Data are means ± SEM, n=5-12 mice per group, *p<0.05, **p<0.01, ***p<0.001 assessed by two-way ANOVA with Tukey post-test on log transformed raw values.

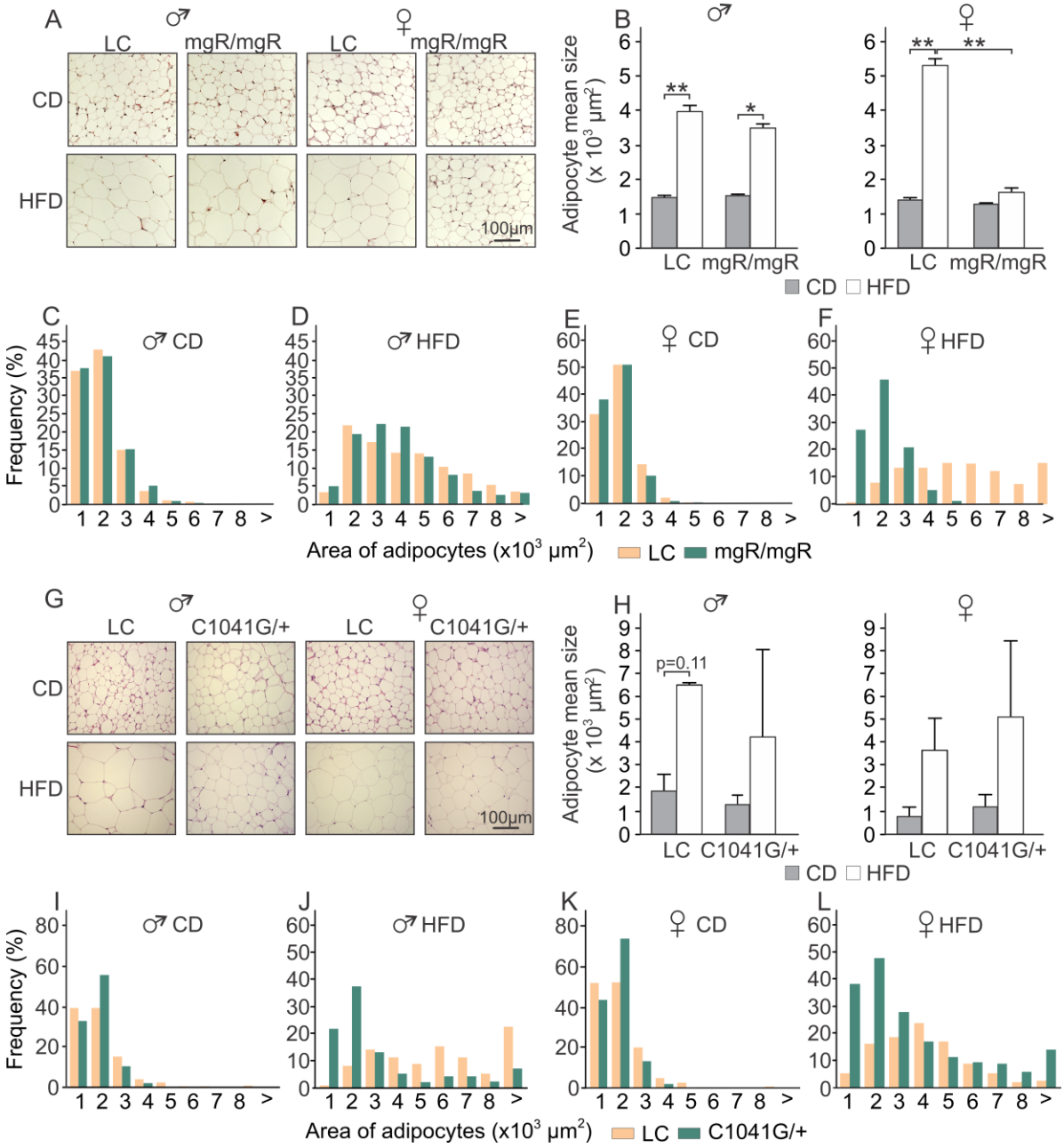

Figure 3.3. Diet-induced changes in adipocyte size of MFS mice and their wild type littermates. Adipocyte size in iWAT were analyzed in male and female mgR/mgR) and C1041G/+ and littermate control (LC) mice fed with CD or HFD on week 12 for mgR/mgR, or week 24 for C1041G/+ after the start of the diet. **(A, G)** Representative images of hematoxylin-eosin stained iWAT from mgR/mgR mice and their LC **(A)** and C1041G/+ mice and their LC **(G)**. **(B, H)** The average adipocyte planar area in iWAT of mgR/mgR **(B)** and C1041G/+ **(H)** mice. Data are means ± SD, n=3 mice/condition, *p<0.05, **p<0.01, ***p<0.001 assessed by two-way ANOVA with Tukey post-test. **(C-F; I-L)** The histograms of relative frequency of adipocyte planar areas binned by 1000 mm^2 in mgR/mgR **(C-F)** and C1041G/+ **(I-L)** mice, n=2-3 mice/condition.

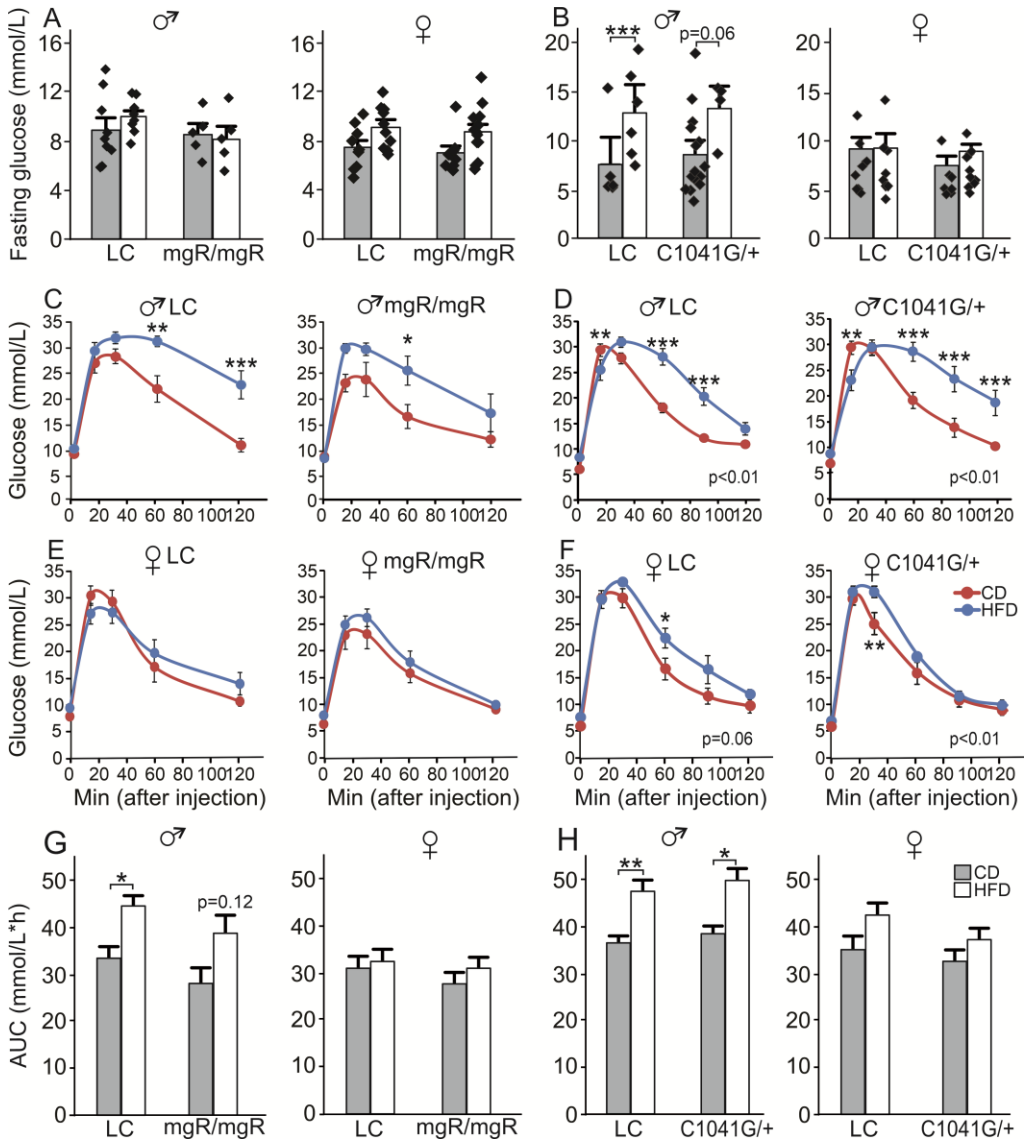

Figure 3.4. Diet-induced changes in glucose homeostasis in MFS mice and their wild type littermates. Starting from 4 weeks of age, male and female wild type and MFS mice were fed with a control diet (CD), or a high fat diet (HFD) and glucose homeostasis was analyzed on week 12 for mgR/mgR, or week 20 for C1041G/+ after the start of the diet. **(A, B)** Fasting glucose levels in mgR/mgR and LC **(A)** and C1041G/+ and LC **(B)** on CD (*grey bars*) or HFD (*white bars*). **(C-H)** Glucose tolerance tests in mgR/mgR and LC **(C, E, G)**, or 1041G/+ and LC **(D, F, H)** male (C, D, G left, H left) and female (E, F, G right, H right) mice fed with control diet (CD, red lines or grey bars), or a high fat diet (HFD, blue lines or white bars). **(C-F)** Average changes in blood glucose following a bolus injection of glucose (2 g/kg). **(G, H)** Average area under the curve for the data shown in (C-F). Data are means ± SEM, n=5-12 mice per group, *p<0.05, **p<0.01, ***p<0.001 analyzed by two-way ANOVA (A, B, G, H) or two-way repeated measures ANOVA (C-F) with Tukey post-test.

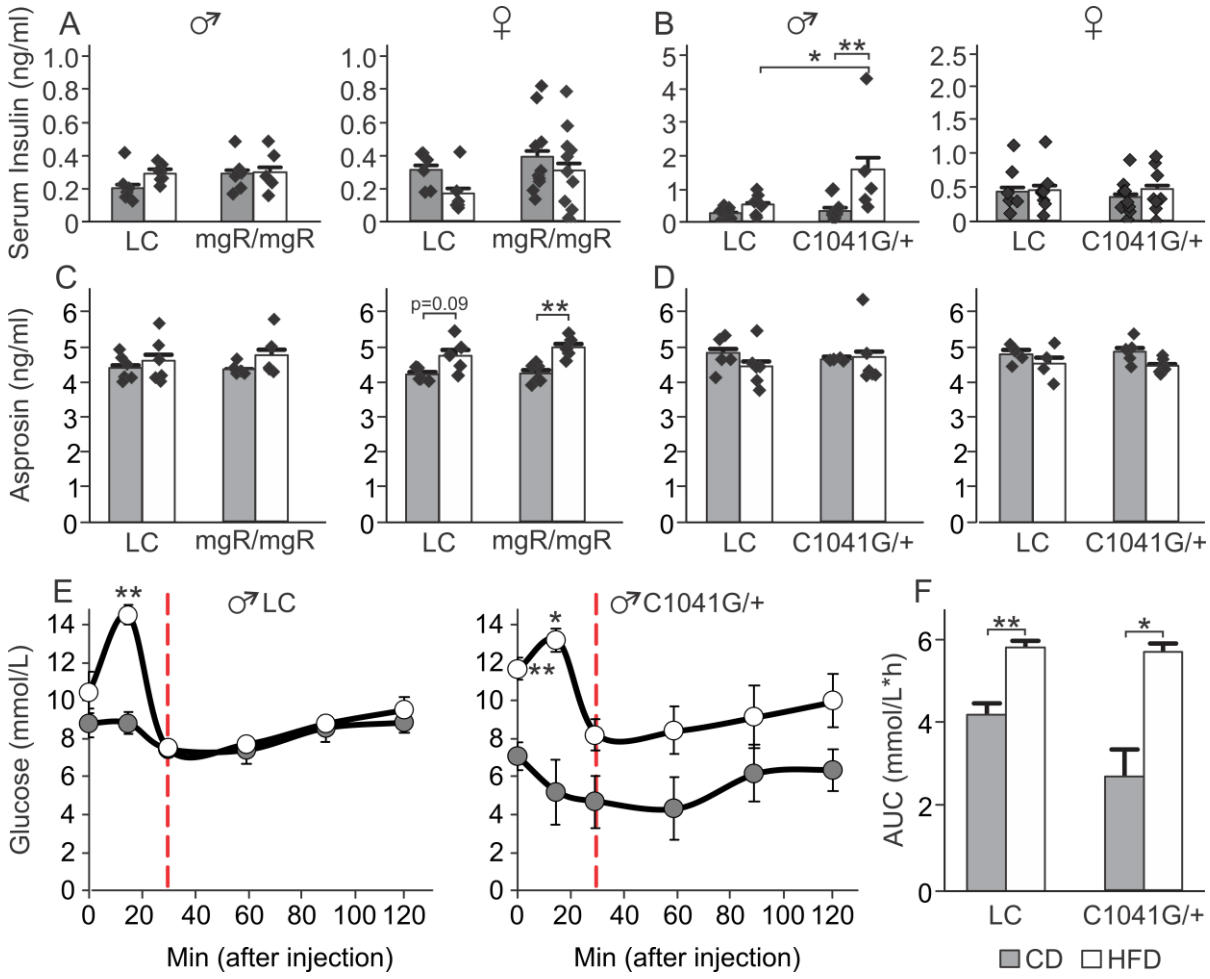

Figure 3.5. Diet-induced changes in insulin homeostasis in MFS mice and their wild type littermates. Starting from 4 weeks of age, male and female wild type and MFS mice were fed with a control diet (CD), or a high fat diet (HFD). **(A, B)** Average serum insulin levels in mgR/mgR mice after 12 weeks on the diets **(A)**, and in C1041G/+ mice after 24 weeks on the diets **(B)**. Data are means ± SEM; n=3-4 mice per group, left panels – male mice, right panels, female mice. **(C, D)** Average serum asprosin levels in mgR/mgR mice after 12 weeks on the diets **(C)**, and in C1041G/+ mice after 24 weeks on the diets **(D)**. Data are means ± SEM; n=4-6 mice per group, left panels – male mice, right panels, female mice. **(E, F)** An insulin tolerance test (ITT) in male C1041G/+ and LC mice fed with control diet (CD), and a high fat diet (HFD) for 20 weeks. **(E)** Average changes in blood glucose concentration following a bolus injection of insulin (0.6 units/kg). **(F)** Average area under the curve for the data shown in C. Data are means ± SEM; n=5-13 mice per group, *p < 0.05 and **p < 0.01 calculated by two-way ANOVA with Tukey post-test.

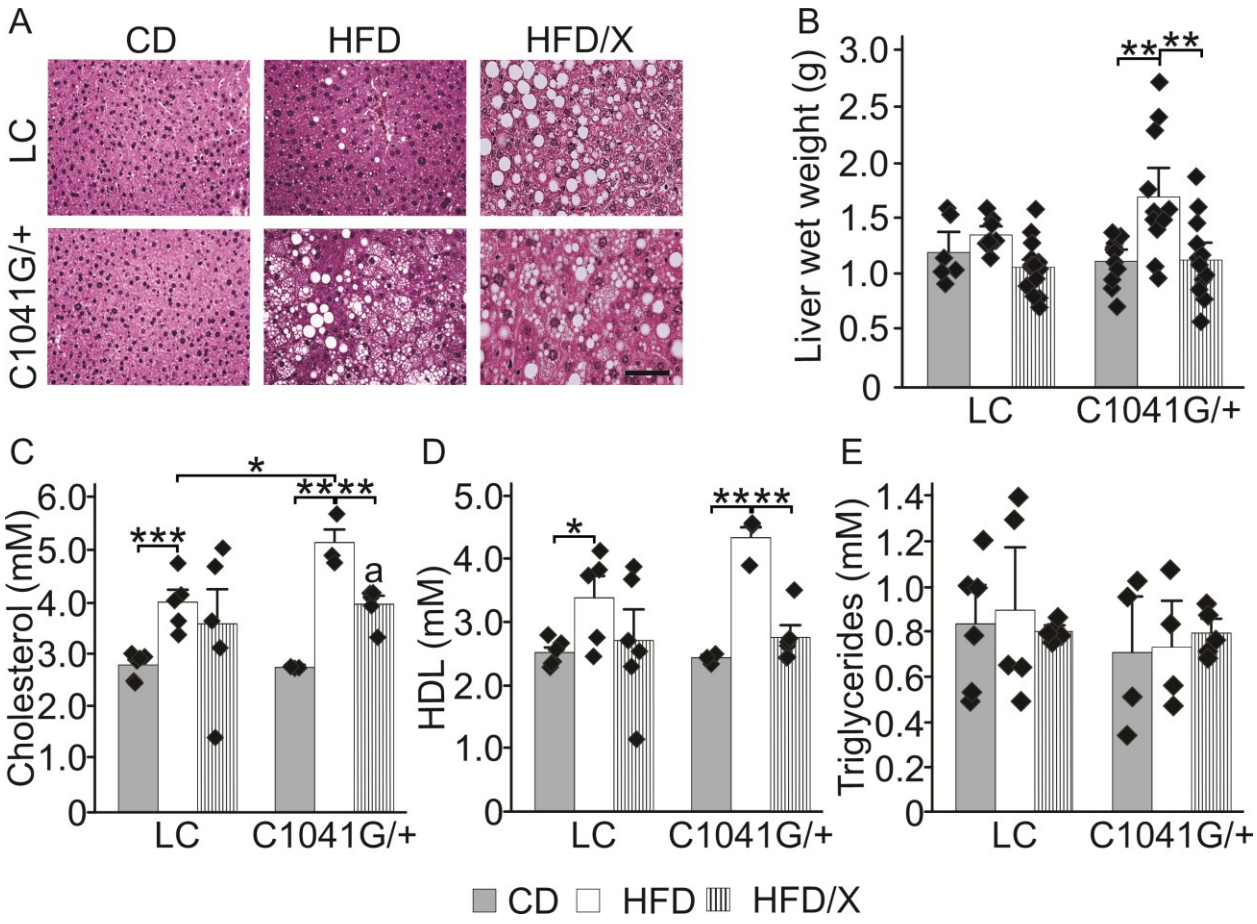

Figure 3.6. Diet-induced changes in liver adiposity in *Fbn1*$^{C1041G/+}$ mice and their wild type littermates. Starting from 4 weeks of age, male and female C1041G/+ and littermate control (LC) mice were fed with a control diet (CD, *grey bars*), or a high fat diet (HFD, *white bars*) for 24 weeks. Livers were analyzed at the experimental endpoints. For orchiectomy, 10–12-week-old male C1041G/+ and LC mice that were on HFD from week 3-4 underwent sham or castration surgery and were maintained on HFD for the remaining 16-18 weeks. **(A)** Representative images of histological liver sections stained with hematoxylin and eosin. **(B)** Average weight of liver tissue. **(C-E)** Average serum levels of cholesterol **(C)**, HDL **(D)** and triglycerides **(E)**. Data are means ± SEM; n=3-4 mice per group; *$p < 0.05$ and **$p < 0.01$ assessed by two-way ANOVA with Tukey post-test.

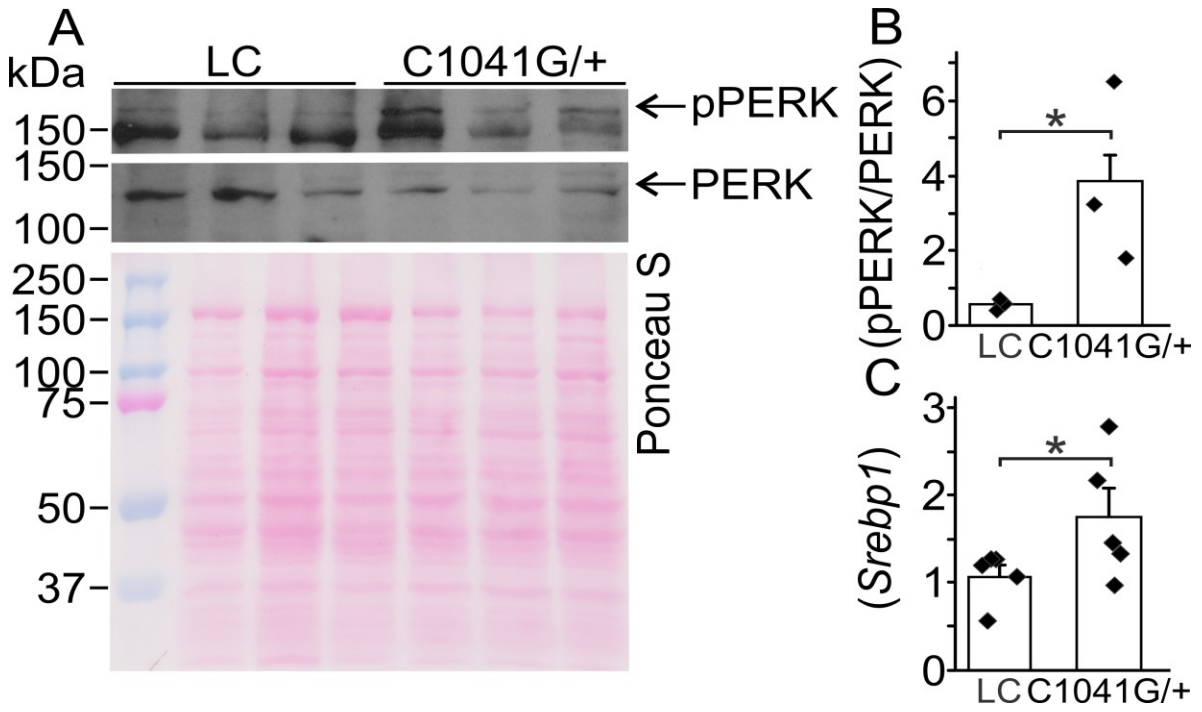

Figure 3.7. ER-stress in the liver of *Fbn1*$^{C1041G/+}$ mice and their wild type littermates. Starting from 4 weeks of age, male C1041G/+ and littermate control (LC) mice were fed with control diet (CD) or a high fat diet (HFD) for 24 weeks. The liver expression of phosphorylated (pPERK) and total PERK were analyzed by immunoblotting. The mRNA expression of a liver lipogenic factor, *Srebp1,* was analyzed by qPCR. **(A)** Representative immunoblots (top) and corresponding control ponceau staining (bottom). **(B)** Average protein levels of pPERK normalized to total PERK. **(C)** Average mRNA expression of *Srebp1*. Data are means ±SEM, n = 3-5 mice per condition, *p < 0.05 determined by one-way ANOVA with Tukey post-test.

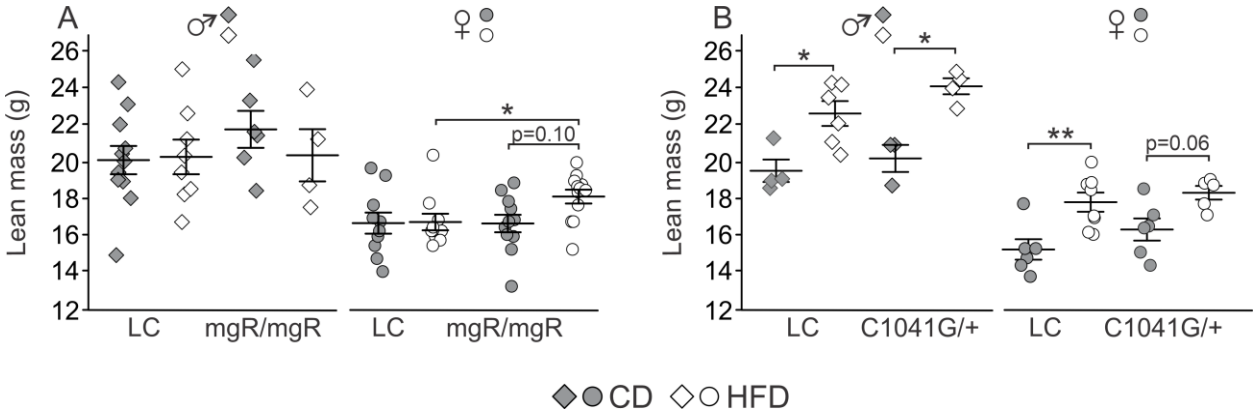

Figure S3.1. Female *Fbn1*$^{mgR/mgR}$ mice increase lean mass when fed with HFD. The lean mass in male (d*iamonds*) and female (*circles*) *Fbn1*$^{mgR/mgR}$ (mgR/mgR) and *Fbn1*$^{C1041G/+}$ (C1041G/+) and littermate control (LC) mice, fed with a control diet (CD, *grey symbols*), or a high fat diet (HFD, *white symbols*) starting from 4 weeks of age for 12 weeks for *Fbn1*$^{mgR/mgR}$, or 24 weeks for *Fbn1*$^{C1041G/+}$ mice, was analyzed using DEXA. **(A-B)** DEXA analysis of the lean mass in mgR/mgR and LC **(A)** and C1041G/+ and LC on CD or HFD **(B)**. Data are means ± SEM, n=3-12 mice per group, *p<0.05, **p<0.01, ***p<0.001 by two-way ANOVA with Tukey post-test on log transformed raw values.

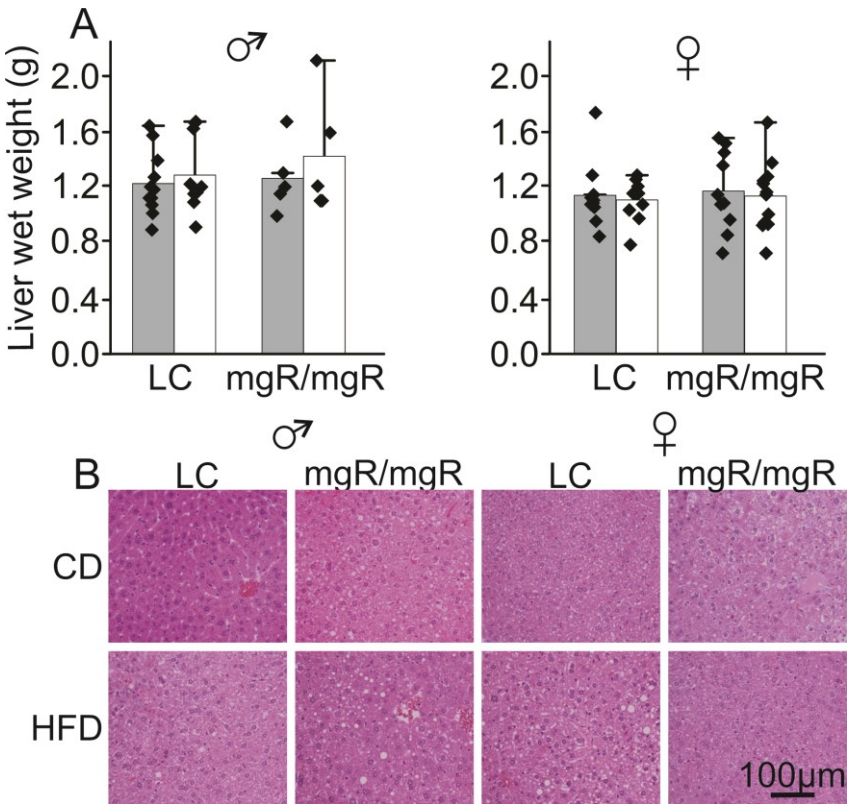

Figure S3.2. Male or female *Fbn1*$^{mgR/mgR}$ mice do not demonstrate liver adiposity when fed HFD. Starting from 4 weeks of age, male and female *Fbn1*$^{mgR/mgR}$ (mgR/mgR) and littermate control (LC) mice were fed with a control diet (CD, *grey bars*), or a high fat diet (HFD, *white bars*) for 12 weeks and livers were analyzed at the experimental endpoints. **A)** Average weight of liver tissue **B)** Representative images of histological liver sections stained with H&E. Data are means ± SEM; n=3-11 mice per group; no significant difference was detected by two-way ANOVA.

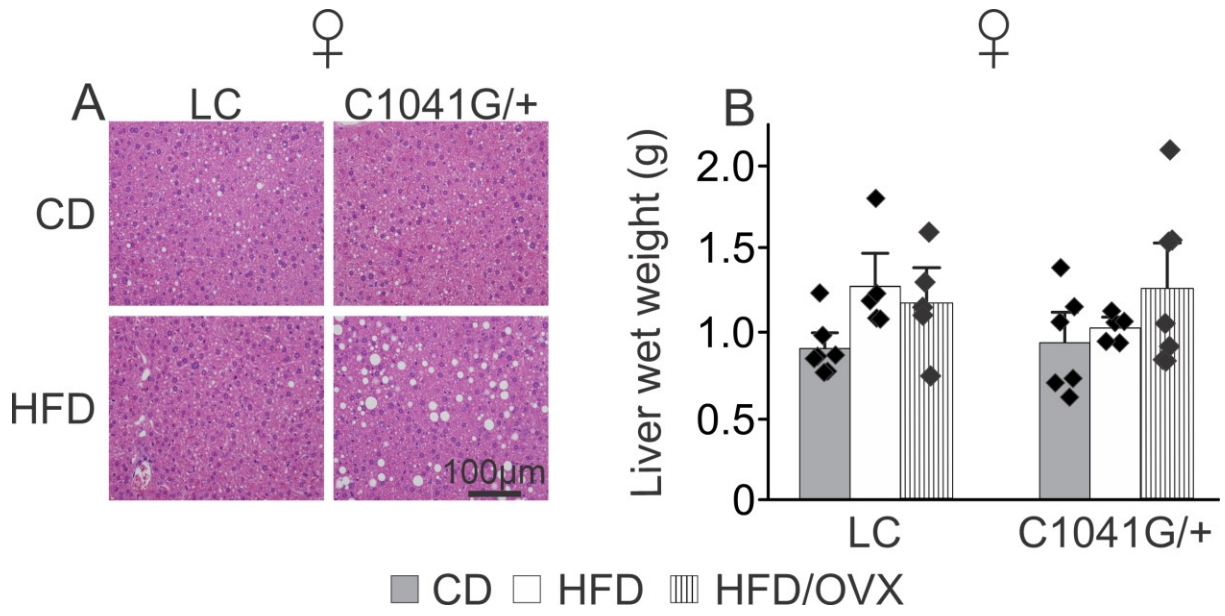

Figure S3.3. Female *Fbn1*$^{C1041G/+}$ demonstrate only a mild lipid accumulation in the liver when fed with HFD. Starting from 4 weeks of age, female *Fbn1*$^{C1041G/+}$ (C1041G/+) and littermate control (LC) mice were fed with a control diet (CD, *grey bars*), or a high fat diet (HFD, *white bars*) for 24 weeks and their livers were analyzed at the experimental endpoints. For ovariectomy, 10–12-week-old female C1041G/+ and LC mice that were on HFD from week 3-4 underwent sham or ovariectomy surgery (HFD/OVX) and were maintained on HFD for the remaining weeks 16-18 weeks. **A)** Representative images of histological liver sections stained with H&E. **B)** Average weight of liver tissue. Data are means ± SEM; n=5-7 mice per group; no significance was detected by two-way ANOVA.

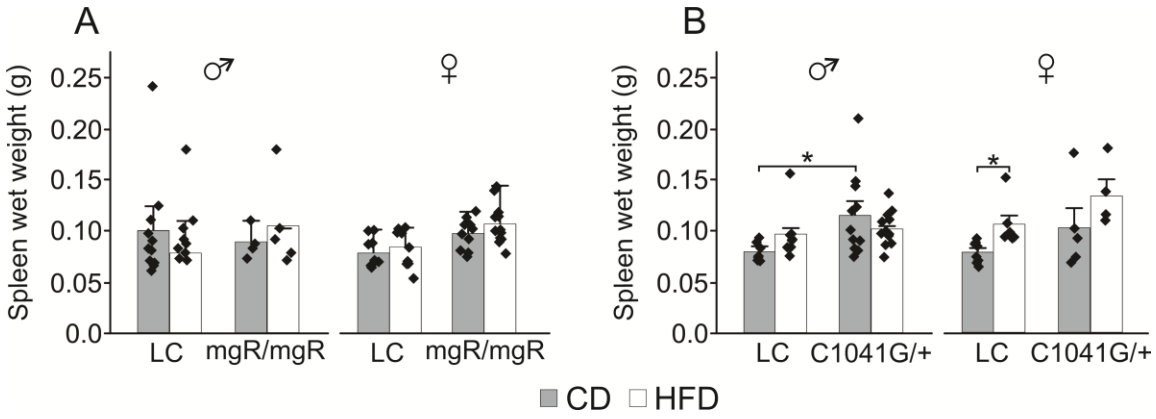

Figure S3.4. The spleen weight is not changed in MFS mutant mice when fed with HFD. Male and female *Fbn1*$^{mgR/mgR}$ (mgR/mgR) and *Fbn1*$^{C1041G/+}$ (C1041G/+) and littermate control (LC) mice were fed with a control diet (CD, *grey bars*), or a high fat diet (HFD, *white bars*) starting from 4 weeks of age. **(A-B)** Average weight of the spleen in mgR/mgR and LC at 16 weeks of age **(A)** and average weight of spleen in C1041G/+ and LC at 28 weeks of age **(B)**. Data are means ± SEM; n=4-14 mice per group, *p < 0.05 determined by two-way ANOVA with Tukey post-test.

3.9 Bibliography for chapter 3

Alan M, Gurlek B, Yilmaz A, Aksit M, Aslanipour B, Gulhan I, Mehmet C, Taner CE. (2019). Asprosin: a novel peptide hormone related to insulin resistance in women with polycystic ovary syndrome. *Gynecol Endocrinol* **35**, 220-223

Aubart M, Gross MS, Hanna N, Zabot MT, Sznajder M, Detaint D, Gouya L, Jondeau G, Boileau C, Stheneur C. (2015). The clinical presentation of Marfan syndrome is modulated by expression of wild-type FBN1 allele. *Hum Mol Genet* **24**, 2764-2770

Boileau C, Jondeau G, Mizuguchi T, Matsumoto N. (2005). Molecular genetics of Marfan syndrome. *Curr Opin Cardiol* **20**, 194-200

Boot-Handford RP, Briggs MD. (2010). The unfolded protein response and its relevance to connective tissue diseases. *Cell Tissue Res* **339**, 197-211

Carta L, Pereira L, Arteaga-Solis E, Lee-Arteaga SY, Lenart B, Starcher B, Merkel CA, Sukoyan M, Kerkis A, Hazeki N, Keene DR, Sakai LY, Ramirez F. (2006). Fibrillins 1 and 2 perform partially overlapping functions during aortic development. *J Biol Chem* **281**, 8016-8023

Collod-Beroud G, Le Bourdelles S, Ades L, Ala-Kokko L, Booms P, Boxer M, Child A, Comeglio P, De Paepe A, Hyland JC, Holman K, Kaitila I, Loeys B, Matyas G, Nuytinck L, Peltonen L, Rantamaki T, Robinson P, Steinmann B, Junien C, Beroud C, Boileau C. (2003). Update of the UMD-FBN1 mutation database and creation of an FBN1 polymorphism database. *Hum Mutat* **22**, 199-208

Davis MR, Arner E, Duffy CR, De Sousa PA, Dahlman I, Arner P, Summers KM. (2016). Expression of FBN1 during adipogenesis: Relevance to the lipodystrophy phenotype in Marfan syndrome and related conditions. *Mol Genet Metab* **119**, 174-185

Despres JP, Lemieux I. (2006). Abdominal obesity and metabolic syndrome. *Nature* **444**, 881-887

Dorn C, Riener MO, Kirovski G, Saugspier M, Steib K, Weiss TS, Gabele E, Kristiansen G, Hartmann A, Hellerbrand C. (2010). Expression of fatty acid synthase in nonalcoholic fatty liver disease. *Int J Clin Exp Pathol* **3**, 505-514

Fang L, Guo F, Zhou L, Stahl R, Grams J. (2015). The cell size and distribution of adipocytes from subcutaneous and visceral fat is associated with type 2 diabetes mellitus in humans. *Adipocyte* **4**, 273-279

Franken R, den Hartog AW, Radonic T, Micha D, Maugeri A, van Dijk FS, Meijers-Heijboer HE, Timmermans J, Scholte AJ, van den Berg MP, Groenink M, Mulder BJ, Zwinderman AH, de Waard V, Pals G. (2015). Beneficial outcome of losartan therapy depends on type of FBN1 mutation in Marfan syndrome. *Circ Cardiovasc Genet* **8**, 383-388

Franken R, Groenink M, de Waard V, Feenstra HM, Scholte AJ, van den Berg MP, Pals G, Zwinderman AH, Timmermans J, Mulder BJ. (2016). Genotype impacts survival in Marfan syndrome. *Eur Heart J* **37**, 3285-3290

Franken R, Teixido-Tura G, Brion M, Forteza A, Rodriguez-Palomares J, Gutierrez L, Garcia Dorado D, Pals G, Mulder BJ, Evangelista A. (2017). Relationship between fibrillin-1 genotype and severity of cardiovascular involvement in Marfan syndrome. *Heart* **103**, 1795-1799

Hasegawa Y, Chen SY, Sheng L, Jena PK, Kalanetra KM, Mills DA, Wan YY, Slupsky CM. (2020). Long-term effects of western diet consumption in male and female mice. *Sci Rep* **10**, 14686

Hilhorst-Hofstee Y, Hamel BC, Verheij JB, Rijlaarsdam ME, Mancini GM, Cobben JM, Giroth C, Ruivenkamp CA, Hansson KB, Timmermans J, Moll HA, Breuning MH, Pals G. (2011). The clinical spectrum of complete FBN1 allele deletions. *Eur J Hum Genet* **19**, 247-252

Hu Q, Mao Y, Liu M, Luo R, Jiang R, Guo F. (2020). The active nuclear form of SREBP1 amplifies ER stress and autophagy via regulation of PERK. *FEBS J* **287**, 2348-2366

Hubmacher D, Tiedemann K, Reinhardt DP. (2006). Fibrillins: From biogenesis of microfibrils to signaling functions. *Curr Top Dev Biol* **75**, 93-123

Hwang LL, Wang CH, Li TL, Chang SD, Lin LC, Chen CP, Chen CT, Liang KC, Ho IK, Yang WS, Chiou LC. (2010). Sex differences in high-fat diet-induced obesity, metabolic alterations and learning, and synaptic plasticity deficits in mice. *Obesity* **18**, 463-469

Jia Y, Yee JK, Wang C, Nikolaenko L, Diaz-Arjonilla M, Cohen JN, French SW, Liu PY, Lue Y, Lee WP, Swerdloff RS. (2018). Testosterone protects high-fat/low-carbohydrate diet-induced nonalcoholic fatty liver disease in castrated male rats mainly via modulating endoplasmic reticulum stress. *Am J Physiol Endocrinol Metab* **314**, E366-E376

Johnson CS, Shively C, Michalson KT, Lea AJ, DeBo RJ, Howard TD, Hawkins GA, Appt SE, Liu Y, McCall CE, Herrington DM, Ip EH, Register TC, Snyder-Mackler N. (2021). Contrasting effects of Western vs Mediterranean diets on monocyte inflammatory gene expression and social behavior in a primate model. *eLife* **10**

Judge DP, Biery NJ, Keene DR, Geubtner J, Myers L, Huso DL, Sakai LY, Dietz HC. (2004). Evidence for a critical contribution of haploinsufficiency in the complex pathogenesis of Marfan syndrome. *J Clin Invest* **114**, 172-181

Knebel B, Haas J, Hartwig S, Jacob S, Kollmer C, Nitzgen U, Muller-Wieland D, Kotzka J. (2012). Liver-specific expression of transcriptionally active SREBP-1c is associated with fatty liver and increased visceral fat mass. *PLoS One* **7**, e31812

Long W, Xie X, Du C, Zhao Y, Zhang C, Zhan D, Li Z, Ning Q, Luo X. (2019). Decreased circulating levels of asprosin in obese children. *Horm Res Paediatr* **91**, 271-277

Lönnqvist L, Reinhardt DP, Sakai LY, Peltonen L. (1998). Evidence for furin-type activity-mediated C-terminal processing of profibrillin-1 and interference in the processing by certain mutations. *Hum Mol Genet* **7**, 2039-2044

Mátyás G, Alonso S, Patrignani A, Marti M, Arnold E, Magyar I, Henggeler C, Carrel T, Steinmann B, Berger W. (2007). Large genomic fibrillin-1 (FBN1) gene deletions provide evidence for true haploinsufficiency in Marfan syndrome. *Hum Genet* **122**, 23-32

McLaughlin T, Sherman A, Tsao P, Gonzalez O, Yee G, Lamendola C, Reaven GM, Cushman SW. (2007). Enhanced proportion of small adipose cells in insulin-resistant vs insulin-sensitive obese individuals implicates impaired adipogenesis. *Diabetologia* **50**, 1707-1715

McLaughlin T, Lamendola C, Coghlan N, Liu TC, Lerner K, Sherman A, Cushman SW. (2014). Subcutaneous adipose cell size and distribution: relationship to insulin resistance and body fat. *Obesity* **22**, 673-680

Muthu ML, Reinhardt DP. (2020). Fibrillin-1 and fibrillin-1-derived asprosin in adipose tissue function and metabolic disorders. *J Cell Commun Signal* **14**, 159-173

Nakamura A, Terauchi Y. (2013). Lessons from mouse models of high-fat diet-induced NAFLD. *Int J Mol Sci* **14**, 21240-21257

Nistala H, Lee-Arteaga S, Carta L, Cook JR, Smaldone S, Siciliano G, Rifkin AN, Dietz HC, Rifkin DB, Ramirez F. (2010). Differential effects of alendronate and losartan therapy on osteopenia and aortic aneurysm in mice with severe Marfan syndrome. *Hum Mol Genet* **19**, 4790-4798

Okamura T, Hamaguchi M, Bamba R, Nakajima H, Yoshimura Y, Kimura T, Nishida K, Hashimoto Y, Fukuda T, Senmaru T, Fukui M. (2020). Immune modulating effects of additional supplementation of estradiol combined with testosterone in murine testosterone-deficient NAFLD model. *Am J Physiol Gastrointest Liver Physiol* **318**, G989-G999

Ozcan U, Cao Q, Yilmaz E, Lee AH, Iwakoshi NN, Ozdelen E, Tuncman G, Gorgun C, Glimcher LH, Hotamisligil GS. (2004). Endoplasmic reticulum stress links obesity, insulin action, and type 2 diabetes. *Science* **306**, 457-461

Parlee SD, Lentz SI, Mori H, MacDougald OA. (2014). Quantifying size and number of adipocytes in adipose tissue. *Methods Enzymol* **537**, 93-122

Pasarica M, Xie H, Hymel D, Bray G, Greenway F, Ravussin E, Smith SR. (2009). Lower total adipocyte number but no evidence for small adipocyte depletion in patients with type 2 diabetes. *Diabetes Care* **32**, 900-902

Passarge E, Robinson PN, Graul-Neumann LM. (2016). Marfanoid-progeroid-lipodystrophy syndrome: a newly recognized fibrillinopathy. *Eur J Hum Genet* **24**, 1244-1247

Pellizzon MA, Ricci MR. (2020). Choice of laboratory rodent diet may confound data interpretation and reproducibility. *Curr Dev Nutr* **4**, nzaa031

Pereira L, Lee SY, Gayraud B, Andrikopoulos K, Shapiro SD, Bunton T, Biery NJ, Dietz HC, Sakai LY, Ramirez F. (1999). Pathogenetic sequence for aneurysm revealed in mice underexpressing fibrillin-1. *Proc Natl Acad Sci USA* **96**, 3819-3823

Pyeritz RE. (2000). The Marfan syndrome. *Annu Rev Med* **51**, 481-510

Ramirez F, Dietz HC. (2007). Fibrillin-rich microfibrils: Structural determinants of morphogenetic and homeostatic events. *J Cell Physiol* **213**, 326-330

Robinson P, Arteaga-Solis E, Baldock C, Collod-Beroud G, Booms P, De Paepe A, Dietz HC, Guo G, Handford PA, Judge DP, Kielty CM, Loeys B, Milewicz DM, Ney A, Ramirez F, Reinhardt DP, Tiedemann K, Whiteman P, Godfrey M. (2006). The molecular genetics of Marfan syndrome and related disorders. *J Med Genet* **43**, 769-787

Robinson PN, Godfrey M. (2000) The molecular genetics of Marfan syndrome and related microfibrillopathies. in *J Med Genet*

Romere C, Duerrschmid C, Bournat J, Constable P, Jain M, Xia F, Saha PK, Del Solar M, Zhu B, York B, Sarkar P, Rendon DA, Gaber MW, LeMaire SA, Coselli JS, Milewicz DM, Sutton VR, Butte NF, Moore DD, Chopra AR. (2016). Asprosin, a fasting-induced glucogenic protein hormone. *Cell* **165**, 566-579

Schneider CA, Rasband WS, Eliceiri KW. (2012). NIH Image to ImageJ: 25 years of image analysis. *Nat Methods* **9**, 671-675

Siegert AM, Garcia Diaz-Barriga G, Esteve-Codina A, Navas-Madronal M, Gorbenko Del Blanco D, Alberch J, Heath S, Galan M, Egea G. (2019). A FBN1 3'UTR mutation variant is associated with endoplasmic reticulum stress in aortic aneurysm in Marfan syndrome. *Biochim Biophys Acta Mol Basis Dis* **1865**, 107-114

Summers KM, Nataatmadja M, Xu D, West MJ, McGill JJ, Whight C, Colley A, Ades LC. (2005). Histopathology and fibrillin-1 distribution in severe early onset Marfan syndrome. *Am J Med Genet* **139**, 2-8

Takenouchi T, Hida M, Sakamoto Y, Torii C, Kosaki R, Takahashi T, Kosaki K. (2013). Severe congenital lipodystrophy and a progeroid appearance: Mutation in the penultimate exon of FBN1 causing a recognizable phenotype. *Am J Med Genet* **161A**, 3057-3062

von Kodolitsch Y, Demolder A, Girdauskas E, Kaemmerer H, Kornhuber K, Muino Mosquera L, Morris S, Neptune E, Pyeritz R, Rand-Hendriksen S, Rahman A, Riise N, Robert L, Staufenbiel I, Szocs K, Vanem TT, Linke SJ, Vogler M, Yetman A, De Backer J. (2019). Features of Marfan syndrome not listed in the Ghent nosology - the dark side of the disease. *Expert Rev Cardiovasc Ther* **17**, 883-915

Walji TA, Turecamo SE, DeMarsilis AJ, Sakai LY, Mecham RP, Craft CS. (2016). Characterization of metabolic health in mouse models of fibrillin-1 perturbation. *Matrix Biol* **55**, 63-76

Wallis DD, Putnam EA, Cretoiu JS, Carmical SG, Cao SN, Thomas G, Milewicz DM. (2003). Profibrillin-1 maturation by human dermal fibroblasts: proteolytic processing and molecular chaperones. *J Cell Biochem* **90**, 641-652

Wang CY, Lin TA, Liu KH, Liao CH, Liu YY, Wu VC, Wen MS, Yeh TS. (2019). Serum asprosin levels and bariatric surgery outcomes in obese adults. *Int J Obes* **43**, 1019-1025

Yetman AT, McCrindle BW. (2010). The prevalence and clinical impact of obesity in adults with Marfan syndrome. *Can J Cardiol* **26**, 137-139

Zhang X, Jiang H, Ma X, Wu H. (2020). Increased serum level and impaired response to glucose fluctuation of asprosin is associated with type 2 diabetes mellitus. *J Diabetes Investig* **11**, 349-355

CHAPTER 4: PRELIMINARY FINDINGS - ADIPOCYTE SPECIFIC DELETION OF FIBRILLIN-1 INHIBITS ADIPOSE TISSUE DEVELOPMENT IN MALE MICE

Preliminary findings - Adipocyte specific deletion of fibrillin-1 inhibits adipose tissue development in male mice

Muthu L. Muthu[1], Dieter P. Reinhardt[1,2#]

[1]Faculty of Medicine and Health Sciences, Department of Anatomy and Cell Biology, McGill University, Montreal, Canada

[2]Faculty of Dental Medicine and Oral Health and Sciences, McGill University, Montreal, Canada

[#]Corresponding author

Keywords: Fibrillin-1, Extracellular matrix, Adipose tissue, Mature adipocytes, Macrophages

4.1 Preamble

In chapter 2 and 3, we used MFS mouse models with global fibrillin-1 haploinsufficiency or a fibrillin-1 missense mutation. However, in addition to the adipose tissue phenotypes observed in these mice, it has been well documented that fibrillin-1 has critical functions in the vasculature which causes a progressive aortic aneurysm phenotype leading to reduced survival (~4 months) in the *Fbn1*$^{mgR/mgR}$ mice. Therefore, the goal of this chapter is to study how local absence of adipocyte specific fibrillin-1 microenvironment contributes to the ability of the adipose tissue to regulate whole body homeostasis. We generated a new mouse model using the Cre-loxP strategy to knockout fibrillin-1 specifically from mature adipocytes. We are now validating the fibrillin-1 deletion particularly in mature adipocytes of these mice. Taking this into consideration, the data presented in this chapter is a preliminary characterization of the metabolic phenotype. Future work will include validation of the mouse models and explore in detail the molecular and metabolic phenotypes of these mice.

4.2 Abstract

Fibrillin-1 is present in the extracellular matrix surrounding each adipocyte. Our recent study demonstrated critical negative roles of fibrillin-1 in the regulation of mesenchymal stem cell commitment, differentiation, and adipose tissue development mediated by the insulin signaling pathway. That study used a hypomorphic mouse model (*Fbn1*$^{mgR/mgR}$) with a global reduction of fibrillin-1 to about 20-25% of wild type mice in the early and late phase of adipocyte differentiation. To identify the cell specific role of fibrillin-1 in mature adipocytes, we generated in the present study an adipose tissue–specific conditional knockout of fibrillin-1 using *Adipoq-Cre* transgenic mice. Deletion of fibrillin-1 in mature adipocytes resulted in a significant reduction of the epididymal white adipose tissue mass in male mice at 16 and 30 weeks of age with no differences in the overall body weight when fed with a normal chow. Fibrillin-1 ablation did not affect the weight of other adipose tissues and liver. Furthermore, adipocyte specific fibrillin-1 deletion did not affect the fasting blood glucose, glucose and insulin tolerance levels leading to normal systemic metabolism. Loss of fibrillin-1 considerably reduced the size of adipocytes, and a tendency of decreased crown-like structures (tissue resident macrophages) was observed in epididymal white adipose tissue at 16 and 30 weeks of age compared to littermate controls. Collectively, these studies demonstrate a critical role of fibrillin-1 in maintenance of mature adipocytes which is different than its role in mesenchymal stem cells, demonstrating its importance in adipose tissue homeostasis.

4.3 Introduction

Fibrillin-1 is a 350 kDa multidomain protein and an important component of microfibrils in the extracellular matrix [*Sakai et al., 1986; Keene et al., 1991; Reinhardt et al., 1996; Lönnqvist et al., 1998*]. Fibrillin microfibrils provide a scaffold for elastic fiber formation in elastic tissues and also regulate the bioavailability of several growth factors and cytokines including TGF-β, BMPs and RANKL [*Isogai et al., 2003; Neptune et al., 2003; Chaudhry et al., 2007; Sengle et al., 2008; Tiedemann et al., 2013; Wohl et al., 2016*]. Fibrillin-1 requires cleavage of N- and C-terminal propeptides by furin proteases during or after secretion to prepare the core protein for assembly [*Milewicz et al., 1995; Lönnqvist et al., 1998; Ritty et al., 1999; Wallis et al., 2003*]. The released C-terminal propeptide was described as a new circulating hunger hormone, termed asprosin [*Romere et al., 2016; Duerrschmid et al., 2017*]. Circulating asprosin was reported to be secreted primarily by white adipose tissue, and it increases hepatic glucose production, drives insulin secretion and appetite stimulation through inter-organ cross talk [*Romere et al., 2016; Duerrschmid et al., 2017*]. Mutations throughout fibrillin-1 cause Marfan syndrome (MFS) with wide clinical variabilities, importantly characterized by dysfunction of adipose tissue among others [*Hubmacher & Reinhardt, 2011*]. Individuals with MFS are often lipodystrophic, characterized by reduced overall body fat [*Moraes et al., 2003; Graul-Neumann et al., 2010; Goldblatt et al., 2011; Horn & Robinson, 2011; Takenouchi et al., 2013; Jacquinet et al., 2014; Romere et al., 2016*]. However, a significant proportion of MFS patients (36%) become overweight or even obese, and most people with MFS accrue adiposity as they age [*Erkula et al., 2002; Yetman & McCrindle, 2010; von Kodolitsch et al., 2019; Hansen et al., 2020*].

Recently, we and others have investigated the role of fibrillin-1 mutations and haploinsufficiency in the adipose tissue pathophysiology of MFS [*Walji et al., 2016*] and (chapter 2). We have identified that male mice hypomorphic for fibrillin-1 exhibit excess adipose tissue deposition mediated by adipocyte hypertrophy. Mechanistically, we showed that early deficiency of fibrillin-1 at the mesenchymal cell stage negatively regulates the adipogenic commitment, differentiation, and development by direct cell binding and insulin sequestration, together suppressing the AKT signaling pathway (chapter 2). Further, we treated MFS mice with a HFD regimen to generate diet-induced obesity and demonstrated that male, but not female, MFS mice were prone to excess fat deposition, insulin resistance and hepatic steatosis. Together, those data clearly show a central role of fibrillin-1 in adipose tissue development and homeostasis under pathological MFS conditions.

In the present study we utilized a conditional knockout strategy to selectively delete the fibrillin-1 gene in mature adipocytes for analysis of specific functions of fibrillin-1 in adipose tissue. This is critical to avoid the severe pathological manifestations in the aorta and bones observed with other mouse models. Importantly, we found that this conditional fibrillin-1 knockout resulted in a lipodystrophic phenotype as seen in many MFS patients. Thus, these mice will serve as a powerful tool to study the physiological role of fibrillin-1 in the development and maintenance of adipose tissue. The model will also be useful to test treatment strategies for fibrillin-1 associated adipose tissue dysfunction.

4.4 Methods

4.4.1 Mice used in this study

All experimental procedures were approved by the McGill University Animal Care Committee in accordance with the guidelines of the Canadian Council on Animal Care (Protocol#2014-7561). Fbn1(flox/flox) (*Fbn1-FL*) mice, kindly provided by Dr. Francesco Ramirez, have 2 loxP sites inserted flanking exon 1 of fibrillin-1 [*Eguchi et al., 2011; Cook et al., 2012; Gao et al., 2019*]. To delete the fibrillin-1 gene and thus expression in mature adipocytes, we first bred *Fbn1-FL* mice with *Adipoq-Cre*–transgenic mice expressing Cre recombinase under control of the mouse adiponectin promoter/enhancer (Jackson Laboratories; B6.FVB-Tg (Adipoq-cre)1Evdr/J). This resulted in mice with a Fbn1(flox/+);Adipoq-Cre/+ genotype. Further breeding of Fbn1(flox/+);Adipoq-Cre/+ mice with Fbn1(flox/flox) mice resulted in the adipocyte-specific fibrillin-1 conditional knockout mice (Fbn1(flox/flox);Adipoq-Cre/+, abbreviation *Fbn1-AKO*). The Cre-negative *Fbn1-FL* mice were used as controls. Due to the striking differences observed in the *Fbn1*$^{mgR/mgR}$ mice, only male mice were used for the preliminary experiments in this study. All mice were housed under standard conditions (12 hours of light-dark cycles) and were fed with conventional grain-based diet. For genotyping, genomic DNA isolated from tail snips were amplified by polymerase chain reaction (PCR) using the protocol and the components of the Mouse Direct PCR Kit (Bimake, Cat#B40015). The sequences of primers used for genotyping mice are published in the original study [*Cook et al., 2012*].

4.4.2 Analysis of systemic metabolism and tissues

One week prior to the experimental endpoints (15 or 29 weeks), insulin tolerance test (ITT) and glucose tolerance test (GTT) were performed after 6 h or 16 h starvation, respectively. Blood glucose was measured using a blood glucometer (Verio Flex, OneTouch) with a drop of blood from the tail tip immediately before (0 min) and after acute intraperitoneal injection of 0.75 U/kg insulin or 2 g/kg glucose, at 15, 30, 60, and 120 min respectively. Mice were euthanized at the experimental endpoint and inguinal white adipose tissue (iWAT), epididymal white adipose tissue (eWAT), and liver were dissected and weighed before further analysis.

4.4.3 Histologic and adipocyte size analysis

Paraffin embedded eWAT was cut in 5 μm sections, and deparaffinized by baking slides at 65°C for 30 min followed by two time of 5 min incubation in CitriSolv (Decon Labs) and hydration using a decreasing ethanol gradient and distilled water (100% ethanol – 0% ethanol), followed by hematoxylin and eosin staining. Images were captured at 100× magnification using an AxioImager M2 bright field microscope (Zeiss) equipped with a AxioCam ICc5 color camera at 2 different areas per sample. Quantification of the number and size of adipocytes were performed using the Adiposoft plugin in ImageJ software (Version 1.53n) following established procedures [*Schneider et al., 2012; Parlee et al., 2014*].

4.4.4 RNA extraction and real-time qPCR

eWAT harvested from mice were used to extract RNA using the RNeasy kit (Qiagen, Cat#74104). cDNA synthesis was performed with 1 μg RNA using the Protoscript First Strand cDNA Synthesis

kit (New England Biolabs, Cat#E6560L). For quantification of *Fbn1* and *Tnfa* gene expression, real-time qPCR was performed using a SYBR Select Master Mix (Applied Biosystems, Cat# LS4472908). Primers for *Fbn1* sense 5'-GGTAGTGGATTCTCTGAGAC-3' and antisense 5'-GGCGTATTGCACATGCTGTG-3', *Tnfa* sense 5'-AGCCCCCAGTCTGTATCCTT-3' and antisense 5'-GGTCACTGTCCCAGCATCTT-3', and *Gapdh* sense 5'-CACTCTTCCACCTTCGATGC-3' and antisense 5'- CACCACCCTGTTGCTGTAGC-3' were purchased from Alpha DNA, Montreal, Canada. Relative gene expression levels were determined using the comparative delta-delta Ct method.

4.4.5 Indirect immunofluorescence

Tissue sections were deparaffinized and rehydrated as described above under *Histologic and adipocyte size analysis.* Heat and protease mediated antigen retrieval was performed and the sections were treated with 2% bovine serum albumin and then incubated with primary antibodies using the α-rF6H polyclonal anti-fibrillin-1 antiserum [*Tiedemann et al., 2001*], anti-fibrillin-2 antiserum at 1:1,000 dilution or anti-CD68 (Abcam, Cat#ab125212) at a 1:500 dilution, overnight at 4°C. Goat anti-rabbit IgG Cyanine 5 (Jackson ImmunoResearch Laboratories, Cat#111-165-003) was used as secondary antibodies for 1 h at ambient temperature at a 1:200 dilution. Vectashield including 4′, 6-diamidino-2-phenylindole (DAPI) (Vector labs, Cat#VECTH1200) was used for nuclear counter staining and mounting. Immunofluorescence images were taken with an Axio Imager M2 microscope fitted with an ORCA-flash4.0 camera. Quantification of crown like structures (CLSs) were performed manually from 5 different representative locations per mouse.

4.4.6 Statistical analysis

Data are represented as means ± Standard Error of the Mean (SEM). $p<0.05$ was considered statistically significant. For experiments with two conditions, significance was evaluated using Student t-test. Statistical analyses for ITT and GTT were performed using two-way ANOVA with repeated measures post-Bonferroni test. All statistical analyses were performed using the OriginPro version 2021 software (OriginLab). Outlier analysis was performed using the Grubb's test with confidence levels of 95%.

4.5 Results

4.5.1 Efficacy of conditional fibrillin-1 deletion in adipocytes

To distinguish the role of fibrillin-1 in mature adipocytes, we developed a conditional Cre-LoxP knockout mouse model, where the *Fbn1* gene is deleted in mature adipocytes (*Fbn1-AKO*), leading to loss of Fbn1 expression in all adipose tissues. The breeding scheme is outlined in Fig. 4.1A. The *Fbn1-AKO* mice were born at the expected Mendelian frequency, viable and fertile. *Fbn1-FL* and *Fbn1-AKO* genotypes were confirmed by genotyping of tail DNA (Fig. 4.1B). To validate the efficacy of Fbn1 deletion in eWAT, real-time qPCR analysis was performed, confirming the deletion of *Fbn1* to a level of 40% compared to *Fbn1-FL* mice (Fig. 4.1C). This is expected, because *Fbn1* is also expressed by other cells in eWAT such as endothelial cells, smooth muscle cells, mesenchymal stem cells, preadipocytes, and macrophages. On the protein level, however, indirect immunofluorescence showed no differences in the fibrillin-1 deposition between the *Fbn1-FL* and *Fbn1-AKO* mice (Fig. 4.1D). Since it is known that deletion of Fbn1 can lead to compensatory enhancement of Fbn2 expression, we tested *Fbn2* mRNA levels in eWAT which was below the detection limits (Fig. 4.1D). Overall, we successfully generated an adipocyte specific fibrillin-1 knockout in mice.

4.5.2 Adipocyte specific deletion of fibrillin-1 significantly reduces specific adipose tissue depots

The overall body weight at 4, 16 and 30 weeks of age was not different between *Fbn1-AKO* mice and *Fbn1-FL* littermates (Fig. 4.2A). However, notably the eWAT weight of male *Fbn1-AKO* mice was significantly lower (~1.2-1.8 fold) at 16 and 30 weeks, compared to *Fbn1-FL* mice (Fig. 4.2B). The weight of other tissues such as iWAT and liver in *Fbn1-AKO* mice remained unchanged (Fig.

4.2C,D). We also monitored the food consumption of *Fbn1-AKO* mice and detected no differences in the food intake compared to *Fbn1-FL* littermates. Taken together, adipocyte-specific deletion of *Fbn1* in mature adipocytes caused substantial weight reduction in eWAT, but not in iWAT and other metabolic organs such as liver.

4.5.3 Deleted adipocyte specific fibrillin-1 does not alter the overall glucose and insulin metabolism

To determine whether the reduced eWAT mass in *Fbn1-AKO* mice affects systemic glucose levels, fasting glucose levels were determined. At baseline, after 6h and 16h of fasting, no differences in the blood glucose levels were observed in the *Fbn1-AKO* mice compared to *Fbn1-FL* littermates Fig. 4.3A,B). Glucose and insulin metabolism were assessed by performing GTT and ITT. Glucose tolerance and insulin sensitivity were normal after acute bolus injections of 2 g/kg glucose or 0.75 U insulin, respectively in *Fbn1-AKO* mice at both 16 and 30 weeks of age (Fig. 4.3C-F).

4.5.4 *Fbn1* gene deletion in adipocytes of male mice reduces cell size

Reduced adipose tissue weight is usually associated with either reduced number or size of adipocytes. Therefore, we assessed these parameters using hematoxylin and eosin staining. This analysis revealed that eWAT adipocytes of *Fbn1-AKO* mice were consistently smaller by ~20-22%, compared to those from *Fbn1-FL* mice at 16 (Fig. 4.4A,B; tendency $p=0.1$) and 30 weeks (Fig. 4.4C,D; $p<0.05$) of age. Frequency distribution of eWAT adipocytes indicated an increase in smaller adipocytes (0-1,000 μm^2) and a decrease in the number of larger adipocytes (1,001-3,500 μm^2) in *Fbn1-AKO* compared to FBN-FL at 16 weeks of age (Fig. 4.4E). This was further enhanced at 30 weeks of age when *Fbn1-AKO* mice showed a higher number of smaller adipocytes

in the 0-2,000 μm^2 range and a lower frequency of larger adipocytes in the 2,001-6,000 μm^2 range (Fig. 4.4F). These data together demonstrates that fibrillin-1 directly impacts cell size of mature adipocytes.

4.5.5 *Fbn1* deletion in adipocytes slightly reduces adipose tissue inflammation

Chronic inflammation is a typical characteristic of adipose tissue dysfunction, which is typically linked to the number and size of adipocytes. This prompted us to investigate potential abnormal macrophage infiltration in adipose tissue of 30-week-old *Fbn1-AKO* mice. Immunofluorescence analysis identified CD68 positive adipose tissue resident macrophages arranged as CLS surrounding dying or dead adipocytes (Fig. 4.5A). A tendency of decreased CLS were observed in *Fbn1-AKO* mice compared to *Fbn1-FL* littermates (Fig. 4.5B). No changes in the inflammatory gene expression marker, *Tnfa* was observed (Fig. 4.5C). In summary, these data suggest that adipose tissue inflammation in the *Fbn1-AKO* adipose tissue is comparable or slightly lower than in *Fbn1-FL* mice.

4.6 Discussion

In this study, we generated a conditional mouse model using Adipoq-Cre transgenic mice crossed with floxed *Fbn1* mice to delete the *Fbn1* gene in mature adipocytes. Adipoq-Cre transgenic mice have been shown to be highly specific (~95%) for adipocytes [*Eguchi et al., 2011; Lee et al., 2013*]. With this *Fbn1-AKO* mouse model we show that specific *Fbn1* deletion in mature adipocytes inhibits eWAT development with substantial decrease in adipocyte size. No defects were observed in the overall growth or in the systemic insulin and glucose metabolism. Although the molecular mechanisms are yet to be identified, this study highlights the essential role of fibrillin-1 in adipocyte maintenance and adipose tissue function.

Adipocyte specific knockout of fibrillin-1 led to 60% reduction of the *Fbn1* gene expression based on the analysis of total RNA extracted from the whole adipose tissue. It is important to note that we did not expect 100% deletion, because eWAT contains other cell types, e.g., endothelial cells, smooth muscle cells, mesenchymal stem cells, preadipocytes, and macrophages [*Cohen & Spiegelman, 2016*]. Therefore, the presence of 40% remaining *Fbn1* mRNA could originate from other cell types in eWAT that express *Fbn1*. However, on the protein level analyzed by immunofluorescence which depicts deposited fibrillin-1, no difference was observed in eWAT harvested from the *Fbn1-AKO* mice versus the control mice. This observation could have several reasons. It is possible that positive staining of fibrillin-1 in blood vessels and capillaries overlays the adipocyte-specific staining. We also considered an compensatory increase of fibrillin-2, but noticed that fibrillin-2 was absent in eWAT of the *Fbn1-AKO* mice, despite the fact that fibrillin-2 can be upregulated in other tissues upon deletion of fibrillin-1 [*Lee et al., 2013*]. Another consideration is that indirect immunofluorescence staining only detects fibrillin-1 that is deposited

into the extracellular matrix around adipocytes, but it cannot account for fibrillin-1 that is secreted from cells but not deposited into the matrix. Future studies will need to include the analysis of the total amount of fibrillin-1 secreted from adipocytes, for example by including Western blotting of conditioned medium. We also will confirm the efficacy of fibrillin-1 deletion in adipocytes by digesting adipose tissue to separate mature adipocytes from the stromal vascular fraction and perform gene expression analysis from the extracted RNA [*Cat & Briones, 2017*]. Since a major portion of an individual adipocyte is filled with a lipid droplet, the ECM surrounding the adipocytes is typically very narrow [*Muthu & Reinhardt, 2020*]. Therefore, in situ hybridization experiments and co-staining of the adipose tissue with endothelial cell markers such as CD31 will be performed to further confirm the efficacy and specificity of the deletion.

Adipose tissue development and function occurs through three critical sequences of events: (1) adipocyte commitment, (2) adipocyte differentiation, and (3) adipocyte maintenance. We have previously shown that the level of *Fbn1* mRNA and fibrillin-1 protein tapered down during differentiation, but still present around the mature adipocytes both in cell culture experiments and in white adipose tissue of mice (chapter 2). We have also shown the negative role of fibrillin-1 in adipocyte commitment and differentiation using a global haplo-insufficient mouse model of fibrillin-1 (chapter 2). However, the function of fibrillin-1 in differentiated adipocyte maintenance was still unclear. Therefore, in the present study we inactivated the *Fbn1* gene in mature adipocytes, which led to significant reduction of eWAT supported by a substantial decrease in adipocyte size. This could be caused either by a developmental phenotype that prevents adipogenesis from correctly occurring or due to lack of adipocyte maintenance mechanisms that lead to adipocyte and adipose tissue dysfunction. Based on our previous studies in combination

with the current preliminary findings, it is possible that fibrillin-1 is required in the early mesenchymal stem cell phase to limit excessive differentiation and in the late phase to support maintenance and function of mature adipocytes to maintain adipose tissue homeostasis. A dual role of fibrillin-1 in different stages of adipogenesis may also provide an explanation why in some context fibrillin-1 deficiency leads to lipodystrophic phenotypes and in others to excessive fat deposition.

A major contributing factor to metabolic dysfunction in obesity is adipose tissue inflammation, which is characterized by increased macrophage infiltration [*Eltzschig & Carmeliet, 2011*]. Infiltrated macrophages assemble into CLS around dying adipocytes [*Li et al., 2020*]. Increased number of CLSs creates a proinflammatory environment which positively correlates with insulin resistance [*Zatterale et al., 2019*]. Analysis of inflammatory markers in *Fbn1-AKO* mice showed a tendency of reduced CLSs and *Tnfa* gene expression in eWAT compared to *Fbn1-FL* control mice. This could be a result of reduced *Fbn1* expression in adipocytes possibly leading to lower levels of fibrotic ECM in eWAT of *Fbn1-AKO* mice, as macrophages usually co-localize to the profibrotic areas with excess ECM deposition [*Khan et al., 2009; Buechler et al., 2015*]. These preliminary data suggests that adipocyte cell death and chronic inflammation in the adipose tissue may not be major contributors of adipose tissue dysfunction in *Fbn1-AKO* mice. This conclusion need to be strengthened further by performing more in depth analysis and analyzing more mice.

Despite the reduced adipose tissue phenotype in the *Fbn1-AKO* mice, liver weight, glucose, and insulin metabolism were similar to control mice. Adipocyte specific deletion of several other key

components involved in adipogenesis such as mTORC1 [*Lee et al., 2016*], AKT [*Shearin et al., 2016*], or basement membrane protein LMNA [*Wojtanik et al., 2009*] also developed significant lipodystrophy or even lipoatrophy. However, those mice were insulin resistant and developed hepatic steatosis. Although our preliminary findings showed that *Fbn1-AKO* mice were not insulin resistant or developed hepatic steatosis up to 30 weeks of age, a HFD challenge would augment the adiposity associated complications. This will provide us with a tool to analyze the role of fibrillin-1 in adipocyte maintenance under diet induced obesity.

Taken together our preliminary findings demonstrate that abolished *Fbn1* expression in mature adipocytes led to reduced adipocyte size and disrupts epididymal white adipose tissue development. Further thorough analysis will delineate the differential role of fibrillin-1 in adipocyte maintenance and adipose tissue homeostasis as a whole.

4.7 Ongoing or immediate future experiments

1. Colocalization studies of endothelial cell marker CD31 and fibrillin-1 by immunofluorescence in eWAT
2. Confirmation analysis of cell proliferation and apoptosis markers in eWAT
3. Plasma analysis of triglycerides, fatty acids, and cholesterol
4. Plasma analysis of insulin and asprosin
5. Analysis of adipogenic, metabolic, inflammatory, fibrotic, and browning markers by real-time qPCR of mRNA from eWAT

6. Western blotting of adipose tissue, liver, and skeletal muscle for alterations in the insulin signaling cascade
7. Perform adipogenic differentiation experiments using bone marrow and adipose tissue derived MSCs derived from these mice
8. High fat diet challenge of *Fbn1-AKO* and control mice to assess adipose tissue function under diet-induced stress

4.8 Acknowledgements

We express our gratitude to Dr. Francesco Ramirez for providing *Fbn1 (flox/flox)* mice. We would also like to thank Kelly Jung for quantifying adipocyte size.

Declarations of Interest: None

Author contributions

MLM and DPR conceptualized the study, contributed to the design of the experiments, and wrote or edited the manuscript. MLM performed all experiments and analyzed the data. DPR supervised, acquired the funding, and provided the resources for the project.

Funding

This work was supported by the Canadian Institutes of Health Research (MOP-137091 and PJT-162099 to DPR), the Marfan Foundation (USA), and the Fonds de recherche de Quebec (fellowship to MLM).

4.9 Figures and supplemental information

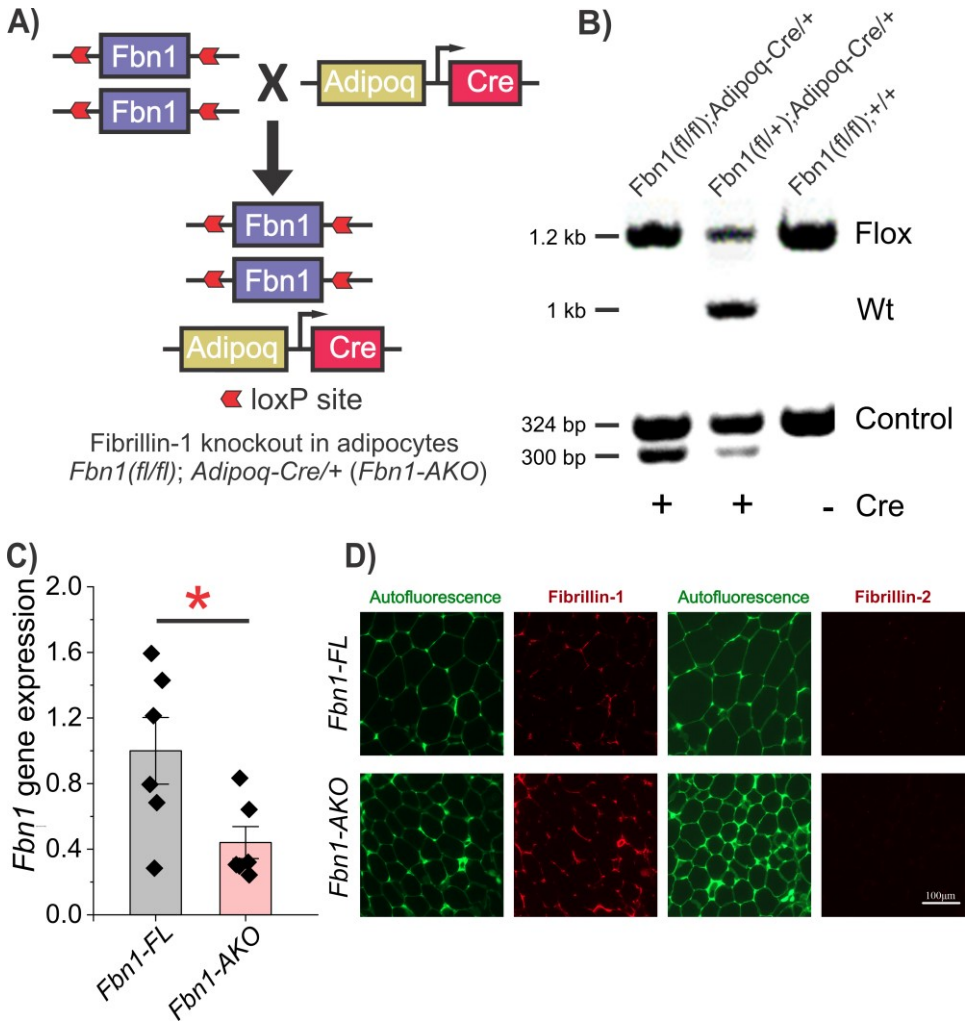

Figure 4.1. Generation of adipocyte specific fibrillin-1 knockout (*Fbn1-AKO*) mice. (A) Schematic diagram of the generation of *Fbn1-AKO* mice from Fbn1 (Fl/Fl) and Adipoq-Cre/+ mice. **(B)** PCR analysis of the Fbn1 and the Cre recombinase gene under the Adipoq promotor using total DNA isolated from tails. Expected bands are 1.2 kb for fibrillin-1 flanked by loxP sites and 300 bp for cre gene. This confirms the successful generation of *Fbn1-AKO* mice (Panel 1 (experimental)- *Fbn1-AKO* and Panel 3 (control)- *Fbn1-FL*). **(C)** eWAT was isolated and analyzed by real-time qPCR for *Fbn1* mRNA levels normalized to *Gapdh* from *Fbn1-FL* and *Fbn1-AKO* mice at 16 weeks. Each data point denotes an individual mouse. Error bars represent ± SEM, n=6 mice per group. Significance was evaluated by unpaired student two tailed t-test. *p<0.05. **(D)** Immunofluorescence analysis of fibrillin-1 and fibrillin-2 deposition in eWAT of *Fbn1-FL* and *Fbn1-AKO* littermates at 16 weeks of age. Green channel represents autofluorescence, red channel represents fibrillin-1 or fibrillin-2 as indicated. n=3 mice per group.

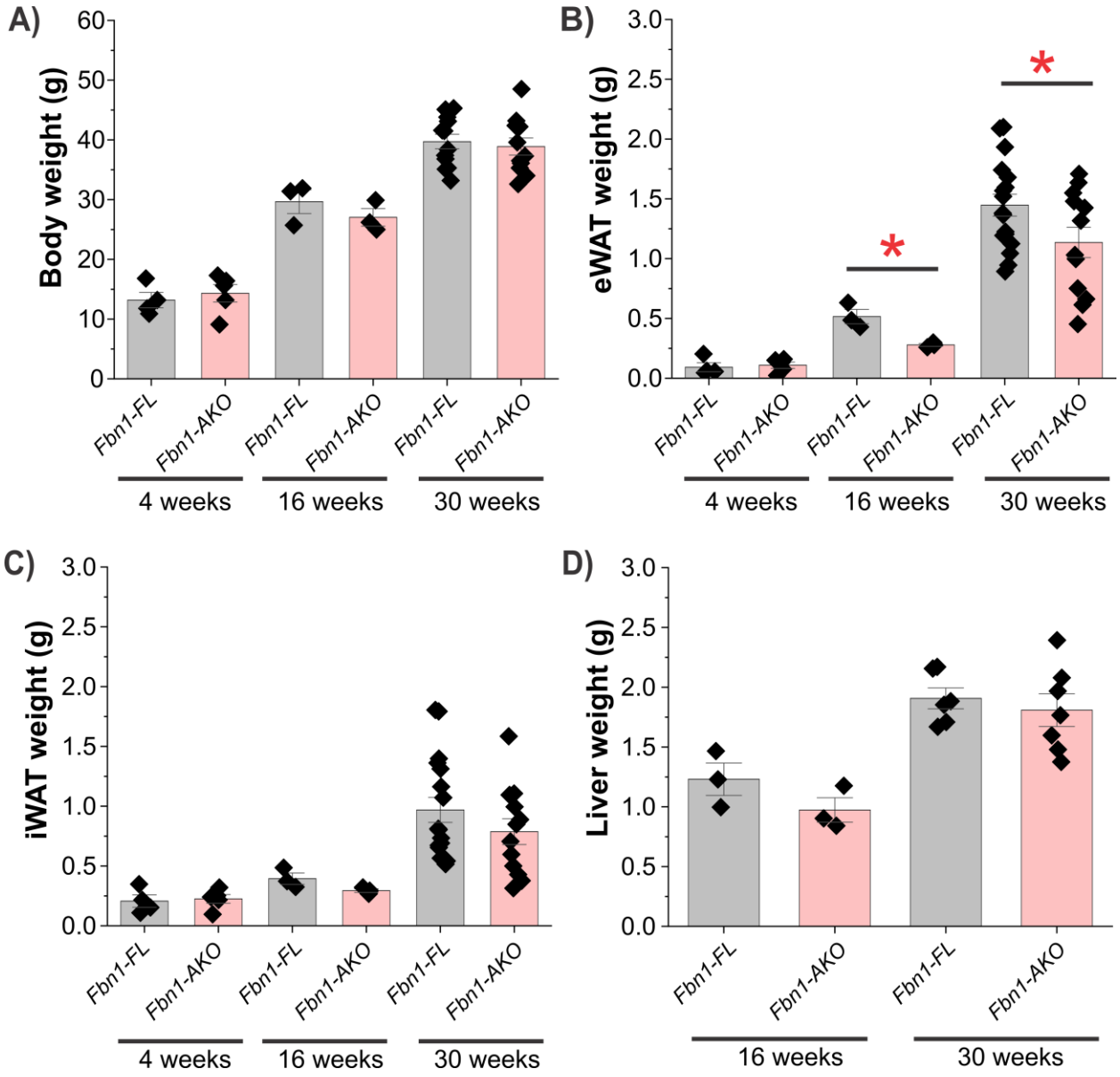

Figure 4.2. Analysis of whole body and tissue weights of adipocyte specific fibrillin-1 knockout mice. Weight of body and metabolic tissues were analyzed in male *Fbn1-FL* and *Fbn1-AKO* mice at 4, 16 or 30 weeks. **(A)** Whole body weight, **(B)** eWAT) weight, **(C)** iWAT weight, **(D)** liver weight. Each data point represents an individual mouse and error bars represent ± SEM, n= 3-14 mice per group. Significance between two conditions were assessed by unpaired student two tailed t-test. *p<0.05.

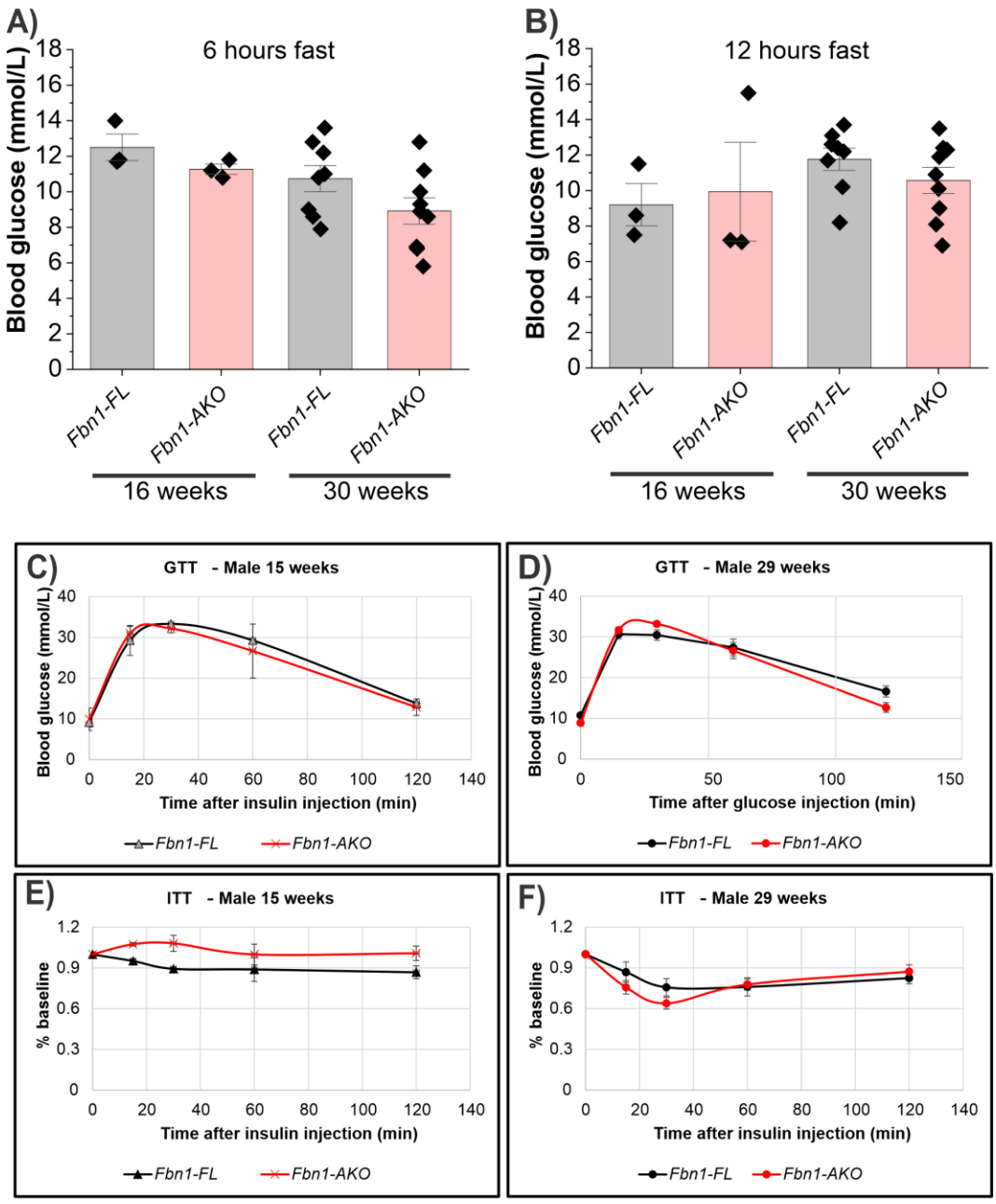

Figure 4.3. Analysis of glucose and insulin metabolism of adipocyte specific fibrillin-1 knockout mice. (A,B) Fasting blood glucose levels (mmol/L) after 6h and 12h were determined with 16 and 30 week old *Fbn1-FL* and *Fbn1-AKO* mice. **(C,D)** Glucose tolerance test (GTT) was performed with 16- and 30-week-old male *Fbn1-FL* and *Fbn1-AKO* mice after overnight fasting and injection of 2mg/kg of glucose. **(E,F)** Insulin tolerance test (ITT) was performed with 16- and 30-week-old male *Fbn1-FL* and *Fbn1-AKO* mice after 6h fasting and injection of 0.75U of insulin. Each data point denotes an individual mouse and error bars represent ± SEM, n= 3-9 mice per group. Significance was assessed by unpaired student two tailed t-test for **(A-B)** and two-way ANOVA with Bonferroni post-test for **(C-F).**

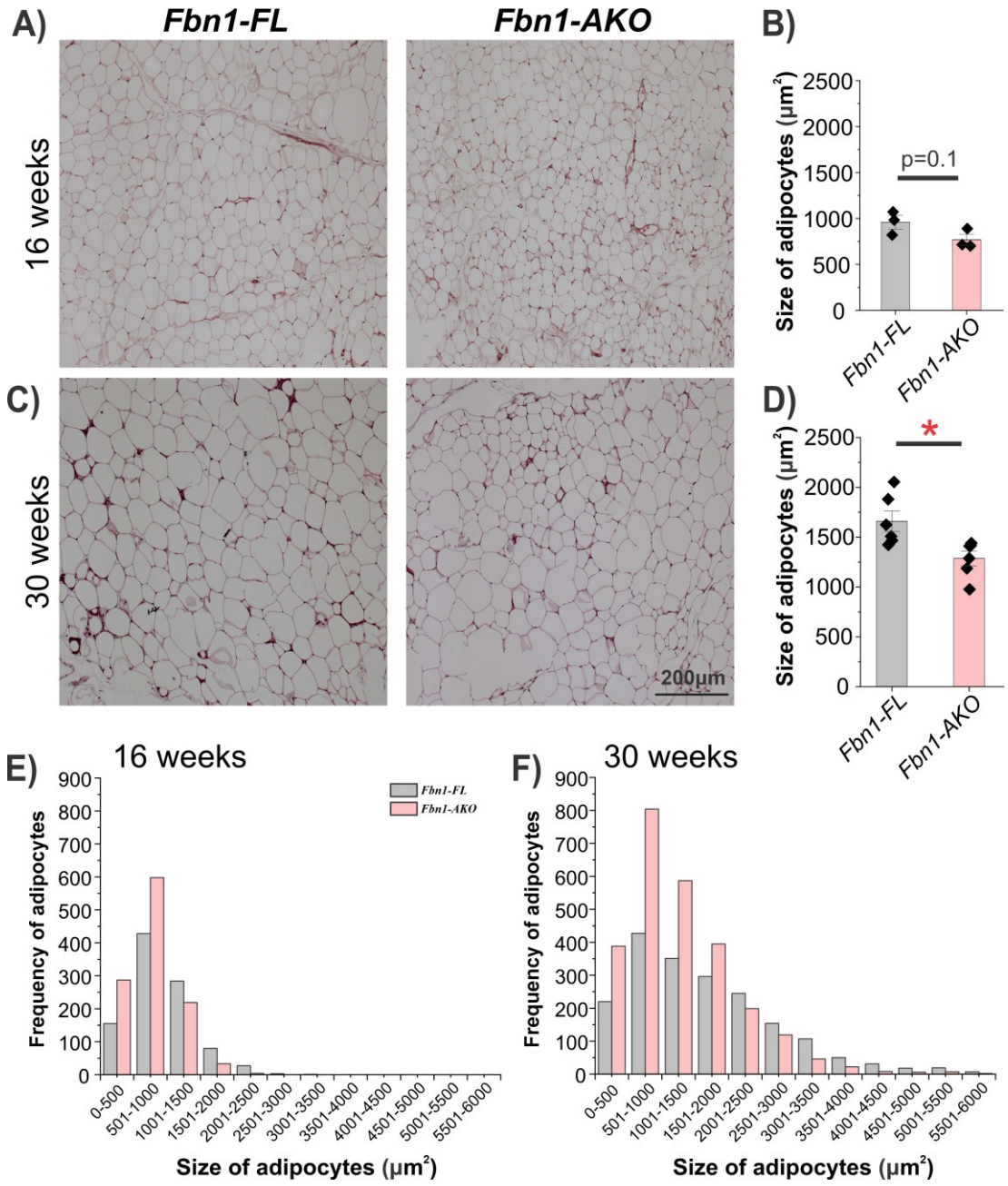

Figure 4.4. Quantification of adipocyte size in eWAT of adipocyte specific *Fbn1-AKO* mice. The adipocyte area in µm^2 was quantified in eWAT of male *Fbn1-FL* and *Fbn1-AKO* mice at 16 and 30 weeks of age, using ImageJ. **(A,C)** Shown are representative images of hematoxylin/eosin-stained tissue sections of eWAT from male *Fbn1-FL* and *Fbn1-AKO* mice. **(B,D)** Quantification of mean areas of adipocytes of images as shown in A and C. Data are shown as means ± SEM; Statistical analysis was performed with the unpaired student two tailed t-test. *p<0.05. **(E,F)** Frequency histograms of eWAT adipocyte areas binned in 500 µm^2 steps of *Fbn1-FL* and *Fbn1-AKO* mice. n=3-6 mice for each condition. The number of analyzed adipocytes for each mouse was >200.

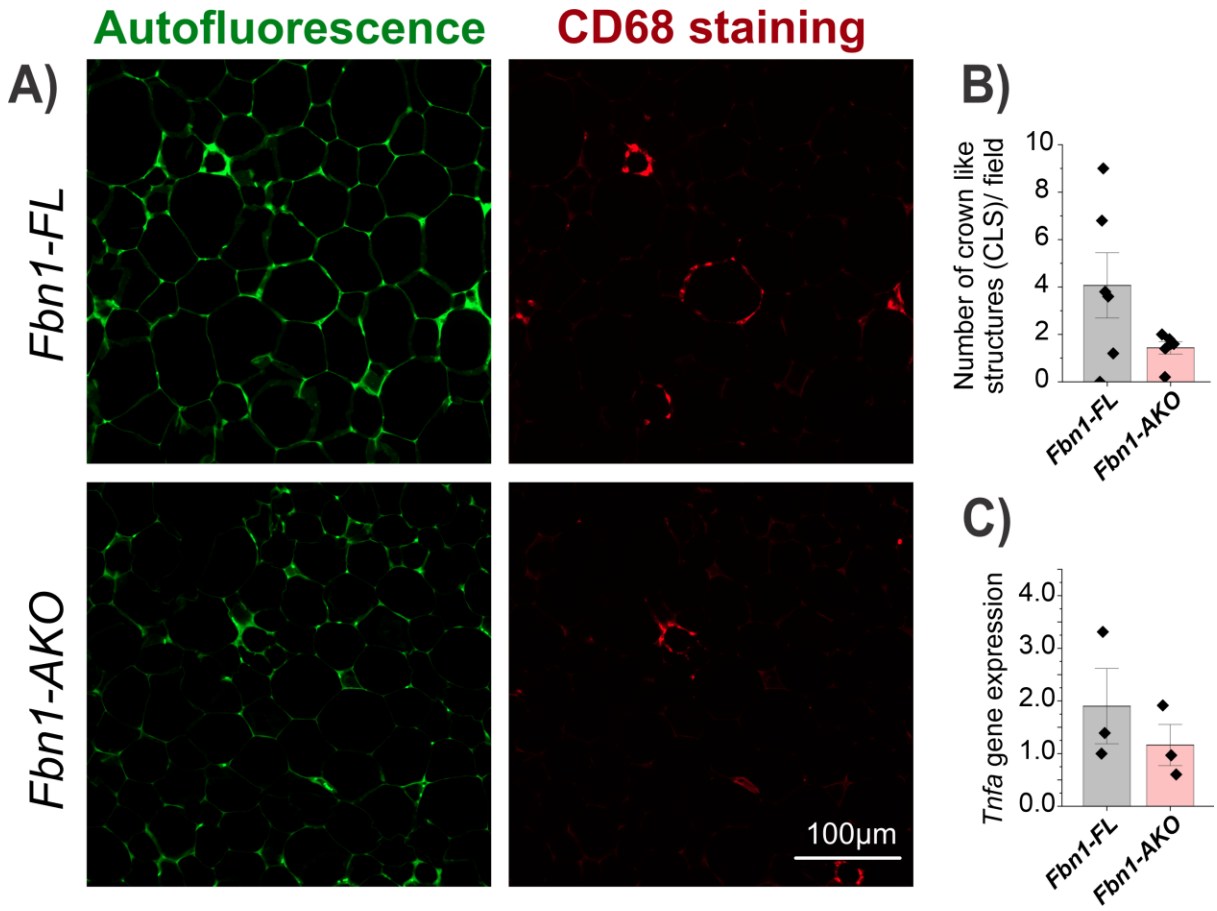

Figure 4.5. Analysis of inflammatory markers in eWAT of adipocyte specific *Fbn1-AKO* knockout mice. (A) Immunofluorescence analysis of macrophage marker (CD68) in eWAT of *Fbn1-FL* and *Fbn1-AKO* littermates at 30 of age. The green channel represents autofluorescence, the red channel represents CD68. **(B)** Quantification of crown like structures (CLS) stained positive for macrophage marker CD68. Each data point represents an individual mouse and error bars are denoted as ± SEM; n= 6 mice per group. **(C)** Real-time qPCR analyses were performed with total RNA extracted from eWAT of male *Fbn1-FL* and *Fbn1-AKO* mice at 16 weeks of age. mRNA expression levels of *Tnfa* relative to *Gapdh* are shown. Each data point represents an individual mouse and error bars are denoted as ± SEM; n= 3 mice per group.

4.10 Bibliography for chapter 4

Buechler C, Krautbauer S, Eisinger K. (2015). Adipose tissue fibrosis. *World J Diabetes* **6**, 548-553

Cat AN, Briones AM. (2017). Isolation of mature adipocytes from white adipose tissue and gene expression studies by real-time quantitative RT-PCR. *Methods Mol Biol* **1527**, 283-295

Chaudhry SS, Cain SA, Morgan A, Dallas SL, Shuttleworth CA, Kielty CM. (2007). Fibrillin-1 regulates the bioavailability of TGF-beta1. *J Cell Biol* **176**, 355-367

Cohen P, Spiegelman BM. (2016). Cell biology of fat storage. *Mol Biol Cell* **27**, 2523-2527

Cook JR, Smaldone S, Cozzolino C, Del SM, Lee-Arteaga S, Nistala H, Ramirez F. (2012). Generation of Fbn1 conditional null mice implicates the extracellular microfibrils in osteoprogenitor recruitment. *Genesis* **50**, 635-641

Duerrschmid C, He Y, Wang C, Li C, Bournat JC, Romere C, Saha PK, Lee ME, Phillips KJ, Jain M, Jia P, Zhao Z, Farias M, Wu Q, Milewicz DM, Sutton VR, Moore DD, Butte NF, Krashes MJ, Xu Y, Chopra AR. (2017). Asprosin is a centrally acting orexigenic hormone. *Nat Med* **23**, 1444-1453

Eguchi J, Wang X, Yu S, Kershaw EE, Chiu PC, Dushay J, Estall JL, Klein U, Maratos-Flier E, Rosen ED. (2011). Transcriptional control of adipose lipid handling by IRF4. *Cell Metab* **13**, 249-259

Eltzschig HK, Carmeliet P. (2011). Hypoxia and inflammation. *N Engl J Med* **364**, 656-665

Erkula G, Jones KB, Sponseller PD, Dietz HC, Pyeritz RE. (2002). Growth and maturation in Marfan syndrome. *Am J Med Genet* **109**, 100-115

Gao H, Guo Y, Yan Q, Yang W, Li R, Lin S, Bai X, Liu C, Chen D, Cao H, Xiao G. (2019). Lipoatrophy and metabolic disturbance in mice with adipose-specific deletion of kindlin-2. *JCI Insight* **4**

Goldblatt J, Hyatt J, Edwards C, Walpole I. (2011). Further evidence for a marfanoid syndrome with neonatal progeroid features and severe generalized lipodystrophy due to frameshift mutations near the 3' end of the FBN1 gene. *Am J Med Genet A* **155A**, 717-720

Graul-Neumann LM, Kienitz T, Robinson PN, Baasanjav S, Karow B, Gillessen-Kaesbach G, Fahsold R, Schmidt H, Hoffmann K, Passarge E. (2010). Marfan syndrome with neonatal progeroid syndrome-like lipodystrophy associated with a novel frameshift mutation at the 3' terminus of the FBN1-gene. *Am J Med Genet A* **152A**, 2749-2755

Hansen LB, von Kodolitsch Y, Schroeder F, Benninghoven D. (2020). Body image in patients with Marfan syndrome. *J Clin Med* **9**

Horn D, Robinson PN. (2011). Progeroid facial features and lipodystrophy associated with a novel splice site mutation in the final intron of the FBN1 gene. *Am J Med Genet* **155A**, 721-724

Hubmacher D, Reinhardt DP. (2011) Microfibrils and fibrillin. In *Biology of Extracellular Matrix* (Mecham RP ed.), Springer, New York. pp 233-265

Isogai Z, Ono RN, Ushiro S, Keene DR, Chen Y, Mazzieri R, Charbonneau NL, Reinhardt DP, Rifkin DB, Sakai LY. (2003). Latent transforming growth factor beta-binding protein 1 interacts with fibrillin and is a microfibril-associated protein. *J Biol Chem* **278**, 2750-2757

Jacquinet A, Verloes A, Callewaert B, Coremans C, Coucke P, de Paepe A, Kornak U, Lebrun F, Lombet J, Pierard GE, Robinson PN, Symoens S, Van Maldergem L, Debray FG. (2014). Neonatal progeroid variant of Marfan syndrome with congenital lipodystrophy results from mutations at the 3' end of FBN1 gene. *Eur J Med Genet* **57**, 230-234

Keene DR, Maddox BK, Kuo HJ, Sakai LY, Glanville RW. (1991). Extraction of extendable beaded structures and their identification as fibrillin-containing extracellular matrix microfibrils. *J Histochem Cytochem* **39**, 441-449

Khan T, Muise ES, Iyengar P, Wang ZV, Chandalia M, Abate N, Zhang BB, Bonaldo P, Chua S, Scherer PE. (2009). Metabolic dysregulation and adipose tissue fibrosis: role of collagen VI. *Mol Cell Biol* **29**, 1575-1591

Lee KY, Russell SJ, Ussar S, Boucher J, Vernochet C, Mori MA, Smyth G, Rourk M, Cederquist C, Rosen ED, Kahn BB, Kahn CR. (2013). Lessons on conditional gene targeting in mouse adipose tissue. *Diabetes* **62**, 864-874

Lee PL, Tang Y, Li H, Guertin DA. (2016). Raptor/mTORC1 loss in adipocytes causes progressive lipodystrophy and fatty liver disease. *Mol Metab* **5**, 422-432

Li Y, Yun K, Mu R. (2020). A review on the biology and properties of adipose tissue macrophages involved in adipose tissue physiological and pathophysiological processes. *Lipids Health Dis* **19**, 164

Lönnqvist L, Reinhardt DP, Sakai LY, Peltonen L. (1998). Evidence for furin-type activity-mediated C-terminal processing of profibrillin-1 and interference in the processing by certain mutations. *Hum Mol Genet* **7**, 2039-2044

Milewicz DM, Grossfield J, Cao SN, Kielty C, Covitz W, Jewett T. (1995). A mutation in FBN1 disrupts profibrillin processing and results in isolated skeletal features of the Marfan syndrome. *J Clin Invest* **95**, 2373-2378

Moraes RC, Blondet A, Birkenkamp-Demtroeder K, Tirard J, Orntoft TF, Gertler A, Durand P, Naville D, Bégeot M. (2003). Study of the alteration of gene expression in adipose tissue of diet-induced obese mice by microarray and reverse transcription-polymerase chain reaction analyses. *Endocrinol Metab Clin North Am* **144**, 4773-4782

Muthu ML, Reinhardt DP. (2020). Fibrillin-1 and fibrillin-1-derived asprosin in adipose tissue function and metabolic disorders. *J Cell Commun Signal* **14**, 159-173

Neptune ER, Frischmeyer PA, Arking DE, Myers L, Bunton TE, Gayraud B, Ramirez F, Sakai LY, Dietz HC. (2003). Dysregulation of TGF-beta activation contributes to pathogenesis in Marfan syndrome. *Nat Genet* **33**, 407-411

Parlee SD, Lentz SI, Mori H, MacDougald OA. (2014). Quantifying size and number of adipocytes in adipose tissue. *Methods Enzymol* **537**, 93-122

Reinhardt DP, Keene DR, Corson GM, Pöschl E, Bächinger HP, Gambee JE, Sakai LY. (1996). Fibrillin 1: Organization in microfibrils and structural properties. *J Mol Biol* **258**, 104-116

Ritty TM, Broekelmann T, Tisdale C, Milewicz DM, Mecham RP. (1999). Processing of the fibrillin-1 carboxyl-terminal domain. *J Biol Chem* **274**, 8933-8940

Romere C, Duerrschmid C, Bournat J, Constable P, Jain M, Xia F, Saha PK, Del Solar M, Zhu B, York B, Sarkar P, Rendon DA, Gaber MW, LeMaire SA, Coselli JS, Milewicz DM, Sutton VR, Butte NF, Moore DD, Chopra AR. (2016). Asprosin, a fasting-induced glucogenic protein hormone. *Cell* **165**, 566-579

Sakai LY, Keene DR, Engvall E. (1986). Fibrillin, a new 350-kD glycoprotein, is a component of extracellular microfibrils. *J Cell Biol* **103**, 2499-2509

Schneider CA, Rasband WS, Eliceiri KW. (2012). NIH Image to ImageJ: 25 years of image analysis. *Nat Methods* **9**, 671-675

Sengle G, Charbonneau NL, Ono RN, Sasaki T, Alvarez J, Keene DR, Bachinger HP, Sakai LY. (2008). Targeting of bone morphogenetic protein growth factor complexes to fibrillin. *J Biol Chem* **283**, 13874-13888

Shearin AL, Monks BR, Seale P, Birnbaum MJ. (2016). Lack of AKT in adipocytes causes severe lipodystrophy. *Mol Metab* **5**, 472-479

Takenouchi T, Hida M, Sakamoto Y, Torii C, Kosaki R, Takahashi T, Kosaki K. (2013). Severe congenital lipodystrophy and a progeroid appearance: Mutation in the penultimate exon of FBN1 causing a recognizable phenotype. *Am J Med Genet* **161A**, 3057-3062

Tiedemann K, Bätge B, Müller PK, Reinhardt DP. (2001). Interactions of fibrillin-1 with heparin/heparan sulfate: Implications for microfibrillar assembly. *J Biol Chem* **276**, 36035-36042

Tiedemann K, Boraschi-Diaz I, Rajakumar I, Kaur J, Roughley P, Reinhardt DP, Komarova SV. (2013). Fibrillin-1 directly regulates osteoclast formation and function by a dual mechanism. *J Cell Sci* **126**, 4187-4194

von Kodolitsch Y, Demolder A, Girdauskas E, Kaemmerer H, Kornhuber K, Muino Mosquera L, Morris S, Neptune E, Pyeritz R, Rand-Hendriksen S, Rahman A, Riise N, Robert L, Staufenbiel I, Szocs K, Vanem TT, Linke SJ, Vogler M, Yetman A, De Backer J. (2019). Features of Marfan syndrome not listed in the Ghent nosology - the dark side of the disease. *Expert Rev Cardiovasc Ther* **17**, 883-915

Walji TA, Turecamo SE, DeMarsilis AJ, Sakai LY, Mecham RP, Craft CS. (2016). Characterization of metabolic health in mouse models of fibrillin-1 perturbation. *Matrix Biol* **55**, 63-76

Wallis DD, Putnam EA, Cretoiu JS, Carmical SG, Cao SN, Thomas G, Milewicz DM. (2003). Profibrillin-1 maturation by human dermal fibroblasts: proteolytic processing and molecular chaperones. *J Cell Biochem* **90**, 641-652

Wohl AP, Troilo H, Collins RF, Baldock C, Sengle G. (2016). Extracellular regulation of bone morphogenetic protein activity by the microfibril component fibrillin-1. *J Biol Chem* **291**, 12732-112746

Wojtanik KM, Edgemon K, Viswanadha S, Lindsey B, Haluzik M, Chen W, Poy G, Reitman M, Londos C. (2009). The role of LMNA in adipose: a novel mouse model of lipodystrophy based on the Dunnigan-type familial partial lipodystrophy mutation. *J Lipid Res* **50**, 1068-1079

Yetman AT, McCrindle BW. (2010). The prevalence and clinical impact of obesity in adults with Marfan syndrome. *Can J Cardiol* **26**, 137-139

Zatterale F, Longo M, Naderi J, Raciti GA, Desiderio A, Miele C, Beguinot F. (2019). Chronic adipose tissue Inflammation linking obesity to insulin resistance and type 2 diabetes. *Front Physiol* **10**, 1607

CHAPTER 5: OVERALL DISCUSSION AND CONCLUSIONS

5.1 Significance of the study

Adipose tissue is a dynamic connective tissue consisting primarily of lipid containing adipocytes and the stromal vascular fraction comprising other cell types such as MSCs, preadipocytes, endothelial cells and macrophages. Adipose tissue is a key regulator of systemic energy homeostasis. There is an increasing need to understand the factors determining adipose tissue function due to its ability to vastly grow or shrink in size based on the metabolic demand. The composition and dynamics of the ECM in adipose tissue is essential for differentiation, development, expansion, maintenance, and function of adipocytes. While there maybe many potential contributors for adipose tissue dysfunction, this study particularly focuses on fibrillin-1, a key component in the ECM. Mutations in fibrillin-1 cause MFS and other heritable disorders. Individuals affected with MFS are characterized by adipose tissue dysfunction and cardiovascular abnormalities, among others.

5.2 Key findings

This study addresses the overarching hypothesis that fibrillin-1 controls the development of adipocytes and plays a crucial role in adipose tissue homeostasis. To test this hypothesis, Chapter 2 and 3 of this dissertation used two MFS mouse models (*Fbn1*$^{mgR/mgR}$ and *Fbn1*$^{C1041G/+}$), and in chapter 4 we generated an adipocyte specific fibrillin-1 knockout using Cre-loxP strategy. In chapter 2, we determined that fibrillin-1 haploinsufficiency in male mice led to excess adipose tissue deposition associated with adipocyte hypertrophy, higher adipogenic gene expression and an insulin resistance phenotype. We also showed that reduction of fibrillin-1 at early mesenchymal cell stages enhanced adipogenic differentiation. Mechanistically, we demonstrated that fibrillin-1 negatively regulates adipogenic differentiation via the insulin signaling pathway by direct cell interaction and through insulin sequestration. Moreover, in chapter 3 HFD treatment of these MFS

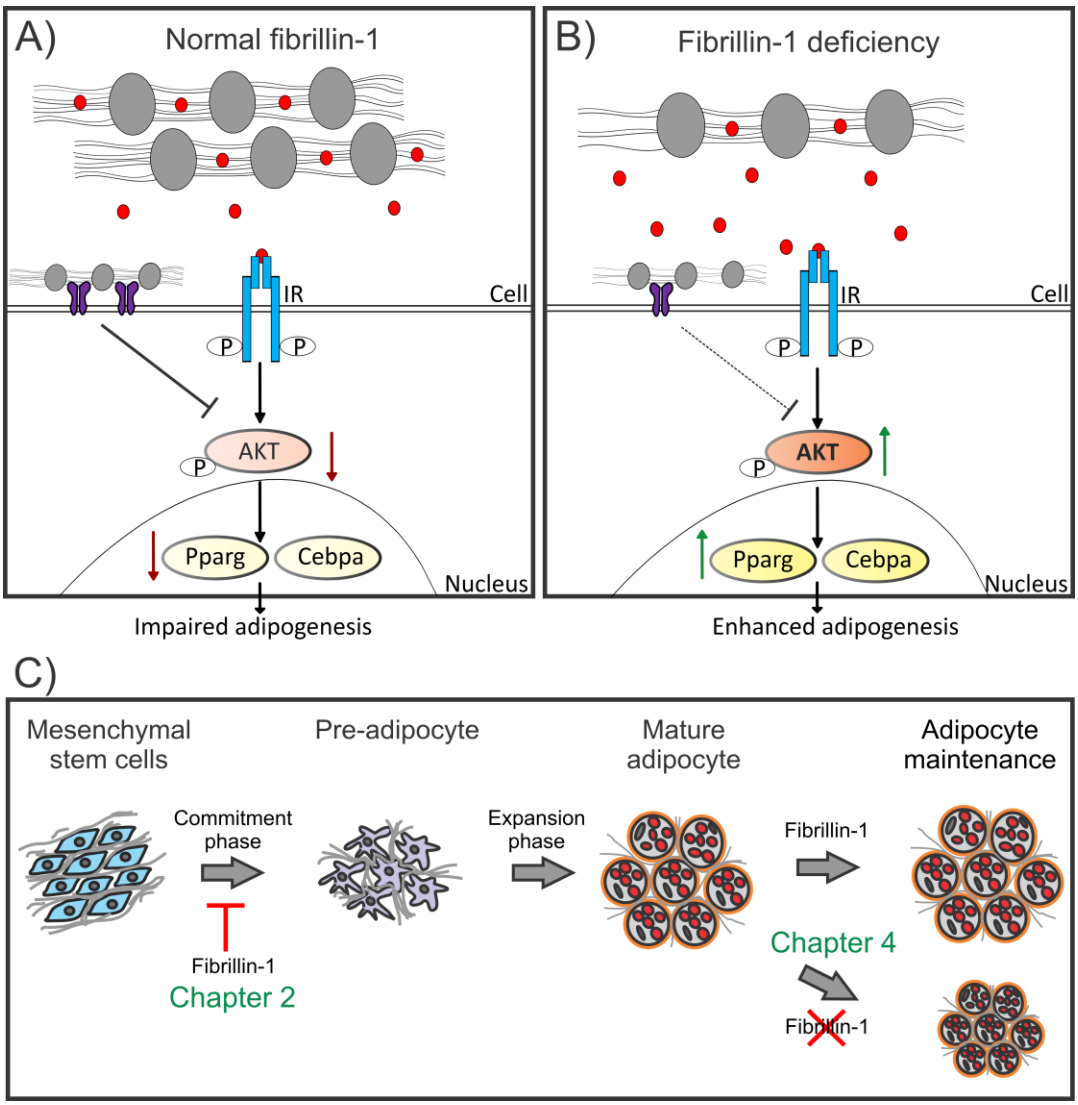

Figure 5.1. Hypothesized working model of fibrillin-1 in adipogenesis and adipose tissue homeostasis Fibrillin-1 controls adipogenesis by modulating the AKT signaling pathway. A) Normal fibrillin-1 was shown to inhibit adipogenic differentiation by direct cell binding and insulin sequestration mechanisms. B) Fibrillin-1 deficiency led to reduced inhibitor activity (dotted line) through cell binding and increased free insulin which in turn enhanced the AKT signaling and adipogenic gene expression. C) Fibrillin-1 functions at the level of MSC stage to inhibit adipogenic commitment and differentiation (Chapter 2) while fibrillin-1 mature adipocyte helps in the maintenance of adipocyte morphology and function (Chapter 4).

mice enhanced obesity, as well as pre-diabetic and non-alcoholic fatty liver phenotype in males, which was abolished in orchiectomized mice. Conversely, female MFS mice were protected from these metabolic and liver phenotypes. Finally in chapter 4, knockout of *Fbn1* gene in mature adipocytes surprisingly reduced WAT depots in these mice, resembling the lipodystrophic phenotype observed in many MFS patients. Overall, this dissertation established a novel biphasic role of fibrillin-1 at different stages of adipogenesis, where fibrillin-1 is required in the early mesenchymal stem cell phase to limit excessive adipogenic differentiation and in the late phase to support maintenance and function of mature adipocytes.

5.3 Overall discussion and future directions

Novel findings of this thesis have been discussed at the end of each chapter in detail. Discussed below are some of the other interesting aspects closely relevant to the project but was beyond the scope of the study.

5.3.1 Regulation of TGF-β signaling by fibrillin-1 in adipose tissue

Chapter 2 of this study developed from the striking observation of excess WAT deposition observed in male mice haplo-insufficient for fibrillin-1 and has severe MFS phenotype. This correlate with the excess adiposity phenotype of MFS patients but not with the lipodystrophic subgroup. These results correlate with another published study using three fibrillin-1 deficient mouse models, heterozygous $Fbn1^{+/-}$ mice, mice lacking the first hybrid domain in fibrillin-1 ($Fbn1^{H1\Delta/H1\Delta}$), and the $Fbn1^{C1041G/+}$ mice also used in our study [*Walji et al., 2016*]. None of these mouse models showed a lipodystrophic phenotype, rather they were slightly heavier than their wild-type littermates. Interestingly, at 24 weeks those mice showed an insulin resistance

phenotype, possibly explained by slightly increased body weight and excess circulating TGF-β levels. To unravel if fibrillin-1 contributes to adipose tissue homeostasis through TGF-β signaling, Walji *et al.* assessed and found no differences in the TGF-β signaling in WAT of all three mouse models, whereas TGF-β was increased in bones. On the other hand, mouse (*Fbn1*$^{NPS/+}$) and rabbit (*Fbn1* het) models harboring mutations in the C-terminal propeptide show severe lipodystrophic phenotypes. Independent of fibrillin-1, TGF-β has been shown to promote the adipocyte commitment of MSCs and positively correlates with increased adipogenesis [*Li & Wu, 2020*]. Obese people and mice are characterized by high levels of circulating TGF-β leading to enhanced TGF-β signaling, a molecular signature that is also found in MFS mice and human patients [*Ramirez et al., 2008; Matt et al., 2009; Franken et al., 2015*]. Fibrillin-1 is known to interact with LTBP-1 and -4 that anchors the large latent TGFβ complex to microfibrils in the ECM [*Isogai et al., 2003*]. Therefore, upregulated circulating TGF-β levels and signaling could potentially represent an independent mechanism causing excess adipose tissue deposition in MFS mouse models. While interesting, this particular aspect was beyond the scope of this study and will be addressed in future studies. It is not clear for MFS patients whether circulating levels of TGF-β differ between those with a lipodystrophic and those with an overweight phenotype. It is possible that MFS patients with lipodystrophic phenotypes have less circulating TGF-β compared to overweight MFS patients, which may also be the case for the respective MFS mouse models. Taken together, excess of circulating TGF-β and the downstream signaling could be a causative factor for the phenotypes observed in MFS conditions. Future studies will investigate the levels of circulating TGF-β and the associated cell signaling in WAT of *Fbn1*$^{mgR/mgR}$ and *Fbn1-AKO* mice.

5.3.2 Potential reasons for sex differences observed in MFS mice

The sex differences in the adipose tissue and the metabolic phenotypes we observed in our study was unexpected. Only male *Fbn1*$^{mgR/mgR}$ mice haplo-insufficient for fibrillin-1 developed excess adipose tissue deposition and metabolic phenotypes, but not the female mice. Also, the enhanced metabolic and liver phenotypes observed in *Fbn1*$^{C1041G/+}$ mice were reduced after orchiectomy pointing towards a role of sex hormones contributing to this phenotype. In the discussion of both chapter 2 and 3 of this dissertation, we provided a detailed explanation of how these sex differences could have occurred in terms of differences in the fibrillin-1 expression. In addition, in the following are other possible reasons for sex differences in adipose tissue and metabolic phenotypes. (i) Depot specific differences: Obesity or excess fat deposition in humans undoubtedly affects both sexes independent of age, culture, race, or other socio-economic factors. But the pattern of fat deposition is different in males and females [*Bjorntorp, 1991; Valencak et al., 2017*]. As mentioned in the introduction of this thesis, females have more fat stores in the subcutaneous or gluteo-femoral regions leading to peripheral obesity compared to men who have significantly higher amount of visceral fat leading to central or abdominal obesity [*Krotkiewski et al., 1983; Bjorntorp, 1991; Valencak et al., 2017*]. Studies show that this increase in the subcutaneous fat protects females from metabolic and cardiovascular complications compared to men, and that sex steroids play a major role [*Valencak et al., 2017*]. (ii) Sex steroids: Estrogen together with estrogen receptor α in females is considered to play a protective role especially in post-menopausal women. Estrogen receptor α knockout in mice show reduced adipocyte triglyceride storage which affects the total adiposity leading to insulin resistance [*Ribas et al., 2010*]. On the other hand, androgens in premenopausal women were shown to have deleterious effects, increasing the size of abdominal adipocytes and reducing insulin sensitivity [*Evans et al., 1983*]. (iii) Adipogenesis: Adipocyte hypertrophy is more characteristic for male adipose tissue, whereas females typically demonstrate

more hyperplasia [*Tchoukalova et al., 2008; Tchoukalova et al., 2010b*]. Females vs. males were found to have increased stromal vascular cells that has the capacity to be differentiated into adipocytes [*Tchoukalova et al., 2010a*]. This directly supported our finding that male *Fbn1*$^{mgR/mgR}$ were characterized by adipocyte hypertrophy while females did not differ compared to their control littermates in grain-based diet. (iv) Adipokine and cytokine secretion: Leptin, adiponectin and resistin are primarily secreted by WAT [*Gavin & Bessesen, 2020*]. These adipokines are known to control various biological functions including glucose and insulin metabolism, adipogenesis, and inflammation. The levels of adipokines increase or decrease in obesity based on their pro- or anti-adipogenic/inflammatory properties [*Gavin & Bessesen, 2020*]. Additionally, proinflammatory cytokines such as TNF-a, IL- 6, IL-1β and adipose tissue macrophages are positively correlated with obesity and highly present in male adipose tissue, while anti-inflammatory cytokines such as IL- 10, IL-1 receptor are negatively correlated with obesity [*Varghese et al., 2019*]. Females are protected against the presence of inflammatory cytokines [*Varghese et al., 2019*]. In our study, there was no difference in the inflammatory markers observed, pointing towards a metabolically healthy phenotype. In the past, many studies considered only one sex to answer specific research questions. More recently, however, it is becoming increasingly clear that potential sex differences must be considered in virtually all preclinical and clinical studies. Ultimately, this will likely lead to new and differential therapeutic avenues for men and women.

5.3.3 Therapeutic potential of fibrillin-1 fragments to target adipogenesis

We discovered that the C-terminal half of fibrillin-1 acts as a negative regulator of adipocyte formation mediated by the insulin signaling pathway. This aspect can be further investigated to develop pharmacological therapies aiming to control adipocyte development. It has been shown

that MFS patients have degraded fragments of fibrillin-1 in circulation [*Marshall et al., 2013*]. Previously the host lab also identified smaller fragments of fibrillin-1 that inhibits osteoclast activity and function. Thus, this could serve as a potential pharmacological tool to improve osteopenia observed in MFS [*Tiedemann et al., 2013*]. Therefore, we can recombinantly produce smaller sub fragments of fibrillin-1 encompassing the C-terminal half that possesses the adipogenic inhibitor activity. Additionally, we have also shown that fibrillin-1 mediates cell adhesion, proliferation and alters cell dynamics through the RGD binding site in the TB4 domain which is present in the C-terminal half of fibrillin-1 [*Pfaff et al., 1996*]. It is known that integrin receptors α5β1, αvβ3 and αvβ6 are present during adipogenesis, which are also the known integrin receptors for fibrillin-1 [*Pfaff et al., 1996; Sakamoto et al., 1996; Jovanovic et al., 2007*]. Fibronectin has been shown to regulate adipogenesis via integrins and altering insulin signaling [*Kamiya et al., 2002; Wang et al., 2010*]. FAK and Src kinase are activated downstream of several integrins and negatively regulate adipocyte differentiation [*Lee et al., 2017; Rubin & Sen, 2017; Hyvari et al., 2018; Kim et al., 2020*]. Therefore, we hypothesize that integrins are the key receptors involved in the fibrillin-1-mediated regulation of adipogenesis. Using various approaches, we can abolish interaction of RGD binding and confirm this hypothesis. i) Use a smaller fragment with a mutation in the RGD site which inactivates integrin binding [*Hubmacher et al., 2014; Zeyer et al., 2019*]. ii) Knockdown of relevant integrins (α5β1, αvβ3 and αvβ6) by siRNA approaches targeting either one or both α and β subunits. iii) Use specific integrin blocking antibodies to test if the effects by fibrillin-1 on adipogenic differentiation and function will be prevented [*Byron et al., 2009*]. Overall, future studies will use this strategy to not only identify the receptor for fibrillin-1 mediated regulation of adipogenesis but also identify potential smaller fragments of fibrillin-1 that can be therapeutically used to manipulate adipogenesis.

5.3.4 Fibrillin-1 and asprosin turnover

We have identified that fibrillin-1 microfibrils are present surrounding the adipocytes in the ECM of the WAT. However, the cellular source of fibrillin-1 in adipose tissue is presently not clear. Besides mesenchymal stem cells, pre-adipocytes, and differentiated adipocytes, other cells such as fibroblasts, pericytes, and endothelial cells could also synthesize fibrillin-1. It is also not known whether fibrillin-1 in the peri-adipocyte matrix is indeed present in the typical beaded microfibrils known from other tissues [*Keene et al., 1991; Davis et al., 2002*]. For example, in skin, fibrillin-1 labeling was in some instances not only localized to microfibrils intersecting with the basement membrane, but also to the lamina densa of the basement membrane in the absence of beaded microfibrils [*Dzamba et al., 2001*]. It is possible that fibrillin-1 in the adipose ECM is associated with the basement membrane that surrounds each adipocyte. High resolution electron microscopy would help to shed light on these important questions to fully understand the source of fibrillin-1.

One important point refers to the cyclic food intake-dependent generation of asprosin (C-terminal propeptide of fibrillin-1) that is inherently coupled to the synthesis of the 350 kDa fibrillin-1. Fluctuating asprosin levels during the course of a day would either require new fibrillin-1 synthesis, or alternatively, release of stored asprosin from intra- or extracellular storage sites. Virtually nothing is known about the turnover of fibrillin-1 and asprosin in the ECM. In elastic tissues the fibrillin-containing microfibrils are located on the surface of elastic fibers, which are characterized by minimal elastin synthesis and persistence during an entire human lifespan [*Shapiro et al., 1991*]. In regenerating skin, the time frame for new microfibrils to form close to the basement membrane is days to months [*Raghunath et al., 1996*]. We also know that microfibrils are heavily cross-linked by transglutaminase and disulfide-bond mediated mechanisms [*Qian & Glanville, 1997*], which presumably slows down protein turnover within a microfibril.

Surprisingly, in the present study, measurement using the serum of CD and HFD fed MFS mice did not show differences in asprosin concentrations. Various variables were different compared to the original study, such as the type of diet, age of the mice, and usage of plasma instead of serum in the analysis [*Romere et al., 2016*]. Future studies will therefore investigate the levels of asprosin in both, *Fbn1*$^{mgR/mgR}$ mice and *Fbn1-AKO* mice after adjusting these variables. Overall, it is presently difficult to understand how fibrillin-1 would rapidly turn over to produce the required amounts of asprosin in a timely manner several times during a day. Therefore, the field urgently needs to understand the turnover of fibrillin-1 in all relevant tissues, as well as how asprosin is possibly stored inside or outside of cells to be readily available when needed.

5.4 Limitations of the study

One of the important limitations of this study is the usage of bone marrow derived MSCs to study the adipogenic process. Indisputably, this is a very good model to study adipogenesis, since it has been shown that bone marrow derived MSCs migrate from the bones to the visceral adipose tissue depots through circulation for adipogenic differentiation [*Gavin et al., 2016*]. Bone marrow derived MSCs also has the capability to differentiate into fat tissue with the presence of adipogenic supplements [*Gerard et al., 2008*]. Additionally, the adipogenic potential of bone marrow derived MSCs are comparable to that of the adipose tissue derived MSCs [*Heo et al., 2016*]. The bone marrow derived MSCs are able to differentiate into multiple lineages, importantly into the adipogenic lineage similar to adipose tissue derived MSCs [*Badimon & Cubedo, 2017*]. However, due to its direct relevance in adipose tissue, future studies will include mouse and human adipose tissue derived MSCs to study the adipogenic process.

5.5 Concluding remarks and broader implications

Altogether, this thesis demonstrated novel and important mechanisms by which fibrillin-1 controls adipogenesis. The knowledge how fibrillin-1 regulates the identity of adipocytes supports the importance of ECM in adipose tissue homeostasis. We predict that the knowledge obtained from this project will help in the development of specific new therapeutic avenues to treat lipodystrophic and obese pathologies associated with MFS and in general population. This should have a profound impact in the long term on the health and quality of life of the affected individuals.

5.6 Bibliography for chapter 1 and 5

Abdennour M, Reggio S, Le Naour G, Liu Y, Poitou C, Aron-Wisnewsky J, Charlotte F, Bouillot JL, Torcivia A, Sasso M, Miette V, Zucker JD, Bedossa P, Tordjman J, Clement K. (2014). Association of adipose tissue and liver fibrosis with tissue stiffness in morbid obesity: links with diabetes and BMI loss after gastric bypass. *J Clin Endocrinol Metab* **99**, 898-907

Aguilar-Salinas CA, Garcia EG, Robles L, Riano D, Ruiz-Gomez DG, Garcia-Ulloa AC, Melgarejo MA, Zamora M, Guillen-Pineda LE, Mehta R, Canizales-Quinteros S, Tusie Luna MT, Gomez-Perez FJ. (2008). High adiponectin concentrations are associated with the metabolically healthy obese phenotype. *J Clin Endocrinol Metab* **93**, 4075-4079

Ahl S, Guenther M, Zhao S, James R, Marks J, Szabo A, Kidambi S. (2015). Adiponectin levels differentiate metabolically healthy vs unhealthy among obese and nonobese white individuals. *J Clin Endocrinol Metab* **100**, 4172-4180

Aikio M, Elamaa H, Vicente D, Izzi V, Kaur I, Seppinen L, Speedy HE, Kaminska D, Kuusisto S, Sormunen R, Heljasvaara R, Jones EL, Muilu M, Jauhiainen M, Pihlajamaki J, Savolainen MJ, Shoulders CC, Pihlajaniemi T. (2014). Specific collagen XVIII isoforms promote adipose tissue accrual via mechanisms determining adipocyte number and affect fat deposition. *Proc Natl Acad Sci USA* **111**, E3043-E3052

Alan M, Gurlek B, Yilmaz A, Aksit M, Aslanipour B, Gulhan I, Mehmet C, Taner CE. (2019). Asprosin: a novel peptide hormone related to insulin resistance in women with polycystic ovary syndrome. *Gynecol Endocrinol* **35**, 220-223

Alkhouli N, Mansfield J, Green E, Bell J, Knight B, Liversedge N, Tham JC, Welbourn R, Shore AC, Kos K, Winlove CP. (2013). The mechanical properties of human adipose tissues and their relationships to the structure and composition of the extracellular matrix. *Am J Physiol Endocrinol Metab* **305**, E1427-E1435

Badimon L, Cubedo J. (2017). Adipose tissue depots and inflammation: effects on plasticity and resident mesenchymal stem cell function. *Cardiovasc Res* **113**, 1064-1073

Bastien M, Dagenais F, Dumont E, Vadeboncoeur N, Dion B, Royer M, Gaudet-Savard T, Poirier P. (2012). Assessment of management of cardiovascular risk factors in patients with thoracic aortic disease. *Blood Press Monit* **17**, 235-242

Bax DV, Mahalingam Y, Cain S, Mellody K, Freeman L, Younger K, Shuttleworth CA, Humphries MJ, Couchman JR, Kielty CM. (2007). Cell adhesion to fibrillin-1: Identification of an Arg-Gly-Asp-dependent synergy region and a heparin-binding site that regulates focal adhesion formation. *J Cell Sci* **120**, 1383-1392

Berry DC, Stenesen D, Zeve D, Graff JM. (2013). The developmental origins of adipose tissue. *Development* **140**, 3939-3949

Berry DC, Jiang Y, Graff JM. (2016). Emerging roles of adipose progenitor cells in tissue development, homeostasis, expansion and thermogenesis. *Trends Endocrinol Metab* **27**, 574-585

Berry R, Rodeheffer MS. (2013). Characterization of the adipocyte cellular lineage in vivo. *Nat Cell Biol* **15**, 302-308

Betteridge DJ. (2011). Thiazolidinediones and fracture risk in patients with Type 2 diabetes. *Diabet Med* **28**, 751-789

Bindlish S, Presswala LS, Schwartz F. (2015). Lipodystrophy: Syndrome of severe insulin resistance. *Postgrad Med* **127**, 511-516

Bjorndal B, Burri L, Staalesen V, Skorve J, Berge RK. (2011). Different adipose depots: their role in the development of metabolic syndrome and mitochondrial response to hypolipidemic agents. *J Obes* **2011**, 490650

Bjorntorp P. (1991). Adipose tissue distribution and function. *Int J Obes* **15 Suppl 2**, 67-81

Bluher M. (2020). Metabolically healthy obesity. *Endocr Rev* **41**

Broekelmann TJ, Bodmer NK, Mecham RP. (2020). Identification of the growth factor-binding sequence in the extracellular matrix protein MAGP-1. *J Biol Chem* **295**, 2687-2697

Bryant NJ, Govers R, James DE. (2002). Regulated transport of the glucose transporter GLUT4. *Nat Rev Mol Cell Biol* **3**, 267-277

Buechler C, Krautbauer S, Eisinger K. (2015). Adipose tissue fibrosis. *World J Diabetes* **6**, 548-553

Byron A, Humphries JD, Askari JA, Craig SE, Mould AP, Humphries MJ. (2009). Anti-integrin monoclonal antibodies. *J Cell Sci* **122**, 4009-4011

Cancello R, Tordjman J, Poitou C, Guilhem G, Bouillot JL, Hugol D, Coussieu C, Basdevant A, Bar Hen A, Bedossa P, Guerre-Millo M, Clement K. (2006). Increased infiltration of macrophages in omental adipose tissue is associated with marked hepatic lesions in morbid human obesity. *Diabetes* **55**, 1554-1561

Carta L, Pereira L, Arteaga-Solis E, Lee-Arteaga SY, Lenart B, Starcher B, Merkel CA, Sukoyan M, Kerkis A, Hazeki N, Keene DR, Sakai LY, Ramirez F. (2006). Fibrillins 1 and 2 perform partially overlapping functions during aortic development. *J Biol Chem* **281**, 8016-8023

Carter N, Duncan E, Wordsworth P. (2000). Bone mineral density in adults with Marfan syndrome. *Rheumatology (Oxford)* **39**, 307-309

Castoldi A, Naffah de Souza C, Camara NO, Moraes-Vieira PM. (2015). The macrophage switch in obesity development. *Front Immunol* **6**, 637

Chang L, Garcia-Barrio MT, Chen YE. (2020). Perivascular adipose tissue regulates vascular function by targeting vascular smooth muscle cells. *Arterioscler Thromb Vasc Biol* **40**, 1094-1109

Charbonneau NL, Carlson EJ, Tufa S, Sengle G, Manalo EC, Carlberg VM, Ramirez F, Keene DR, Sakai LY. (2010). In vivo studies of mutant fibrillin-1 microfibrils. *J Biol Chem* **285**, 24943-24955

Chau YY, Bandiera R, Serrels A, Martinez-Estrada OM, Qing W, Lee M, Slight J, Thornburn A, Berry R, McHaffie S, Stimson RH, Walker BR, Chapuli RM, Schedl A, Hastie N. (2014). Visceral and subcutaneous fat have different origins and evidence supports a mesothelial source. *Nat Cell Biol* **16**, 367-375

Chaudhry SS, Cain SA, Morgan A, Dallas SL, Shuttleworth CA, Kielty CM. (2007). Fibrillin-1 regulates the bioavailability of TGF-beta1. *J Cell Biol* **176**, 355-367

Chawla A, Lazar MA. (1994). Peroxisome proliferator and retinoid signaling pathways co-regulate preadipocyte phenotype and survival. *Proc Natl Acad Sci USA* **91**, 1786-1790

Choe SS, Huh JY, Hwang IJ, Kim JI, Kim JB. (2016). Adipose tissue remodeling: Its role in energy metabolism and metabolic disorders. *Front Endocrinol (Lausanne)* **7**, 30

Cinti S, Mitchell G, Barbatelli G, Murano I, Ceresi E, Faloia E, Wang S, Fortier M, Greenberg AS, Obin MS. (2005). Adipocyte death defines macrophage localization and function in adipose tissue of obese mice and humans. *J Lipid Res* **46**, 2347-2455

Collod-Beroud G, Le Bourdelles S, Ades L, Ala-Kokko L, Booms P, Boxer M, Child A, Comeglio P, De Paepe A, Hyland JC, Holman K, Kaitila I, Loeys B, Matyas G, Nuytinck L, Peltonen L, Rantamaki T, Robinson P, Steinmann B, Junien C, Beroud C, Boileau C. (2003). Update of the UMD-FBN1 mutation database and creation of an FBN1 polymorphism database. *Hum Mutat* **22**, 199-208

Connell JO, Lynch L, Cawood TJ, Kwasnik A, Nolan N, Geoghegan J, McCormick A, O'Farrelly C, O'Shea D. (2010). The relationship of omental and subcutaneous adipocyte size to metabolic disease in severe obesity. *PLoS One* **5**, e9997

Corson GM, Chalberg SC, Dietz HC, Charbonneau NL, Sakai LY. (1993). Fibrillin binds calcium and is coded by cDNAs that reveal a multidomain structure and alternatively spliced exons at the 5' end. *Genomics* **17**, 476-484

Corson GM, Charbonneau NL, Keene DR, Sakai LY. (2004). Differential expression of fibrillin-3 adds to microfibril variety in human and avian, but not rodent, connective tissues. *Genomics* **83**, 461-472

Corvera S, Gealekman O. (2014). Adipose tissue angiogenesis: impact on obesity and type-2 diabetes. *Biochim Biophys Acta* **1842**, 463-472

Crewe C, An YA, Scherer PE. (2017). The ominous triad of adipose tissue dysfunction: inflammation, fibrosis, and impaired angiogenesis. *J Clin Invest* **127**, 74-82

Czech MP. (2017). Insulin action and resistance in obesity and type 2 diabetes. *Nat Med* **23**, 804-814

D'Souza A M, Neumann UH, Glavas MM, Kieffer TJ. (2017). The glucoregulatory actions of leptin. *Mol Metab* **6**, 1052-1065

Dalmas E, Toubal A, Alzaid F, Blazek K, Eames HL, Lebozec K, Pini M, Hainault I, Montastier E, Denis RG, Ancel P, Lacombe A, Ling Y, Allatif O, Cruciani-Guglielmacci C, Andre S, Viguerie N, Poitou C,

Stich V, Torcivia A, Foufelle F, Luquet S, Aron-Wisnewsky J, Langin D, Clement K, Udalova IA, Venteclef N. (2015). Irf5 deficiency in macrophages promotes beneficial adipose tissue expansion and insulin sensitivity during obesity. *Nat Med* **21**, 610-618

Dam-Larsen S, Franzmann M, Andersen IB, Christoffersen P, Jensen LB, Sorensen TI, Becker U, Bendtsen F. (2004). Long term prognosis of fatty liver: risk of chronic liver disease and death. *Gut* **53**, 750-755

Davis EC, Roth RA, Heuser JE, Mecham RP. (2002). Ultrastructural properties of ciliary zonule microfibrils. *J Struct Biol* **139**, 65-75

Davis MR, Andersson R, Severin J, de Hoon M, Bertin N, Baillie JK, Kawaji H, Sandelin A, Forrest AR, Summers KM, Consortium F. (2014). Transcriptional profiling of the human fibrillin/LTBP gene family, key regulators of mesenchymal cell functions. *Mol Genet Metab* **112**, 73-83

Davis MR, Arner E, Duffy CR, De Sousa PA, Dahlman I, Arner P, Summers KM. (2016). Expression of FBN1 during adipogenesis: Relevance to the lipodystrophy phenotype in Marfan syndrome and related conditions. *Mol Genet Metab* **119**, 174-185

Denroche HC, Huynh FK, Kieffer TJ. (2012). The role of leptin in glucose homeostasis. *J Diabetes Investig* **3**, 115-129

Dietz HC, Cutting GR, Pyeritz RE, Maslen CL, Sakai LY, Corson GM, Puffenberger EG, Hamosh A, Nanthakumar EJ, Curristin SM, Stetten G, Meyers DA, Francomano CA. (1991). Marfan syndrome caused by a recurrent de novo missense mutation in the fibrillin gene. *Nature* **352**, 337-339

Divoux A, Clement K. (2011). Architecture and the extracellular matrix: the still unappreciated components of the adipose tissue. *Obes Rev* **12**, e494-503

Downing AK, Knott V, Werner JM, Cardy CM, Campbell ID, Handford PA. (1996). Solution structure of a pair of calcium-binding epidermal growth factor-like domains: implications for the Marfan syndrome and other genetic disorders. *Cell* **85**, 597-605

Duerrschmid C, He Y, Wang C, Li C, Bournat JC, Romere C, Saha PK, Lee ME, Phillips KJ, Jain M, Jia P, Zhao Z, Farias M, Wu Q, Milewicz DM, Sutton VR, Moore DD, Butte NF, Krashes MJ, Xu Y, Chopra AR. (2017). Asprosin is a centrally acting orexigenic hormone. *Nat Med* **23**, 1444-1453

Dzamba BJ, Keene DR, Isogai Z, Charbonneau NL, Karaman-Jurukovska N, Simon M, Sakai LY. (2001). Assembly of epithelial cell fibrillins. *J Invest Dermatol* **117**, 1612-1620

Erkula G, Jones KB, Sponseller PD, Dietz HC, Pyeritz RE. (2002). Growth and maturation in Marfan syndrome. *Am J Med Genet* **109**, 100-115

Eto H, Suga H, Matsumoto D, Inoue K, Aoi N, Kato H, Araki J, Yoshimura K. (2009). Characterization of structure and cellular components of aspirated and excised adipose tissue. *Plast Reconstr Surg* **124**, 1087-1097

Evans DJ, Hoffmann RG, Kalkhoff RK, Kissebah AH. (1983). Relationship of androgenic activity to body fat topography, fat cell morphology, and metabolic aberrations in premenopausal women. *J Clin Endocrinol Metab* **57**, 304-310

Fain JN, Tichansky DS, Madan AK. (2005). Transforming growth factor beta1 release by human adipose tissue is enhanced in obesity. *Metabolism* **54**, 1546-1551

Fajas L, Auboeuf D, Raspe E, Schoonjans K, Lefebvre AM, Saladin R, Najib J, Laville M, Fruchart JC, Deeb S, Vidal-Puig A, Flier J, Briggs MR, Staels B, Vidal H, Auwerx J. (1997). The organization, promoter analysis, and expression of the human PPARgamma gene. *J Biol Chem* **272**, 18779-18789

Finkbohner R, Johnston D, Crawford ES, Coselli J, Milewicz DM. (1995). Marfan syndrome. Long-term survival and complications after aortic aneurysm repair. *Circulation* **91**, 728-733

Fontana L, Chen Y, Prijatelj P, Sakai T, Fassler R, Sakai LY, Rifkin DB. (2005). Fibronectin is required for integrin alphavbeta6-mediated activation of latent TGF-beta complexes containing LTBP-1. *FASEB J* **19**, 1798-1808

Franken R, Radonic T, den Hartog AW, Groenink M, Pals G, van Eijk M, Lutter R, Mulder BJ, Zwinderman AH, de Waard V, group Cs. (2015). The revised role of TGF-beta in aortic aneurysms in Marfan syndrome. *Neth Heart J* **23**, 116-121

French DD, Margo CE, Harman LE. (2012). Ocular pseudoexfoliation and cardiovascular disease: a national cross-section comparison study. *N Am J Med Sci* **4**, 468-473

Fried SK, Bunkin DA, Greenberg AS. (1998). Omental and subcutaneous adipose tissues of obese subjects release interleukin-6: depot difference and regulation by glucocorticoid. *J Clin Endocrinol Metab* **83**, 847-850

Fruhbeck G. (2008). Overview of adipose tissue and its role in obesity and metabolic disorders. *Methods Mol Biol* **456**, 1-22

Furlan AG, Spanou CES, Godwin ARF, Wohl AP, Zimmermann LA, Imhof T, Koch M, Baldock C, Sengle G. (2021). A new MMP-mediated prodomain cleavage mechanism to activate bone morphogenetic proteins from the extracellular matrix. *FASEB J* **35**, e21353

Galgani J, Ravussin E. (2008). Energy metabolism, fuel selection and body weight regulation. *Int J Obes (Lond)* **32 Suppl 7**, S109-S119

Garcia-Rubio J, Leon J, Redruello-Romero A, Pavon E, Cozar A, Tamayo F, Caba-Molina M, Salmeron J, Carazo A. (2018). Cytometric analysis of adipose tissue reveals increments of adipocyte progenitor cells after weight loss induced by bariatric surgery. *Sci Rep* **8**, 15203

Garg A. (2006). Adipose tissue dysfunction in obesity and lipodystrophy. *Clin Cornerstone* **8 Suppl 4**, S7-S13

Garg A, Xing C. (2014). De novo heterozygous FBN1 mutations in the extreme C-terminal region cause progeroid fibrillinopathy. *Am J Med Genet A* **164A**, 1341-1345

Garofalo RS, Orena SJ, Rafidi K, Torchia AJ, Stock JL, Hildebrandt AL, Coskran T, Black SC, Brees DJ, Wicks JR, McNeish JD, Coleman KG. (2003). Severe diabetes, age-dependent loss of adipose tissue, and mild growth deficiency in mice lacking Akt2/PKB beta. *J Clin Invest* **112**, 197-208

Gavin KM, Gutman JA, Kohrt WM, Wei Q, Shea KL, Miller HL, Sullivan TM, Erickson PF, Helm KM, Acosta AS, Childs CR, Musselwhite E, Varella-Garcia M, Kelly K, Majka SM, Klemm DJ. (2016). De novo generation of adipocytes from circulating progenitor cells in mouse and human adipose tissue. *FASEB J* **30**, 1096-1108

Gavin KM, Bessesen DH. (2020). Sex differences in adipose tissue function. *Endocrinol Metab Clin North Am* **49**, 215-228

Geisler CE, Renquist BJ. (2017). Hepatic lipid accumulation: cause and consequence of dysregulated glucoregulatory hormones. *J Endocrinol* **234**, R1-R21

Gerard C, Blouin K, Tchernof A, Doillon CJ. (2008). Adipogenesis in nonadherent and adherent bone marrow stem cells grown in fibrin gel and in the presence of adult plasma. *Cells Tissues Organs* **187**, 186-198

Gesta S, Tseng YH, Kahn CR. (2007). Developmental origin of fat: tracking obesity to its source. *Cell* **131**, 242-256

Giordano A, Murano I, Mondini E, Perugini J, Smorlesi A, Severi I, Barazzoni R, Scherer PE, Cinti S. (2013). Obese adipocytes show ultrastructural features of stressed cells and die of pyroptosis. *J Lipid Res* **54**, 2423-2436

Goldblatt J, Hyatt J, Edwards C, Walpole I. (2011). Further evidence for a marfanoid syndrome with neonatal progeroid features and severe generalized lipodystrophy due to frameshift mutations near the 3' end of the FBN1 gene. *Am J Med Genet A* **155A**, 717-720

Graul-Neumann LM, Kienitz T, Robinson PN, Baasanjav S, Karow B, Gillessen-Kaesbach G, Fahsold R, Schmidt H, Hoffmann K, Passarge E. (2010). Marfan syndrome with neonatal progeroid syndrome-like lipodystrophy associated with a novel frameshift mutation at the 3' terminus of the FBN1-gene. *Am J Med Genet A* **152A**, 2749-2755

Gray JR, Davies SJ. (1996a). A clinical severity grading scale for Marfan syndrome. *J Med Genet* **33**, 758-759

Gray JR, Davies SJ. (1996b). Marfan syndrome. *J Med Genet* **33**, 403-408

Gregoire FM, Smas CM, Sul HS. (1998). Understanding adipocyte differentiation. *Physiol Rev* **78**, 783-809

Gregory KE, Ono RN, Charbonneau NL, Kuo CL, Keene DR, Bächinger HP, Sakai LY. (2005). The prodomain of BMP-7 targets the BMP-7 complex to the extracellular matrix. *J Biol Chem* **280**, 27970-27980

Groth KA, Hove H, Kyhl K, Folkestad L, Gaustadnes M, Vejlstrup N, Stochholm K, Ostergaard JR, Andersen NH, Gravholt CH. (2015). Prevalence, incidence, and age at diagnosis in Marfan syndrome. *Orphanet J Rare Dis* **10**, 153

Habashi JP, Judge DP, Holm TM, Cohn RD, Loeys BL, Cooper TK, Myers L, Klein EC, Liu G, Calvi C, Podowski M, Neptune ER, Halushka MK, Bedja D, Gabrielson K, Rifkin DB, Carta L, Ramirez F, Huso DL, Dietz HC. (2006). Losartan, an AT1 antagonist, prevents aortic aneurysm in a mouse model of Marfan syndrome. *Science* **312**, 117-121

Habashi JP, Doyle JJ, Holm TM, Aziz H, Schoenhoff F, Bedja D, Chen Y, Modiri AN, Judge DP, Dietz HC. (2011). Angiotensin II type 2 receptor signaling attenuates aortic aneurysm in mice through ERK antagonism. *Science* **332**, 361-365

Halberg N, Khan T, Trujillo ME, Wernstedt-Asterholm I, Attie AD, Sherwani S, Wang ZV, Landskroner-Eiger S, Dineen S, Magalang UJ, Brekken RA, Scherer PE. (2009). Hypoxia-inducible factor 1alpha induces fibrosis and insulin resistance in white adipose tissue. *Mol Cell Biol* **29**, 4467-4483

Handford PA, Mayhew M, Baron M, Winship PR, Campbell ID, Brownlee GG. (1991). Key residues involved in calcium-binding motifs in EGF-like domains. *Nature* **351**, 164-167

Hanna-Mitchell AT, Wolf-Johnston A, Roppolo JR, Buffington TC, Birder LA. (2014). Corticotropin-releasing factor family peptide signaling in feline bladder urothelial cells. *J Endocrinol* **222**, 113-121

Hansen LB, von Kodolitsch Y, Schroeder F, Benninghoven D. (2020). Body image in patients with Marfan syndrome. *J Clin Med* **9**

Henninger AM, Eliasson B, Jenndahl LE, Hammarstedt A. (2014). Adipocyte hypertrophy, inflammation and fibrosis characterize subcutaneous adipose tissue of healthy, non-obese subjects predisposed to type 2 diabetes. *PLoS One* **9**, e105262

Heo JS, Choi Y, Kim HS, Kim HO. (2016). Comparison of molecular profiles of human mesenchymal stem cells derived from bone marrow, umbilical cord blood, placenta and adipose tissue. *Int J Mol Med* **37**, 115-125

Herranz P, de Lucas R, Perez-Espana L, Mayor M. (2008). Lipodystrophy syndromes. *Dermatol Clin* **26**, 569-578, ix

Hildebrand S, Stumer J, Pfeifer A. (2018). PVAT and its relation to brown, beige, and white adipose tissue in development and function. *Front Physiol* **9**, 70

Hill JO, Melanson EL, Wyatt HT. (2000). Dietary fat intake and regulation of energy balance: implications for obesity. *J Nutr* **130**, 284S-288S

Hill JO, Wyatt HR, Peters JC. (2012). Energy balance and obesity. *Circulation* **126**, 126-132

Hirani R, Hanssen E, Gibson MA. (2007). LTBP-2 specifically interacts with the amino-terminal region of fibrillin-1 and competes with LTBP-1 for binding to this microfibrillar protein. *Matrix Biol* **26**, 213-223

Hirsch J, Han PW. (1969). Cellularity of rat adipose tissue: effects of growth, starvation, and obesity. *J Lipid Res* **10**, 77-82

Hirsch J, Knittle JL. (1970). Cellularity of obese and nonobese human adipose tissue. *Fed Proc* **29**, 1516-1521

Holm TM, Habashi JP, Doyle JJ, Bedja D, Chen Y, van Erp C, Lindsay ME, Kim D, Schoenhoff F, Cohn RD, Loeys BL, Thomas CJ, Patnaik S, Marugan JJ, Judge DP, Dietz HC. (2011). Noncanonical TGFbeta signaling contributes to aortic aneurysm progression in Marfan syndrome mice. *Science* **332**, 358-361

Horn D, Robinson PN. (2011). Progeroid facial features and lipodystrophy associated with a novel splice site mutation in the final intron of the FBN1 gene. *Am J Med Genet* **155A**, 721-724

Hotamisligil GS, Arner P, Caro JF, Atkinson RL, Spiegelman BM. (1995). Increased adipose tissue expression of tumor necrosis factor-alpha in human obesity and insulin resistance. *J Clin Invest* **95**, 2409-2415

Huber J, Loffler M, Bilban M, Reimers M, Kadl A, Todoric J, Zeyda M, Geyeregger R, Schreiner M, Weichhart T, Leitinger N, Waldhausl W, Stulnig TM. (2007). Prevention of high-fat diet-induced adipose tissue remodeling in obese diabetic mice by n-3 polyunsaturated fatty acids. *Int J Obes* **31**, 1004-1013

Hubmacher D, El-Hallous E, Nelea V, Kaartinen MT, Lee ER, Reinhardt DP. (2008). Biogenesis of extracellular microfibrils: Multimerization of the fibrillin-1 C-terminus into bead-like structures enables self-assembly. *Proc Natl Acad Sci USA* **105**, 6548-6553

Hubmacher D, Reinhardt DP. (2011) Microfibrils and fibrillin. In *Biology of Extracellular Matrix* (Mecham RP ed.), Springer, New York. pp 233-265

Hubmacher D, Sabatier L, Annis DS, Mosher DF, Reinhardt DP. (2011). Homocysteine modifies structural and functional properties of fibronectin and interferes with the fibronectin-fibrillin-1 interaction. *Biochemistry* **50**, 5322-5332

Hubmacher D, Bergeron E, Fagotto-Kaufmann C, Sakai LY, Reinhardt DP. (2014). Early fibrillin-1 assembly monitored through a modifiable recombinant cell approach. *Biomacromolecules* **15**, 1456-1468

Hyvari L, Ojansivu M, Juntunen M, Kartasalo K, Miettinen S, Vanhatupa S. (2018). Focal adhesion kinase and ROCK signaling are switch-like regulators of human adipose stem cell differentiation towards osteogenic and adipogenic lineages. *Stem Cells Int* **2018**, 2190657

Hyytiäinen M, Penttinen C, Keski-Oja J. (2004). Latent TGF-beta binding proteins: extracellular matrix association and roles in TGF-beta activation. *Crit Rev Clin Lab Sci* **41**, 233-264

Isogai Z, Ono RN, Ushiro S, Keene DR, Chen Y, Mazzieri R, Charbonneau NL, Reinhardt DP, Rifkin DB, Sakai LY. (2003). Latent transforming growth factor beta-binding protein 1 interacts with fibrillin and is a microfibril-associated protein. *J Biol Chem* **278**, 2750-2757

Jacquinet A, Verloes A, Callewaert B, Coremans C, Coucke P, de Paepe A, Kornak U, Lebrun F, Lombet J, Pierard GE, Robinson PN, Symoens S, Van Maldergem L, Debray FG. (2014). Neonatal progeroid variant of Marfan syndrome with congenital lipodystrophy results from mutations at the 3' end of FBN1 gene. *Eur J Med Genet* **57**, 230-234

Jensen SA, Iqbal S, Lowe ED, Redfield C, Handford PA. (2009). Structure and interdomain interactions of a hybrid domain: a disulphide-rich module of the fibrillin/LTBP superfamily of matrix proteins. *Structure* **17**, 759-768

Jensen SA, Aspinall G, Handford PA. (2014). C-terminal propeptide is required for fibrillin-1 secretion and blocks premature assembly through linkage to domains cbEGF41-43. *Proc Natl Acad Sci USA* **111**, 10155-10160

Jiang Y, Berry DC, Tang W, Graff JM. (2014). Independent stem cell lineages regulate adipose organogenesis and adipose homeostasis. *Cell Rep* **9**, 1007-1022

Jovanovic J, Takagi J, Choulier L, Abrescia NG, Stuart DI, van der Merwe PA, Mardon HJ, Handford PA. (2007). αVß6 is a novel receptor for human fibrillin-1: Comparative studies of molecular determinants underlying integrin-RGD affinity and specificity. *J Biol Chem* **282**, 6743-6751

Judge DP, Biery NJ, Keene DR, Geubtner J, Myers L, Huso DL, Sakai LY, Dietz HC. (2004). Evidence for a critical contribution of haploinsufficiency in the complex pathogenesis of Marfan syndrome. *J Clin Invest* **114**, 172-181

Judge DP, Dietz HC. (2005). Marfan's syndrome. *Lancet* **366**, 1965-1976

Jung TW, Kim HC, Kim HU, Park T, Park J, Kim U, Kim MK, Jeong JH. (2019). Asprosin attenuates insulin signaling pathway through PKCdelta-activated ER stress and inflammation in skeletal muscle. *J Cell Physiol* **234**, 20888-20899

Junghyo J, Oksana G, Stephanie PW, J. , Shawn M, Anne ES, Samuel WCaV, P. (2009). Hypertrophy and/or hyperplasia: dynamics of adipose tissue growth. *PLoS Comput Biol* **3**, e1000324

Kajimura S, Spiegelman BM, Seale P. (2015). Brown and beige fat: physiological roles beyond heat generation. *Cell Metab* **22**, 546-559

Kamiya S, Kato R, Wakabayashi M, Tohyama T, Enami I, Ueki M, Yajima H, Ishii T, Nakamura H, Katayama T, Takagi J, Fukai F. (2002). Fibronectin peptides derived from two distinct regions stimulate adipocyte differentiation by preventing fibronectin matrix assembly. *Biochemistry* **41**, 3270-3277

Kantola AK, Keski-Oja J, Koli K. (2008). Fibronectin and heparin binding domains of latent TGF-beta binding protein (LTBP)-4 mediate matrix targeting and cell adhesion. *Exp Cell Res* **314**, 2488-2500

Kassi E, Pervanidou P, Kaltsas G, Chrousos G. (2011). Metabolic syndrome: definitions and controversies. *BMC Med* **9**, 48

Keene DR, Maddox BK, Kuo HJ, Sakai LY, Glanville RW. (1991). Extraction of extendable beaded structures and their identification as fibrillin-containing extracellular matrix microfibrils. *J Histochem Cytochem* **39**, 441-449

Khan T, Muise ES, Iyengar P, Wang ZV, Chandalia M, Abate N, Zhang BB, Bonaldo P, Chua S, Scherer PE. (2009). Metabolic dysregulation and adipose tissue fibrosis: role of collagen VI. *Mol Cell Biol* **29**, 1575-1591

Kido Y, Nakae J, Accili D. (2001). Clinical review 125: The insulin receptor and its cellular targets. *J Clin Endocrinol Metab* **86**, 972-979

Kim JI, Huh JY, Sohn JH, Choe SS, Lee YS, Lim CY, Jo A, Park SB, Han W, Kim JB. (2015). Lipid-overloaded enlarged adipocytes provoke insulin resistance independent of inflammation. *Mol Cell Biol* **35**, 1686-1699

Kim JY, van de Wall E, Laplante M, Azzara A, Trujillo ME, Hofmann SM, Schraw T, Durand JL, Li H, Li G, Jelicks LA, Mehler MF, Hui DY, Deshaies Y, Shulman GI, Schwartz GJ, Scherer PE. (2007). Obesity-associated improvements in metabolic profile through expansion of adipose tissue. *J Clin Invest* **117**, 2621-2637

Kim JY, Park S, Lee HJ, Lew H, Kim GJ. (2020). Functionally enhanced placenta-derived mesenchymal stem cells inhibit adipogenesis in orbital fibroblasts with Graves' ophthalmopathy. *Stem Cell Res Ther* **11**, 469

Kim S, Kim Y. (2012). Variations in LOXL1 associated with exfoliation glaucoma do not affect amine oxidase activity. *Mol Vis* **18**, 265-270

Kim SM, Lun M, Wang M, Senyo SE, Guillermier C, Patwari P, Steinhauser ML. (2014). Loss of white adipose hyperplastic potential is associated with enhanced susceptibility to insulin resistance. *Cell Metab* **20**, 1049-1058

Kissebah AH, Krakower GR. (1994). Regional adiposity and morbidity. *Physiol Rev* **74**, 761-811

Klemm DJ, Leitner JW, Watson P, Nesterova A, Reusch JE, Goalstone ML, Draznin B. (2001). Insulin-induced adipocyte differentiation. Activation of CREB rescues adipogenesis from the arrest caused by inhibition of prenylation. *J Biol Chem* **276**, 28430-28435

Kloting N, Fasshauer M, Dietrich A, Kovacs P, Schon MR, Kern M, Stumvoll M, Bluher M. (2010). Insulin-sensitive obesity. *Am J Physiol Endocrinol Metab* **299**, E506-E515

Kohlmeier L, Gasner C, Marcus R. (1993). Bone mineral status of women with Marfan syndrome. *Am J Med* **95**, 568-572

Kohlmeier L, Gasner C, Bachrach LK, Marcus R. (1995). The bone mineral status of patients with Marfan syndrome. *J Bone Miner Res* **10**, 1550-1555

Koli K, Saharinen J, Hyytiäinen M, Penttinen C, Keski-Oja J. (2001). Latency, activation, and binding proteins of TGF-beta. *Microsc Res Tech* **52**, 354-362

Kralova Lesna I, Kralova A, Cejkova S, Fronek J, Petras M, Sekerkova A, Thieme F, Janousek L, Poledne R. (2016). Characterisation and comparison of adipose tissue macrophages from human subcutaneous, visceral and perivascular adipose tissue. *J Transl Med* **14**, 208

Krauss RM, Siri PW. (2004). Metabolic abnormalities: triglyceride and low-density lipoprotein. *Endocrinol Metab Clin North Am* **33**, 405-415

Kriz W, Elger M, Lemley K, Sakai T. (1990). Structure of the glomerular mesangium: a biomechanical interpretation. *Kidney Int Suppl* **30**, S2-S9

Krotkiewski M, Bjorntorp P, Sjostrom L, Smith U. (1983). Impact of obesity on metabolism in men and women. Importance of regional adipose tissue distribution. *J Clin Invest* **72**, 1150-1162

Kubo Y, Kaidzu S, Nakajima I, Takenouchi K, Nakamura F. (2000). Organization of extracellular matrix components during differentiation of adipocytes in long-term culture. *In Vitro Cellular & Developmental Biology - Animal* **36**, 38-44

Kubota N, Terauchi Y, Miki H, Tamemoto H, Yamauchi T, Komeda K, Satoh S, Nakano R, Ishii C, Sugiyama T, Eto K, Tsubamoto Y, Okuno A, Murakami K, Sekihara H, Hasegawa G, Naito M, Toyoshima Y, Tanaka S, Shiota K, Kitamura T, Fujita T, Ezaki O, Aizawa S, Kadowaki T, et al. (1999). PPAR gamma mediates high-fat diet-induced adipocyte hypertrophy and insulin resistance. *Mol Cell* **4**, 597-609

Lack J, O'Leary JM, Knott V, Yuan X, Rifkin DB, Handford PA, Downing AK. (2003). Solution structure of the third TB domain from LTBP1 provides insight into assembly of the large latent complex that sequesters latent TGF-beta. *J Mol Biol* **334**, 281-291

Lee H, Lee YJ, Choi H, Seok JW, Yoon BK, Kim D, Han JY, Lee Y, Kim HJ, Kim JW. (2017). SCARA5 plays a critical role in the commitment of mesenchymal stem cells to adipogenesis. *Sci Rep* **7**, 14833

Lee T, Yun S, Jeong JH, Jung TW. (2019). Asprosin impairs insulin secretion in response to glucose and viability through TLR4/JNK-mediated inflammation. *Mol Cell Endocrinol* **486**, 96-104

Lee YH, Petkova AP, Mottillo EP, Granneman JG. (2012). In vivo identification of bipotential adipocyte progenitors recruited by beta3-adrenoceptor activation and high-fat feeding. *Cell Metab* **15**, 480-491

Lepper C, Fan CM. (2010). Inducible lineage tracing of Pax7-descendant cells reveals embryonic origin of adult satellite cells. *Genesis* **48**, 424-436

Li E, Shan H, Chen L, Long A, Zhang Y, Liu Y, Jia L, Wei F, Han J, Li T, Liu X, Deng H, Wang Y. (2019). OLFR734 mediates glucose metabolism as a receptor of asprosin. *Cell Metab* **30**, 319-328 e318

Li SN, Wu JF. (2020). TGF-beta/SMAD signaling regulation of mesenchymal stem cells in adipocyte commitment. *Stem Cell Res Ther* **11**, 41

Lin M, Liu Z, Liu G, Zhao S, Li C, Chen W, Coban Akdemir Z, Lin J, Song X, Wang S, Xu Q, Zhao Y, Wang L, Zhang Y, Yan Z, Liu S, Liu J, Chen Y, Zuo Y, Yang X, Sun T, Yang XZ, Niu Y, Li X, You W, Qiu B, Ding C, Liu P, Zhang S, Carvalho CMB, Posey JE, Qiu G, Deciphering Disorders Involving S, study CO, Lupski JR, Wu Z, Zhang J, Wu N. (2019). Genetic and molecular mechanism for distinct clinical phenotypes conveyed by allelic truncating mutations implicated in FBN1. *Mol Genet Genomic Med*, e1023

Lönnqvist L, Reinhardt DP, Sakai LY, Peltonen L. (1998). Evidence for furin-type activity-mediated C-terminal processing of profibrillin-1 and interference in the processing by certain mutations. *Hum Mol Genet* **7**, 2039-2044

Low FN. (1962). Microfibrils: fine filamentous components of the tissue space. *Anat Rec* **142**, 131-137

Lumeng CN, Deyoung SM, Saltiel AR. (2007). Macrophages block insulin action in adipocytes by altering expression of signaling and glucose transport proteins. *Am J Physiol Endocrinol Metab* **292**, E166-E174

Mariman EC, Wang P. (2010). Adipocyte extracellular matrix composition, dynamics and role in obesity. *Cell Mol Life Sci* **67**, 1277-1292

Marshall LM, Carlson E, O'Malley JP, Snyder CK, Charbonneau N, Hayflick S, Coselli JS, Lemaire SA, Sakai LY. (2013). Thoracic aortic aneurysm frequency and dissection are associated with fibrillin-1 fragment concentrations in circulation. *Circ Res* **113**, 1159-1168

Martinez-Santibanez G, Singer K, Cho KW, DelProposto JL, Mergian T, Lumeng CN. (2015). Obesity-induced remodeling of the adipose tissue elastin network is independent of the metalloelastase MMP-12. *Adipocyte* **4**, 264-272

Matt P, Schoenhoff F, Habashi J, Holm T, van Erp C, Loch D, Carlson OD, Griswold BF, Fu Q, J. DB, Loeys B, Huso DL, McDonnell NB, Van Eyk JE, Dietz HC. (2009). Circulating transforming growth factor-beta in Marfan syndrome. *Circulation* **120**, 526-532

Milewicz DM, Grossfield J, Cao SN, Kielty C, Covitz W, Jewett T. (1995). A mutation in FBN1 disrupts profibrillin processing and results in isolated skeletal features of the Marfan syndrome. *J Clin Invest* **95**, 2373-2378

Minokoshi Y, Haque MS, Shimazu T. (1999). Microinjection of leptin into the ventromedial hypothalamus increases glucose uptake in peripheral tissues in rats. *Diabetes* **48**, 287-291

Moura B, Tubach F, Sulpice M, Boileau C, Jondeau G, Muti C, Chevallier B, Ounnoughene Y, Le Parc JM. (2006). Bone mineral density in Marfan syndrome. A large case-control study. *Joint Bone Spine* **73**, 733-735

Mueller E, Drori S, Aiyer A, Yie J, Sarraf P, Chen H, Hauser S, Rosen ED, Ge K, Roeder RG, Spiegelman BM. (2002). Genetic analysis of adipogenesis through peroxisome proliferator-activated receptor gamma isoforms. *J Biol Chem* **277**, 41925-41930

Murdoch JL, Walker BA, Halpern BL, Kuzma JW, McKusick VA. (1972). Life expectancy and causes of death in the Marfan syndrome. *N Engl J Med* **286**, 804-808

Muthu ML, Reinhardt DP. (2020). Fibrillin-1 and fibrillin-1-derived asprosin in adipose tissue function and metabolic disorders. *J Cell Commun Signal* **14**, 159-173

Neptune ER, Frischmeyer PA, Arking DE, Myers L, Bunton TE, Gayraud B, Ramirez F, Sakai LY, Dietz HC. (2003). Dysregulation of TGF-beta activation contributes to pathogenesis in Marfan syndrome. *Nat Genet* **33**, 407-411

Nistala H, Lee-Arteaga S, Carta L, Cook JR, Smaldone S, Siciliano G, Rifkin AN, Dietz HC, Rifkin DB, Ramirez F. (2010). Differential effects of alendronate and losartan therapy on osteopenia and aortic aneurysm in mice with severe Marfan syndrome. *Hum Mol Genet* **19**, 4790-4798

O'Neill B, Simha V, Kotha V, Garg A. (2007). Body fat distribution and metabolic variables in patients with neonatal progeroid syndrome. *Am J Med Genet* **143A**, 1421-1430

Okuno A, Tamemoto H, Tobe K, Ueki K, Mori Y, Iwamoto K, Umesono K, Akanuma Y, Fujiwara T, Horikoshi H, Yazaki Y, Kadowaki T. (1998). Troglitazone increases the number of small adipocytes without the change of white adipose tissue mass in obese Zucker rats. *J Clin Invest* **101**, 1354-1361

Olefsky JM. (1999). Insulin-stimulated glucose transport minireview series. *J Biol Chem* **274**, 1863

Ono RN, Sengle G, Charbonneau NL, Carlberg V, Bachinger HP, Sasaki T, Lee-Arteaga S, Zilberberg L, Rifkin DB, Ramirez F, Chu ML, Sakai LY. (2009). Latent transforming growth factor beta-binding proteins and fibulins compete for fibrillin-1 and exhibit exquisite specificities in binding sites. *J Biol Chem* **284**, 16872-16881

Orio F, Jr., Palomba S, Cascella T, Savastano S, Lombardi G, Colao A. (2007). Cardiovascular complications of obesity in adolescents. *J Endocrinol Invest* **30**, 70-80

Pajvani UB, Trujillo ME, Combs TP, Iyengar P, Jelicks L, Roth KA, Kitsis RN, Scherer PE. (2005). Fat apoptosis through targeted activation of caspase 8: a new mouse model of inducible and reversible lipoatrophy. *Nat Med* **11**, 797-803

Pasarica M, Gowronska-Kozak B, Burk D, Remedios I, Hymel D, Gimble J, Ravussin E, Bray GA, Smith SR. (2009). Adipose tissue collagen VI in obesity. *J Clin Endocrinol Metab* **94**, 5155-5162

Passarge E, Robinson PN, Graul-Neumann LM. (2016). Marfanoid-progeroid-lipodystrophy syndrome: a newly recognized fibrillinopathy. *Eur J Hum Genet* **24**, 1244-1247

Pellegrinelli V, Heuvingh J, du Roure O, Rouault C, Devulder A, Klein C, Lacasa M, Clement E, Lacasa D, Clement K. (2014). Human adipocyte function is impacted by mechanical cues. *J Pathol* **233**, 183-195

Pereira L, D'Alessio M, Ramirez F, Lynch JR, Sykes B, Pangilinan T, Bonadio J. (1993). Genomic organization of the sequence coding for fibrillin, the defective gene product in Marfan syndrome. *Hum Mol Genet* **2**, 961-968

Pereira L, Lee SY, Gayraud B, Andrikopoulos K, Shapiro SD, Bunton T, Biery NJ, Dietz HC, Sakai LY, Ramirez F. (1999). Pathogenetic sequence for aneurysm revealed in mice underexpressing fibrillin-1. *Proc Natl Acad Sci USA* **96**, 3819-3823

Pfaff M, Reinhardt DP, Sakai LY, Timpl R. (1996). Cell adhesion and integrin binding to recombinant human fibrillin-1. *FEBS Lett* **384**, 247-250

Pierleoni C, Verdenelli F, Castellucci M, Cinti S. (1998). Fibronectins and basal lamina molecules expression in human subcutaneous white adipose tissue. *Eur J Histochem* **42**, 183-188

Piha-Gossack A, Sossin WS, Reinhardt DP. (2012). The evolution of extracellular fibrillins and their functional domains. *PLoS One* **7**, e33560

Pyeritz RE. (2000). The Marfan syndrome. *Annu Rev Med* **51**, 481-510

Qian RQ, Glanville RW. (1997). Alignment of fibrillin molecules in elastic microfibrils is defined by transglutaminase-derived cross-links. *Biochemistry* **36**, 15841-15847

Raghunath M, Bächi T, Meuli M, Altermatt S, Gobet R, Bruckner-Tuderman L, Steinmann B. (1996). Fibrillin and elastin expression in skin regenerating from cultured keratinocyte autografts: morphogenesis of microfibrils begins at the dermo-epidermal junction and precedes elastic fiber formation. *J Invest Dermatol* **106**, 1090-1095

Raghunath M, Putnam EA, Ritty T, Hamstra D, Park ES, Tschödrich-Rotter M, Peters R, Rehemtulla A, Milewicz DM. (1999). Carboxy-terminal conversion of profibrillin to fibrillin at a basic site by PACE/furin-like activity required for incorporation in the matrix. *J Cell Sci* **112**, 1093-1100

Ramirez F, Carta L, Lee-Arteaga S, Liu C, Nistala H, Smaldone S. (2008). Fibrillin-rich microfibrils - Structural and instructive determinants of mammalian development and physiology. *Connect Tissue Res* **49**, 1-6

Rauch F, Plotkin H, DiMeglio L, Engelbert RH, Henderson RC, Munns C, Wenkert D, Zeitler P. (2008). Fracture prediction and the definition of osteoporosis in children and adolescents: the ISCD 2007 Pediatric Official Positions. *J Clin Densitom* **11**, 22-28

Reinhardt DP, Keene DR, Corson GM, Pöschl E, Bächinger HP, Gambee JE, Sakai LY. (1996a). Fibrillin 1: Organization in microfibrils and structural properties. *J Mol Biol* **258**, 104-116

Reinhardt DP, Sasaki T, Dzamba BJ, Keene DR, Chu ML, Göhring W, Timpl R, Sakai LY. (1996b). Fibrillin-1 and fibulin-2 interact and are colocalized in some tissues. *J Biol Chem* **271**, 19489-19496

Ribas V, Nguyen MT, Henstridge DC, Nguyen AK, Beaven SW, Watt MJ, Hevener AL. (2010). Impaired oxidative metabolism and inflammation are associated with insulin resistance in ERalpha-deficient mice. *Am J Physiol Endocrinol Metab* **298**, E304-E319

Rifkin DB. (2005). Latent transforming growth factor-beta (TGF-beta) binding proteins: orchestrators of TGF-beta availability. *J Biol Chem* **280**, 7409-7412

Robinson P, Arteaga-Solis E, Baldock C, Collod-Beroud G, Booms P, De Paepe A, Dietz HC, Guo G, Handford PA, Judge DP, Kielty CM, Loeys B, Milewicz DM, Ney A, Ramirez F, Reinhardt DP, Tiedemann K, Whiteman P, Godfrey M. (2006). The molecular genetics of Marfan syndrome and related disorders. *J Med Genet* **43**, 769-787

Romere C, Duerrschmid C, Bournat J, Constable P, Jain M, Xia F, Saha PK, Del Solar M, Zhu B, York B, Sarkar P, Rendon DA, Gaber MW, LeMaire SA, Coselli JS, Milewicz DM, Sutton VR, Butte NF, Moore DD, Chopra AR. (2016). Asprosin, a fasting-induced glucogenic protein hormone. *Cell* **165**, 566-579

Rong JX, Qiu Y, Hansen MK, Zhu L, Zhang V, Xie M, Okamoto Y, Mattie MD, Higashiyama H, Asano S, Strum JC, Ryan TE. (2007). Adipose mitochondrial biogenesis is suppressed in db/db and high-fat diet-fed mice and improved by rosiglitazone. *Diabetes* **56**, 1751-1760

Rosen ED, Sarraf P, Troy AE, Bradwin G, Moore K, Milstone DS, Spiegelman BM, Mortensen RM. (1999). PPAR gamma is required for the differentiation of adipose tissue in vivo and in vitro. *Mol Cell* **4**, 611-617

Rosen ED, Walkey CJ, Puigserver P, Spiegelman BM. (2000). Transcriptional regulation of adipogenesis. *Genes Dev* **14**, 1293-1307

Rosen ED, MacDougald OA. (2006). Adipocyte differentiation from the inside out. *Nat Rev Mol Cell Biol* **7**, 885-896

Rubin J, Sen B. (2017). Actin up in the nucleus: Regulation of actin structures modulates mesenchymal stem cell differentiation. *Trans Am Clin Climatol Assoc* **128**, 180-192

Rurali E, Perrucci GL, Pilato CA, Pini A, Gaetano R, Nigro P, Pompilio G. (2018). Precise therapy for thoracic aortic aneurysm in Marfan syndrome: a puzzle nearing its solution. *Prog Cardiovasc Dis* **61**, 328-335

Sabatier L, Miosge N, Hubmacher D, Lin G, Davis EC, Reinhardt DP. (2011). Fibrillin-3 expression in human development. *Matrix Biol* **30**, 43-52

Saely CH, Geiger K, Drexel H. (2012). Brown versus white adipose tissue: a mini-review. *Gerontology* **58**, 15-23

Saharinen J, Taipale J, Keski-Oja J. (1996). Association of the small latent transforming growth factor-ß with an eight cysteine repeat of its binding protein (LTBP-1). *EMBO J* **15**, 245-253

Saharinen J, Keski-Oja J. (2000). Specific sequence motif of 8-Cys repeats of TGF-beta binding proteins, LTBPs, creates a hydrophobic interaction surface for binding of small latent TGF-beta. *Mol Biol Cell* **11**, 2691-2704

Sakamoto H, Broekelmann T, Cheresh DA, Ramirez F, Rosenbloom J, Mecham RP. (1996). Cell-type specific recognition of RGD- and non-RGD-containing cell binding domains in fibrillin-1. *J Biol Chem* **271**, 4916-4922

Salans LB, Cushman SW, Weismann RE. (1973). Studies of human adipose tissue. Adipose cell size and number in nonobese and obese patients. *J Clin Invest* **52**, 929-941

Saltiel AR, Olefsky JM. (2017). Inflammatory mechanisms linking obesity and metabolic disease. *J Clin Invest* **127**, 1-4

Samad F, Yamamoto K, Pandey M, Loskutoff DJ. (1997). Elevated expression of transforming growth factor-beta in adipose tissue from obese mice. *Mol Med* **3**, 37-48

Samuel VT, Petersen KF, Shulman GI. (2010). Lipid-induced insulin resistance: unravelling the mechanism. *Lancet* **375**, 2267-2277

Sanchez-Gurmaches J, Guertin DA. (2014). Adipocytes arise from multiple lineages that are heterogeneously and dynamically distributed. *Nat Commun* **5**, 4099

Sanchez-Gurmaches J, Hsiao WY, Guertin DA. (2015). Highly selective in vivo labeling of subcutaneous white adipocyte precursors with Prx1-Cre. *Stem Cell Rep* **4**, 541-550

Scherer LR, Arn PH, Dressel DA, Pyeritz RM, Haller JA, Jr. (1988). Surgical management of children and young adults with Marfan syndrome and pectus excavatum. *J Pediatr Surg* **23**, 1169-1172

Schultze JL. (2015). Global transcriptional regulation in the immune system. *Semin Immunol* **27**, 1-3

Seale P, Bjork B, Yang W, Kajimura S, Chin S, Kuang S, Scime A, Devarakonda S, Conroe HM, Erdjument-Bromage H, Tempst P, Rudnicki MA, Beier DR, Spiegelman BM. (2008). PRDM16 controls a brown fat/skeletal muscle switch. *Nature* **454**, 961-967

Seale P, Kajimura S, Spiegelman BM. (2009). Transcriptional control of brown adipocyte development and physiological function--of mice and men. *Genes Dev* **23**, 788-797

Sengle G, Ono RN, Lyons KM, Bachinger HP, Sakai LY. (2008). A new model for growth factor activation: type II receptors compete with the prodomain for BMP-7. *J Mol Biol* **381**, 1025-1039

Sengle G, Ono RN, Sasaki T, Sakai LY. (2011). Prodomains of transforming growth factor beta (TGFbeta) superfamily members specify different functions: extracellular matrix interactions and growth factor bioavailability. *J Biol Chem* **286**, 5087-5099

Shan T, Liu W, Kuang S. (2013). Fatty acid binding protein 4 expression marks a population of adipocyte progenitors in white and brown adipose tissues. *FASEB J* **27**, 277-287

Shapiro SD, Endicott SK, Province MA, Pierce JA, Campbell EJ. (1991). Marked longevity of human lung parenchymal elastic fibers deduced from prevalence of D-aspartate and nuclear weapons-related radiocarbon. *J Clin Invest* **87**, 1828-1834

Shi M, Zhu J, Wang R, Chen X, Mi L, Walz T, Springer TA. (2011). Latent TGF-beta structure and activation. *Nature* **474**, 343-349

Silverman DI, Burton KJ, Gray J, Bosner MS, Kouchoukos NT, Roman MJ, Boxer M, Devereux RB, Tsipouras P. (1995). Life expectancy in the Marfan syndrome. *Am J Cardiol* **75**, 157-160

Singh MN, Lacro RV. (2016). Recent clinical drug trials evidence in Marfan syndrome and clinical implications. *Can J Cardiol* **32**, 66-77

Smith RE, Horwitz BA. (1969). Brown fat and thermogenesis. *Physiol Rev* **49**, 330-425

Smith U. (2002). Impaired ('diabetic') insulin signaling and action occur in fat cells long before glucose intolerance--is insulin resistance initiated in the adipose tissue? *Int J Obes Relat Metab Disord* **26**, 897-904

Spalding KL, Arner E, Westermark PO, Bernard S, Buchholz BA, Bergmann O, Blomqvist L, Hoffstedt J, Naslund E, Britton T, Concha H, Hassan M, Ryden M, Frisen J, Arner P. (2008). Dynamics of fat cell turnover in humans. *Nature* **453**, 783-787

Spencer M, Unal R, Zhu B, Rasouli N, McGehee RE, Jr., Peterson CA, Kern PA. (2011). Adipose tissue extracellular matrix and vascular abnormalities in obesity and insulin resistance. *J Clin Endocrinol Metab* **96**, E1990-E1998

Sponseller PD, Hobbs W, Riley LH, 3rd, Pyeritz RE. (1995). The thoracolumbar spine in Marfan syndrome. *J Bone Joint Surg* **77**, 867-876

Sponseller PD, Sethi N, Cameron DE, Pyeritz RE. (1997). Infantile scoliosis in Marfan syndrome. *Spine* **22**, 509-516

Stephens JM, Bailey JL, Hang H, Rittell V, Dietrich MA, Mynatt RL, Elks CM. (2018). Adipose tissue dysfunction occurs independently of obesity in adipocyte-specific oncostatin receptor knockout mice. *Obesity* **26**, 1439-1447

Summers KM, Nataatmadja M, Xu D, West MJ, McGill JJ, Whight C, Colley A, Ades LC. (2005). Histopathology and fibrillin-1 distribution in severe early onset Marfan syndrome. *Am J Med Genet* **139**, 2-8

Summers KM, Raza S, van Nimwegen E, Freeman TC, Hume DA. (2010). Co-expression of FBN1 with mesenchyme-specific genes in mouse cell lines: implications for phenotypic variability in Marfan syndrome. *Eur J Hum Genet* **18**, 1209-1215

Takamiya T, Zaky WR, Edmundowics D, Kadowaki T, Ueshima H, Kuller LH, Sekikawa A. (2004). World Health Organization-defined metabolic syndrome is a better predictor of coronary calcium than the adult treatment panel III criteria in American men aged 40-49 years. *Diabetes Care* **27**, 2977-2979

Takenouchi T, Hida M, Sakamoto Y, Torii C, Kosaki R, Takahashi T, Kosaki K. (2013). Severe congenital lipodystrophy and a progeroid appearance: Mutation in the penultimate exon of FBN1 causing a recognizable phenotype. *Am J Med Genet* **161A**, 3057-3062

Tchoukalova YD, Koutsari C, Karpyak MV, Votruba SB, Wendland E, Jensen MD. (2008). Subcutaneous adipocyte size and body fat distribution. *Am J Clin Nutr* **87**, 56-63

Tchoukalova YD, Koutsari C, Votruba SB, Tchkonia T, Giorgadze N, Thomou T, Kirkland JL, Jensen MD. (2010a). Sex- and depot-dependent differences in adipogenesis in normal-weight humans. *Obesity* **18**, 1875-1880

Tchoukalova YD, Votruba SB, Tchkonia T, Giorgadze N, Kirkland JL, Jensen MD. (2010b). Regional differences in cellular mechanisms of adipose tissue gain with overfeeding. *Proc Natl Acad Sci USA* **107**, 18226-18231

Tiedemann K, Sasaki T, Gustafsson E, Göhring W, Bätge B, Notbohm H, Timpl R, Wedel T, Schlötzer-Schrehardt U, Reinhardt DP. (2005). Microfibrils at basement membrane zones interact with perlecan via fibrillin-1. *J Biol Chem* **280**, 11404-11412

Tiedemann K, Boraschi-Diaz I, Rajakumar I, Kaur J, Roughley P, Reinhardt DP, Komarova SV. (2013). Fibrillin-1 directly regulates osteoclast formation and function by a dual mechanism. *J Cell Sci* **126**, 4187-4194

Tontonoz P, Hu E, Spiegelman BM. (1994). Stimulation of adipogenesis in fibroblasts by PPAR gamma 2, a lipid-activated transcription factor. *Cell* **79**, 1147-1156

Trayhurn P. (2013). Hypoxia and adipose tissue function and dysfunction in obesity. *Physiol Rev* **93**, 1-21

Unger RH, Scherer PE. (2010). Gluttony, sloth and the metabolic syndrome: a roadmap to lipotoxicity. *Trends Endocrinol Metab* **21**, 345-352

Vaicik MK, Thyboll Kortesmaa J, Moverare-Skrtic S, Kortesmaa J, Soininen R, Bergstrom G, Ohlsson C, Chong LY, Rozell B, Emont M, Cohen RN, Brey EM, Tryggvason K. (2014). Laminin alpha4 deficient mice exhibit decreased capacity for adipose tissue expansion and weight gain. *PLoS One* **9**, e109854

Valencak TG, Osterrieder A, Schulz TJ. (2017). Sex matters: The effects of biological sex on adipose tissue biology and energy metabolism. *Redox Biology* **12**, 806-813

van Karnebeek CD, Naeff MS, Mulder BJ, Hennekam RC, Offringa M. (2001). Natural history of cardiovascular manifestations in Marfan syndrome. *Arch Dis Child* **84**, 129-137

Varghese M, Griffin C, McKernan K, Eter L, Lanzetta N, Agarwal D, Abrishami S, Singer K. (2019). Sex differences in inflammatory responses to adipose tissue lipolysis in diet-induced obesity. *Endocrinology* **160**, 293-312

Virtue S, Vidal-Puig A. (2010). Adipose tissue expandability, lipotoxicity and the metabolic syndrome - an allostatic perspective. *Biochim Biophys Acta* **1801**, 338-349

von Kodolitsch Y, Demolder A, Girdauskas E, Kaemmerer H, Kornhuber K, Muino Mosquera L, Morris S, Neptune E, Pyeritz R, Rand-Hendriksen S, Rahman A, Riise N, Robert L, Staufenbiel I, Szocs K, Vanem TT, Linke SJ, Vogler M, Yetman A, De Backer J. (2019). Features of Marfan syndrome not listed in the Ghent nosology - the dark side of the disease. *Expert Rev Cardiovasc Ther* **17**, 883-915

Wajchenberg BL. (2000). Subcutaneous and visceral adipose tissue: their relation to the metabolic syndrome. *Endocr Rev* **21**, 697-738

Walji TA, Turecamo SE, DeMarsilis AJ, Sakai LY, Mecham RP, Craft CS. (2016). Characterization of metabolic health in mouse models of fibrillin-1 perturbation. *Matrix Biol* **55**, 63-76

Wallace RN, Streeten BW, Hanna RB. (1991). Rotary shadowing of elastic system microfibrils in the ocular zonule, vitreous, and ligament nuchae. *Curr Eye Res* **10**, 99-109

Wallis DD, Putnam EA, Cretoiu JS, Carmical SG, Cao SN, Thomas G, Milewicz DM. (2003). Profibrillin-1 maturation by human dermal fibroblasts: proteolytic processing and molecular chaperones. *J Cell Biochem* **90**, 641-652

Wang CY, Lin TA, Liu KH, Liao CH, Liu YY, Wu VC, Wen MS, Yeh TS. (2019). Serum asprosin levels and bariatric surgery outcomes in obese adults. *Int J Obes* **43**, 1019-1025

Wang Q, Somwar R, Bilan PJ, Liu Z, Jin J, Woodgett JR, Klip A. (1999). Protein kinase B/Akt participates in GLUT4 translocation by insulin in L6 myoblasts. *Mol Cell Biol* **19**, 4008-4018

Wang QA, Tao C, Gupta RK, Scherer PE. (2013). Tracking adipogenesis during white adipose tissue development, expansion and regeneration. *Nat Med* **19**, 1338-1344

Wang Y, Zhao L, Smas C, Sul HS. (2010). Pref-1 interacts with fibronectin to inhibit adipocyte differentiation. *Mol Cell Biol* **30**, 3480-3492

Weinbaum JS, Broekelmann TJ, Pierce RA, Werneck CC, Segade F, Craft CS, Knutsen RH, Mecham RP. (2008). Deficiency in microfibril-associated glycoprotein-1 leads to complex phenotypes in multiple organ systems. *J Biol Chem* **283**, 25533-25543

Weisberg SP, McCann D, Desai M, Rosenbaum M, Leibel RL, Ferrante AW, Jr. (2003). Obesity is associated with macrophage accumulation in adipose tissue. *J Clin Invest* **112**, 1796-1808

Wernstedt Asterholm I, Tao C, Morley TS, Wang QA, Delgado-Lopez F, Wang ZV, Scherer PE. (2014). Adipocyte inflammation is essential for healthy adipose tissue expansion and remodeling. *Cell Metab* **20**, 103-118

Weyer C, Foley JE, Bogardus C, Tataranni PA, Pratley RE. (2000). Enlarged subcutaneous abdominal adipocyte size, but not obesity itself, predicts type II diabetes independent of insulin resistance. *Diabetologia* **43**, 1498-1506

Wilcox G. (2005). Insulin and insulin resistance. *Clin Biochem Rev* **26**, 19-39

Williams AS, Kang L, Wasserman DH. (2015). The extracellular matrix and insulin resistance. *Trends Endocrinol Metab* **26**, 357-366

Wipff PJ, Rifkin DB, Meister JJ, Hinz B. (2007). Myofibroblast contraction activates latent TGF-beta1 from the extracellular matrix. *J Cell Biol* **179**, 1311-1323

Wohl AP, Troilo H, Collins RF, Baldock C, Sengle G. (2016). Extracellular regulation of bone morphogenetic protein activity by the microfibril component fibrillin-1. *J Biol Chem* **291**, 12732-112746

Wolever TM. (1990). The glycemic index. *World Rev Nutr Diet* **62**, 120-185

Wright DW, Mayne R. (1988). Vitreous humor of chicken contains two fibrillar systems: an analysis of their structure. *J Ultrastruct Mol Struct Res* **100**, 224-234

Wronska A, Kmiec Z. (2012). Structural and biochemical characteristics of various white adipose tissue depots. *Acta Physiol (Oxf)* **205**, 194-208

Wu J, Bostrom P, Sparks LM, Ye L, Choi JH, Giang AH, Khandekar M, Virtanen KA, Nuutila P, Schaart G, Huang K, Tu H, van Marken Lichtenbelt WD, Hoeks J, Enerback S, Schrauwen P, Spiegelman BM. (2012). Beige adipocytes are a distinct type of thermogenic fat cell in mouse and human. *Cell* **150**, 366-376

Wu Z, Bucher NL, Farmer SR. (1996). Induction of peroxisome proliferator-activated receptor gamma during the conversion of 3T3 fibroblasts into adipocytes is mediated by C/EBPbeta, C/EBPdelta, and glucocorticoids. *Mol Cell Biol* **16**, 4128-4136

Wu Z, Rosen ED, Brun R, Hauser S, Adelmant G, Troy AE, McKeon C, Darlington GJ, Spiegelman BM. (1999). Cross-regulation of C/EBP alpha and PPAR gamma controls the transcriptional pathway of adipogenesis and insulin sensitivity. *Mol Cell* **3**, 151-158

Xu H, Barnes GT, Yang Q, Tan G, Yang D, Chou CJ, Sole J, Nichols A, Ross JS, Tartaglia LA, Chen H. (2003). Chronic inflammation in fat plays a crucial role in the development of obesity-related insulin resistance. *J Clin Invest* **112**, 1821-1830

Yadav H, Quijano C, Kamaraju AK, Gavrilova O, Malek R, Chen W, Zerfas P, Zhigang D, Wright EC, Stuelten C, Sun P, Lonning S, Skarulis M, Sumner AE, Finkel T, Rane SG. (2011). Protection from obesity and diabetes by blockade of TGF-beta/Smad3 signaling. *Cell Metab* **14**, 67-79

Yaribeygi H, Farrokhi FR, Butler AE, Sahebkar A. (2019). Insulin resistance: Review of the underlying molecular mechanisms. *J Cell Physiol* **234**, 8152-8161

Yetman AT, McCrindle BW. (2010). The prevalence and clinical impact of obesity in adults with Marfan syndrome. *Can J Cardiol* **26**, 137-139

Yuan X, Downing AK, Knott V, Handford PA. (1997). Solution structure of the transforming growth factor ß-binding protein-like module, a domain associated with matrix fibrils. *EMBO J* **16**, 6659-6666

Zatterale F, Longo M, Naderi J, Raciti GA, Desiderio A, Miele C, Beguinot F. (2019). Chronic adipose tissue Inflammation linking obesity to insulin resistance and type 2 diabetes. *Front Physiol* **10**, 1607

Zeyer KA, Zhang RM, Kumra H, Hassan A, Reinhardt DP. (2019). The fibrillin-1 RGD integrin binding site regulates gene expression and cell function through microRNAs. *J Mol Biol* **431**, 401-421

Zhang H, Apfelroth SD, Hu W, Davis EC, Sanguineti C, Bonadio J, Mecham RP, Ramirez F. (1994a). Structure and expression of fibrillin-2, a novel microfibrillar component preferentially located in elastic matrices. *J Cell Biol* **124**, 855-863

Zhang H, Hu W, Ramirez F. (1995). Developmental expression of fibrillin genes suggests heterogeneity of extracellular microfibrils. *J Cell Biol* **129**, 1165-1176

Zhang X, Jiang H, Ma X, Wu H. (2019). Increased serum level and impaired response to glucose fluctuation of asprosin is associated with type 2 diabetes mellitus. *J Diabetes Investig*

Zhang Y, Proenca R, Maffei M, Barone M, Leopold L, Friedman JM. (1994b). Positional cloning of the mouse obese gene and its human homologue. *Nature* **372**, 425-432

APPENDIX

Dr. Kerstin Tiedemann
Shriners Hospital for Children
1003 Décarie Boulevard
Montréal, QC, H4A 0A9
work: 514-282-8250
cell: 514-862-9512

November 24, 2021

Reg: Agreement on the use of manuscript in a manuscript-based thesis at McGill University

I hereby confirm that I will not use the two manuscripts listed below for a manuscript-based thesis at McGill University. In this manuscript, Muthu L. Muthu and I are listed as co-first authors. I agree to that my co-first author, Muthu L. Muthu, will use it in her manuscript-based PhD thesis.

1. Muthu ML*, Tiedemann K*, Fradette J, Komarova S#, Reinhardt DP#, *co-first authors, #co-senior authors "Fibrillin-1 is a key regulator of white adipose tissue development, homeostasis, and function" (Submitted manuscript).

2. Tiedemann K*, Muthu ML*, Reinhardt DP#, Komarova S#, *co-first authors, #co-senior authors "Male mice with fibrillin-1 deficiency are predisposed to high-fat diet induced obesity, diabetes, and fatty liver" (Submitted manuscript).

Sincerely,
Kerstin Tiedemann, PhD